Thermosensory Neurons Control Germline Transposons and Modulate Genetic Inheritance

Inaugural-Dissertation
zur
Erlangung des Doktorgrades
der Mathematisch-Naturwissenschaftlichen Fakultät
der Universität zu Köln

vorgelegt von

Péter Richárd Szántó

Aus Szeged, Ungarn

Köln, 2025

Accepted in the year 2025

The work described in this dissertation was conducted from September 2020 to May 2025 under the supervision of Prof. Dr. Björn Schumacher at the Institute for Genome Stability in Ageing and Disease, CECAD research center, University of Cologne.

Chapter 3.1 “Thermosensory neurons control genetic inheritance through regulation of germline transposons” of this thesis have been published:

Szántó, P.R., Meyer, D.H., Teichman, G., Pérez-Llanos, F.J., Rickert, D., Köhrer, K.-E., Rechavi, O., and Schumacher, B. (2024). Thermosensory neurons control genetic inheritance through regulation of germline transposons. Preprint at bioRxiv, https://doi.org/10.1101/2024.12.02.626368.

Table of Contents

List of Abbreviations ..... *I*

List of Figures ..... *II*

List of Tables ..... *IV*

Summary ..... *V*

1. Introduction *6*

1.1 Revisiting evolution: From Darwin through Weismann to genomic flexibility 6

1.2 Transposable elements: mobile code in a dynamic genome 8

1.3 Classification of transposable elements 9

1.4 Evolutionary origins and evolutionary roles of transposable elements 13

1.5 Regulation of Transposable Elements by small RNAs, piRNAs, Epigenetic Mechanisms, and DNA Repair Pathways 17

1.5.1 Small RNA and piRNA-Mediated Silencing of Transposons 17

1.5.2 Somatic piRNA Functions and Non-Canonical Roles 19

1.5.3 Tissue-specific control of transposons by DNA repair and epigenetic 20

1.5.4 Evolutionary implications 21

1.6 Transposable Elements in Development and Decline 21

1.6.1 Reproductive Biology and Aging: From Germline Regulation to Fertility Decline 21

1.6.2 Immune Function and Autoimmunity: TE-Derived Innovation and Risk 23

1.6.3 Nervous System Development, Neuronal Mosaicism and Neurodegeneration 24

1.6.4 Stem cell biology, senescence, and cancer 25

1.7 Methods for studying transposable elements 25

1.7.1 Functional and phenotypic assays 26

1.7.2 Genome assembly and annotation of TEs 26

1.7.3 Long-read DNA sequencing techniques 26

1.7.4 Mapping reads to repetitive regions 28

1.7.5 Quantifying TE expression 28

1.7.6 Further assays to track TEs 28

1.8 *Caenorhabditis elegans* a model to study evolution, aging and TE biology 29

1.8.1 *C. elegans* as a Model Organism 29

1.8.2 Using *C. elegans* to study evolution 30

1.8.3 Small RNA-mediated epigenetic inheritance in *C. elegans* 30

1.8.4 Heat stress induced TE activation and neuronal thermosensory regulation in *C. elegans* 31

1.8.5 Caenorhabditis elegans as a Model for Studying Aging and Reproductive Senescence 32

1.9 Aim of the study 32

2. Materials and methods *33*

2.1 *C. elegans* culture and maintenance 33

2.1.1 Strain Acquisition and Maintenance 33

2.1.2 Preparation of culture on NGM 33

2.1.3 Culture handling and synchronization 35

Contamination management 36

2.1.4 Freezing and thawing protocols 36

2.1.5 Crossing and backcrossing *C. elegans* 37

2.1.6 Genotyping *C. elegans* strains 37
2.2 Generation of the BJS1062 "AFD:HisCl1" strain 40
2.3 RNA extraction for RT-qPCR and RNA sequencing 40
2.4 cDNA synthesis 41
2.5 Quantitative real-time PCR (RT-qPCR) 42
2.6 Proteomics sample preparation 44
2.7 Proteomics data acquisition and proteomics sample processing 44
2.8 Mutation accumulation experiment design and strain handling 44
2.9 High molecular weight genomic DNA extraction from *C. elegans* 45
2.10 Tc1 Transposon mobilization assay – twitching screen 45
2.11 Bioinformatic analysis 46
2.12 Brood size quantification assay 46
2.13 Germ cell apoptosis assay, ... 46
2.14 Reproductive lifespan assay in *fog-2(q71)* mutants 47
2.15 *C. elegans* lifespan assay 47
2.16 Data quantification, handling, statistical analysis and visualization 48
2.17 *C. elegans* strains used for this study 48
2.18 Primers used for this study 48
2.19 Key resources, consumables, instruments used for this study 50
2.20 Use of generative AI and AI-assisted technologies in the writing process. 51
3 Results I: Thermosensory neurons control genetic inheritance through regulation of germline transposons 52
3.1 Thermosensory neurons control genetic inheritance through regulation of germline transposons ..52
3.2 Effect of candidate mediator genes that link AFD neuron signaling to germline transposable element activity 110
3.3 The effect of AFD neuron impairment on fertility and germ cell apoptosis 113
4 Results II: The impact of transposable element activity on aging and fertility in C. elegans ..116
4.1 Transposase inhibitor: Raltegravir 116
4.2 Establishing Raltegravir treatment and conducting a brood size assay. 116
4.3 The effect of transposon inhibitor treatment on fertility in wild type under normal and mild heat stress conditions. 120
4.4 The effect of transposon inhibitor treatment on fertility and reproductive aging in *fog-2* feminized *C. elegans* 121
4.5 The effect of transposon inhibitor treatment on the lifespan of *C. elegans* 122

5 Discussion *129*
6 Conclusion *136*
References *136*

List of Abbreviations

Full name	**Abreviation**
Caenorhabditis elegans	*C. elegans*
Clustered regularly interspaced short palindromic repeats	CRISPR
DNA damage response	DDR
Endogenous retroviruses	ERV
Heat shock factor 1	HSF-1
Horizontal gene transfer	HGT
Insertion / deletion	indel
Long interspersed nuclear elements	LINE
Long terminal repeat	LTR
Lysogeny broth	LB
Miniature Inverted-repeat Transposable Elements	MITE
Mutator-like element	MULE
Nematode growth medium	NGM
Penelope-like elements	PLE
Piwi-interacting RNA	piRNA
Post-transcriptional gene silencing	PTGS
Reactive oxygen species	ROS
Reverse transcriptase	RT
RNA-dependent RNA polymerases	RdRP
Short interspersed nuclear elements	SINE
Single worm lysis buffer	SWLB
small RNA	sRNA
Target-primed reverse transcription	TPRT
Terminal inverted repeats	TIR
Transcription factor	TF
Transcription factor binding site	TFBS
Transposable element	TE
Tyrosine Recombinase	YR
Untranslated region	UTR
Variable number tandem repeats	VNTR
Worm-specific Argonaute	WAGO

List of Figures

Figure number	Figure title	Contribution/ origin
Figure 1.1	Schematic representation of the Weismann barrier	Péter Richárd Szántó
Figure 1.2	Summary of classification and transposition mechanisms of Class I and Class II transposable element subtypes	Han et al. 2023[1]
Figure 1.3	Overview of RNAi-based transposon silencing in *C. elegans*	Fischer 2024[2]
Figure 3.1	AFD dysfunction triggers transposon expression	Szántó et al. 2024[3]
Figure 3.2	Transcriptome and Proteome analysis reveal desilencing mechanisms triggers in AFD triple mutants	Szántó et al. 2024[3]
Figure 3.3	Transcriptome analysis identifies AFD-germline pathway regulating TE expression	Szántó et al. 2024[3]
Figure 3.4	Phenotypic and genetic analysis shows de novo Tc1 insertion mutagenesis	Szántó et al. 2024[3]
Figure 3.5	AFD neurons control inheritable TE insertion accumulation	Szántó et al. 2024[3]
Figure 3. S1	RT-qPCR measurement of differential expression of transposase mRNA primer pairs "A"	Szántó et al. 2024[3]
Figure 3. S2	Genotyping *mut-16(mg461)* background	Szántó et al. 2024[3]
Figure 3. S3	Gene set enrichment analyses (GSEA) for transposable elements	Szántó et al. 2024[3]
Figure 3. S4	The distribution of genes significantly downregulated or upregulated genes	Szántó et al. 2024[3]
Figure 3. S5	Heatmap of the public datasets shown in Figure 3.3F	Szántó et al. 2024[3]
Figure 3. S6	Single GSEA plots of the sRNA regulation related genes for Figure 3.3F.	Szántó et al. 2024[3]
Figure 3.6	RT-qPCR measurement of differential expression of transposase mRNA in the AFD neuron-germ line signaling mediator candidate *C. elegans* strains	Péter Richárd Szántó
Figure 3.7	Brood size of AFD neuron-depleted strains	Péter Richárd Szántó

Figure 3.8	Germ cell apoptosis and fertility of the AFD triple mutant.	Péter Richárd Szántó
Figure 4.1	Differential expression of transposase mRNA level of the Tc1 and Mirage	Péter Richárd Szántó
Figure 4.2	Brood size of *mut-16(pk710)I C. elegans*	Péter Richárd Szántó
Figure 4.3	Apoptotic change in response to reltegravir treatment in *mut-16(pk710)I C. elegans*	Péter Richárd Szántó
Figure 4.4	Brood size of wild-type *C. elegans* following raltegravir treatment at 25°C	Lahav, n.d. [302]
Figure 4.5	The effect of raltegravir treatment on brood size and reproductive lifespan in *fog-2(q71)V*	Titash Chandra Sarker; Péter Richárd Szántó
Figure 4.6	Lifespan of wild-type N2 *C. elegans* at 20 °C upon raltegravir and FUdR treatment	Lahav, n.d. [302]
Figure 4.7	Lifespan of wild-type N2 *C. elegans* at 20 °C upon raltegravir treatment	Titash Chandra Sarker; Péter Richárd Szántó
Figure 4.8	Lifespan of wild-type N2 *C. elegans* at 25 °C upon raltegravir treatment	Péter Richárd Szántó
Figure 4.9	Incidence of death by internal hatching in wild-type *C. elegans* at 25°C	Péter Richárd Szántó
Figure 4.10	Lifespan of AFD triple mutant *C. elegans* at 20 °C upon raltegravir treatment	Titash Chandra Sarker; Péter Richárd Szántó
Figure 4.11	Incidence of death by internal hatching in wild-type and AFD triple mutant *C. elegans* at 20°C	Titash Chandra Sarker; Péter Richárd Szántó
Figure 5.1	Working model	Szántó et al. 2024[3]
Figure 5.2	Proposed signaling pathway mechanism linking the AFD neuron to the germline	David Helmut Meyer; Péter Richárd Szántó

List of Tables

Table 2.1 nematode growth medium (NGM)
Table 2.2 lysogeny broth (LB) liquid medium
Table 2.3 lysogeny broth (LB) solid agar medium
Table 2.4 M9 buffer composition
Table 2.5 Bleaching solution composition
Table 2.6 Freezing buffer composition
Table 2.7 single worm lysis buffer (SWLB)
Table 2.8 single worm lysis incubation protocol
Table 2.9 MangoTaq Master Mix
Table 2.10 MangoTaq PCR program
Table 2.11 Q5 Master Mix
Table 2.12 Q5 PCR program
Table 2.13 cDNA synthesis master mixes and preparation procedure
Table 2.14 cDNA synthesis incubation protocol
Table 2.15 RT-qPCR template mater mix
Table 2.16 RT-qPCR template primer mix
Table 2.17 RT-qPCR program
Table 2.18 Nicotine solution

Summary

Transposable elements (TEs) constitute a significant portion of the genome and pose both evolutionary driver potential and mutagenic threat. In the germline, small RNA (sRNA) pathways act as critical repressors of TE activity, safeguarding genome integrity across generations. Traditionally, it has been assumed that somatic signals cannot influence the germline genome, a concept rooted in August Weismann's barrier. However, recent discoveries in epigenetic inheritance have begun to challenge this view by demonstrating that environmental signals sensed by somatic tissues can modulate germline gene expression.

The central aim of my study was to test whether neuronal sensing of heat stress in *Caenorhabditis elegans* (*C. elegans*) can influence germline TE activity, thereby altering genetic inheritance. Specifically, I investigated the role of the AFD thermosensory neuron in regulating TE silencing and mobilization. Using models of AFD neuron dysfunction, I demonstrated that disruption of thermosensory neuron leads to TE desilencing in germ cells. This results in *de novo* insertions of the Tc1 TE family, and an increased frequency of heritable mutations. These findings reveal a non-cell-autonomous regulation linking somatic neuron activity to induce mutations in the germline genome, thereby breaching the Weismann barrier.

Exploratory transcriptomic and proteomic analyses identified two potential parallel stress-responsive pathways downstream of AFD function that converge on the inhibition of germ line specific sRNA pathways, leading to transposon derepression. Preliminary experimental data show that *tph-1* mutants exhibit elevated TE activation under heat stress, while *pmk-1* mutants display reduced TE induction, supporting their respective roles as positive and negative regulators of TE expression. These findings suggest a neuro-germline communication axis that modulates TE silencing in response to environmental stress.

In the second part of this study, I investigated the role of age-related TE activation, which has been proposed to drive genomic instability and inflammaging, contributing to both somatic and reproductive aging. To assess whether TE activity influences these processes, I applied a pharmacological approach using the TE inhibitor raltegravir. The treatment enhanced fertility, maintained germline integrity, and reduced reproductive abnormalities, especially under heat stress. These results suggest that pharmacological inhibition of TE activity may offer a promising strategy to support reproductive health and promote healthy aging.

1. Introduction

1.1 Revisiting evolution: From Darwin through Weismann to genomic flexibility

To frame the implications of my thesis for evolutionary biology, regarding how the major thermosensory neurons of *C. elegans* influence germline TE activity and TE-driven mutagenesis, it is important to begin with the revisit development of evolutionary theory and how it has shaped our understanding of inheritance and genome dynamics.

The concept of evolution by natural selection was first formalized by Charles Darwin in "On the Origin of Species", where he proposed that advantageous heritable traits become more common across generations[4]. The rediscovery of Gregor Mendel's work in the early 20th century provided a clear genetic basis for inheritance, establishing the idea that traits are passed down through discrete hereditary units, later identified as genes[5]. These insights laid the foundation for the Modern Synthesis of the 1930s and 1940s, which unified Darwinian natural selection with Mendelian genetics[5]. This framework integrated population genetics and mutation theory, emphasizing random mutations as the primary source of genetic variation acted upon by selection[5]. A central concept in this synthesis was August Weismann's germ plasm theory, formulated in 1893, which introduced a strict division between somatic and germline cells[6,7]. This led to the formulation of the Weismann barrier, the idea that hereditary information flows unidirectionally from germline to soma and not in the reverse direction[6,7]. According to this model, genetic mutations in germ cells arise spontaneously and randomly, without influence from somatic cells or environmental conditions acting directly on the organism **(Figure 1.1)** [6]. In this framework, the environment plays a role only as a selective force, shaping the evolutionary process by favoring or eliminating genetic variants after they have arisen[5]. Evolutionary change is therefore driven solely by random mutations in the germline, and the environment influences which of these mutations persist through natural selection[6,7]. This model explicitly rejected Lamarckian inheritance, which proposed that traits acquired in somatic tissues could be transmitted to offspring[6,7]. Subsequent advances in developmental biology and molecular genetics provided strong support for this view by showing that the separation between soma and germline is actively maintained[8–10]. This is achieved through mechanisms such as the early embryonic segregation of germline precursor cells, the establishment of specialized nuclear architecture, highly efficient DNA repair systems, tightly regulated chromatin modifications, and apoptosis to eliminate defective cells[8–10]. These processes help preserve the integrity of the germline genome and prevent it from being altered by somatic changes or damage. Throughout most of the 20th century, the Weismann barrier was considered impermeable, reinforcing the foundational belief of the Modern Synthesis that only changes originating within germ cells could contribute to evolutionary outcomes[5].

With the advent of molecular biology, our understanding of the genome shifted from viewing it as a static blueprint to recognizing it as a dynamic and complex system. In addition to protein-coding genes, the genome includes regulatory elements, non-coding RNA loci, centromeres, telomeres, and a large fraction of mobile genetic elements known as transposable elements[11,12]. TEs play a

significant role in shaping genome structure and regulation, and they contribute to evolutionary innovation[11,12]. Genetic changes arise from several sources, including replication errors, environmental mutagens, cellular stress, recombination, and TE activity[11,12]. These mutations vary in effect, with some being neutral, others deleterious, and a few beneficial[13].

To safeguard genome integrity, cells rely on a range of DNA repair mechanisms, such as base excision repair, nucleotide excision repair, mismatch repair, homologous recombination, and non-homologous end joining[14]. In addition, TEs are tightly regulated to prevent harmful insertions[15]. The DNA damage response (DDR) serves to detect and resolve DNA lesions, and when damage is beyond repair, it can trigger apoptosis to eliminate defective cells[14]. This is particularly important in germ cells, where maintaining genome stability is essential for successful reproduction and the prevention of inherited defects[14]. Despite these safeguards, some mutations escape repair and become fixed in the germline[14]. Harmful mutations tend to be removed by natural selection, while others provide the genetic variation necessary for evolutionary change.

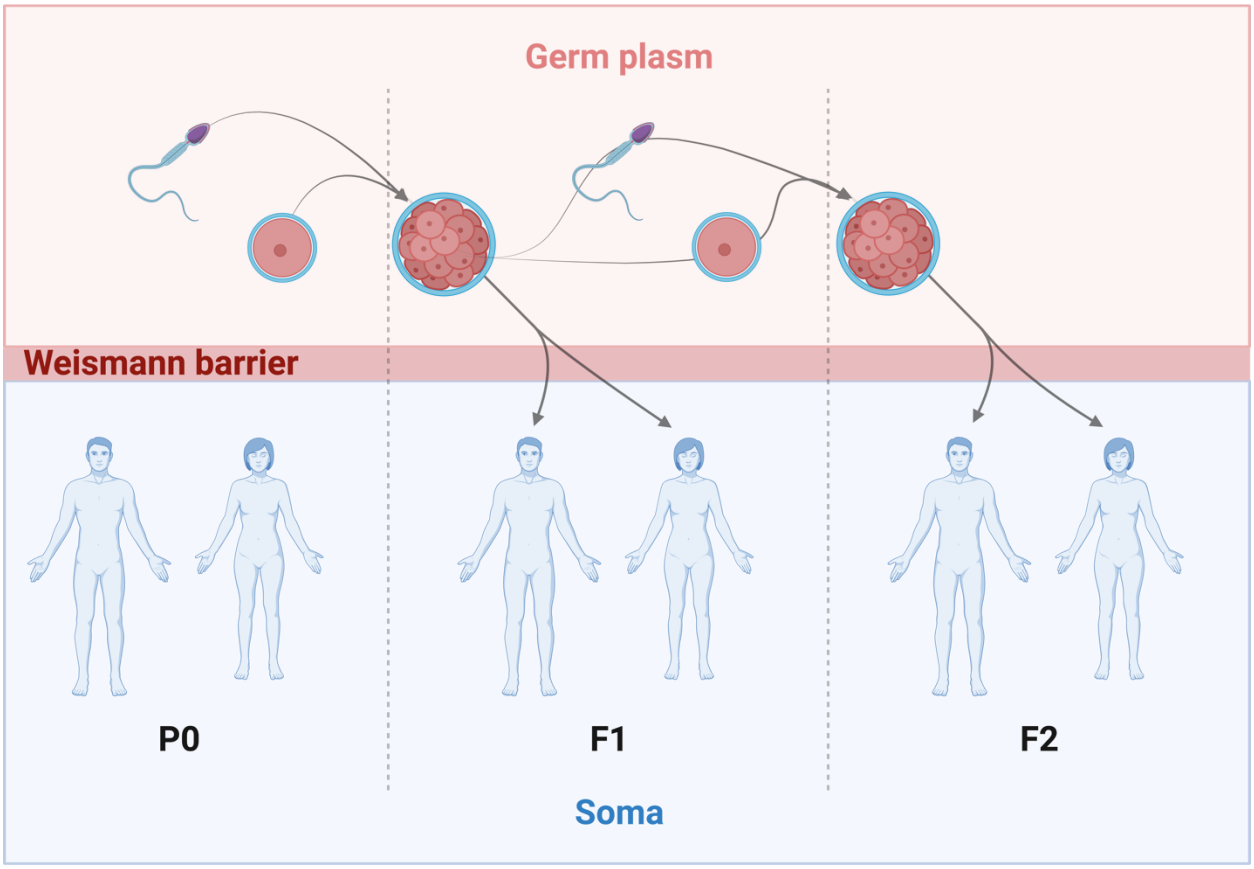

Figure 1.1 Schematic representation of the Weismann barrier. Arrows indicate the unidirectional flow of genetic information, which is segregated from direct somatic influence.

Recent discoveries in epigenetics and sRNA mediated transgenerational inheritance have begun to challenge the impermeability of the Weismann barrier[16,17]. Epigenetic mechanisms such as DNA methylation, histone modifications, and sRNAs regulate gene expression without altering the DNA

sequence, and in some cases, these changes can be inherited across generations. Environmental stressors can induce epigenetic modifications in somatic tissues that, under certain conditions, are transmitted to the germline[18]. In *C. elegans*, it has been shown that environmental cues sensed by somatic neurons can influence gene expression in germ cells through sRNA signaling pathways[18]. This points to a form of soma-to-germline communication that has begun to redefine the classical gene-centric models of evolution[19].

These insights suggest that the germline genome is not a closed system but one that can respond to environmental inputs in a heritable way[19]. Evolution may not be driven solely by random mutation and natural selection but may also involve adaptive regulatory mechanisms that incorporate environmental information into epigenetic inheritance[19]. While the DNA sequence remains the primary medium of inheritance, the recognition that epigenetic signals can influence heritable traits implies that the Weismann barrier is more permeable than previously thought.

This highlights the central focus of my study. Environmentally and somatically induced sRNAs and epigenetic modifications, which have been shown to bypass the Weismann barrier, may also regulate TEs. If environmental stimuli sensed by neurons can influence TE activity in the germline, this would challenge the final standing postulate of the Weismann barrier: that somatic signaling cannot induce heritable changes in DNA sequence. Given their mutagenic potential, TEs must be tightly regulated in germ cells to prevent genomic instability[15]. At the same time, their ability to generate genetic diversity positions them as key contributors to evolutionary innovation[15]. The following section explores the biology and evolutionary significance of transposable elements in greater depth.

1.2 Transposable elements: mobile code in a dynamic genome

Seventy years ago, Barbara McClintock made a discovery that would challenge the very foundation of how we perceive the genome[20]. She found that certain sequences of DNA were not bound by the constraints of static inheritance but were instead capable of moving across the genome, reshuffling the genetic code in ways previously unimagined[20]. What seemed, at first, an obscure anomaly has since transformed our understanding of the genome as a dynamic, ecosystem, continuously rewritten by the activity of TEs. These DNA wanderers have traversed the tree of life, shaping genetic landscapes, their influence embedded in the very essence of evolution[21]. They have a varying abundance in different organisms, within the *C. elegans* genome, constituting 12% of the total DNA[22], in others, they are sprawling across more than 90% of the genome, as in some plants[23]. In the human genome, they constituting approximately 45% of our genome[25]. TEs are not passive relics of evolutionary history, these elements continue to sculpt the genomic landscape. As both agents of disruption and sources of genetic innovation, TEs reflect the paradox of life itself, balancing order and randomness[24].

Despite their reputation as genomic parasites, TEs have also been co-opted for essential cellular functions[26]. They have influenced the evolution of gene regulatory networks, facilitated the emergence of novel exons, and even given rise to entire protein-coding genes[26]. Their activity plays a dual role, driving genetic diversity while also posing risks such as mutations, genome

instability, and associations with disease[27]. There is an ongoing evolutionary arms race between TEs and host genomes[27]. To mitigate TE activity, hosts have developed sophisticated defense mechanisms, including epigenetic repression such as, DNA methylation, histone modifications, and sRNA pathways[28,29]. However, TEs persist, evolving counterstrategies to evade suppression, which has led to a dynamic interplay that continues to influence genomic architecture and function[28,29]. Beyond this conflict, TE domestication has transformed some elements from invaders into essential components of cellular biology[30]. Many have been repurposed to serve functions in immune response and embryonic development, integrating into host regulatory networks[31,32]. As both disruptors and architects of genomes, TEs exemplify the evolutionary balance between constraint and innovation, leaving a lasting imprint on genome evolution[31,32].

TEs have also become valuable tools in biotechnology and biomedical research, contributing to genetic screening, genetic engineering, and high-throughput sequencing[1,33]. The advent of long-read sequencing technologies, such as nanopore and PacBio, has propelled TE research, allowing unprecedented insights into their structure, diversity, and evolutionary dynamics[34]. These advances, coupled with CRISPR-based TE insertion systems, have opened new avenues for targeted genome modifications[35,36]. As sequencing technologies continue to improve, TE research stands to make even greater contributions to genetics and synthetic biology[35,36].

Understanding the classification, diversity, and mechanisms of TEs is essential to fully decipher their impact on genome biology[37]. Their remarkable adaptability has allowed them to become not just genomic passengers but powerful evolutionary agents, influencing species diversification and the emergence of novel biological functions[21].

1.3 Classification of transposable elements

TEs are primarily classified based on their transposition mechanism, a system originally proposed by David Finnegan in 1989[38]. They are broadly divided into two major classes: Class I retrotransposons, which mobilize via an RNA intermediate and require reverse transcription, and Class II DNA transposons, which move through a direct DNA-based mechanism. Each class is further subdivided into orders, superfamilies, and families, reflecting their evolutionary relationships and structural features[39].

1.3.1 Class I: retrotransposons

Class I retrotransposons, also known as RNA transposons, mobilize via a "copy-and-paste" mechanism involving transcription into RNA, reverse transcription into DNA, and reintegration into the genome. Because the original sequence remains intact, this process significantly contributes to genome expansion. Retrotransposons are divided into three major subclasses based on their integration mechanisms: long terminal repeat (LTR) elements, non-LTR elements, and Tyrosine Recombinase (YR)-mobilized elements[40].

LTR retrotransposons, including the Ty3/Gypsy and Ty1/Copia superfamilies, share structural and mechanistic similarities with retroviruses[41–43]. These elements contain protein genes, encoding: reverse transcriptase, RNase H, and integrase, which facilitate their mobilization.

Endogenous retroviruses (ERVs), a distinct LTR subgroup, originate from ancient viral infections that became permanently integrated into host genomes[41–43]. Some ERVs have been domesticated to regulate gene expression, such as in mammalian placenta formation **(Figure 1.2 A)**[41–43].

Non-LTR retrotransposons, which lack terminal repeats, are further categorized into long interspersed nuclear elements (LINEs), short interspersed nuclear elements (SINEs), and Penelope-like elements (PLEs)[44]. **LINEs**, such as LINE-1 in mammals, encode an endonuclease and a reverse transcriptase, allowing autonomous retrotransposition. Their transposition is mediated by target-primed reverse transcription (TPRT), a process where the endonuclease cleaves genomic DNA, and the reverse transcriptase copies the RNA template into a complementary DNA strand**(Figure 1.2 B)**[45,46]. **SINEs**, including the primate-specific Alu elements, do not encode proteins but hijack LINE-encoded enzymes for their mobilization. These elements often originate from noncoding RNA genes, and amplify within genomes through a parasitic relationship with LINEs **(Figure 1.2 C)**[47]. Similarly, **Miniature Inverted-repeat Transposable Elements (MITEs)** are non-autonomous but maintain structural features that allow them to be mobilized by autonomous transposons[48]. A lesser-known subclass, **YR retrotransposons**, utilizes a tyrosine recombinase instead of integrase for genomic integration[49]. Their replication mechanism remains poorly understood, but they appear to be functionally distinct from LTR and non-LTR retrotransposons[50]. **PLEs** represent another distinct lineage, exhibiting structural similarities with telomerase and playing a role in maintaining genome stability across various eukaryotic lineages[51].

1.3.2 Class II: DNA transposons

Class II DNA transposons, often referred to as "cut-and-paste" elements, mobilize through direct DNA excision and reintegration. This process is typically catalyzed by a transposase enzyme that recognizes specific terminal inverted repeats (TIRs), excises the transposon from one genomic locus, and inserts it elsewhere[39]. Unlike retrotransposons, this mechanism does not inherently increase TE copy number, although some DNA transposons can amplify through replication-associated processes for example, during the S phase of the cell cycle or when gene conversion copies a heterozygous insertion into the homologous locus[52]. Class II elements are diverse and can be grouped into four major subclasses based on their distinct mobilization strategies: DDE transposases, Cryptons, rolling-circle transposons (Helitrons), and Mavericks (Polintons)[39].

DDE transposases represent the most widespread and evolutionary significant subclass. Named after their conserved catalytic triad (aspartic acid, aspartic acid, glutamic acid), these transposases mediate precise DNA excision and integration **(Figure 1.2 D)**. Major superfamilies include Tc1/mariner, hAT (hobo-Ac-Tam3), Mutator-like elements (MULEs), and PiggyBac transposons[21]. These elements differ in target site preferences, transposition efficiency, and evolutionary impact. Some, like PiggyBac, are actively used in genome engineering due to their high transposition efficiency and precise excision mechanism, which leaves no mutation scars at the excision site[53]. Others like the Tc1/mariner due to its high activity had a large-scale expansion becoming one of the widest spread family[54]. **Cryptons**, another subclass, differ fundamentally by utilizing a tyrosine recombinase rather than a transposase for mobilization. While less prevalent

than DDE transposons, Cryptons contribute to TE diversity across eukaryotes[55]. **Rolling-circle transposons**, or **Helitrons**, employ a distinctive "peel-and-paste" mechanism **(Figure 1.2 E)**. Instead of excision, they create a single-stranded DNA intermediate that is copied and integrated at new genomic sites. Helitrons lack TIRs and encode a Rep/Helicase protein related to bacterial rolling-circle replication enzymes[56]. Their ability to mobilize large genomic fragments has contributed significantly to genome evolution in various eukaryotic lineages, including plants, insects, and vertebrates, for example the diversification of *C. elegans* heat shock response elements happened via Helitron activity[57]. **Mavericks**, also known as **Polintons**, are among the most enigmatic and complex DNA transposons. Spanning up to 20 kilobases, they encode multiple proteins, including a DNA polymerase, integrases, and capsid-like proteins. Their structural similarities to certain dsDNA viruses suggest an ancient evolutionary link between transposons and viral elements. Some hypotheses propose that Mavericks played a role in the evolution of large DNA viruses and early eukaryotic genome organization[58]. Their role in horizontal gene transfer (HGT) and potential viral interactions remains an active area of research[58].

Advancements of long-read sequencing technologies have greatly enhanced our ability to characterize transposons, revealing previously hidden structural complexities and novel transposition mechanisms[34]. These tools have also facilitated the discovery of new TE families, further refining our understanding of their evolutionary history and functional significance[34].

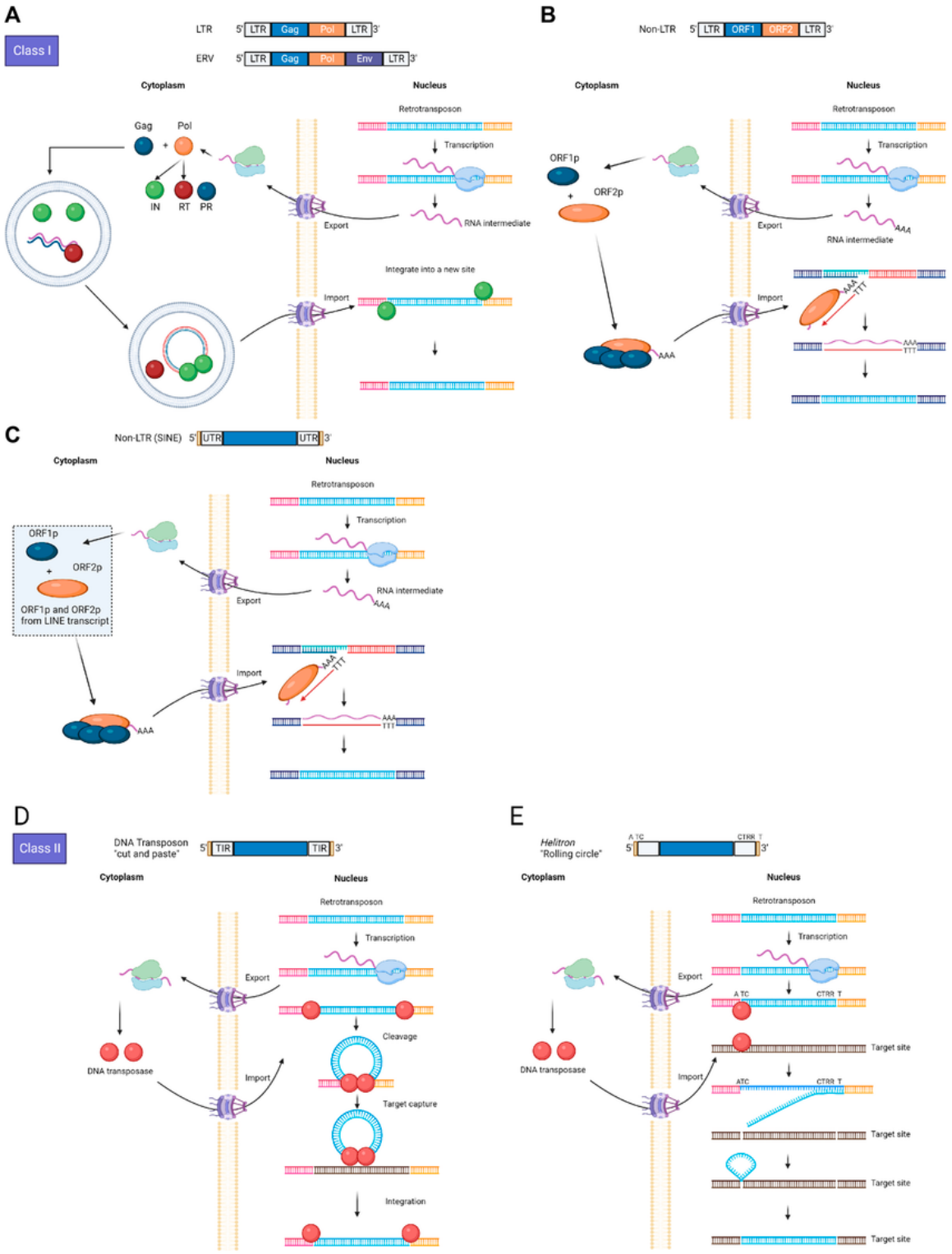

Figure 1.2 Summary of classification and transposition mechanisms of Class I and Class II transposable element subtypes. **A)** Schematic overview of the key steps in the transposition cycle of LTR retrotransposons and ERVs. **B)** Transposition cycle of non-LTR retrotransposons (LINEs), highlighting reverse transcription and target-primed integration. **C)** Transposition cycle of SINEs,

which rely on LINE-encoded proteins for mobilization. **D)** Classical "cut-and-paste" mechanism of DNA transposons, involving excision and reintegration into a new genomic locus. **E)** "Rolling-circle" replication mechanism of Helitrons, a distinct subclass of DNA transposons. **Abbreviations:** LTR, long terminal repeat; ERV, endogenous retrovirus; LINE, long interspersed nuclear element; SINE, short interspersed nuclear element; IN, integrase; PR, protease; RT, reverse transcriptase; Pol, polyprotein; UTR, untranslated region; TIR, terminal inverted repeat. (Adapted from Han et al. 2023[1])

1.3.3 Autonomous and non-autonomous elements

TEs can also be classified based on their ability to mobilize independently. Autonomous TEs, such as LINEs and LTR retrotransposons, encode the enzymatic machinery necessary for their own transposition, including reverse transcriptase or transposase[27,40]. In contrast, non-autonomous TEs, such as SINEs and MITEs, lack these essential proteins and rely on autonomous elements to facilitate their movement[27,40]. This parasitic relationship enables non-autonomous elements to propagate within genomes despite their lack of coding capacity, often reaching high copy numbers by hijacking the enzymatic activity of related autonomous elements[59]. The evolutionary persistence of non-autonomous TEs highlights their adaptability, allowing them to evade host defense mechanisms while contributing to genome plasticity and regulatory complexity through for example transcription factor binding site (TFBS) reshuffling[59].

The classification of transposable elements provides a foundation for examining their evolutionary significance. Their capacity to replicate, rearrange, and interact with host genomes has played a central role in shaping genome architecture across species throughout evolution.

1.4 Evolutionary origins and evolutionary roles of transposable elements

TEs are part of the genome as part of a biocoenosis, an ecosystem of sequences with diverse origins that interact, co-evolve, and potentially self-engineer[26]. Their origins stretch back to the dawn of eukaryotic life, with phylogenomic analyses revealing that the major TE subclasses were present early in eukaryotic evolution[60]. Core catalytic domains such as DDE-transposase, reverse transcriptase, tyrosine recombinase, and rolling-circle Rep/Helicase have their evolutionary roots extend to the primordial procaryotic world[61]. Some DNA transposons, including Tc1/mariner and PiggyBac, show homology to prokaryotic insertion sequences, indicating that these elements may have predated the eukaryotic-prokaryotic split[58]. In contrast, retrotransposons seem to have evolved independently within eukaryotes[21].

The evolutionary trajectory of TEs has not followed a simple linear path, but rather one that is modular and mosaic, defined by the recurrent assembly, disassembly, and reshuffling of functional genetic modules[36,61,62]. One of the most striking features of TE evolution is its reliance on the reuse and recombination of protein domains across different element types and even across biological domains. This modular evolution is evident in the frequent domain swapping events between unrelated TEs, viruses, and plasmids. For example, TEs often share structural domains like

integrase, reverse transcriptase, and RNase H with retroviruses, indicating that these protein modules can be co-opted or exchanged across lineages[21,63,64].

In this context, HGT emerges as a major force accelerating TE evolution and dispersal. Unlike vertical transmission, where genetic material is inherited from parent to offspring, HGT allows TEs to leap across species boundaries, introducing novel sequences into unrelated genomes[65]. This occurs through several mechanisms: via viral intermediates, host-parasite interactions, or even ingestion and cellular uptake of foreign DNA. HGT is particularly common among DNA transposons, whose compact structure and autonomous mobility make them ideal candidates for cross-species transfer[66,67]. Members of the Tc1/mariner superfamily have been identified in distantly related taxa, often with higher sequence identity than expected based on their evolutionary distance, suggesting multiple independent horizontal transfer events[66,67]. Likewise, the BovB retrotransposon, originally discovered in cattle, has been horizontally transferred between reptiles, ruminants, and marsupials, possibly via blood-feeding parasites[68]. Such events dramatically alter recipient genomes, injecting mobile elements with ready-to-use transposition machinery that can rapidly proliferate and reshape genome architecture. HGT thus acts as both a catalyst for TE diversification and a vehicle for their global distribution, blurring phylogenetic boundaries[65].

This modularity has led to the formation of chimeric TEs, hybrid elements composed of sequences from multiple ancestral sources. A well-known example of this is the hypothesized origin of LTR retrotransposons. These elements appear to have evolved from a fusion between non-LTR retrotransposons and cut-and-paste DNA transposons[69]. Evidence for this fusion model comes from the shared structural characteristics between these elements, despite their overall evolutionary distance[69]. These fused domains granted the new elements with a distinct transposition mechanism and regulatory capabilities, setting the stage for the proliferation of LTR elements across diverse genomes[69].

Similarly, the emergence of SINEs, SVA elements, and Helitrons underscores the creative potential of modular evolution. SINEs are non-autonomous elements that derive from host sRNAs or tRNAs and are mobilized by LINE machinery[59]. Many SINEs, such as the primate-specific Alu elements, arose from the fusion of multiple ancient SINE copies, acquiring additional sequences that enhance their mobility and regulatory influence[59]. SVAs, in turn, represent a higher-order composite structure that emerged from a combination of Alu, variable number tandem repeats (VNTRs), and endogenous retroviral sequences[70,71]. Helitrons, which use a rolling-circle replication mechanism, further exemplify this trend by frequently capturing host gene fragments and splicing them into new genomic contexts, contributing to novel gene architectures[56,72].

Taken together, these examples illustrate how TEs evolve and can shape evolution, not just by insertions, deletions and duplication, but through domain shuffling, structural recombination, and horizontal gene transfer. This modular architecture enables TEs to rapidly acquire new functions, circumvent host defense systems, and diversify the genome.

Beyond their highly flexible nature and origin of virus like ability to mutate, reshuffle and change, the evolutionary success of TEs has depended on complex host–element dynamics[21]. While many

insertions are neutral or deleterious, host genomes have occasionally co-opted TE sequences to generate new regulatory elements, protein domains, and even entire genes [24,26]. As in *C. elegans*, Helitrons have contributed reshuffling heat shock factor 1 (HSF-1) binding motifs, rewiring stress response pathway[57]. These TE insertions, particularly in gene promoters, demonstrate how TEs can rapidly innovate gene regulatory networks, often under selective pressure[24,73]. A genome-wide survey in *C. elegans* has shown that approximately 10% of all transcription factor motifs occur within TEs, and many of these motifs are bound by their cognate TFs and reside in accessible chromatin[74].

TEs are also central to population-level evolutionary processes. Natural variation in TE copy number and insertion sites is shaped by both genetic drift and selection[75]. Wild isolates of *C. elegans* reveal substantial lineage-specific TE activity[76]. Importantly, TEs can generate novel genetic material through five primary mechanisms:

1. Domestication, where TE-encoded proteins (like transposases, reverse transcriptases or envelope genes) are repurposed by the host genome to serve essential biological functions[21,24]. This process has left a deep imprint across diverse lineages. In *Drosophila*, for example, telomere elongation is maintained not by the canonical telomerase enzyme, but through the targeted insertion of domesticated retrotransposons like HeT-A and TART, which transpose specifically to chromosome ends[77,78]. In vertebrates, the RAG1 gene, which is indispensable for the somatic V(D)J recombination processes underlying adaptive immunity, is originated from a domesticated transposase derived from an ancient Transib DNA element[79,81]. Another intriguing case is that of Syncytins, proteins derived from the envelope genes of endogenous retroviruses, which have been repeatedly co-opted across mammalian evolution to mediate trophoblast cell fusion during placental development[80,82].

2. Exaptation, where TE sequences are repurposed into exons or regulatory elements, often resulting in novel splicing variants or enhancers. These changes can affect how, when, and where a gene is expressed, sometimes creating entirely new regulatory connections or gene functions[84].

3. Regulatory innovation, where insertions near host genes modify expression patterns, as seen in industrial melanism in the peppered moth and heat stress response diversification via Helitron elements in nematodes[57,83]. By inserting into promoter or enhancer regions, TEs can bring new transcription factor binding sites or disrupt existing ones, altering gene expression levels and timing[85]. New TF binding sites upstream of genes, rewiring stress-responsive transcriptional programs[57]. Such regulatory changes can have immediate phenotypic consequences and may be subject to natural selection.

4. Retrogene formation, where retrotransposon activity reverse-transcribes host mRNA into new, potentially functional gene copies. These "retrogenes" are typically intronless and inserted to another locus in the genome, sometimes near active regulatory elements that allow their expression[86,87]. While many of these copies remain nonfunctional, since they are free to mutate without pressure on fitness, some acquire novel functions or expression patterns distinct from their parental genes[88]. For example, in dogs, a retrocopy of the *fgf4* gene contributes to chondrodysplasia, the short-legged phenotype seen in certain breeds like dachshunds[89].

5. Genomic plasticity, where ectopic recombination and rearrangements fueled by TEs drive structural variation[21]. Transposable elements act as potent endogenous mutagens by creating new genetic variation through a variety of mechanisms. These include, most commonly, **insertions** (where a TE integrates into a new genomic location)[27], **deletions** (caused when TE excision is imperfect or when recombination removes flanking sequences)[90], and **duplications** (arising from replication slippage or transposition-associated errors)[91]. Additionally, **inversions** can occur when two TEs copies in opposite orientation recombine, flipping the intervening sequence[92], and **translocations** may result from non-allelic homologous recombination between TEs copies on different chromosomes[93]. TEs also facilitate **ectopic recombination**, where non-homologous sequences at different TE copy loci misalign during meiosis, leading to rearrangements and copy number variations[94]. These structural changes can impact gene dosage, disrupt coding regions, or generate new regulatory interactions, contributing significantly to genome evolution and phenotypic diversity[24].

Stress-induced TE activation is a particularly powerful route for generating adaptive diversity. In periods of environmental upheaval, when cellular defense systems like HSP90-piRNA interactions are overwhelmed, TEs can escape repression and transpose[95]. This can result in rapid genomic restructuring, potentially conferring advantageous traits. The "epi-transposon hypothesis" and "TE-thrust hypothesis" propose that TEs may serve as evolutionary accelerators, particularly during population bottlenecks or habitat shifts[97]. These ideas are supported by findings in invasive species like the ant, Cardiocondyla obscurior, whose TE-rich "islands" appear to concentrate genes relevant for environmental sensing and adaptation[96].

A wide range of stressors beyond environmental instability have been shown to activate TEs, acting as genomic triggers that destabilize epigenetic silencing. **Thermal stress** is one of the most documented inducers: in both plants and animals, elevated temperatures can lead to the derepression of heat-sensitive elements. In *C. elegans*, heat stress activates transposons in the male germline, leading to an increase in DNA double-strand breaks during spermatogenesis, independent of the canonical SPO-11 pathway[98]. This damage is linked to the mobilization of Tc1 elements, which show an increase in new insertions in spermatocytes however, oocytes remain largely resistant[98]. In *Drosophila*, for example, heat shock destabilizes heterochromatin and derepresses the hobo and gypsy TEs[99,100]. Similarly, in *Arabidopsis*, heat exposure activates the ONSEN retrotransposon[101]. **Oxidative stress** is another potent activator, where increased reactive oxygen species (ROS) can damage DNA and alter chromatin states, facilitating TE mobilization[102]. In *C. elegans*, exposure to hydrogen peroxide increases excision frequencies of DNA transposons like Tc1 and CemaT1, especially when combined with *hsp-90* knockdown, suggesting that oxidative stress can compromise TE silencing and promote heritable genome instability[102]. In mammals, TE activation under oxidative stress has been linked to neurodegeneration and tumorigenesis, indicating a broader impact on organismal health[103]. **Nutritional deprivation**, particularly amino acid or folate deficiency, also affects the epigenetic landscape and has been shown to activate LINE elements in mammalian cells[104]. **Pathogen exposure and immune**

challenges similarly alter host transcriptional programs and can lead to temporary windows of TE expression. Viral infections are particularly notable; for instance, influenza and HIV infections can stimulate LINE-1 and ERV expression in human cells by disrupting heterochromatin or hijacking transcriptional machinery[105,106]. Although most TE insertions are neutral or deleterious, the occasional beneficial insertion can sweep to fixation under positive selection[76,107]. This dynamic is evident in *C. elegans*, where experimental evolution has shown that under relaxed selection, derepression of specific TE families (e.g. Tc1, Turmoil2) occurs[76,107]. This is accompanied by changes in 22G-RNA silencing and chromatin context, reflecting the complex molecular environment governing TE expression[108]. These mechanisms illustrate how TEs not only provide raw mutational material but also participate in lineage-specific regulatory evolution. Stress appears to act as a catalyst, releasing the latent potential of TEs to generate variation, reorganize genomes, and drive adaptation.

Understanding how host genomes respond to and regulate TE activity through sRNA-mediated silencing, piRNA pathways, and epigenetic mechanisms is essential to fully appreciate their evolutionary significance and their ongoing influence across biological systems.

1.5 Regulation of Transposable Elements by small RNAs, piRNAs, Epigenetic Mechanisms, and DNA Repair Pathways

As TEs present both potential and peril within genomes, necessitating stringent regulation to maintain genomic stability while allowing evolutionary flexibility. Mechanisms controlling TE activity involve intricate interactions among sRNA pathways, PIWI-interacting RNAs (piRNAs), and epigenetic silencing systems. These regulatory pathways, conserved across diverse species yet specialized by evolutionary pressures, illustrate the dynamic balance maintained between TEs and host genomes[28,109,110].

1.5.1 Small RNA and piRNA-Mediated Silencing of Transposons

sRNA-mediated pathways form a foundational line of defense against TE activity. The major classes primarily regulating endogenous gene expression are miRNAs and siRNAs, however piRNAs are uniquely specialized to detect and silence TEs, particularly in the germline. piRNAs (typically 21–31 nucleotides in length) are defined by their association with PIWI proteins, a subfamily of Argonaute proteins[111]. Their functions extend beyond TE suppression, encompassing roles in gene regulation, stem cell biology, transgenerational epigenetic inheritance, and disease[112]. While siRNAs and miRNAs are processed from double-stranded RNA precursors via Dicer, piRNAs are generated from long single-stranded precursors through a Dicer-independent pathway[113]. These precursors are transcribed from genomic regions called piRNA clusters, which are typically enriched in fragmented or degenerate TE sequences. As such, these clusters serve as genomic archives of past TE invasions[110]. piRNA clusters are generally transcribed by RNA polymerase II and can be organized in either unidirectional or bidirectional orientations, with transcriptional initiation mechanisms differing across taxa[112]. Functionally, the organization and role of piRNA clusters bear a strong resemblance to CRISPR arrays in prokaryotes: both systems

encode short RNA sequences derived from non-self genetic elements, which are then processed and used by the host as a form of sequence-specific immune memory to recognize and silence foreign nucleic acids[114].

After transcription from piRNA clustrs the primary piRNA processing involves endonucleolytic cleavage by ZUCCHINI/PLD6, helicases such as Armitage (*Drosophila*) or MOV10L1 (mammals), and mitochondrial localization of processing factors. This processing can occur in phase (phased piRNAs) or via a secondary "ping-pong" amplification cycle. The resulting piRNAs often carry a 5′ uridine bias and have 3′ ends protected through 2′-O-methylation by HENN1[110,115–120]. The ping-pong cycle, prominent in germline cells of many species, involves reciprocal cleavage by two PIWI proteins, reinforcing silencing of TEs and expanding the piRNA pool[110]. TUDOR domain-containing proteins, such as Krimper, scaffold these interactions and ensure specificity[121]. Additional processing yields phased piRNAs, generated downstream of cleavage sites, further diversifying the regulatory repertoire[118].

piRNA biogenesis and function are spatially organized within ribonucleoprotein condensates, nuage granules in Drosophila, chromatoid bodies in mammals, and Yb bodies in somatic cells, formed through liquid–liquid phase separation. These structures facilitate co-localization of pathway components, with proteins like VASA and TDRDs ensuring granule integrity[122–125].

In mammals, MILI and MIWI2 direct piRNA-guided TE silencing during embryonic spermatogenesis[126]. MILI initiates ping-pong and phased processing, while MIWI2 shuttles to the nucleus, recognize actively transcribing TE regions and recruiting DNA methyltransferases and histone modifiers to silence TEs epigenetically[127]. In later stages, MIWI-pachytene piRNAs modulate mRNA stability and translation, essential for spermiogenesis[128].

In *C. elegans*, a functionally analogous system is centered on 21U-RNAs. These short, single-stranded RNAs are transcribed from thousands of genomic loci that share a conserved upstream motif[129]. Their biogenesis involves initiation by the USTC transcription factor complex, transcription by RNA polymerase II, and processing by specialized factors such as PETISCO, PARN-1, and HENN-1[130]. Mature 21U-RNAs are loaded onto the Piwi-clade Argonaute PRG-1 and PPW-2 forming complexes that survey the germline transcriptome[132]. PRG-1 does not cleave targets directly, as the ping-pong amplification cycle is absent in *C. elegans*[131]. Instead, it recruits the endonuclease RDE-8[131]. Following cleavage in the mutator focus, RDE-3 (also known as MUT-2) adds a poly(UG) tail, which facilitates recognition by RNA-dependent RNA polymerases (RdRP), leading to the synthesis of secondary 22G-RNAs.[131]. These secondary siRNAs associate with a diverse set of worm-specific Argonautes (WAGOs) that mediate both post-transcriptional gene silencing (PTGS) (e.g., WAGO-1) and transcriptional silencing through nuclear WAGOs such as HRDE-1. HRDE-1 transports the secondary 22G-RNAs into the nucleus, where it scans actively transcribing regions[133]. Upon target recognition, it initiates epigenetic silencing. Nuclear WAGOs promote heterochromatin formation via the NRDE complex, leading to the recruitment of histone methyltransferases (HMT) and deposition of H3K9me3 and H3K27me3 marks and establishing long-term, heritable repression known as RNA-induced epigenetic silencing **(Figure 1.3)**[134,135]. The 21U-RNA pathway is finely tuned to discriminate between self and non-self-

transcripts. Endogenous germline genes are protected by competing regulatory inputs: CSR-1-bound 22G-RNAs promote gene expression, while PATC (Periodic An/Tn Cluster) motifs inhibit silencing[136]. This balance is crucial as it prevents inappropriate repression of essential genes while maintaining genome defense[136]. In addition to TE control, piRNA-like pathways in *C. elegans* regulate endogenous genes, support fertility, mediate stress responses and establish transgenerational epigenetic memory. Dysfunction of the aforementioned pathways results in the progressive loss of the germline integrity, ultimately leading to sterility after couple of generations when cultured at 20 °C or higher, known as the mortal germline phenotype, underscoring their essential role in maintaining germline immortality[137].

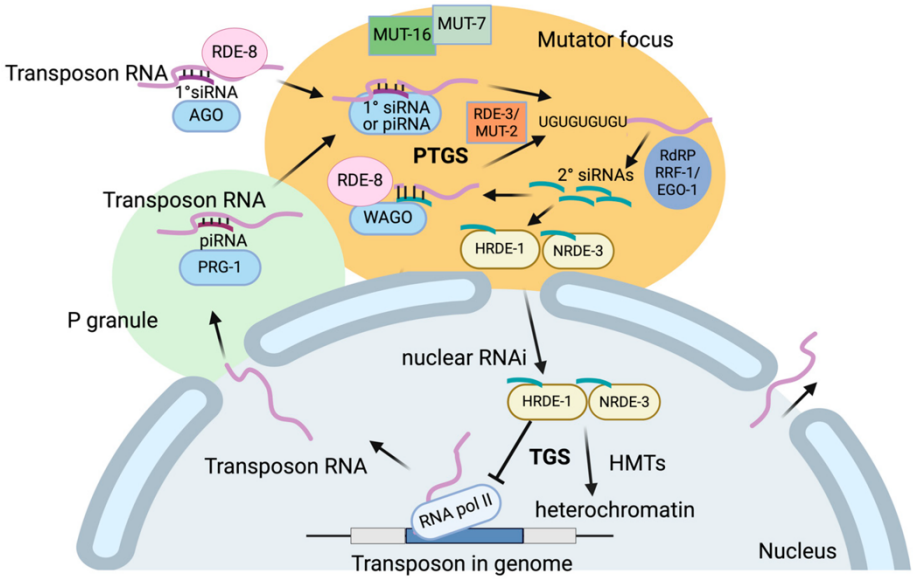

Figure 1.3 Overview of RNAi-based transposon silencing in *C. elegans*. In this pathway, transposon-derived RNAs are initially recognized by piRNAs bound to the Argonaute protein PRG-1. Upon target recognition, RDE-8 or related nucleases cleave the RNA, allowing RDE-3/MUT-2 to add a poly(UG) tail. This modification recruits an RdRP, which synthesizes secondary siRNAs. These siRNAs mediate post-transcriptional silencing by associating with WAGO Argonautes within the mutator focus, where they are stabilized by scaffolding proteins such as MUT-16 and MUT-7. Amplification of secondary 22G-RNAs by RdRP further reinforces silencing. In parallel, these siRNAs initiate transcriptional silencing via the nuclear Argonautes HRDE-1 and NRDE-3, resulting in stable and heritable repression of transposon activity. (Adapted from Fischer 2024[2])

1.5.2 Somatic piRNA Functions and Non-Canonical Roles

Initially characterized as germline-restricted, piRNA pathways are now recognized to function in somatic tissues as well, this paradigm shift highlights their broader regulatory scope and reinforces the novelty of somatic TE control mechanisms across many taxa. In *C. elegans*, 21U-RNAs remain germline-enriched, but their downstream effectors (22G-RNAs and WAGO Argonautes such as

NRDE-3) mediate somatic silencing. This allows maternally inherited sRNAs (21U- and 26G-RNAs) to initiate somatic 22G-RNA production, contributing to developmental gene regulation, stress resilience, and cellular identity, also to imprint transgenerationally persisting epigenetic memory[138–140].

As a broader outlook, in planarians, the homologue PIWI proteins SMEDWI-1/2/3 mediate both transcriptional and post-transcriptional TE repression and regulate chromatin via histone mRNA translation[141]. In Hydra, HYWI and HYLI proteins operate canonical ping-pong cycles[142]. In both organisms their function is essential for somatic stem cell maintenance and their extraordinary regenerative potential[142].

In mammals, somatic and stem cells express PIWI proteins and piRNAs with diverse functions[112]. In adult neural progenitors, MILI/piRNAs suppress translation-related genes, maintaining stemness and preventing differentiation[143]. In bone marrow stromal cells, piRNAs regulate lineage commitment, either promoting or inhibiting osteogenesis[144]. Human embryonic stem cells exhibit dynamic PIWI expression patterns that likely regulate stem cell maintenance and differentiation timing. piRNAs also mediate antiviral defense[145]. In neural stem cells, exosomal piRNAs target HIV and SARS-CoV-2 RNAs[145]. In mosquitoes and other invertebrates, piRNAs silence viral genomes, indicating that piRNA-based immunity operates beyond the germline[146].

1.5.3 Tissue-specific control of transposons by DNA repair and epigenetic

piRNA-mediated silencing is tightly linked to epigenetic regulation and genome maintenance. In mammals, PIWI–piRNA complexes recruit DNMT3 family methyltransferases to establish repressive DNA methylation at TE loci[112]. In *C. elegans*, PRG-1–initiated silencing triggers the generation of 22G-RNAs and recruitment of WAGO Argonautes, leading to histone modifications. Two histone methyltransferases, MET-2 and SET-25, deposit H3K9me2 and H3K9me3, respectively, modifications critical for silencing repetitive elements and transposons[147]. Loss of MET-2 results in derepression, DNA damage, and replication stress[147]. When combined with BRCA1/BARD1 inactivation, this leads to synthetic sterility, suggesting functional crosstalk between heterochromatin formation and DNA repair[147]. Artificial activation of repeats induces germline apoptosis, further highlighting H3K9me2's genome-protective role[147].

TE excision introduces DNA double-strand breaks, which are repaired differently across tissues. In the *C. elegans* germline, homologous recombination repair restores excised TEs, masking mobilization[148]. In somatic cells, repair occurs via non-homologous end joining, promoting detectable TE movement[148]. For instance, Tc1 transposition is ~1000-fold more frequent in soma than germline. Disruption of NHEJ components (*nhj-1, lig-4, cku-70, cku-80*) significantly reduces Tc1 mobilization, demonstrating that repair pathway choice directly shapes TE dynamics and lack of sufficient repair forms a negative feedback regulation on TE excision[148]. Together, these systems, RNA-guided silencing, chromatin remodeling, and tissue-specific DNA repair, constitute a multilayered defense against transposon-induced genomic instability[148].

1.5.4 Evolutionary implications

piRNA pathways exemplify evolutionary plasticity, linking their rapid evolution to the functional diversification and regulatory mechanisms explored throughout this chapter[112]. Their dynamic co-evolution with transposable elements drives continual innovation in genomic defense strategies, adapting the sRNA landscape to species-specific challenges and regulatory needs[149]. PIWI proteins and piRNA clusters evolve rapidly, often in response to TE pressures. In some nematodes, such as *C. briggsae* and *C. remanei*, the number of piRNA loci and Argonaute proteins exceeds that of *C. elegans*[150]. Conversely, some nematode lineages have lost *prg*-1 and 21U-RNAs entirely, relying on siRNA pathways[151].

This rapid divergence allows species-specific adaptation, as newly invading TEs may become assimilated into piRNA clusters. As such, piRNA pathways act as evolutionary sensors, continually reshaping the genome's defensive architecture[152].

The molecular regulation of transposable elements integrates sRNA silencing, chromatin remodeling, and DNA repair into a coordinated, evolutionarily responsive system[28]. These mechanisms manage TE activity across developmental stages and tissue types, supporting genome integrity while enabling adaptive potential[133]. Positioned between TE origin and TE function, this regulatory layer contextualizes TEs as both parasitic elements and regulatory partners, genomic actors with the capacity to shape both species evolution and individual physiology. Understanding the complex regulatory networks that manage transposable element activity reveals not only their evolutionary persistence but also their integral roles throughout organismal life[140].

1.6 Transposable Elements in Development and Decline

TEs are vital not only on an evolutionary scale, generating genetic variation and contributing to species phylogenesis, but also at the ontogenetic level. Many developmental and physiological processes involve regulated, moderate TE activity, underscoring a co-option between the host genome and TEs that reflects a more symbiotic relationship[24,153]. However, this balance is disrupted during aging: the dysregulation of TEs can lead to genomic instability, chronic inflammation, and the onset of various age-related diseases[24,153].

1.6.1 Reproductive Biology and Aging: From Germline Regulation to Fertility Decline

The reproductive system and the germline are the most prominent sites of TE activity. Given their potential for genomic disruption, TEs must be tightly regulated, yet they also contribute to essential physiological processes[28,154,155]. Later in life, however, their reactivation appears to drive reproductive decline. This section follows TE activity and involvement in the reproductive system from fertilization through to the end of the reproductive lifespan[28,154,155].

In mammalian models, immediately after fertilization during the preimplantation stage of embryonic development, global epigenetic reprogramming transiently permits TE expression[156]. This permissive chromatin landscape allows TEs to act as regulatory elements, driving gene expression during zygotic genome activation and supporting large-scale chromatin reorganization[157]. As discussed earlier, many TEs harbor regulatory motifs that appear essential

for early development[158,159]. In parallel, this early burst of TE activity may be linked to the resetting of the epigenome to a 'ground zero' state, erasing age-associated epigenetic marks. Elements such as LINE-1 and MERVL contribute to transcriptional activation, totipotency regulation, and placental development by harboring regulatory sequences[158,159].

As germ cell development proceeds, TE-derived long non-coding RNAs and alternative promoters modulate genes involved in oocyte maturation and spermatogenesis. While tight control by piRNA pathways typically preserves genomic integrity across generations, occasional bursts of TE activity may reflect their evolutionary role in regulatory innovation[156].

With aging, the epigenetic control of TEs in reproductive tissues begins to deteriorate. In oocytes, this manifests as the loss of repressive heterochromatin marks such as H3K9me2, H3K27me3, and HP1γ, along with a decline in sRNA-mediated silencing mechanisms[160]. This erosion of repression permits the transcriptional activation of retrotransposons, notably LINE-1, which accumulate at both RNA and protein levels in aged oocytes[161]. The resulting activity induces DNA damage, as evidenced by increased γH2AX foci and Rad51 localization, accompanied by elevated double-stranded RNA processing, cytoplasmic accumulation, and retrotransposon protein expression[161,162]. Importantly, these deleterious changes precede widespread aneuploidy, suggesting that TE activation may represent an early, and possibly causal, event in reproductive decline[161].

Experimental manipulation further supports this relationship. Pharmacological disruption of heterochromatin in young oocytes, using compounds such as Chaetocin (an H3K9 methyltransferase inhibitor) or TSA (a histone deacetylase inhibitor), induces aging-like phenotypes, elevating retrotransposon activity, increasing DNA damage, and impairing oocyte maturation[155,160]. Interestingly, treatment with AZT, a reverse transcriptase inhibitor, partially preserves genome integrity and oocyte quality by inhibiting retrotransposition, though it does not restore heterochromatin marks[161].

Mouse studies reveal that these processes begin as early as nine months of age, before the onset of significant chromosomal segregation errors, highlighting the significance of epigenetic deterioration and TE reactivation as early events in reproductive aging[161,163,164].

Human data mirror these findings. In oocytes retrieved during IVF procedures, levels of the heterochromatin mark H3K9me2 decline linearly with age, paralleling the observations in mice and reinforcing the universality of this mechanism across mammals[165–167]. A corresponding reduction in Rec8, a cohesin subunit essential for chromosomal segregation, further supports the link between epigenetic and structural deterioration in reproductive senescence[168–170].

Collectively, these data support a model in which age-related loss of heterochromatin initiates a cascade of events: derepression of retrotransposons, accumulation of DNA damage, impairment of chromosomal cohesion, and ultimately compromised oocyte maturation[154,161,162].

In *C. elegans*, germline expression of the Cer1 retrotransposon, a member of the Ty3/Gypsy family, is tightly regulated by both age and environmental conditions. Notably, capsid formation occurs only at lower temperatures (~15 °C), a pattern opposite to that of other Class II DNA transposon families such as Tc1/Mariner and in older adults[171,172]. Cer1 capsids accumulate in

germ cells during meiotic progression[171,172]. These observations suggest that, even in systems with tight repression, aging can permit retrotransposon reactivation that interferes with fertility[137,137,173]. In *Drosophila*, similar patterns emerge. Aging is associated with downregulation of Piwi expression in the germline stem cell niche, permitting activation of the Ty3/gypsy retrotransposon[174]. This, in turn, triggers Toll–GSK3 signaling, degradation of β-catenin, disruption of stem cell–niche adhesion, and eventual stem cell loss[175,176]. These conserved pathways illustrate how TE activity, inflammation, and stem cell exhaustion are tightly interconnected in reproductive aging across species[177,178]. Moreover, the temperature- and age-dependent activation of TEs may reflect not only a breakdown in repression but also an evolved, context-specific regulatory strategy in the germline[179,180].

1.6.2 Immune Function and Autoimmunity: TE-Derived Innovation and Risk

TEs have emerged as both drivers of immune innovation and potential instigators of immune dysfunction[32]. While the full extent of their influence remains incompletely understood, growing evidence demonstrates that TEs are deeply embedded in immune physiology, far beyond their role as passive triggers of innate immune pathways such as cGAS–STING or inducers of sterile inflammation[181].

TEs have played pivotal roles in shaping the evolutionary architecture of the immune system. Ancient DNA transposons gave rise to the RAG1/2 recombinases, enabling V(D)J recombination and the advent of adaptive immunity[79,81]. Endogenous retroviruses have been co-opted to bolster antiviral defense and immune sensing[32,183]. TE-derived enhancers, such as MER41B, regulate interferon-stimulated genes during thymic development, enhancing host responsiveness[32,182]. In thymic epithelial cells, TE-derived peptides contribute to the education of developing T cells, while in plasmacytoid dendritic cells, TE-derived double-stranded RNAs maintain tonic interferon-α production[184]. These examples illustrate the extensive domestication of TEs for fine-tuning immune surveillance and function.

However, this domestication carries inherent risks. Loss of TE silencing, whether due to aging, oncogenic transformation, heritable mutation, or epigenetic dysregulation, can lead to the accumulation of TE-derived nucleic acids, which aberrantly activate recognition receptors such as cGAS[164]. This chronic activation fuels persistent interferon responses and sterile inflammation, a hallmark of autoimmune diseases like multiple sclerosis[185,187]. In these conditions, the immune system fails to distinguish endogenous TEs from viral invaders, transforming once-beneficial elements into sources to trigger autoimmunity[186].

Intriguingly, this same capacity for viral mimicry and innate immune activation may serve as a tumor surveillance mechanism. During malignant transformation, transcriptomic remodeling frequently results in TE derepression. While tumors may exploit TEs to enhance regulatory plasticity and genomic microevolution, the resulting TE activity can also trigger cytoplasmic sensing pathway cGAS–STING, promoting immunogenic cell death and apoptosis[188,189]. This mechanism is exemplified by the blind mole rat, a rodent species with exceptional cancer resistance[190]. Their naturally low DNA (cytosine-5)-methyltransferase-1 (DNMT1) levels lead to

spontaneous TE derepression and interferon-mediated cell death[190]. Similar TE-based immune surveillance mechanisms operate in mice and humans, indicating a conserved anti-cancer strategy[191,192].

Thus, TEs may function as endogenous alarm systems for pre-malignant states, capable of triggering intrinsic immune responses that constrain tumorigenesis[188,193]. This raises promising therapeutic possibilities: deliberate TE reactivation, for example via DNA-demethylating agents, could sensitize cancer cells to immune clearance[194]. However, such strategies must be approached with caution, as chronic TE activity also contributes to inflammaging and immune dysregulation during aging[194].

1.6.3 Nervous System Development, Neuronal Mosaicism and Neurodegeneration

TEs are active contributors to brain development and function[196]. During neurogenesis, LINE-1 elements can undergo somatic retrotransposition in neural progenitor cells (NPC), contributing to neuronal mosaicism[195]. This process, confirmed in both rodent and human brains, may increase neuronal plasticity and individual variability in brain function[197,198]. Somatic LINE-1 insertions are especially enriched in brain regions such as the hippocampus and can affect gene regulation in cis by introducing new promoters, enhancers, or splice sites[197,199]. These insertions may shape neural circuitry on a per-cell basis[196].

Beyond insertional mutagenesis, TE-derived cis-regulatory elements, including enhancers, polyadenylation signals, and transcription factor binding sites, are frequently repurposed in the brain to influence gene expression[200,201]. In addition, TE-derived long lncRNAs and exapted TE coding genes, such as *Arc*, are implicated in synaptic function and neurodevelopment[202]. Collectively, these observations support a model in which controlled TE activity provides a substrate for neuronal complexity[196].

Repression of TE activity in the nervous system is maintained by DNA methylation, histone modifications such as H3K9me3, and repressive complexes involving KRAB-ZFP and KAP1[203–205]. These mechanisms are robust in NPCs but become relaxed in mature neurons, where low-level TE activity may serve physiological roles[206]. However, this delicate balance is increasingly disrupted during aging and disease[207]. Age-related epigenetic alterations, including global heterochromatin loss, DNA hypomethylation, and SIRT6 depletion, lead to the derepression of evolutionarily young retrotransposons such as LINE-1, SVA, and HERV-K[154,205]. This derepression results in the accumulation of cytoplasmic nucleic acids, which activate innate immune pathways including the cGAS–STING axis and type I interferon (IFN-I) responses[190,208]. This inflammatory cascade is implicated in disorders like ALS/FTD, Alzheimer's, Ataxia-Telangiectasia, Rett syndrome, and Aicardi-Goutières syndrome, where TE activation contributes to neurotoxicity[209–211]. In these contexts, TEs shift from developmental regulators to endogenous danger signals that drive neuroinflammation[212].

Therapeutic strategies targeting TE activity, such as NRTIs or antisense oligonucleotides, show promise in models of aging and neurodegeneration[213,214].

1.6.4 Stem cell biology, senescence, and cancer

TEs are integral to gene regulation in stem cells. In embryonic and induced pluripotent stem cells (ESCs, iPSCs), TE families such as HERV-H, SVA, and LTR5_Hs function as enhancers, promoters, and splicing modules for core pluripotency genes like OCT4, SOX2, and NANOG[215,216]. These elements support naïve and primed pluripotency and are reactivated during cellular reprogramming, facilitating chromatin remodeling and identity transitions. In extraembryonic tissues, co-opted ERVs like *syncytin* are essential for placental development, underscoring the physiological roles of TE domestication[216].

With aging, this regulatory capacity can become pathological. Heterochromatin loss, global hypomethylation, and RNAi pathway decline allow TEs, especially LINE-1, to reactivate. In senescent cells, these elements generate cytoplasmic cDNAs that activate cGAS–STING and INF-1, promoting chronic inflammation and reinforcing the senescence-associated secretory phenotype (SASP).

In cancer, widespread epigenetic erosion unmasks TE-derived enhancers and promoters, activating oncogenes (e.g., via MER11, LTR12, HERV-K)[217,218]. As TEs are potent drivers of evolution they can also drive the microevolution of malignant tumor line[217,218]. Genome-wide screens show that over half of active enhancers in some cancers overlap with TEs, and they can also disrupt tumor suppressors or produce chimeric oncogenic RNAs[217]. Domesticated TE genes like *PEG10*, *TERT*, and *LDOC1* are frequently dysregulated in tumors[217].

Paradoxically, this TE reactivation presents therapeutic potential. As described above TE-derived RNAs mimic viral infection, triggering innate immune responses and enhancing tumor immunogenicity. The potential to exploit this viral mimicry, and TE-derived peptides may bring neoantigens for immunotherapy[192,219].

Thus, TEs emerge as double-edged swords, acting as drivers of evolution and regulators during development while posing potential threats during aging and disease. A locus-specific understanding of their regulation will be essential for harnessing their dual roles in medicine and for deepening our insight into their contributions to both development and pathology. Various techniques exist to track TE activity, and the next chapter focuses on those most relevant to the aims of this thesis.

1.7 Methods for studying transposable elements

TEs have long posed a formidable challenge in genomic analysis due to their repetitive nature, sequence similarity, and polymorphic insertion patterns[37]. Although they constitute a substantial fraction of most eukaryotic genomes, they were traditionally filtered out from sequencing datasets due to technical limitations[220]. However, as our understanding of their roles in gene regulation, development, evolution, and disease has expanded, so has the need for accurate tools to study them[24]. This chapter outlines the current state-of-the-art techniques, computational and experimental that enable researchers to analyze TEs.

1.7.1 Functional and phenotypic assays

Phenotypic assays offer powerful, direct readouts of TE activity and provide a crucial complement to molecular analyses. In experimental models such as *C. elegans* and *Drosophila*, well-established assays allow for the visualization and quantification of TE mobilization.

In *C. elegans*, the *unc-22* twitching assay is a classic example: TE insertion induced mutation in the *unc-22* gene disrupt muscle integrity, causing a distinct twitching phenotype that can be identified visually. TE activity can be induced through stress exposure or genetic manipulation, such as *hsp-90* knockdown, leading to increased Tc1 insertions in this locus[102,221,222]. This phenotypic screen thus provides a sensitive, live readout of TE mobilization events.

Similarly, in *Drosophila*, eye mosaicism serves as a classic model for monitoring somatic TE mobilization. Somatic excision of elements like P-elements or Ty3/gypsy during eye development leads to mosaic pigmentation pattern in the compound eye. These visible mosaics reflect the activity of transposons during development and provide an effective system for investigating TE regulation[223,224].

1.7.2 Genome assembly and annotation of TEs

A critical first step in the study of TEs is the generation of a high-quality genome assembly with detailed repeat annotation. This foundational resource allows for the accurate identification of TE insertion sites, copy numbers, and their structural and regulatory context. However, assembling repetitive DNA presents inherent challenges, particularly when using short-read sequencing technologies, which often result in fragmented or misassembled repeat-rich regions, since the read length cannot span the repeat lenght[225].

Recent advances in long-read sequencing technologies have transformed genome assembly practices, enabling researchers to resolve complex genomic regions that were previously intractable. Technologies such as Pacific Biosciences (PacBio) and Oxford Nanopore Technologies (ONT) can span full-length TEs and their flanking sequences, making them invaluable for comprehensive analysis[226–228].

Annotation of TEs is typically guided by established databases. RepBase is a widely used, subscription-based repository of consensus TE sequences, while Dfam provides TE family profiles based on hidden Markov models (HMMs), enabling sensitive and specific repeat classification[220,229]. Tools such as RepeatMasker utilize these databases to annotate repeats in genomic sequences and are commonly integrated into genome browsers like UCSC[220,229].

Species-specific databases also support annotation efforts in model organisms. Moreover, de novo annotation tools facilitate the discovery of novel, lineage-specific, or polymorphic TEs. This is particularly crucial in evolutionary and population genomic studies, where TE content can vary significantly across individuals or strains[230].

1.7.3 Long-read DNA sequencing techniques

One of the most promising advancements for the study of TEs lies in long-read DNA sequencing technologies. These methods offer the ability to span full-length TEs and their flanking sequences,

enabling accurate localization of insertions, detection of structural variation, and resolution of nested and polymorphic transposons. Long-read data enhances the assembly of repeat-rich genomic regions, refines annotations, and facilitates locus-specific quantification of TE expression[1].

Oxford Nanopore Technologies employs biological nanopores embedded in a synthetic membrane to sequence DNA by measuring disruptions in ionic current as nucleotides pass through the pore[231,231–234]. This method enables the sequencing of ultra-long fragments, that can theoretically exceed 1 Mb in length, which is particularly advantageous for resolving structural variants, nested TEs, and complex insertion sites[231,231–234]. The portability of ONT devices, such as the MinION, makes them suitable for field-based applications, while real-time sequencing and basecalling provide rapid insights into genomic regions[231,231–234]. Despite a higher intrinsic raw error rate compared to other sequencing platforms, recent advances in signal processing algorithms (e.g., Guppy), basecalling software, and error correction pipelines (e.g., Medaka, Racon) have significantly improved ONT accuracy[231,231–234]. Hybrid assembly approaches, combining ONT with Illumina short reads, also bolster precision and coverage[231,231–234]. Notably, ONT supports direct RNA sequencing, bypassing reverse transcription and PCR amplification steps, thereby reducing biases and enabling the characterization of full-length TE-derived transcripts and RNA modifications[231,231–234]. In addition to transcriptomics, ONT can directly detect epigenetic modifications like 5-methylcytosine without requiring bisulfite conversion. This feature enables high-resolution methylation profiling at TE loci and offers new insights into TE regulation under various biological conditions[235].

Pacific Biosciences (PacBio) Single Molecule Real-Time (SMRT) sequencing offers high-fidelity long reads using circular consensus sequencing (HiFi). By sequencing circularized DNA templates multiple times, this approach yields highly accurate long reads ranging up to 25 kb[228,236–238]. These HiFi reads are particularly effective in assembling TE-rich genomic regions and identifying TE insertions that occur in GC-rich, structurally complex, or low-mappability regions[228,236–238]. PacBio excels at resolving repetitive structures and distinguishing among near-identical TE insertions, making it a preferred platform for reference-grade genome assemblies and locus-specific annotation of active transposons[228,236–238]. It is also useful for capturing full-length isoforms of TE-containing transcripts and for characterizing chimeric fusion events between TEs and host genes[228,236–238]. Due to its high base accuracy and long read length, PacBio is often used in studies requiring both structural insight and sequence precision[228,236–238]. PacBio SMRT technology can also detect base modifications such as 5-methylcytosine and 6-methyladenine based on changes in DNA polymerase kinetics[228,236–238]. This allows for the simultaneous measurement of TE sequence and methylation status, facilitating studies of epigenetic regulation at the single-molecule level[239].

Together, ONT and PacBio offer complementary advantages, ONT provides unmatched read length and real-time flexibility, while PacBio delivers accuracy, making them indispensable tools in the sequencing of TEs[240].

1.7.4 Mapping reads to repetitive regions

Accurately assigning sequencing reads to repetitive regions is essential for analyzing TE activity. Traditional aligners like STAR, HISAT2, and GSNAP often misrepresent TE-derived reads due to their multimapping nature. Tools such as MMR and Telescope use expectation-maximization algorithms to probabilistically resolve these ambiguities, improving expression accuracy[220,241,242]. For sRNAs, tools like ShortStack, Manatee, and TEsmall are specifically designed to manage short, repetitive reads, while machine learning-based predictors like piRNAPredictor and Piano enable piRNA detection and quantification[243–247]. For the long-read platforms ONT and PacBio aligners such as Minimap2 and GraphMap supporting their error-corrected data[227,236,236,248].

1.7.5 Quantifying TE expression

Quantifying TE expression requires both sensitivity and precision, and PCR-based methods continue to play a central role in this task. RT-qPCR remains a widely used and accessible technique for measuring TE expression. It is especially useful for targeted validation, enabling sensitive quantification of individual TE subfamilies or insertion loci. RT-qPCR assays can be designed with TE-specific primers to distinguish closely related elements or to encompass whole TE families[249,250]. Digital PCR (dPCR) builds upon this foundation by enabling absolute quantification of transcripts without reference genes[251]. Through partitioning the PCR mixture into thousands of nanoliter-scale reactions, dPCR can detect low-abundance or rare TE transcripts with high precision and reproducibility[251]. This is particularly valuable for validating low-copy insertions, profiling TE expression in rare cell populations, or detecting subtle changes associated with development, stress, or disease[251]. Complementing these experimental approaches, recent computational tools have significantly advanced RNA sequencing-based quantification. Algorithms such as TEtranscripts and TETools provide family-level expression estimates by aggregating reads across TE subfamilies[252,253]. Meanwhile, tools like SQuIRE and Telescope achieve locus-specific resolution, mapping expression to individual TE insertions[242,254]. Specialized packages like TeXP are tailored to disentangle genuine transcriptional activity from background noise, especially in highly active families such as LINE-1[255]. These developments have made it possible to connect TE expression with regulatory effects and phenotypic outcomes more accurately than ever before.

1.7.6 Further assays to track TEs

Fusion Transcript Detection: Transposable elements often contribute novel regulatory elements or promoters, leading to fusion transcripts with host genes. The LIONS pipeline identifies such TE-host chimeras in RNA-seq data, offering insight into gene regulation and potential TE-driven innovation, particularly in cancer[256]. **ChIP, CLIP, and RIP-seq Analysis:** Protein-DNA and protein-RNA interaction studies frequently intersect with TEs. ChIP-seq (e.g., for H3K9me3), CLIP-seq, and RIP-seq experiments often encounter high TE content. Tools like CSEM and CLAM apply statistical methods to redistribute ambiguously mapped reads, while MapRRCon uses TE consensus sequences to simplify binding site detection across repeat landscapes[245,257].

DNA Methylation Profiling: TE silencing is heavily regulated by DNA methylation. WGBS remains a key technique, supported by tools such as Bismark, BS-Seeker3, and MOABS. TEPID and epiTEome extend methylation profiling to TE loci. Nanopore and PacBio allow direct, chemical-free detection of methylation marks, granting detailed views of epigenetic landscapes at TE loci[258–261]. **Single-Cell TE Transcriptomics:** Single-cell RNA-seq has begun to uncover TE expression heterogeneity. While many protocols underrepresent TEs, full-length and 5'-end capture methods enhance detection. Tools like Repsc promise improved TE resolution at the single-cell level, unlocking new avenues for developmental and disease-related research[262].

Future Directions, despite methodological advances, challenges in mapping, resolution, and detection sensitivity persist, especially for young, lowly expressed, or intronic TEs. The integration of long-read technologies, refined alignment strategies, and multi-omic approaches and machine learning analysis will be essential to fully elucidate TE functions and dynamics in complex biological systems[227,227,263].

1.8 *Caenorhabditis elegans* a model to study evolution, aging and TE biology

1.8.1 *C. elegans* as a Model Organism

Since Sydney Brenner established *C. elegans* in the 1960s as a model organism due to its genetic simplicity and suitability for laboratory research, it has become a cornerstone of developmental biology, genetics, neuroscience, and aging research[264]. Its rapid and consistent developmental cycle, approximately 3.5 days from egg to reproductive adult at room temperature, facilitates experimentation and allows the observation of multiple generations within short periods[265]
. The genome of *C. elegans*, comprising approximately 20,000 genes, shows remarkable genetic conservation with humans; 83% (15,344 sequences) of human genes have clearly defined orthologs in this nematode[22]. This genetic similarity underscores the relevance of findings from *C. elegans* research to human biology, making it an invaluable model for exploring fundamental biological processes. A defining characteristic of *C. elegans* is its highly predictable and invariant cell lineage. Each adult hermaphrodite consistently develops exactly 959 somatic cells, all mapped from fertilization through adulthood[266]. This precise developmental framework has been crucial for elucidating key biological processes such as apoptosis, developmental timing, cellular differentiation, and aging. Predominantly hermaphroditic, *C. elegans* individuals produce both sperm and eggs, enabling self-fertilization that yields genetically uniform offspring, an advantageous trait for genetic analyses and functional genomics studies. Males naturally occur at a low frequency (0.1 – 0.2%)[267]. Research using *C. elegans* has significantly advanced our understanding of diverse cellular and molecular pathways, including apoptosis, RNAi, insulin signaling pathways, and the mechanisms underlying aging[268]. It has also played an essential role in the development and refinement of advanced genetic and molecular technologies, such as CRISPR-Cas9 genome editing, RNAi-based gene knockdown, and transgenic methods employing fluorescent proteins for live-cell imaging[269]. The success of *C. elegans* as a model organism is supported by an active and collaborative global research community. Resources such as

WormBase, WormAtlas, and WormBook provide comprehensive genomic, anatomical, and experimental information[270–272].

1.8.2 Using *C. elegans* to study evolution

C. elegans is an indispensable model for investigating the genetic, developmental, and evolutionary underpinnings of life history traits[273]. Its utility in evolutionary biology stems from a distinctive combination of features: the short generation time, a fully sequenced and well-annotated genome, powerful genetic tools (including CRISPR, RNAi, and high-throughput phenotyping), and a reproductive mode, primarily self-fertilization, that allows precise control over genetic backgrounds and different lineages[274,275]. Additionally, the growing availability of natural isolates and comparative genomic data from closely related *Caenorhabditis* species has enabled population-level studies of selection, adaptation, and genome evolution in a metazoan context[274,275]. As reviewed by Braendle and Paaby (2024), *C. elegans* serves as a model for understanding how complex life history strategies evolve in fluctuating environments, offering insights into trade-offs between traits such as reproduction and longevity, stress resistance and developmental rate, or fecundity and survival[276]. These trade-offs are deeply embedded in the regulatory logic of development and physiology, often orchestrated by endocrine pathways such as insulin-like signaling[277]. The genetic architecture underlying such traits, including genotype-by-environment interactions (GxE), polygenicity, and epistasis, is increasingly well characterized in *C. elegans*, aided by resources such as wild isolates and multiparental panels like CeMEE[278]. A growing body of research also suggests that *C. elegans* is particularly well suited to studying the role of TEs in evolutionary processes[76,279]. Studies across wild isolates have shown that TEs contribute to heritable variation in gene expression, reproductive output, and stress responses[76,279]. Given the tightly regulated genome surveillance mechanisms in *C. elegans*, notably through sRNA pathways, the species is a great model to study how organisms maintain genome integrity while balancing the evolutionary potential of TEs[279,280]. Furthermore, the ability to experimentally manipulate TE activity, either by introducing genetic mutations in silencing pathways or by inducing stress, and to track the consequences across generations makes *C. elegans* a powerful model for linking TE biology to evolutionary landscapes[281]. Importantly, research in *C. elegans* is also bridging molecular and evolutionary biology by investigating not only how traits are encoded and regulated, but also how they are maintained, altered, or co-opted across generations[279]. This connection becomes particularly interesting in light of emerging evidence for sRNA–mediated transgenerational epigenetic inheritance[135,172].

1.8.3 Small RNA-mediated epigenetic inheritance in *C. elegans*

Recent studies have revealed that sRNAs can mediate the inheritance of acquired traits, such as antiviral resistance and behavioral responses[135,172]. These non-Mendelian effects can persist across multiple generations and often depend on maternal "inheritance states" that by the conserved transcription factor HSF-1[282]. These inheritance states determine the uniformity and duration of sRNA-induced gene silencing within a lineage and can predict progeny responses to environmental

stress[283]. The longer a silencing response persists, the more likely it is to be transmitted to subsequent generations, a phenomenon termed transgenerational momentum[283]. HSF-1 shapes these inheritance states by regulating endogenous sRNA levels and the expression of silencing factors, including Argonaute proteins and germ granule components. High HSF-1 activity promotes silencer states, while reduced HSF-1 activity favors non-silencing states[282]. Thus, the global inheritance state determines how specific gene-silencing responses unfold. sRNAs, some of neuronal origin, can cross soma-to-germline boundaries via the transmembrane channel SID-1 and are subsequently amplified by RdRPs[284,285]. Nuclear Argonauts, such as HRDE-1, by facilitating the placement of histone modifications like H3K9me3, help stabilize these inherited silencing responses[133]. sRNAs not only transmit adaptive information but also reshape chromatin and regulate gene expression, often in locus-specific ways. Feedback between histone methylation (mediated by factors such as MET-2 and SET-25) and sRNAs further contributes to the duration and stability of inherited silencing[286]. *C. elegans* thus exemplifies how environment-induced RNA-based signals can be transgenerationally encoded.

1.8.4 Heat stress induced TE activation and neuronal thermosensory regulation in *C. elegans*

Environmental stress, particularly acute heat exposure, can drive TE mobilization in *C. elegans*, with significant consequences for genome integrity and fertility[98,287]. A temperature increase induces a rise in DNA double-strand breaks in spermatocytes, up to a 25-fold increase during meiotic prophase I. Crucially, this damage occurs independently of SPO-11, the conserved endonuclease typically responsible for programmed meiotic DSBs. Instead, it correlates with the activation and mobilization of Tc1/mariner transposons[98,287]. Heat-induced expression of Tc1 transposase increases significantly, leading to both intra- and interchromosomal TE insertions that compromise genome stability and reduce progeny viability[98,287]. In contrast, oocytes effectively suppress heat-induced TE activation, highlighting a dimorphic vulnerability to thermal stress[98,287]. This heat-sensitive TE mobilization could be embedded within broader physiological sensing systems, the major research question addressed in this thesis. Central to this is the AFD thermosensory neuron, which enables *C. elegans* to detect thermal fluctuations, as small as 0.01°C, across a broad temperature range[288]. AFD neurons adapt both their response threshold and output based on recent temperature experiences integrating environmental cues with internal physiological states[289]. These neurons not only guide behavioral thermotaxis but also orchestrate systemic responses, including the organism-wide heat shock response and temperature-dependent regulation of lifespan[290–292]. AFD-mediated signaling influences somatic and germline physiology through neuromodulators such as serotonin and neuropeptides like FLP-6[293]. Remarkably, optogenetic activation of AFD is sufficient to trigger HSF-1 activation in germ cells, illustrating a top-down coordination of stress responses. AFD neurons also promote longevity at elevated temperatures through CMK-1-dependent transcriptional regulation, indicating a dual role in both acute stress adaptation and long-term physiological adjustment[295]. The potential interface between AFD neuronal thermosensation and TE regulation raises the intriguing possibility of a direct neuronal influence on genomic integrity. The hypothetic connection of neuronal thermosensation

and germline TE regulation suggests a complex system in which environmental information could be transduced into heritable genomic changes, challenging one of the last standing postulates of the Weismann barrier. If neuronal signaling can directly influence mutation rates through TE mobilization, this would represent a paradigm shift in our understanding of how environmental cues can impact genome evolution. Such a mechanism may drive stress-induced increases in genetic diversity, a process particularly relevant for a predominantly self-fertilizing species like *C. elegans*. Therefore, investigating this connection has been addressed as a major research focus of this thesis.

1.8.5 Caenorhabditis elegans as a Model for Studying Aging and Reproductive Senescence

C. elegans is an invaluable model for aging research due to its short lifespan, well-characterized genetics, ease of cultivation, and distinct aging phenotypes, especially in reproductive senescence[22,264]. Additionally, the rapid generational turnover and the availability of genetic manipulation tools make it an ideal system for dissecting the molecular and cellular mechanisms driving reproductive aging and for testing interventions that may mitigate or reverse age-associated declines[294]. Reproductive aging in *C. elegans* exhibits many hallmarks that parallel those observed in later-diverging taxa with increased biological complexity, including humans, making it an invaluable model for translational aging research. Age-related fertility decline in *C. elegans* manifests through reduced germline cell proliferation, deterioration of oocyte quality and viability, increased chromosomal segregation errors, and diminished embryo survival rates[296]. These cumulative impairments progressively lead to reduced reproductive capability and eventual sterility; a trajectory reminiscent of reproductive senescence in mammals[296]. A critical mechanistic feature that could contribute to reproductive aging in *C. elegans* is the gradual loss of genomic stability, including the dysregulation of TEs. Under normal physiological conditions, TEs are effectively suppressed by sRNA-dependent silencing pathways, preserving genomic integrity by limiting TE mobilization[154]. However, with progressing age, the efficiency of these sRNA-mediated mechanisms declines, leading to the activation of TEs[297]. This heightened mobilization contributes to genomic instability, impairing germline function and reproductive success[154]. Apoptosis, also plays a critical role in maintaining oocyte quality and overall fertility[268,298]. In *C. elegans*, physiological apoptosis selectively eliminates defective germ cells during oogenesis, thereby preserving the health of the surviving oocytes[268,298]. Dysregulation of apoptotic processes with age may contribute to the accumulation of defective oocytes, declining embryo quality, and reduced fertility[268,298].

1.9 Aim of the study

The last intact postulate of August Weismann, which states that somatic influences cannot directly affect the germline genome, still holds. However, recent advances in transgenerational epigenetic inheritance and findings that germline gene expression can be regulated by neuronal sensing of environmental conditions have begun to partially erode this barrier. In particular, the observation

that heat stress can induce TE activity, so far demonstrated only in a cell-autonomous manner within germ cells, raises a compelling question.
Can heat stress sensation through neurons influence sRNA pathways in the germline, thereby impairing the transposon silencing machinery and induce TE mobilization?
This is the central aim of my study. Using *C. elegans* as a model organism, I aimed to investigate whether disruption of the AFD thermosensory neuron affects germline TE activity, and whether such neuronal input can influence genetic inheritance.
Furthermore, since age-related TE activation has been shown to contribute to genomic instability in aging germ cells and somatic tissues, I aimed to search for a method to inhibit TE activity and test whether this could influence reproductive aging and lifespan.

2. Materials and methods

2.1 *C. elegans* culture and maintenance

2.1.1 Strain Acquisition and Maintenance

New nematode strains were obtained from the Caenorhabditis Genetics Center (CGC) at the University of Minnesota, USA. Strains were maintained on nematode growth medium (NGM) agar plates seeded with the bacterium Escherichia coli strain OP50 as a food source.
For routine laboratory maintenance, nematodes were cultured at 20°C. Medium-term storage of nematode strains was carried out at 15°C, while long-term preservation involved freezing freshly starved L1–L2 stage larvae at -80°C in freezing buffer containing glycerol. Prior to experimentation, worms were acclimated to 20°C for at least two generations to ensure consistent physiological states.

2.1.2 Preparation of culture on NGM

NGM plates were prepared by combining agar with NaCl, peptone, and distilled water, autoclaving, and then supplementing with cholesterol, $CaCl_2$, $MgSO_4$, and potassium phosphate buffer after cooling. Media were dispensed into Petri dishes with a peristaltic pump and stored at 4°C **(Table 2.1)**. The E. coli OP50 srain, serving as the food source, was cultured overnight at 37°C on lysogeny broth (LB) liquid media **(Table 2.2)**. NGM plates were seeded with 0.05–0.3 ml of bacterial culture and incubated overnight at 37°C to establish a bacterial lawn suitable for routine culture or experimental analyses.

NGM Agar For 1L	
Component	**Amount**
Bacto Peptone	2.5 g
NaCl	3 g
Serva Agar	17 g
Distilled H_2O	970 ml
Autoclave at 121°C for 20min	
Cool down to 56°C before adding:	
1M $CaCl_2$	1 mL
1M $MgSO_4$	1 mL
5 mg/mL Cholesterol	1 mL
1M KPO_4	25 mL
Nystatin (1000 units/mL)	2.5 mL

Table 2.1 nematode growth medium (NGM)

LB Medium For 400 mL	
Component	**Amount**
NaCl	4 g
Tryptone	4 g
Yeast extract	2 g
ddH_2O	Fill up to 400 mL

Table 2.2 lysogeny broth (LB) liquid medium

LB Agar For 400 mL	
Component	**Amount**
Tryptone	4 g
Yeast extract	2 g
NaCl	4 g
Serva Agar	7.2 g
ddH_2O	Fill up to 400 ml

Table 2.3 lysogeny broth (LB) solid agar medium

2.1.3 Culture handling and synchronization

Transfers between culture plates were performed either by agar chunking or individual worm picking. For chunk transfers, a sterilized metal spatula was used to cut a piece of NGM agar from the old plate, which was then placed onto a bacteria-free area of a fresh plate, allowing nematodes to migrate away from potential contaminants. Individual worms were precisely transferred using platinum-wire picks. Plates were routinely sealed with Parafilm to maintain sterility and moisture content. Developmental synchronization of nematodes was performed by hypochlorite treatment ("bleaching"). Fully grown adult nematodes and eggs were collected with M9 buffer (**Table 2.4)** into tubes and incubated in alkaline hypochlorite "bleach" solution (10% sodium hypochlorite, 5 M NaOH) (**Table 2.5**) for 5 minutes with on a rotating mixer. Embryos were recovered by centrifugation, washed three times with M9 buffer, and incubated overnight in fresh buffer at room temperature on a rotating mixer. The resulting synchronized, developmentally arrested L1 larvae were filtered (11 µM hydrophilic filter) prior to plating. Worm concentrations were determined microscopically by averaging counts from two 5 µL drops per strain if experimentation required precise amount of worm plating. Alternatively, egg-laying synchronization was performed by allowing adult worms to lay eggs on fresh plates for 3–5 h before removal, resulting in synchronized progeny.

M9 buffer For 1L	
Component	**Amount**
KH_2PO_4	3 g
Na_2HPO_4	6 g
NaCl	5 g
ddH_2O	Fill up to 1L
Autoclave at 121°C for 20min	
Cool down to RT before adding:	
1M $MgSO_4$	1 mL

Table 2.4 M9 buffer composition

Bleaching Solution	
Component	**Amount**
5M NaOH	3 mL
10% Sodium hypochlorite	6 mL
M9 buffer	41 mL

Table 2.5 Bleaching solution composition

Contamination management

Mold contaminants were eliminated by transferring agar chunks containing worms to clean plates, allowing worms to migrate away from contamination. Bacterial or yeast contaminants were removed by hypochlorite treatment, isolating viable eggs subsequently placed on uncontaminated, seeded plates.

2.1.4 Freezing and thawing protocols

For long-term storage, nematodes were frozen using either Liquid Freezing Solution. Gradual freezing at -80°C was conducted within insulated containers. Stocks frozen in liquid freezing solution were stored long-term in liquid nitrogen, and were maintained at -80°C. Frozen nematode stocks were thawed by transferring aliquots onto fresh NGM plates seeded with E. coli OP50. Post-thaw viability and strain integrity checks were performed regularly.

For long-term storage, nematodes were frozen using Liquid Freezing Solution (**Table 2.6)**. Starved mixed-stage worm populations containing predominantly L1 and L2 larvae, were collected and washed in M9 buffer, then resuspended in fresh M9 buffer. Worm suspensions were mixed at a 1:1 ratio with 2x Freezing Buffer, aliquoted into cryotubes, and gradually cooled to -80°C using a Cryo 1°C Freezing Container (Nalgene) filled with 2-propanol or alternatively within insulated

Styrofoam boxes. Following freezing, stocks were stored long-term at -80°C as working stocks, and at -196°C (liquid nitrogen) for permanent preservation. To thaw frozen stocks, aliquots were transferred onto fresh NGM plates seeded with E. coli OP50, and regular checks were performed to assess viability and confirm strain integrity.

2x Freezing buffer For 1L	
Component	**Amount**
NaCl	5.8 g
KH2PO4	6.8 g
Glycerol/Glycerin	300 g
5 M NaOH	1.12 mL
ddH2O	Fill up to 1L
Autoclave at 121°C for 20min	
Cool down to RT before using	

Table 2.6 Freezing buffer composition

The protocols, including reagent and material compositions, were based on standard methods described in WormBook[271].

2.1.5 Crossing and backcrossing *C. elegans*

C. elegans crosses and backcrosses were performed by transferring 1-3 L4 hermaphrodites from one strain onto NGM agar plates seeded with a small E. coli OP50 bacterial lawn (5-20µl), along with 5-10 adult males from the other strain. Successful mating was confirmed by the presence of high incidence of male progeny in the F1 generation. To prevent further mating in subsequent generations, five to ten F1 L4 hermaphrodites were individually transferred to fresh plates and allowed to reproduce exclusively by self-fertilization. For the F2 generation, 20-30 hermaphrodites were singled onto new plates if crossing involved alleles on different chromosomes, or more, dependent on the genetic distance, if the alleles were on the same chromosome. After laying eggs to produce the F3 generation, these F2 mothers were genotyped to identify homozygous double mutants, thereby establishing new strains. Final strain confirmation involved genotyping 10 individual worms.

2.1.6 Genotyping *C. elegans* strains

For genotyping strains single worms were individually transferred into 0.2 ml PCR tubes containing single worm lysis buffer (SWLB) (**Table 2.7**) supplemented with proteinase K, and lysed by incubation at 65°C for 90 minutes, followed by enzyme inactivation at 95°C for 20 minutes (**Table 2.8)**. Genomic regions of interest were amplified by PCR using specifically designed primer pairs. Insertions and deletions were resolved through agarose gel electrophoresis,

while single nucleotide variants were identified by sequencing. For PCR products smaller than 2 kb, amplification was carried out using MangoTaq™ DNA polymerase (Meridian Bioscience) (**Table 2.9, Table 2.10)**, whereas larger fragments required Q5® High-Fidelity DNA Polymerase (New England BioLabs) (**Table 2.11, Table 2.12)**. PCR products were visualized on 1% (w/v) agarose gels containing ethidium bromide in TAE buffer, documented with a Gel Doc XR+ system (Bio-Rad). Sequencing involved purification of PCR products using the NucleoSpin® Gel and PCR Clean-up kit (Macherey-Nagel), followed by Sanger sequencing conducted by Eurofins Genomics. Sequencing data were analyzed using Benchling, a web-based platform for molecular biology that enables DNA sequence visualization, alignment, annotation, and editing. (https://www.benchling.com/).

SWLB For 100 mL	
Component	**Amount**
1M KCl	5 mL
1M Tris (pH 8.3)	1 mL
1M MgCl2	250 µL
Tween-20	450 µL
ddH2O	Fill up to 100 mL
Autoclave at 121°C for 20min	
Cool down to RT before adding:	
Gelatin	0.01 g
Before each use, add:	
Proteinase K (20 mg/mL) 1:10 Dilution	

Table 2.7 single worm lysis buffer (SWLB)

Step Temperature Time	
Temperature (°C)	**Time**
60°C	60 min
95°C	15 min
16 °C	∞

Table 2.8 single worm lysis incubation protocol

MangoTaq Master Mix	
Component	**V[µl]**
ddH_2O	12.2
5x mango reaction buffer	4
[50mM] $MgCl_2$	0.6
[10mM] dNTP	0.5
[2,5um] forward prmier	1
[2,5um] Reverse prmier	1
MangoTaq DNA polymerase	0.2
Worm lysate	0.5
SUM	**20**

Table 2.9 MangoTaq Master Mix

MangoTaq Genotyping PCR program			
STEP	**TEMP**	**TIME**	**Cycle**
Initial Denaturation	95°C	03:00 min	1x
Denaturation	95°C	00:30 min	35x
Annealing	56°C	00:30 min	
Extension	72°C	01:00 min/kb	
Final Extension	72°C	05:00 min	1x
Hold	12°C	∞	1x

Table 2.10 MangoTaq PCR program

Q5 PCR program			
STEP	**TEMP**	**TIME**	**Cycle**
Initial Denaturation	98°C	03:00 min	1x
Denaturation	98°C	00:30 min	35x
Annealing	56°C	00:30 min	
Extension	72°C	00:30 min/kb	
Final Extension	72°C	05:00 min	1x
Hold	12°C	∞	1x

Table 2.11 Q5 Master Mix

Q5 Master Mix	
Component	**V[µl]**
5X Q5 Reaction Buffer	5
10 mM dNTPs	0.5
10 µM Forward Primer	1.25
10 µM Reverse Primer	1.25
Template DNA	0.1
Q5 High-Fidelity DNA Polymerase	0.25
5X Q5 High GC Enhancer (optional)	(5 µl)
Nuclease-Free Water	to 25 µl
SUM	**25**

Table 2.12 Q5 PCR program

2.2 Generation of the BJS1062 "AFD:HisCl1" strain

A starved population, containing several thousand (3-5000) mixed staged worms on a L-plate (d= 90 mm), of the BFF96 strain was subjected to gamma irradiation at a dose of 90 Gy, with a Biobeam 8000 containing a Cs137 radionucleotide source. This strain contains an extrachromosomal transgenic construct encoding a histamine-gated chloride channel, along with a transcriptional fusion mCherry reporter and a rol-6 selection marker, all driven by the AFD neuron-specific gcy-8 promoter *[pgcy-8::HisCl1::SL2::mCherry::rab-3 3'UTR, pgcy-8::GCaMP6::rab-3 3'UTR; rol-6(GOF)]*. Following irradiation, the progeny was screened over six generations to select worms displaying 100% identifiable mCherry fluorescence, indicating successful integration of the transgenic construct. The resulting strain was then backcrossed four times with the wild-type strain to ensure genetic consistency and remove potential background mutations, then confirmed again for the 100% penetrance of the mCherry fluorescence. As a result we established the BJS1062 strain, that carries the integrated *[pgcy-8::HisCl1::SL2::mCherry::rab-3 3'UTR, pgcy-8::GCaMP6::rab-3 3'UTR]* transgene. In the following sections of this work the AFD:HisCl1 will refer to this strain.

2.3 RNA extraction for RT-qPCR and RNA sequencing

All RNA extractions in this study were performed using a combined TRIzol® (Thermo Fisher Scientific) and RNeasy® Mini Kit (Qiagen) protocol, optimized for high-quality RNA recovery from *C. elegans*.

Worms were harvested from L-plates by washing them off the surface using M9 buffer and transferred into 15 mL Falcon. Then they were washed 3–5 times with M9 buffer until the supernatant became clear.

Following the final wash, the worm pellet was concentrated into the smallest possible volume of M9 and transferred into 2 mL Eppendorf Safe-Lock Tubes. A volume of 1 mL TRIzol® reagent was added to each sample for RNA lysis. Homogenization was performed via freeze cracking: samples were flash-frozen in liquid nitrogen and immediately thawed in a 40–50°C incubator. This freeze-thaw cycle was repeated 3 times.

After homogenization, 100 µL of bromochloropropane (BCP; Sigma-Aldrich) was added to each tube. Samples were vortexed for 15 seconds and incubated for 2 minutes at room temperature. Centrifugation was then carried out at 12,000 × g for 15 minutes at 4°C. The upper aqueous phase (approximately 600 µL) was carefully transferred to a new RNase-free microcentrifuge tube.

To facilitate RNA binding to the spin column membrane, the aqueous phase was mixed with an equal volume of 70% ethanol and vortexed. The mixture was applied to an RNeasy® Mini spin column and centrifuged at ≥8000 × g for 15 seconds.

For removal of genomic DNA, on-column DNase digestion was performed using the RNase-Free DNase Set (Qiagen). First, 350 µL Buffer RW1 was added to the column and centrifuged for 15 seconds at ≥8000 × g to pre-wash the membrane. A DNase incubation mix (prepared by mixing 10 µL DNase I with 70 µL Buffer RDD) was then applied directly onto the membrane and incubated at room temperature (20–30°C) for 15 minutes. Following digestion, another 350 µL Buffer RW1 wash was performed.

The column was then washed twice with 500 µL of Buffer RPE. The first wash was centrifuged for 15 seconds, and the second for 2 minutes at ≥8000 × g to fully dry the membrane. An additional centrifugation step was carried out in a clean collection tube at full speed for 1 minute to eliminate any residual Buffer RPE or ethanol.

For RNA elution, the spin column was transferred to a 1.5 mL RNase-free collection tube, and 30–50 µL of preheated (50–60°C) RNase-free water was applied directly to the membrane. After 1 minute of incubation, the column was centrifuged for 1 minute at ≥8000 × g to elute the RNAExtracted RNA was quantified using a Thermo Scientific™ NanoDrop™ spectrophotometer, and RNA integrity was assessed on 1% gelelectrophoresis, indirectly by the integrity of the ribosomal bands.

2.4 cDNA synthesis

The SuperScript® III Reverse Transcriptase (Invitrogen) kit was used for reverse transcription reactions of isolated RNA samples. cDNA synthesis was performed in a 20 µL reaction mixture. The initial reaction mixture included 12 µL of RNA solution (1 µg RNA), 1 µL of random hexamer, and 1 µL of dNTP. This mixture was incubated at 65°C for 5 minutes and then subjected to a brief centrifugation (**Table 2.13, Table 2.14)**. Following this, the mixture was placed on ice for 5 minutes.

Subsequently, 4 µL of 5x First Strand Reaction Buffer, 1 µL of DTT, 1 µL of RNase Out Recombinant RNase Inhibitor, and 1 µL of SuperScript III RT (200 U/µL) were added to the mixture. The contents were gently mixed by pipetting. The reaction was then incubated under the following conditions: 25°C for 5 minutes, 50°C for 60 minutes, and 70°C for 5 minutes.

Following the incubation, the cDNA was diluted to a final volume of 100 µL by adding 80 µL of double-distilled water (ddH2O). The resultant cDNA was evaluated using a control PCR to verify successful synthesis.

cDNA synthesis	
Component	**Volume**
RNA (100µg/µl)	10 µl
Random hexamer primer or oligo(dT)	1 µl
10 mM dNTP Mix	1 µl
Sterile, distilled water	To 14 µl
Heat mixture to 65 C for 5 minutes	
Incubate on ice for at least 1 minute	

Prepare Master Mix:	
Component	**Volume**
5 x First-Strand Buffer	4 µl
0.1 M DTT	1 µl
SS III RT enzyme	1 µl
Add 6 µl Master Mix to the sample	
Mix by pipetting gently up and down	

Table 2.13 cDNA synthesis master mixes and preparation procedure

Incubation in thermocycler	
25°C	5 minutes
50 C°	90 min
70 C°	5 min

Table 2.14 cDNA synthesis incubation protocol

2.5 Quantitative real-time PCR (RT-qPCR)

Quantitative real-time PCR (RT-PCR) was carried out using the PowerUp™ SYBR™ Green Master Mix (Thermo Fisher Scientific) on white 96-well qPCR plates (Bioplastics B60101), sealed with optically clear film (Bio-Rad MSB-1001). Reactions were performed using Bio-Rad CFX Connect and CFX96 Touch Real-Time PCR Detection Systems.

Each 20 µL reaction contained 10 µL of 2× PowerUp™ SYBR™ Green Master Mix, 0.25 µL of cDNA template (typically 0.1–10 ng RNA input), 0.75 µL of nuclease-free water, and 9 µL of Primer Master Mix. The Primer Master Mix was freshly prepared at a final primer concentration of 1.1 µM by mixing 5.5 µL each of 100 µM forward and reverse primers with 489 µL of nuclease-free water to a total volume of 500 µL.

For each well, 11 µL of Template Master Mix (containing SYBR Green Master Mix, cDNA, and water) and 9 µL of Primer Master Mix were combined. All samples were run in biological triplicates with technical replicates, and no-template controls were included to assess contamination (**Table 2.15, Table 2.16)**.
Gene expression levels were normalized against a panel of validated housekeeping genes: act-1, tbg-1, lmn-1, eif-3.C, vha-6, and rpl-32. qPCR cycling was performed using the standard PowerUp™ SYBR™ protocol recommended by the manufacturer, with real-time fluorescence detection. Melt curve analysis was performed following amplification to verify product specificity. Data acquisition and preliminary analysis were performed using Bio-Rad CFX Manager Software. Further data processing, normalization, and statistical analysis were conducted using Microsoft Excel 2019, R version 4.3.2, and GraphPad Prism 9 (**Table 2.17)**.

Tempate Master Mix	
Buffer	**Volume (µL/well)**
PowerUp™ SYBR™ Green Master Mix (2X)	10 µl
cDNA template (0.1-10ng total input)	0.25 µl
Nuclease-Free Water	0.75 µl
Total	11 µl

Table 2.15 RT-qPCR template mater mix

Primer Mix	
Primer	**Volume for 500 µl**
Primer fwd stock 100µM	5.5µl
Primer rev stock 100µM	5.5µl
Nuclease-Free Water	489µl

Table 2.16 RT-qPCR template primer mix

RT-qPCR program				
Step	**Temperature (°C)**	**Time**	**Description**	**Repeats**
1	50	2:00 min	UDG activation	1
2	95	2:00 min	Initial denaturation	1
3	95	0:15 min	Denaturation	40
4	56	0:15 min	Annealing	
5	72	1:00 min	Extension + Plate Read	
6			Cycle GOTO Step 3	
7	95	0:15 min	Denaturation before melt curve	1
8	56.5 → 98.0	0:05 per °C	Melt curve (0.5°C increments) + Read	1

Table 2.17 RT-qPCR program

2.6 Proteomics sample preparation

Whole-animal protein extracts were prepared from a homogenized population of 3,000 C. elegans. Samples were lysed in 8 M urea buffer with 50 mM triethylammonium bicarbonate (TEAB), supplemented with a 50x protease inhibitor cocktail (Roche). For chromatin degradation, Benzonase HC nuclease was added at a concentration of 25 units, followed by incubation at 37°C for 30 minutes to ensure complete chromatin degradation. The lysates were centrifuged at 20,000 × g for 15 minutes to remove cell debris, and protein concentrations were measured using a standard assay. For reduction and alkylation, 50 µg of protein was transferred to a 1.5 mL microcentrifuge tube. Dithiothreitol (DTT) was added to a final concentration of 5 mM, followed by incubation at 25°C for 1 hour. Chloroacetamide (CAA) was then added to a final concentration of 40 mM, and the samples were incubated in the dark for 30 minutes. Trypsin was then added at a 1:75 enzyme-to-substrate ratio, and the samples were incubated overnight at 25°C for complete proteolysis. On the following day, the enzymatic digestion was stopped by acidification with formic acid to a final concentration of 1%. The samples were subsequently purified using SDB-RP StageTips packed with two layers of SDB-RPS discs in 200 µL pipette tips. The StageTips were equilibrated by sequential centrifugation at 800 × g for 1 minute with 20 µL methanol, 20 µL buffer B (0.1% formic acid in 80% acetonitrile), and twice with 20 µL buffer A (0.1% formic acid in water). Acidified samples were centrifuged, and the supernatant was loaded onto the StageTips, followed by washing with buffer A and buffer B. The StageTips were then dried and stored at 4°C and submitted to the CECAD Proteomics Facility. All reagents mentioned in this preparation were provide by the CECAD Proteomics Facility (https://proteomics.cecad-labs.uni-koeln.de/home).

2.7 Proteomics data acquisition and proteomics sample processing

Was performed by the CECAD proteomics facility, the related matherials and mathods are avaible in the corresponding section of the attached paper[3]

2.8 Mutation accumulation experiment design and strain handling

For the mutation accumulation experiment, a single mother was isolated from each strain to establish independent lineages. These mothers were used to generate synchronized populations via bleaching, which served as the P0 founder generation. The resulting populations were collected into 15 mL Falcon tubes, washed five times with M9 buffer to remove residual bacteria, and stored at −80°C.

From these initial populations, five mothers were isolated and placed on separate plates, serving as the founding mothers of the experiment (N=5). Throughout the experiment, one L4 stage larva from each strain was transferred individually to a new plate in every generation, spanning 30 generations.

Upon reaching the F30 generation, populations were again propagated and synchronized by bleaching. Approximately 3000 young adult nematodes were collected per population and cleaned by repeated M9 buffer washes (×5) and stored at −80°C for downstream whole-genome

sequencing. In parallel, frozen nematode stocks were established for long-term preservation of the evolved lineages.

2.9 High molecular weight genomic DNA extraction from *C. elegans*

High molecular weight genomic DNA was extracted from *C. elegans* using the QIAGEN Puregene Cell Kit. Approximately 3000 nematodes were grown on NGM agar plates with E. coli OP50 strain and collecting into 15ml falcon tubes using M9 buffer and washing 5 times. The harvested worms were stored at –80°C until DNA extraction.

The extraction process commenced by adding 3 mL of Cell Lysis Solution and 15 µL of Proteinase K to the frozen worm pellet, allowing it to thaw. Once thawed, the pellet was resuspended by pipetting with a 1 mL wide-bore tip. The sample was incubated at 50°C for 2 hours, with gentle inversion of the tube every 30 minutes to ensure homogeneity.

Following incubation, 15 µL of RNase A was added, and the mixture was incubated at 37°C for 30 minutes. Subsequently, 1 mL of Protein Precipitation Solution was added, and the tube was mixed by inversion 15-20 times before being placed on ice for 2 minutes. The sample was centrifuged at 2000 x g for 10 minutes at 4°C. The resulting supernatant, containing the DNA, was transferred to a fresh 15 mL Falcon tube containing 3 mL of isopropanol. The solution was gently inverted 50 times to promote DNA precipitation and centrifuged at 2000 × g for 5 minutes. The DNA pellet was washed with 3 mL of 70% ice-cold ethanol, gently mixed by inversion, and centrifuged at 2000 × g for 2 minutes. The supernatant was discarded, and any residual ethanol was carefully removed by inverting the tube onto sterile paper wipes and allowing the pellet to air-dry briefly. The DNA was eluted in 600 µL of TE buffer (10 mM Tris-HCl, 1 mM EDTA, pH 8.0) and incubated overnight at room temperature to maximize yield. The quantity and quality of the extracted DNA were assessed using a Thermo Scientific Nanodrop spectrophotometer, agarose gel electrophoresis and the Agilent TapeStation System.

2.10 Tc1 Transposon mobilization assay – twitching screen

To assess Tc1 transposon activity, a phenotype-based screen was performed. The insertion of Tc1 into the *unc-22* locus results in an observable twitching phenotype due to muscle spasms. To perform the assay a single nematode, confirmed to have no twitching phenotype, was isolated and propagated into a large population of approximately 300,000-500,000 individuals in several subsequent generations. Then the population was then synchronized using a bleach synchronization method.

Once the developmentally synchronized population reached the young adult stage, before egg-laying began, the worms were collected and washed with M9 buffer. Nicotine was added to a final concentration of 2%, **Table 2.18** which paralyzed all worms, allowing the twitching phenotype to become observable, as it is unaffected by nicotine.

The culture was dispersed into L-plates, containing a thin 1(w/v%) agarose layer, and screened under a dissecting microscope to identify twitching individuals. This allowed for the assessment of Tc1 transposon activity based on the presence of the twitching phenotype.

Nicotine solution For 8 ml	
Nicotine	160 µl
M9 Buffer	8 ml

Table 2.18 Nicotine solution

2.11 Bioinformatic analysis

The methods used for bioinformatic analysis of RNA sequencing, proteomics, and PacBio whole genome sequencing are explained in detail in the Materials and Methods section of the attached paper, corresponding to the Results I chapter. These include protocols for: total RNA sequencing analysis, RNA-seq processing, enrichment analyses, analysis of public transcriptomic datasets, PacBio whole genome sequencing, WGS filtering, Circos plot generation, background mutation analysis, identification of transposable element insertions, analysis of repeat elements near breakpoints, and CeNDR-based variant analysis.

2.12 Brood size quantification assay

For the assay, nematodes were developmentally synchronized by timed egg laying. 5 gravid adult hermaphrodites were placed on individual S-plates and allowed to lay eggs for 3 hours, after which the mothers were removed. From the resulting progeny, individuals at the L4 larval stage were selected and transferred to fresh S-plates for individual tracking.

On the first day of adulthood, each worm was transferred daily to a new plate until the end of its reproductive period. After each daily transfer, the number of eggs laid was counted. Two days later, the number of hatched larvae and remaining unhatched eggs on each plate was counted.

Brood size was determined by summing the total number of eggs laid across all days. Reproductive output was assessed based on the cumulative number of total number of eggs, viable progeny (hatched worms) and unhatched eggs. Quantifications were performed by visual examination using a Leica M80 stereomicroscope.

2.13 Germ cell apoptosis assay,

To induce apoptosis, worms were exposed to gamma irradiation using a Biobeam 8000 equipped with a Cs-137 radionuclide source. Apoptotic corpses were quantified 6 hours after treatment. To further assess progeny survival, treated worms were individually plated and allowed to lay eggs for 24 hours. Progeny survival was assessed over the following two days based on hatching rates.

To assess germ cell apoptosis, adult *C. elegans* were stained using acridine orange (AO). The working solution was prepared by diluting 7.5 µL of 10 mg/mL AO stock in 1 mL M9 buffer. Adult worms were placed on fresh NGM plates and treated with 500 µL of the AO solution, ensuring full plate coverage. Worms were incubated at room temperature in the dark for 1 hour. After staining, animals were washed with M9 buffer and transferred to unseeded NGM plates for destaining in the dark for 1 hour. Worms were then mounted on agar pads and imaged using a fluorescence microscope. Apoptotic germ cell corpses were identified as brightly fluorescent puncta within the

gonad. For quantification, the number of fluorescent corpses per gonad arm was recorded and also double verified under DIC channel.

2.14 Reproductive lifespan assay in *fog-2(q71)* mutants

To assess reproductive lifespan and oocyte aging independently of endogenous sperm influence, the feminized *C. elegans* strain *fog-2(q71) V* was used. In this mutant background, hermaphrodites do not produce functional sperm and thus behave as females, requiring mating for fertilization. Nematodes were developmentally synchronized by timed egg laying. Five fertilized adult females were placed on individual S-plates and allowed to lay eggs for 3 hours, after which the mothers were removed. From the resulting synchronized progeny, individual L4-stage animals were selected and transferred to fresh S-plates for individual monitoring. Beginning on the first day of adulthood, each female was transferred daily to a new plate until the end of their reproductive lifespan. To ensure consistent fertilization and exclude effects of male sperm aging, a cohort of five young adult males was added to each plate daily. After each transfer, the number of eggs laid was recorded. Two days later, hatched larvae and any remaining unhatched eggs were counted. Brood size was calculated as the total number of eggs laid over the reproductive lifespan. Reproductive output was further characterized by quantifying the number of viable progeny (hatched larvae) and unhatched eggs across all reproductive days.

2.15 *C. elegans* lifespan assay

Lifespan assays were conducted using synchronized populations of *C. elegans*. Developmental synchronization was achieved by timed egg laying. Upon reaching the YA stage, worms were transferred to S-plates, 20 animals per plate, totaling approximately 100–120 animals distributed across 5–6 plates per experimental group. The precise number of animals used for each condition is indicated in the corresponding figure legends. Starting on the first day of adulthood (day 1), worms were transferred to fresh plates daily during the reproductive period to prevent progeny confusion. After reproduction ceased, animals were transferred less frequently (every 3–4 days). Survival was assessed once daily. Worms were considered alive if they displayed signs of vitality, including pharyngeal pumping or spontaneous movement. In advanced age, animals were evaluated using a gentle touch assay with a platinum or eyelash worm pick; lack of response to repeated stimulation was used to confirm death. Worms that died due to non-age-related causes, such as internal hatching or accidental desiccation, were censored from the analysis. Survival data were analyzed using GraphPad Prism version 10.1.0. Kaplan-Meier survival curves were generated from time of death data, with censored subjects indicated. Statistical significance between groups was assessed using both the log-rank (Mantel-Cox) test and the Gehan–Breslow–Wilcoxon test. Standard error SE or 95% confidence intervals CI computed from the Kaplan-Meier estimates.

2.16 Data quantification, handling, statistical analysis and visualization

All data are presented as mean ± standard deviation (SD) or indicated in the figures and corresponding figure legends. The number of independent experiments (ℕ), biological replicates (N), and individual organisms (nematodes, n) are specified in the figures and corresponding figure legends. The specific statistical tests applied are detailed in the figure legends, with p-values reported directly in the diagrams. Boxplots are shown with the center line depicting the median value, the box limits showing the top and bottom quartiles, and the whiskers showing the 1.5x interquartile range. Linear regression plots are shown with the 95% confidence interval. Data handling, statistical testing, and plotting were conducted using Microsoft Excel 2019, R version 4.3.2, GraphPad Prism 9 and 10, and with Seaborn-0.11.0[299] and Matplotlib-3.3.0[300] in Python 3.6.10. Illustrative figures were made with bioRender https://www.biorender.com/ and InkScape 1.2.

2.17 *C. elegans* strains used for this study

Strain	**description**	**Genotype**	**origin**
N2 Bristol	wild type		CGC
GN112	AFD split caspase ablated - AFD:SCA	*pgIs2 [gcy-8p::TU#813 + gcy-8p::TU#814 + unc-122p::GFP + gcy-8p::mCherry + gcy-8p::GFP + ttx-3p::GFP].*	CGC
BFF96	AFD neuron specific trangenic hitamine gated cloride channel expressing strain	*pgcy-8::HisCl1::SL2::mCherry::rab-3 3'UTR, pgcy-8::GCaMP6::rab-3 3'UTR; rol-6(GOF)*	Rechavi lab
BJS1062	The integrated version of of the BFF96 - AFD:HisCl1	*pgcy-8::HisCl1::SL2::mCherry::rab-3 3'UTR, pgcy-8::GCaMP6::rab-3 3'UTR; rol-6(GOF)*	Generated by us
IK597	AFD triple mutant	*gcy-23(nj37) gcy-8(oy44) gcy-18(nj38) IV.*	CGC
NL1810		*mut-16(pk710) I.*	CGC
CB4108		*fog-2(q71) V.*	CGC
VC2324		*flp-6 (ok3065) V*	CGC
PY1589		*cmk-1(oy21) IV*	CGC
MG15434		*tph-1 (mg280) II*	CGC
KU25		*pmk-1 (km25) IV*	CGC

2.18 Primers used for this study

Name	**Purpose**	**Sequence 5' - 3'**
tbg-1F	RT-qPCR housekeeper gene	CAATGTGCCCATCAATTCGG
tbg-1R	RT-qPCR housekeeper gene	AACAAGAAGCGAGTGACGTC
act-1-F	RT-qPCR housekeeper gene	CCACCATGTACCCAGGAATT
act-1-R	RT-qPCR housekeeper gene	AGAGGGAAGCGAGGATAGAT
eif-3.C-F	RT-qPCR housekeeper gene	ACACTTGACGAGCCCACCGAC
eif-3.C-R	RT-qPCR housekeeper gene	TGCCGCTCGTTCCTTCCTGG

rpl-32 - F	RT-qPCR housekeeper gene	CAAGGTCGTCAAGAAGAAGC
rpl-32 - R	RT-qPCR housekeeper gene	GGCTACACGACGGTATCTGT
Tc1(A) - F	RT-qPCR target gene	ACCAGCACTTCCATGGGCCC
Tc1(A) - R	RT-qPCR target gene	ACGAAGCCACGGCCCACATT
Tc1(B) - F	RT-qPCR target gene	TCGCTTTGAGAATCTCGCCCGG
Tc1(B) - R	RT-qPCR target gene	CGTGGCGGTCCTATGCGGAT
Mirage(A) - F	RT-qPCR target gene	AGCTTCTCCCCAGGCCCTCA
Mirage(A) - R	RT-qPCR target gene	ATCCGCTTTCCAGGCCACTCC
Mirage(B) - F	RT-qPCR target gene	ACGGGGAAATTCGTTATCCGGTCG
Mirage(B) - R	RT-qPCR target gene	ACAGTTGACTTCGCTCGTCGCA
unc-22B-F1	genotyping *unc-22:Tc1* locus	TTTTGAGACACCCGACGCTT
unc-22B-R1	genotyping *unc-22:Tc1* locus	GTGGTGGTGGCAGGATGATT
unc-22B-F2	genotyping *unc-22:Tc1* locus	CGTGTCACTGGACTTCGTCA
unc-22B-R2	genotyping *unc-22:Tc1* locus	ATGGGCGGTGAGTCCAAAAT
unc-22B-F3	genotyping *unc-22:Tc1* locus	TCACGGAAGGCCACGAATAC
unc-22B-R3	genotyping *unc-22:Tc1* locus	GAAGTCCAGTGACACGAGCA
unc-22B-F4	genotyping *unc-22:Tc1* locus	ACAACATTTTGATTTTCAGTTCCG
unc-22B-R4	genotyping *unc-22:Tc1* locus	TGGAGCAGACGGTCTATCTT
unc-22B-F5	genotyping *unc-22:Tc1* locus	CCATCTGCAATGCGATCTGA
unc-22B-R5	genotyping *unc-22:Tc1* locus	GACACGGAACTGAAAATCAAAATG
unc-22B-F6	genotyping *unc-22:Tc1* locus	ACTTCTTATTTCAGAACCGCCG
unc-22B-R6	genotyping *unc-22:Tc1* locus	TTCCGCATTCTTGCCAGTCT
unc-22B-F7	genotyping *unc-22:Tc1* locus	TACGCCACGTGTAAGACCAC
unc-22B-R7	genotyping *unc-22:Tc1* locus	GGCAACGGGTTCAGGAAACT
gcy-8-F1	genotyping AFD triple mutant	ATGGGTCTTCCCACGAGAAAAC
gcy-8-R1	genotyping AFD triple mutant	GAGAACATTGGATTCACGGACC
gcy-8-F2	genotyping AFD triple mutant	AATCCCAAAGAAGCTGGCCTAC
gcy-8-R2	genotyping AFD triple mutant	GACAGCTAGTACATGGGTGAGC
gcy-18-F1	genotyping AFD triple mutant	ATCGCTACAAACACCGGAAG
gcy-18-R1	genotyping AFD triple mutant	CCGATGAATAAAGCTTCGGA
gcy-18-F2	genotyping AFD triple mutant	TCGAAGAAATCATGCACAGG
gcy-18-R2	genotyping AFD triple mutant	CGTAGGCTGGTAGGAGTTGG
gcy-23-F1	genotyping AFD triple mutant	CGGTTTATGCGGCATTCTAT
gcy-23-R1	genotyping AFD triple mutant	AGACTCCATTCTCGAGGCAA
gcy-23-F2	genotyping AFD triple mutant	AACTGGATTCTGGCCGTCTA
gcy-23-R2	genotyping AFD triple mutant	ATAGGCAATAACGAGGTGCG
mut-16(mg461)F	genotyping AFD triple mutant for *mut-16(mg461)* background	CCCGCCGATACAGAAACTAA

mut-16(mg461)R	genotyping AFD triple mutant for *mut-16(mg461)* background	AATATTCGATCGGCAAGCAG

2.19 Key resources, consumables, instruments used for this study

Reagents:	**Source**	**Identifier**
Nematode growth medium (NGM) agar	[301]	
M9 buffer	[301]	
Trizol® reagent	Invitrogen	15596018
Bromochloropropane (BCP)	Sigma-Aldrich	B9673
SuperScript® III Reverse Transcriptase	Invitrogen	18080085
PowerUp™ SYBR™ Green Master Mix	Thermo Fisher Scientific	A25742
Histamine dihydrochloride	Sigma	H7250-10G
Nicotine	Sigma	N3876
Raltegravir Potassium	Sigma-Aldrich	CDS023737-25MG
Dimethylsulfoxid	Merck	200-664-3
FUDR (5-Fluor-2′-Desoxyuridin)	Merck	F0503
Materials:		
qPCR plates (96 x 0.1 ml plate)	BIOplastics	B60101
200 µl wide-bore pipette tips	Merck	AXYT205WBCRS
1 ml wide-bore pipette tips	Merck	AXYT1005WBCRS
E. coli OP50 strain	CGC	N/A
E. coli NA22 strain	CGC	N/A
QIAGEN Puregene Cell and Tissue Kit	QIAGEN	158388
Qiagen RNeasy Mini Kit®	QIAGEN	175032139
Instruments and Machines:		
Biobeam 8000	Eckert & Ziegler, Gamma Service Medical GmbH	
Centrifuge	Eppendorf	5424 R
Nanodrop spectrophotometer	Thermo Scientific	N/A
CFX Connect real-time PCR detection system	BioRad	#1855201
CFX96 Touch real-time PCR detection system	BioRad	#1854096
Agilent TapeStation System	Agilent	Agilent
Dissecting microscope	Leica	CLS 150X
Axio Imager.M2	Carl Zeiss	N/A
Softwares:		

CFX Manager Software	BioRad	#1845000
Microsoft Excel 2019	Microsoft	
R version 4.3.2		
GraphPad Prism 9	GraphPad	

2.20 Use of generative AI and AI-assisted technologies in the writing process.

AI-assisted literature mining was performed using PerplexityAI, an AI-powered search and synthesis platform. During the preparation of this work OpenAI ChatGPT-4o was employed for text editing and the refinement of scientific writing. After using these tools/services, I have reviewed and edited the content as needed and take full responsibility for the content.

3 Results I: Thermosensory neurons control genetic inheritance through regulation of germline transposons

3.1 Thermosensory neurons control genetic inheritance through regulation of germline transposons

The first results section presents findings from the main project conducted during my PhD. At the time of thesis preparation, the work was available as a preprint on bioRxiv (first version posted on December 5, 2024). In the following section, the preprint is included in its original, unaltered form as submitted for publication.

Szántó, P.R., Meyer, D.H., Teichman, G., Pérez-Llanos, F.J., Rickert, D., Köhrer, K.-E., Rechavi, O., and Schumacher, B. (2024). Thermosensory neurons control genetic inheritance through regulation of germline transposons. Preprint at bioRxiv, https://doi.org/10.1101/2024.12.02.626368.

Author contributions:

Conceptualization: P.R.S., D.H.M., G.T., O.R., B.S.; Experimentation: P.R.S.; Bioinformatics: D.H.M., P.R.S.; Data analysis: P.R.S., D.H.M.; PacBio sequencing experiment lead: K.K. ,F.J.P.- L; PacBio data curation and bioinformatics analysis: F.J.P.-L., D.R.; Manuscript writing: P.R.S., D.H.M, B.S.; Visualization: P.R.S., D.H.M; Supervision: B.S.; Funding acquisition: O.R., B.S.

bioRxiv preprint doi: https://doi.org/10.1101/2024.12.02.626368; this version posted December 5, 2024. The copyright holder for this preprint (which was not certified by peer review) is the author/funder. All rights reserved. No reuse allowed without permission.

Thermosensory neurons control genetic inheritance through regulation of germline transposons

Péter R. Szántó[1,2], David H. Meyer[1,2], Guy Teichman[3], Francy J. Pérez-Llanos[4], Daniel Rickert[4], Karl-Erich Köhrer[4], Oded Rechavi[3], Björn Schumacher[1,2,*]

[1]Institute for Genome Stability in Aging and Disease, Medical Faculty, University of Cologne, Germany
[2]Cologne Excellence Cluster for Cellular Stress Responses in Ageing-Associated Diseases (CECAD), Center for Molecular Medicine Cologne (CMMC), University of Cologne, Joseph-Stelzmann-Str. 26, 50931 Cologne, Germany
[3]School of Neurobiology, Biochemistry and Biophysics, Wise Faculty of Life Sciences & Sagol School of Neuroscience, Tel Aviv University, Tel Aviv, Israel.
[4]West German Genome Center, Biological and Medical Research Center (BMFZ), Medical Faculty and University Hospital Düsseldorf, Heinrich-Heine-University, Universitätsstraße 1, 40225 Düsseldorf, Germany.

[*]correspondence: B.S., bjoern.schumacher@uni-koeln.de

Epigenetic inheritance can be influenced by environmental conditions and somatic inputs originating from different tissues. Such transgenerational inheritance is reversable as it does not lead to mutations and thus alterations in the genetic information. Epigenetic mechanisms such as small RNAs (sRNAs) in the germline silence transposable elements (TEs), which comprise a significant portion of the genome. TE mobility can be mutagenic and is thought to contribute to genome evolution by altering genome structure and diversification. In *C. elegans* elevated temperature leads to desilencing of TEs in the germline, suggesting that environmental conditions could impact the integrity of inheritable genomes. Here, we show that dysfunction of the AFD thermosensory neurons leads to desilencing of TEs in the germline. The TE activity results in *de novo* insertions and mutagenesis. Our data indicate that neuronal sensing of environmental conditions can alter genetic inheritance through stress-induced TE mutagenesis thus shaping genome evolution.

bioRxiv preprint doi: https://doi.org/10.1101/2024.12.02.626368; this version posted December 5, 2024. The copyright holder for this preprint (which was not certified by peer review) is the author/funder. All rights reserved. No reuse allowed without permission.

Introduction

Inheritable genomes are protected by sophisticated DNA repair mechanisms and the DNA damage response (DDR) that ensures the integrity of genomes in the germline and thus the stability of the inheritable genetic information[1,2,3]. The potentially mutagenic transposable elements (TEs) are silenced by mechanisms such as regulatory small RNAs, particularly in the germline, to prevent harmful mutations that can occur if these elements insert into open reading frames or regulatory sequences [4,5]. Ever since the introduction of Weismann's germplasm theory of genetic inheritance in the late 19th century, it is widely thought that the control of genetic inheritance is ensured autonomously by germ cells[6]. Thus far only epigenetic factors were shown to influence transgenerational inheritance in response to changes in the environment[7], while it is not known whether the sensing of environmental factors could also alter genetic, DNA-based information.

Here, we employ the paradigm of temperature control of TE silencing in *C. elegans*[8–10]. The nematode has served as pivotal model system to investigate the mechanisms of TE silencing[11–15] and interactions between somatic tissues and the germline[16–18]. TE activity in germ cells is normally suppressed by small RNA-mediated silencing[19–22]. At elevated temperatures, the Tc1 transposon has been shown to mobilize in germ cells[8,10]. Thus far, it has been unexplored whether this desilencing is a cell autonomous effect in germ cells or a temperature sensing controlled mechanism. Environmental temperature status and change are sensed primarily by a pair of amphid sensory AFD neurons[23–26], it has been established that the cellular heat shock response in *C. elegans* is non-cell autonomously controlled by thermosensory neurons[27]. Manipulation of small RNA biosynthesis in neurons was previously shown to trigger transgenerational epigenetic inheritance in *C. elegans* [28,29]. Here, we tested whether the AFD neurons might mediate transposon silencing and thus regulate TE activity and mutagenesis in the germline.

We report that dysfunction of the AFD pair of thermosensory neurons by distinct experimental paradigms leads to the desilencing of TEs in the germline. We establish that the AFD controlled activation of the Tc1 transposon leads to *de novo* insertions in the genome and thus mutagenesis. The AFD-mediated mutagenesis is inheritable throughout generations and becomes genetically ingrained thus altering genome evolution. Our data established that neurons can control genetic inheritance by regulating the stability and mutagenesis of germline genomes.

Results

bioRxiv preprint doi: https://doi.org/10.1101/2024.12.02.626368; this version posted December 5, 2024. The copyright holder for this preprint (which was not certified by peer review) is the author/funder. All rights reserved. No reuse allowed without permission.

AFD neuron-dependent transposase expression induction

To assess TE activity, we first employed a RT-qPCR based assay that measures the transposase enzyme expression level of a given TE family. We chose the Tc1 and Mirage TE families since they have been reported as highly expressed in *C. elegans* mutant strains where the TE silencing mechanism of the germ cells is impaired, such as the *mut-16* mutant background[30]. To ensure accuracy, we targeted the perfect consensus region of the given TE family with two independent primer pairs, Tc1(A), Tc1(B), Mirage1(A), Mirage1(B) (**Supplementary Figure S1A**). To test the role of the AFD thermosensory neurons, we employed three distinct experimental paradigms of AFD impairment. First, we examined a AFD split caspase ablated strain, hereafter referred to as AFD:SCA. This strain contains a transgenic construct that expresses split caspases under the control of the *gcy-8* promoter, which induces apoptotic ablation of the AFD neuron[26]. We found that in the AFD:SCA strain the Tc1 family remains unaffected, whereas the expression of the Mirage transposase is significantly induced, exhibiting approximately a 9-fold increase in mRNA level compared to wild type (WT) controls (**Figure 1A, Supplementary Figure S1B**).

To confirm that the TE expression is specifically due to the involvement of the AFD neuron, we employed alternative methods to manipulate AFD neuron function. We utilized a transgenic strain that expresses a histamine-gated chloride channel[31] under the control of the *gcy-8* promoter hereafter referred to as AFD:HisCl1. In this strain the AFD neuron is constantly hyperpolarized in the presence of histamine, rendering the AFD neuron inactivate. We performed RT-qPCR in the AFD:HisCl1 strain under normal conditions and following supplementation with 1 mM histamine, which activates the chloride channel. In WT animals histamine supplementation on its own did not significantly alter the expression of Tc1 and Mirage transposases. In the AFD:HisCl1 strain, the Mirage transposase was significantly induced, both under normal conditions and upon histamine supplementation, while Tc1 transposase expression remained unaffected (**Figure 1B, Supplementary Figure S1C**). The observed induction of Mirage transposase mRNA without histamine supplementation is potentially due to the previously suggested leakiness of the transgenic chloride channels, allowing Cl^- ion influx and causing neuron hyperpolarization even in the absence of histamine[31–33].

To more specifically investigate the effect of functional impairment of the AFD neurons on TE expression, we next examined the well-characterized "AFD triple mutant"[27,34]. This strain lacks three key AFD neuron-specific guanylyl cyclase enzymes, *gcy-8, gcy-18* and *gcy-23,* that together

bioRxiv preprint doi: https://doi.org/10.1101/2024.12.02.626368; this version posted December 5, 2024. The copyright holder for this preprint (which was not certified by peer review) is the author/funder. All rights reserved. No reuse allowed without permission.

are crucial for the thermosensory response in *C. elegans* (**Figure 1C**)[34–36]. In the context of prolonged heat stress, the diminished activity of these guanylyl cyclases leads to reduced intracellular Ca^{2+} levels, which is the transducer for long term heat adaptation[23,24,36–38]. In the AFD triple mutant these receptor guanylyl cyclases are absent, therefore the physiological temperature sensing and downstream signaling is disrupted [23,24,36–38]. AFD triple mutant animals displayed a similar induction of Mirage transposase induction as the two AFD dysfunctional models above (**Figure 1D, Supplementary Figure S1D**). Moreover, also the Tc1 transposase showed marked induction compared to WT suggesting a distinct consequence of compromised chronic heat stress sensing.

Given that various forms of heat stress have been reported to induce Tc1 activity in germ cells[10], we further explored the role of AFD neurons in transposase regulation in the context of chronic heat stress. We compared Tc1 and Mirage1 transposase expression in young adulthood in AFD triple mutant and WT nematodes, under normal temperature of 20 °C and chronic heat stress condition by cultivating worms at 25 °C before shifting them to 26 °C at the L4 larval stage preceding adulthood (see methods for details). Transposase derived from both TE families were significantly induced upon heat stress in WT nematodes, while the AFD triple mutants showed strongly elevated Tc1 and Mirage1 expression at ambient temperature that was only slightly further elevated upon heat stress (**Figure 1D, Supplementary Figure S1D**).

To ensure that the effect on TE desilencing is not confounded by the *mut-16(mg461)* background mutation that was reported in several *C. elegans* strains[39], we confirmed the absence of this background mutation in the AFD triple mutant strain (**Supplementary Figure S2**).

To probe whether the AFD neurons could have a general effect on TE desilencing, we examined the transcriptome of the animals carrying dysfunctional AFD neurons. To comprehensively sequence transposon transcripts, we conducted total RNA sequencing (ribo-minus, see methods for details) in the three AFD neuron-impaired strains, i.e. AFD::SCA, AFD:HisCl1, and the AFD triple mutant, and, additionally, in the WT and AFD triple mutant under both normal temperature and chronic heat-stressed condition as applied above. Consistent with our RT-qPCR results, we observed a positive average induction across all TE families in all comparisons, including an additive effect of heat stress and the AFD triple mutant (**Figure 1E**). TEs showed a significant enrichment in the upregulated genes in the AFD:SCA strain, the AFD triple mutant, upon heat stress in WT worms, an additive upregulation upon heat stress in the AFD triple mutant, and a

bioRxiv preprint doi: https://doi.org/10.1101/2024.12.02.626368; this version posted December 5, 2024. The copyright holder for this preprint (which was not certified by peer review) is the author/funder. All rights reserved. No reuse allowed without permission.

non-significant positive enrichment in the AFD:HisCl1 mutant upon Histamine treatment (**Supplementary Figure S3A-G**). Mirage1 showed the most consistent average upregulation and enrichment in all comparisons, while Tc1 showed the strongest effect in the AFD triple mutant and heat-stress, mirroring our RT-qPCR results (**Supplementary Figure S3H, I**).

Our results using three independent paradigms of AFD dysregulation demonstrate that TE RNA expression is induced amid dysfunction of the thermosensory AFD neuron. However, the different types of AFD impairment distinctively affect the expression of the different TE families, likely due to their distinctive consequence on AFD function. The AFD:SCA model induces apoptosis and this strain exhibits severe impairments in fertility, development, and temperature resistance and shows lethality upon elevated temperature thus precluding heat stress experiments. The AFD:HisCl1 model induces hyperpolarization; however, the channel has been shown to be leaky, resulting in sustained hyperpolarization even in the absence of histamine[31,32], complicating experimentation and requiring precise histamine control. In contrast, in the AFD triple mutant the neurons remain intact except for its thermosensory function [23,24,37,38]. Furthermore, a hierarchical clustering of the enrichment scores of TE families clustered the AFD triple mutant together with heat-stressed WT transcriptomes, suggesting that a chronic heat stress response is mounted in the AFD triple mutant (**Supplementary Figure S3I**). In conclusion, the transcriptome analysis confirms the induction of TE expression upon AFD dysfunction. Moreover, our data suggest that the AFD triple mutant provides a suitable model for an animal under a chronic heat stress. Consistently, it has been reported that the AFD triple mutant mounts a chronic stress response, as evidenced by increased peroxide resistance[40]. Our data, combined with evidence from the literature, suggest that the AFD triple mutant behaves as if it was under chronic heat perception, based on the examined phenotypes. Therefore, we proceeded to utilize the AFD triple mutant as our primary model for investigating the role of neuronal thermosensory regulation on TE activity.

Disruption of TE regulation and the sRNA pathway in AFD triple mutants

To investigate the mechanistic basis of the TE induction in the AFD triple mutant, we analyzed the overall RNA sequencing data, which we further complemented with proteomics. First, we focused on gene expression changes that behave in a similar additive pattern as the average logFC of TEs (**Figure 1E**), i.e. genes that are significantly up- (respective down-) regulated upon heat-stress in WT, in the AFD triple mutant, and further upon heat-stress in the AFD triple mutant

bioRxiv preprint doi: https://doi.org/10.1101/2024.12.02.626368; this version posted December 5, 2024. The copyright holder for this preprint (which was not certified by peer review) is the author/funder. All rights reserved. No reuse allowed without permission.

(**Figure 2A**). Intriguingly, *csr-1* and *ckk-1* were AFD mutant and heat-stress dependently repressed and induced, respectively, mirroring the TE expression levels in the AFD triple mutants and the additive effect of heat stress (**Figure 2A**). The argonaute protein CSR-1 was shown to regulate gene expression in the germ cells[41–43], while the calmodulin kinase kinase CKK-1 operates in the thermosensory intracellular signal transduction in the AFD neurons. Consistent with the TE desilencing, a pathway enrichment analysis revealed significant enrichments in transgene expression and transposon silencing pathways in the additively downregulated genes (**Figure 2B**). The mechanisms responsible for silencing transgenes and transposons in the germline rely on a similar molecular machinery to recognize 'non-self' transcripts[11,12,15,44]. Intriguingly, the transgene silencing mechanisms that we find repressed here, were experimentally linked to the AFD neuron function in the accompanying manuscript by Teichman et al.

We next complemented the transcriptome analysis with proteomics comparing the AFD triple mutant and WT at ambient and elevated temperature as described above. Both methods yielded highly consistent results with a strong correlation between the transcriptome and proteome results (**Figure 2C**). Consistently with the role of sRNAs in silencing TEs in the germline, we found that in the AFD triple mutant many genes that function in sRNA biogenesis or processing were down regulated on the transcriptomics as well as proteomics level (**Figure 2D).**

In different organisms, TE silencing is mediated by the deposition of repressive histone modifications[45]. In line with the desilencing of TEs, the epigenetic silencing machinery (*hpl-2*, *mes-4*, *set-32*, *set-25*, and *lin-13*) is significantly downregulated in the AFD triple mutant (**Figure 2D**). We therefore wondered whether we could detect the remodeling of histone modifications, which are mediating epigenetic TE silencing. For this we computed the overlap of histone modification peaks of public ChIP-seq data (see methods for details) with genes that were upregulated in the AFD triple mutant. Consistent with the involvement of the heterochromatin machinery in mediating the gene desilencing in the thermosensory mutant, we found the repressive H3K23me3, H3K27me3, and H3K9me2/3 histone marks were strongly enriched in the genes that we found upregulated in the AFD triple mutant (**Figure 2E**).

In conclusion, we present strong evidence that many components of the sRNA machinery are downregulated in the AFD triple mutant at both the transcriptomic and proteomic levels. This is marked by the downregulation of sRNA biogenesis factors, sRNA processing genes, Argonaute

bioRxiv preprint doi: https://doi.org/10.1101/2024.12.02.626368; this version posted December 5, 2024. The copyright holder for this preprint (which was not certified by peer review) is the author/funder. All rights reserved. No reuse allowed without permission.

proteins, and the post-transcriptional, as well as transcriptional gene silencing pathways, including the epigenetic silencing machinery involving a heterochromatin remodeling.

Exploration of the pathway connecting the AFD neuron and germ cells

We next aimed to elucidate the signaling mechanism from the AFD neuron to the germline. First, we examined genes that have previously been reported to operate in or be influenced by the AFD neuron and to have an epistatic relationship with it [46–48]. Consistent with compromised AFD function, we found those genes differentially expression upon heat stress and in the AFD triple mutant (**Figure 3A**). Strikingly, we detected a pronounced induction of a range of neuropeptides in AFD triple mutants in line with a chronic thermosensatory activation (**Figure 3B**). To further investigate the signaling mechanism through which the AFD could impact on TE regulation, we computed a gene set enrichment analysis with publicly available differentially expressed gene sets with the significantly up-, respective down-, regulated genes in the AFD triple mutant (see Methods for details, **Supplementary Table 2**). The transcription factor *crh-1* was reported to be a major heat stress response regulator that mediates the expression of neuropeptides [48]. In line with this reported role, the loss-of-function *crh-1(tz2)* mutant exhibits opposite patterns of gene expression compared to the AFD triple mutant (**Figure 3C, Supplementary Figure 4A**). A similar opposite gene expression pattern can be observed in loss-of-function *pmk-1(km25)* mutants (**Figure 3C, Supplementary 4 B**). PMK-1 is known to transmit somatic stress signals from the soma to germ cells via the secretion of SYSM-1 to regulate germ cell apoptosis and control stress-induced aneuploidy in the offspring[49]. Consistently, we observe a significant upregulation of the PMK-1 target gene *sysm-1* in the AFD triple mutant (logFC=1.31, FDR=7e-14).

In contrast, the loss-of-function *emb-4(hc60),* the loss-of-function *miR-243(n4759),* and the constitutive-active *atfs-1(et15)* mutants show a similar gene expression pattern as the AFD triple mutants (**Figure 3C, Supplementary Figure 4C-E**). The helicase *emb-4* has been reported to physically interact with the nuclear Argonaute *hrde-1*, a critical component in the heritable silencing of genes and transposable elements. EMB-4/AQR facilitates this process by removing intronic barriers that otherwise impede the nuclear RNAi pathway, thereby enabling efficient silencing by HRDE-1 [50]. This helicase has also been implicated in temperature tolerance in *C. elegans*[51]. miR-243 has been reported to interact with RDE-1, another argonaute, and plays a role in silencing endogenous RNA targets[52]. ATFS-1 is a transcription factor involved in the

bioRxiv preprint doi: https://doi.org/10.1101/2024.12.02.626368; this version posted December 5, 2024. The copyright holder for this preprint (which was not certified by peer review) is the author/funder. All rights reserved. No reuse allowed without permission.

mitochondrial unfolded protein response and multiple stress response pathways, including the *hif-1* mediated hypoxia response, *skn-1* mediated oxidative stress response, and *daf-16* mediated stress response[53]. Notably, genes regulated by ATFS-1 are enriched in the differentially expressed genes of the AFD triple mutant on the transcriptome as well as the proteome level (**Figure 3D, Supplementary Figure 4E**). Analyzing the transcription factor binding motifs present in the promoters of genes that are upregulated at the RNA level in our AFD triple mutant revealed a highly significant enrichment of HIF-1 transcription factor binding motifs, indicative of a role of HIF-1 in the mediator pathway (**Figure 3 E**).

To further investigate the potential mediators from the AFD neuron to the sRNA pathway in the germline, we analyzed relevant public datasets to assess the enrichment of sRNA pathway genes in relevant mutants and conditions (**Figure 3F, Supplementary Figure S5, S6**). In addition to the aforementioned mutants, we included a hypoxia treatment as a potent activator of HIF-1 [54,55]; a treatment with the pathogen PA14 as an activator of PMK-1[56]; and a knock down of *inx-14*, which has been shown to mediate signal from the soma to the germline[57]. The majority of datasets exhibit significant downregulation of sRNA pathway genes, consistent with the downregulation observed in the AFD triple mutant, as shown in Figure 2E. Notably, only the *pmk-1(km25)* mutant dataset displays opposite sRNA pathway regulation behavior (**Figure 3F, Supplementary Figure S4, S5, S6**).

Based on our combined transcriptomic and proteomic analyses, along with comparisons to public datasets, and the genetic evidence for mediators of AFD regulated germline transgene silencing in the accompanying Teichman et al. paper, we derived a plausible signaling link from the AFD neurons to the induction of TE expression in germ cells. In the AFD triple mutant, we observed an induction of *crh-1* and upregulation of neuropeptides. Downstream mediators include PMK-1[58,59], a repressor of *hsf-1*, which is downregulated and functions as important regulator of the heat stress response in germ cells[60]. We also propose the involvement of *hif-1*, a key stress response mediator known to affect serotonin signaling [61], which has been reported to mediate the AFD neurogenic heat stress response to germ cells[47], impacting *hsf-1* and chromatin maintenance[62]. Serotonin was shown to regulate HSF-1 activation in the germ cells in AFD neuron dependent manner[47] and serotonin was also shown to activate *atfs-1*[63,64], and constitutive active *atfs-1(et15)* mutant leads to downregulation of *emb-4*, which in turn was shown to mediate *hrde-1* dependent gene and transposon silencing specifically in germ cells[50]. These gene regulation changes are highly

bioRxiv preprint doi: https://doi.org/10.1101/2024.12.02.626368; this version posted December 5, 2024. The copyright holder for this preprint (which was not certified by peer review) is the author/funder. All rights reserved. No reuse allowed without permission.

consistent with the genetic results of the accompanying paper by Teichman et al. implicating AFD-mediated serotonin signaling in the HSF-1 mediated regulation of the small RNA machinery in the germline.

Impaired AFD neuron function leads to inheritable Tc1 induced mutations.

Since heat stress can lead to the de-silencing of TEs in germ cells[10] and we detected a strong downregulation of the germline sRNA pathway (**Figure 2**), we hypothesized that AFD neuron impairment-induced activation of TE expression may affect the germline and potentially influence genome inheritance. As both our RT-qPCR (**Figure 1D**) and transcriptomic analyses (**Supplementary Figure 3H, I**) revealed an induction of Tc1 transposase RNA expression in the AFD triple mutant, we chose to investigate Tc1 insertion and its heritability. We utilized the well-established phenotype-based "twitching assay", which has been validated in several studies as a reliable indicator of Tc1 transposon *de novo* insertion activity[65–67]. The twitching assay relies on spontaneous Tc1 transposon insertions into the *unc-22* locus, a 38 kb genomic sequence encoding the *C. elegans* homologue of the titin gene, essential for proper muscle function. When a Tc1 transposon insertion disrupts UNC-22 function, the nematodes display non-neurogenic muscle spasms, which becomes evident upon nicotine treatment that paralyzes WT, while *unc-22::Tc1* insertion mutants exhibit a twitching phenotype[65–67]. This assay serves as a robust genetic indicator of Tc1 transposon insertion activity, determined by the penetrance of the twitching phenotype in a given population derived from a single confirmed non-twitching founder hermaphrodite (**Figure 4A**).

While none of the WT animals displayed a twitching phenotype in each of the four independent experiments, we observed a penetrance of the twitching phenotype of $5e^{-6}$ to $25e^{-6}$ AFD triple mutant animals (**Figure 4B**). These results provide visually observable, phenotype-based evidence that the induction of transposase expression in the AFD triple mutant leads to increased Tc1 transposon mobilization and mutagenesis. To assess whether the observed AFD-dependent mutations were stably inheritable, we independently recovered five twitching nematodes and established separate lines (A-E) from each and assessed the F1 progeny of these lines. The results demonstrated that the twitching phenotype was present in the F1 generation with 100% penetrance, confirming that the mutation is inheritable (**Figure 4C**).

bioRxiv preprint doi: https://doi.org/10.1101/2024.12.02.626368; this version posted December 5, 2024. The copyright holder for this preprint (which was not certified by peer review) is the author/funder. All rights reserved. No reuse allowed without permission.

To confirm that the inheritable twitching phenotype was, as expected, caused by a *de novo* Tc1 insertion in the AFD triple mutant, we performed single-worm PCR in the *unc-22* locus in one of the isolated lines (line D) from the twitching screen. We detected an insertion in the *unc-22* locus (**Figure 4 D**). Sequencing of the PCR product confirmed the insertion of Tc1 into the coding region of the *unc-22* gene, 33,091 base pairs downstream of the start codon (**Figure 4 F**). These findings indicate that in the thermosensory AFD triple mutant the increased Tc1 transposon activity results in a higher frequency of Tc1 insertion-induced inheritable mutations.

AFD neuron impairment drives genome-wide *de novo* transposon insertions.

Following the observation of inheritable mutations resulting from AFD neuron impairment, we expanded our investigation to encompass the entire transposon-insertion landscape of the genome. We conducted a mutation accumulation experiment spanning thirty generations. We compared a founder P0 population with five independent progeny lines up to the F30 generation, which were derived from the P0 by transferring a single nematode prior to reaching reproductive age, thereby minimizing the effects of natural selection. PacBio HiFi whole-genome sequencing (WGS) was used to analyze the genomic changes to determine whether the depletion of AFD neurons leads to a higher frequency of mutation events compared to the WT controls (**Figure 5A**).

To ensure that no background mutation was responsible for our phenotype, we first determined that no structural variants (SVs), small deletions (DELs), small insertions (INS), or single nucleotide variants (SNVs) in our sequenced samples impacted genes known to influence transposon activity (**Supplementary Table 3, 4**). While some genes within the list exhibited mutations – primarily of modifier impact - these were scattered across different strains, or present in most samples and thus not associated with our phenotype (**Supplementary Table 3, 4**). Having ruled out that a background mutation might affect our mutation accumulation analyses, we next analyzed the overall *de novo* mutation landscape of our samples after filtering out any mutation that existed already in the P0 generation of the respective strain (see methods for details).

First, we examined overall translocations and strikingly, observed that the AFD triple mutant strain exhibited a stark increase in the number of translocations (**Figure 5B,C,E**). We confirmed the presence of the *gcy* mutations in the AFD triple mutant lines but had to omit one line that was WT for the *gcy* alleles and thus not a triple mutant. The heterozygous translocations in the AFD triple mutant were especially enriched to be nearby known Tc1 positions in the genome (**Figure 5D**).

bioRxiv preprint doi: https://doi.org/10.1101/2024.12.02.626368; this version posted December 5, 2024. The copyright holder for this preprint (which was not certified by peer review) is the author/funder. All rights reserved. No reuse allowed without permission.

Further genomic analysis revealed that the AFD triple mutant strain also exhibited a strong increase in homozygous insertions compared to WT (**Figure 5E**). The inserted sequences were highly enriched in Tc1 transposons, indicating an increased Tc1 activity (**Figure 5F**).

Finally, we wondered why the *de novo* transposition events were specific to Tc1 but absent in other TE types despite their RNA expression. To assess whether the Tc1 transposon family might still be active in nematodes, we determined the number of transposon insertions in 152 wild isotypes of *C. elegans* from the Natural Diversity Resource (see methods for details). The *C. elegans* Tc1 transposon is related to the Mariner family of TEs, which is one of the most widely occurring TE type across species[68,69]. Consistently, we indeed found that the Tc1/Mariner TE family accounts for an overwhelming proportion of TE insertions in the wild isolates suggesting that it is responsible for the evolutionary genomic expansion of TEs (**Supplementary Table 5**).

In conclusion, our findings reveal a profound Tc1 mutagenesis in the AFD triple mutant strain, that leads to transposon accumulation in the inheritable genomes throughout generations of animals.

Discussion

Weismann's germplasm theory has served as foundational concept of genetic inheritance for over a century and posited that the inheritable genome is protected from somatic influences through the Weismann barrier[6]. Thus far only transient somatic epigenetic effects or yolk deposition were observed to be carried into the next generation. The hardwired genetic information is primarily preserved by the DNA damage response (DDR), the full range of DNA repair systems acting in the germline[1,2,3], and the epigenetic repression particularly of TEs to prevent their mutagenic effects [4,5]. Under certain environmental conditions such as heat stress in *C. elegans*, the silencing mechanisms are alleviated resulting in TE expression and subsequent *de novo* insertions[10]. These insertions can be mutagenic, as for instance when they insert into the *unc-22* locus[65–67]. Here we posed the question whether somatic influences could impinge on TE activity and thus contribute to genome evolution. We found that the impairment of the AFD thermosensory neurons leads to a dramatic increase in many TE expression resulting in *de novo* insertions overwhelmingly due to Tc1 mobilization. These insertions become fixed in the germline genomes and thus become part of the species' genetic makeup.

bioRxiv preprint doi: https://doi.org/10.1101/2024.12.02.626368; this version posted December 5, 2024. The copyright holder for this preprint (which was not certified by peer review) is the author/funder. All rights reserved. No reuse allowed without permission.

In this study, we focused on the *genetic* outcome, i.e. TE mobilization, that results from dysfunctions in the activity of the AFD neurons. TE silencing is mediated by sRNAs, which function as "the guardians of the genome" [19,20]. The accompanying Teichman et al. paper reports that AFD neuron dysfunctions also has *epigenetic* consequences, as it disrupts the transgenerational inheritance of sRNA, leading to de-silencing of foreign genes in the germline. Substantial evidence indicates that transgene silencing and transposon silencing in the *C. elegans* germline rely on overlapping molecular machinery, with several key findings supporting this connection[11,12,15,44]. The highly consistent effects of the AFD neuron affecting transgenerational sRNA inheritance and TE desilencing leading to epigenetic and genetic alterations in germline genomes, respectively, suggest a common mechanism likely emanating from a chronic heat stress response in the AFD neuron. Mechanistically, our transcriptome and proteome analysis implicated known mediators of AFD signaling, i.e. HIF-1 mediated serotonin signaling impacting the transcription factor ATFS-1 and its effector EMB-4 in parallel to PMK-1 induced SYSM-1 and repression of HSF-1 converging on the repression of the sRNA machinery leading to TE desilencing and consequent *de novo* Tc1 driven germline mutagenesis. These AFD effector mechanisms are highly consistent with the genetic analysis of the accompanying Teichman et al. paper.

The *de novo* mutations were specifically caused by the Tc1 but no other TE families, such as Mirage1, despite their RNA expression. This might be explained by the evolutionary history of TEs since several studies have highlighted the activity of the Tc1 and the closely related Mariner family, both of which are classified as the Tc1/Mariner superfamily[70]. It is well documented that the Tc1 family is evolutionarily younger and remains highly active, as many of its copies still encode fully functional proteins[71–74]. The Tc1/Mariner TE family is reportedly the most abundant and active[14,70–74]. It is also known that only a small percentage of Tc1 transcripts are correctly processed, yet this is sufficient to translate a functional transposase and drive transposition, highlighting the mobility of Tc1 over the dormancy of other TE families, despite others also being upregulated at the RNA level[11]. In contrast, evolutionarily older TE families may transcribe only nonfunctional RNAs, often residing in intronic or untranslated regions[74]. However, these transcripts do not result in the translation of functional transposase and thus cannot mediate mobilization, as reported[75]. Our investigation of *C. elegans* wild isotypes also revealed that the Tc1/Mariner TE family has indeed been the most active in the recent evolutionary history

bioRxiv preprint doi: https://doi.org/10.1101/2024.12.02.626368; this version posted December 5, 2024. The copyright holder for this preprint (which was not certified by peer review) is the author/funder. All rights reserved. No reuse allowed without permission.

(**Supplementary Table 5**). Finally, we observed many upregulated TE-related transcripts following AFD neuron impairment, but the reportedly most active Tc1 family is contributing overwhelmingly to transposon mediated *de novo* mutations that also get inherited and accumulate over generations creating new genetic variants.

Our results transform the current understanding of genetic inheritance as for the first time, we show here that neurons can control genetic inheritance. As the AFD neurons sense environmental stimuli, our results suggest that environmental conditions that are neuronally sensed could be conferred to the genetic makeup in germ cells and thus alter the course of a species evolution. It is thus conceivable that neuronal sensing of stressful temperatures translates to increased transposition, to increase genetic variability amid altered environmental conditions. Environmentally controlled mutagenesis has previously been observed in microorganisms, e.g., genetically regulated stress-induced mutagenesis in *Escherichia coli* [76,77]. We propose that our findings of environmental stress sensing mediated induction of inheritable transposon mutagenesis provides the first example of stress-induced mutagenesis in animals that might enable the animals to generate genomic diversity potentially allowing new adaptations to changing environmental conditions.

Ackowledgements

We thank the Regional Computing Center of the University of Cologne (RRZK) for providing computing time on the DFG-funded High Performance Computing (HPC) system CHEOPS as well as support and the Zentrum für Informations- und Medientechnologie, especially the HPC team at Heinrich Heine University. Worm strains were provided by the National Bioresource Project (supported by The Ministry of Education, Culture, Sports, Science and Technology, Japan), the Caenorhabditis Genetics Center (funded by the NIH National Center for Research Resources, US), and the C. elegans Gene Knockout Project at the Oklahoma Medical Research Foundation (part of the International C. elegans Gene Knockout Consortium). We thank Wen Chen for providing the list with all transposable elements and their clustering into families for the WS291 reference.

O.R. and B.S. acknowledge funding from the Deutsche Forschungsgemeinschaft (DFG) project 437407415 (SCHU 2494/10-1) and the John Templeton Foundation Grant (61734), B.S. from the

bioRxiv preprint doi: https://doi.org/10.1101/2024.12.02.626368; this version posted December 5, 2024. The copyright holder for this preprint (which was not certified by peer review) is the author/funder. All rights reserved. No reuse allowed without permission.

DFG (Reinhart Koselleck-Project 524088035, FOR 5504 project 496650118, SCHU 2494/24-1 540136447, SCHU 2494/3-1, SCHU 2494/11-1, SCHU 2494/15-1, CECAD EXC 2030 – 390661388), the Deutsche Krebshilfe (70114555), Deutsche José Carreras Leukämie-Stiftung (DJCLS 04 R/2023), the European Research Council ERC-2023-SyG 101118919, and the Hevolution Foundation HF-GRO-23-1199212-35. This work was supported by the DFG Research Infrastructure West German Genome Center, project 407493903, as part of the Next Generation Sequencing (NGS) Competence Network, project 423957469. NGS and analyses were carried out at the West German Genome Center Düsseldorf. B.S. received the DFG grant SCHU 2494/7-1 as part of the DFG Sequencing call #1.

Author contributions

Conceptualization: P.R.S., D.H.M., G.T., O.R., B.S.; *Experimentation*: P.R.S.; *Bioinformatics*: D.H.M., P.R.S.; *Data analysis*: P.R.S., D.H.M.; *PacBio sequencing experiment lead:* K.K. ,F.J.P.-L; *PacBio data curation and bioinformatics analysis:* F.J.P.-L., D.R.; *Manuscript writing*: P.R.S., D.H.M, B.S.; *Visualization*: P.R.S., D.H.M; *Supervision*: B.S.; *Funding acquisition*: O.R., B.S.

Declaration of Interests

All authors declare no competing interests.

Materials and methods

C. elegans culture and maintenance

Nematodes were cultured on nematode growth medium (NGM) agar plates. Strains were maintained at 15°C for medium-term storage, and long-term storage by freezing stocks at -80°C in freezing buffer. Prior to experiments, nematodes were acclimated to 20°C for at least two generations. All experiments were conducted at 20°C unless otherwise specified. In all cases during heat stress experiments, synchronized populations were cultured at 25 °C and at the L4 larval stage shifted to 26 °C until collection on the first day of adulthood. Developmental synchronization was achieved using a bleaching solution. Collection and washing of nematodes was done with M9 buffer. The protocols, including reagent and material compositions, were based on standard methods described in WormBook[78].

bioRxiv preprint doi: https://doi.org/10.1101/2024.12.02.626368; this version posted December 5, 2024. The copyright holder for this preprint (which was not certified by peer review) is the author/funder. All rights reserved. No reuse allowed without permission.

Generation of the BJS1062 "AFD:HisCl1"

strain, a starved population of the BFF96 strain was subjected to gamma irradiation at a dose of 90 Gy, with a Biobeam 8000 containing a Cs137 radionucleotide source. This strain contains an extrachromosomal transgenic construct encoding a histamine-gated chloride channel, along with a transcriptional fusion mCherry reporter and a rol-6 selection marker, all driven by the AFD neuron-specific gcy-8 promoter *[pgcy-8::HisCl1::SL2::mCherry::rab-3 3'UTR, pgcy-8::GCaMP6::rab-3 3'UTR; rol-6(GOF)]*. Following irradiation, the progeny was screened over six generations to select worms displaying 100% identifiable mCherry fluorescence, indicating successful integration of the transgenic construct. The resulting strain was then backcrossed four times with the wild-type strain to ensure genetic consistency and remove potential background mutations, then confirmed again for the 100% penetrance of the mCherry fluorescence. As a result we established the BJS1062 strain, that carries the integrated *[pgcy-8::HisCl1::SL2::mCherry::rab-3 3'UTR, pgcy-8::GCaMP6::rab-3 3'UTR]* transgene.

RNA Extraction for RT-qPCR and RNA sequencing

All RNA extractions for this study were performed using the following method. Worms were collected in a tube and washed with M9 buffer, followed by the addition of 1 mL Trizol® reagent. The sample was homogenized by freeze cracking, which involved dropping it into liquid nitrogen and then melting it in an incubator. Subsequently, 100 µL of bromochloropropane (BCP) was added for phase separation. The sample was incubated at room temperature for 2 minutes and then centrifuged at 12,000 rcf for 15 minutes at 4°C. The upper, clear phase (~600 µL) was collected into a fresh RNase-free tube, mixed with an equal volume (~600 µL) of 70% ethanol, and vortexed. The mixture was then processed using the Qiagen RNeasy Mini Kit® according to the manufacturer's instructions, including on-column DNase digestion. The RNA was eluted in 50 µL of RNase-free water. The extracted RNA was quantified and its integrity assessed using Thermo Scientific Nanodrop spectrophotometer to ensure suitability for downstream applications.

cDNA Synthesis

The SuperScript® III Reverse Transcriptase (Invitrogen) kit was used for reverse transcription reactions of isolated RNA samples. cDNA synthesis was performed in a 20 µL reaction mixture.

bioRxiv preprint doi: https://doi.org/10.1101/2024.12.02.626368; this version posted December 5, 2024. The copyright holder for this preprint (which was not certified by peer review) is the author/funder. All rights reserved. No reuse allowed without permission.

The initial reaction mixture included 12 µL of RNA solution (1 µg RNA), 1 µL of random hexamer, and 1 µL of dNTP. This mixture was incubated at 65°C for 5 minutes and then subjected to a brief centrifugation. Following this, the mixture was placed on ice for 5 minutes.

Subsequently, 4 µL of 5x First Strand Reaction Buffer, 1 µL of DTT, 1 µL of RNase Out Recombinant RNase Inhibitor, and 1 µL of SuperScript III RT (200 U/µL) were added to the mixture. The contents were gently mixed by pipetting. The reaction was then incubated under the following conditions: 25°C for 5 minutes, 50°C for 60 minutes, and 70°C for 5 minutes.

Following the incubation, the cDNA was diluted to a final volume of 100 µL by adding 80 µL of double-distilled water (ddH2O). The resultant cDNA was evaluated using a control PCR to verify successful synthesis.

Quantitative Real-Time PCR (qPCR)

Quantitative Real-Time PCR was performed using the PowerUp™ SYBR™ Green Master Mix (Thermo Fisher Scientific). The reaction mixture consisted of 10 µL of 2X PowerUp™ SYBR™ Green Master Mix, 9 µL of 1.1 µM forward and reverse primers, and 0.25 µL of cDNA template, with the total reaction volume adjusted to 20 µL using nuclease-free water. Each sample was measured in biological triplicates from each technical replicate.

A Template Master Mix was prepared by combining 10 µL of PowerUp™ SYBR™ Green Master Mix, 0.25 µL of cDNA template (50 ng/µL), and 0.1 µL of nuclease-free water per reaction, yielding a total volume of 11 µL per well. Separately, a Primer Master Mix was prepared at a concentration of 1.1 µM by mixing 5.5 µL each of 100 µM forward and reverse primer stocks with 489 µL of nuclease-free water to reach a final volume of 500 µL.

Each well of the qPCR plate was aliquoted with 11 µL of Template Master Mix and 9 µL of Primer Master Mix. The qPCR assays were conducted using a CFX Connect and CFX96 Touch real-time PCR detection system (BioRad). The expression levels of target genes were normalized to the reference genes tbg-1, act-1, eif-3.C, and rpl-32. Data acquisition and analysis were performed using CFX Manager Software (BioRad), with subsequent data processing carried out in Microsoft Excel 2019, R version 4.3.2, and GraphPad Prism 9.

Total RNA sequencing

bioRxiv preprint doi: https://doi.org/10.1101/2024.12.02.626368; this version posted December 5, 2024. The copyright holder for this preprint (which was not certified by peer review) is the author/funder. All rights reserved. No reuse allowed without permission.

Libraries were prepared from 500ng total. Enzymatic depletion of ribosomal RNA with the Illumina Ribo-Zero Gold rRNA Depletion Kit was followed by library preparation with the Illumina TruSeq Stranded Total RNA sample preparation kit. The depleted RNA was fragmented and reverse transcribed with random hexamer primers, second strand synthesis with dUTPs was followed by A-tailing, adapter ligation and library amplification (15 cycles). Next library validation and quantification (Agilent Tape Station) was performed, followed by pooling of equimolar amounts of library. The pool itself was then quantified using the Peqlab KAPA Library Quantification Kit and the Applied Biosystems 7900HT Sequence Detection System and sequenced on an Illumina NovaSeq6000 sequencing instrument with an PE100 protocol aiming for 30 million clusters per sample.

Proteomics sample preparation

Whole-animal protein extracts were prepared from a homogenized population of 3,000 C. elegans. Samples were lysed in 8 M urea buffer with 50 mM triethylammonium bicarbonate (TEAB), supplemented with a 50x protease inhibitor cocktail (Roche). For chromatin degradation, Benzonase HC nuclease was added at a concentration of 25 units, followed by incubation at 37°C for 30 minutes to ensure complete chromatin degradation. The lysates were centrifuged at 20,000 × g for 15 minutes to remove cell debris, and protein concentrations were measured using a standard assay. For reduction and alkylation, 50 µg of protein was transferred to a 1.5 mL microcentrifuge tube. Dithiothreitol (DTT) was added to a final concentration of 5 mM, followed by incubation at 25°C for 1 hour. Chloroacetamide (CAA) was then added to a final concentration of 40 mM, and the samples were incubated in the dark for 30 minutes. Trypsin was then added at a 1:75 enzyme-to-substrate ratio, and the samples were incubated overnight at 25°C for complete proteolysis. On the following day, the enzymatic digestion was stopped by acidification with formic acid to a final concentration of 1%. The samples were subsequently purified using SDB-RP StageTips packed with two layers of SDB-RPS discs in 200 µL pipette tips. The StageTips were equilibrated by sequential centrifugation at 800 × g for 1 minute with 20 µL methanol, 20 µL buffer B (0.1% formic acid in 80% acetonitrile), and twice with 20 µL buffer A (0.1% formic acid in water). Acidified samples were centrifuged, and the supernatant was loaded onto the StageTips, followed by washing with buffer A and buffer B. The StageTips were then dried and stored at 4°C

bioRxiv preprint doi: https://doi.org/10.1101/2024.12.02.626368; this version posted December 5, 2024. The copyright holder for this preprint (which was not certified by peer review) is the author/funder. All rights reserved. No reuse allowed without permission.

and submitted to the CECAD Proteomics Facility. All reagents mentioned in this preparation were provide by the CECAD Proteomics Facility (https://proteomics.cecad-labs.uni-koeln.de/home).

Proteomics Data Acquisition

Samples were analyzed by the CECAD Proteomics Facility on an Orbitrap Exploris 480 (Thermo Scientific, granted by the German Research Foundation under INST 1856/71-1 FUGG) mass spectrometer equipped with a FAIMSpro differential ion mobility device that was coupled to an UltiMate 3000 (Thermo Scientific). Samples were loaded onto a precolumn (Acclaim 5µm PepMap 300 µ Cartridge) for

2 min at 15 ul flow before reverse-flushed onto an in-house packed analytical column (30 cm length, 75 µm inner diameter, filled with 2.7 µm Poroshell EC120 C18, Agilent). Peptides were chromatographically separated at a constant flow rate of 300 nL/min and the following gradient: initial 6% B (0.1% formic acid in 80 % acetonitrile), up to 32% B in 72 min, up to 55% B within 7.0 min and up to 95% solvent B within 2.0 min, followed by column wash with 95% solvent B and reequilibration to initial condition. The FAIMS pro was operated at -50V compensation voltage and electrode temperatures of 99.5 °C for the inner and 85 °C for the outer electrode.

For the Gas-phase fractionated library, a pool generated from all samples was analyzed in six individual runs covering the range from 400 m/z to 1000 m/z in 100 m/z increments. For each run, MS1 was acquired at 60k resolution with a maximum injection time of 98 ms and an AGC target of 100%. MS2 spectra were acquired at 30k resolution with a maximum injection time of 60 ms. Spectra were acquired in staggered 4 m/z windows, resulting in nominal 2 m/z windows after deconvolution using ProteoWizard [79].

For the samples, MS1 scans were acquired from 399 m/z to 1001 m/z at 15k resolution. Maximum injection time was set to 22 ms and the AGC target to 100%. MS2 scans ranged from 400 m/z to 1000 m/z and were acquired at 15 k resolution with a maximum injection time of 22 ms and an AGC target of 100%. DIA scans covering the precursor range from 400 - 1000 m/z and were acquired in 60 x 10 m/z windows with an overlap of 1 m/z. All scans were stored as centroid.

Proteomics Sample Processing:

bioRxiv preprint doi: https://doi.org/10.1101/2024.12.02.626368; this version posted December 5, 2024. The copyright holder for this preprint (which was not certified by peer review) is the author/funder. All rights reserved. No reuse allowed without permission.

The gas-phase fractionated library was build using DIA-NN 1.8.1 (Demichev 2020) using C. elegans WormBase database (PRJNA13758, downloaded 24/01/23) with settings matching acquisition parameters.

Samples were analyzed in DIA-NN 1.8.1 as well using the previously generated library and identical database. DIA-NN was run with the additional command line prompts "—report-lib-info" Further output settings were: filtered at 0.01 FDR, N-terminal methionine excision enabled, maximum number of missed cleavages set to 1, min peptide length set to 7, max peptide length set to 30, min precursor m/z set to 400, max precursor m/z set to 1000, cysteine carbamidomethylation enabled as a fixed modification. Afterwards, DIA-NN output was further filtered on library q-value and global q-value <= 0.01 and at least two unique peptides per protein using R (4.1.3). Finally, LFQ values calculated using the DIA-NN R-package. Afterwards, analysis of results was performed in Perseus 1.6.15[80].

Mutation Accumulation Experiment Design and Strain Handling

For this experiment, a single mother was isolated from each of the strains. These isolated mothers were used to propagate populations, which were synchronized by bleaching. This synchronized population served as the P0 founder population for the experiment. The populations were collected and stored at -80°C.

From these initial populations, five mothers were isolated and placed on separate plates, serving as the founding mothers of the experiment (N=5). Throughout the experiment, one L4 stage larva from each strain was transferred individually to a new plate in every generation, spanning 30 generations.

Upon reaching the F30 generation, a population was propagated and synchronized via bleaching to collection for whole genome sequencing (n=3000). All the synchronized populations were collected at the young adult stage by washing with M9 buffer and stored at -80°C, and frozen nematode stocks were established for long-term storage.

High Molecular Weight Genomic DNA Extraction from *C. elegans*

High molecular weight genomic DNA was extracted from *C. elegans* using the QIAGEN Puregene Cell Kit. Approximately 3000 nematodes were grown on NGM agar plates with E. coli OP50 strain and harvested using M9 buffer. The harvested worms were stored at –80°C until DNA extraction.

bioRxiv preprint doi: https://doi.org/10.1101/2024.12.02.626368; this version posted December 5, 2024. The copyright holder for this preprint (which was not certified by peer review) is the author/funder. All rights reserved. No reuse allowed without permission.

The extraction process commenced by adding 3 mL of Cell Lysis Solution and 15 µL of Proteinase K to the frozen worm pellet, allowing it to thaw. Once thawed, the pellet was resuspended by pipetting with a 1 mL wide-bore tip. The sample was incubated at 50°C for 2 hours, with gentle inversion of the tube every 30 minutes to ensure homogeneity.

Following incubation, 15 µL of RNase A was added, and the mixture was incubated at 37°C for 30 minutes. Subsequently, 1 mL of Protein Precipitation Solution was added, and the tube was mixed by inversion 15-20 times before being placed on ice for 2 minutes. The sample was centrifuged at 2000 x g for 10 minutes, and DNA was precipitated from the supernatant using 3 mL of isopropanol. The tube was gently inverted 50 times and centrifuged at 2000 x g for 5 minutes. The supernatant was discarded, and the DNA pellet was washed with 3 mL of 70% ice-cold ethanol. The tube was gently inverted to mix and then centrifuged at 2000 x g for 2 minutes. The supernatant was discarded, and any remaining ethanol was removed using sterile paper wipes. The DNA was eluted in 600 µL of TE buffer and incubated overnight at room temperature to maximize yield. The quantity and quality of the extracted DNA were assessed using a Thermo Scientific Nanodrop spectrophotometer and the Agilent TapeStation System.

PacBio whole genome sequencing

HiFi Whole Genome Library Preparation

DNA quality and quantity were assessed using a NanoDrop spectrophotometer, the Qubit BR DNA assay (ThermoFisher), and the Femto Pulse system (Agilent) with the FP-1002 protocol (165 kb) to evaluate fragment size distribution.

Long-read whole-genome sequencing libraries were prepared using the HiFi low-input protocol as described in the SMRTbell® Prep Kit 3.0 (Version 02; March 2023). Genomic DNA (1,500–7,900 ng) in Low TE buffer was used as input for library preparation. DNA shearing was performed with a MegaRuptor3 (Diagenode) using long hydropores at a shearing speed of 27–30, targeting a fragment size of 10–15 kb when appropriate. Samples with a pre-sheared average fragment size suitable for library preparation were not further processed. Sheared DNA was purified using the DNeasy PowerClean Pro Cleanup Kit (Qiagen) according to the manufacturer's instructions, eluting the DNA in 50 µl of water. For samples with limited DNA, up to three sequential 50 µl elutions were performed on the same column, with eluates pooled to minimize DNA loss.

bioRxiv preprint doi: https://doi.org/10.1101/2024.12.02.626368; this version posted December 5, 2024. The copyright holder for this preprint (which was not certified by peer review) is the author/funder. All rights reserved. No reuse allowed without permission.

Pooled samples were concentrated to a final volume of 50 µl using a SpeedVac at room temperature. DNA quantification was performed at all steps using the Qubit dsDNA assay (ThermoFisher). Fragment size distribution was assessed using a Femto Pulse (Agilent) with the FP-1002 protocol (165 kb) by diluting the sheared DNA to 0.1 ng/µl. Sheared samples were further purified with 1X SMRTbell cleanup beads (PacBio), washed twice with 80% ethanol, and eluted in 47 µl of Low TE buffer (PacBio). DNA concentration was again determined using the Qubit dsDNA HS assay (Thermo Fisher). For library preparation, 46 µl (480–4,000 ng) of each sample was used, following the manufacturer's protocol. This process included DNA repair, A-tailing, adapter ligation, and a nuclease treatment step. AMPure bead size selection was performed to remove fragments smaller than 5 kb, and final libraries were eluted in 11–15 µl of Elution Buffer (PacBio).

A 1:10 dilution of the eluted library was prepared for quality control. Library concentration was measured using Qubit (Thermo Fisher), and size distribution was analyzed with the Femto Pulse (Agilent) using the FP-1002 protocol. Four to six libraries were pooled equimolarly based on their average fragment size and total DNA amount, with each library containing a unique barcode. The final library pool concentration was verified using the Qubit dsDNA HS assay (Thermo Fisher), and fragment size distribution was confirmed on the Femto Pulse. A total of seven final library pools were prepared and stored at 4°C until sequencing.

HiFi Whole Genome Single Molecule Real-Time Sequencing

Sequencing of each SMRTbell library pool was conducted following PacBio's standard sample preparation and sequencing guidelines (SMRT Link version 11.1.0.166339). Sequencing primers and polymerase were bound to each library pool using the Sequel® II Binding Kit 3.2 (PacBio). Polymerase-bound SMRTbell complexes were purified, achieving a recovery rate of ≥75%, as confirmed using the Qubit dsDNA HS assay (Thermo Fisher). Each library pool, including internal control, was sequenced on an SMRT Cell 8M with an on-plate loading concentration of 70–85 pM. Run conditions included a 120-minute pre-extension time and an 1800-minute movie time. Sequencing was performed on Sequel II and Sequel IIe systems.

PacBio Data Analysis

Raw subreads were obtained after filtering polymerase reads and then subjected to Circular Consensus Sequencing (CCS) analysis resulting in HiFi reads using SMRT Link (version 11.1.0.166339 and **13.0.0.207600**). HiFi reads were further demultiplexed using Lima resulting

bioRxiv preprint doi: https://doi.org/10.1101/2024.12.02.626368; this version posted December 5, 2024. The copyright holder for this preprint (which was not certified by peer review) is the author/funder. All rights reserved. No reuse allowed without permission.

with a barcode score threshold of 96. On average, the sequencing generated ~360,000 HiFi reads per genome with a quality value of ≥20, an N50 read length of approximately 8.6 kb, a predicted base accuracy of 99%, and a minimum of three passes per molecule. Datasets were organized into generations: P0, F30 for the wild type and AFD triple mutant respectively, with one P0 sample rep and five samples corresponding for the F30 descendants of the five independent lines. Each analysis was performed individually on sample replicates, with datasets merged where applicable, resulting in one dataset per sample.

HiFi Mapping

HiFi reads were mapped to the *Caenorhabditis elegans* reference genome (PMID: 31123080) using the pbmm2 tool based on minimap2. The PacBio data analysis was performed using SMRT Link version 13.0.0.207600. Parameters included a minimum CCS Phred scale of 20, a minimum gap-compressed identity of 70%, and a minimum mapped length of 50 bp. The mean concordance of reads that mapped to the reference ranged from 98.51% to 99.32%. Approximately 338,158 CCS reads were mapped, with a 95th percentile read length of ~15 kb and an average read length of 8.6 kb. The mean depth of coverage across the reference sequence was 26x.

Structural Variant Calling

HiFi reads (CCS BAM input) were aligned to the reference genome, and structural variation signatures were identified from the aligned BAMs. Variant calling and genotype assignment were conducted using the pbsv tool, detecting insertions, deletions, inversions, duplications, translocations homozygous and heterozygous variables. Parameters included a min CCS Phred scale of 20, minimum gap-compressed identity of 70%, minimum mapped length of 50 bp, minimum 10% read support for the variant (any one sample), and a minimum of 3 reads supporting the variant (total over all samples). Variants were called for structural variants of a minimum length of 500 bp.

Variant Calling

For each sample, mapped BAM files were merged using samtools (version 1.2.0) if multiple BAM files were available. Variants were called against the reference using deepconsensus (version 1.6.1) with default parameters and options "--model_type PACBIO --num_shards 12" (PMID: 30247488).

Tc1 Transposon Mobilization Assay – Twitching Screen

bioRxiv preprint doi: https://doi.org/10.1101/2024.12.02.626368; this version posted December 5, 2024. The copyright holder for this preprint (which was not certified by peer review) is the author/funder. All rights reserved. No reuse allowed without permission.

To assess Tc1 transposon activity, a phenotype-based screen was performed. The insertion of Tc1 into the *unc-22* locus results in an observable twitching phenotype due to muscle spasms. To perform the assay a single nematode, confirmed to have no twitching phenotype, was isolated and propagated into a large population of approximately 300,000-500,000 individuals. The population was then synchronized using a bleach synchronization method.

Once the developmentally synchronized population reached the young adult stage, before egg-laying began, the worms were collected and washed with M9 buffer. Nicotine was added to a final concentration of 2%, which paralyzed all worms, allowing the twitching phenotype to become observable, as it is unaffected by nicotine.

The culture was screened under a dissecting microscope to identify twitching individuals. This allowed for the assessment of Tc1 transposon activity based on the presence of the twitching phenotype.

RNA-seq processing

First, we preprocessed the raw samples with Fastp v0.20.0[81] with the parameters -g -x -q 30 -e 30. The preprocessed samples were subsequently mapped with Salmon v1.1[82] with the parameters –validateMappings –seqBias –gcBias and a decoy-aware reference genome based on WS281 including transposon transcripts from Wormbase[83] .The mapped transcript-level counts were combined to the gene-level with tximport v1.14.2[84] .filterByExpr was used to remove lowly expressed genes retaining 17674 genes for further analyses. edgeR v3.40.2[85] was used for differential gene expression analysis. We identified three WT control outlier from batch 1, and 2 histamine treated WT outlier in a PCA and removed them from subsequent analyses.

Enrichment analyses

The 961 additively downregulated genes in the in heat-stressed WT, the AFD triple mutant, and heat-stressed AFD triple mutants were identified by selecting only those genes that were significantly (FDR<0.05) downregulated in all three pairwise comparisons. STRING v12[86] was used for functional enrichment analysis, using all 17674 genes that remained after filtering as the statistical background. The histone modification enrichment analysis was done with the Enrichment Analysis from https://chip-atlas.org/[87] for *C. elegans* (ce11), the experiment type "ChIP:Histone", cell type class "Adult", threshold for significance of 50, all significant up-

bioRxiv preprint doi: https://doi.org/10.1101/2024.12.02.626368; this version posted December 5, 2024. The copyright holder for this preprint (which was not certified by peer review) is the author/funder. All rights reserved. No reuse allowed without permission.

regulated genes (FDR<0.05) as dataset A, all 17674 genes as dataset B, and a distance of -1kb <= TSS<= +1kb. Histone modifications for which more than 3 samples for whole worm samples that were over-enriched (fold change >1) exist were plotted. WormExp with a background gene set of all 17674 genes[88] was used to compute enrichment for publicly available datasets. Gene set enrichment analysis (GSEA) for all transposable element transcripts, transposable element families, transcription factor motifs, and the sRNA-related genes were done with fgsea::fgseaMultilevel[89]. For the transcription factor motif analysis we downloaded all available curated motifs from the 10th release (2024) of JASPAR[90] and identified genes whose promoter region contained the motif with HOMER's[91] findMotifs.pl function and a motif score of at least 7. The identified genes were used for a GSEA.

Public transcriptomic data analysis

The OP50-fed *inx-14 RNAi*[92] data was downloaded from GSE216879. The processed ribozero emb-4(hc60) samples (GSE94455)[93], and the lin-14 samples (GSE87523) were downloaded via Archs4[94]. The *atfs-1(et15)* data (GSE110984) was downloaded from the supplementary data of PMID30563508[53]. The hypoxia microarray dataset (GSE228851)[95], and the *pmk-1(km25)* microarray dataset (GSE53732)[96] were reanalyzed with GEO2R[97]. The pathogen PA14 dataset was downloaded from GSE122544[98]. The *hsf-1* samples (GSE241011) were downloaded from the supplementary data of PMID38895933[99].

WGS Filtering

We had to omit one of the F30 AFD triple mutant line that was WT for the gcy alleles and thus not a triple mutant.

To identify *de novo* F30 structural variants (SV) we filtered variants of each F30 generation sample that appeared in the respective P0 sample. For this we checked if the genomic region of each F30 SV is overlapping with any SV in the corresponding P0 sample. For imprecisely called SVs we extended the area of overlap by the length of the SV.

Circos plots

The R v4.2.2 package circlize[100] v.0.4.16 was used to draw the circos plots for all *de novo* F30 translocations (BNDs).

bioRxiv preprint doi: https://doi.org/10.1101/2024.12.02.626368; this version posted December 5, 2024. The copyright holder for this preprint (which was not certified by peer review) is the author/funder. All rights reserved. No reuse allowed without permission.

Background mutation analysis

Genomic variants, including single nucleotide variants(SNVs), small insertions and deletions (INDELs), and structural variants (SVs), were annotated with SnpEFF 4.3t[101] to assess the potential impact of each variant on gene function, allowing for the identification of possible background mutations.

Transposable element insertions

The inserted sequences for all homozygous *de novo* F30 insertions were used as input for a BLASTN[102] query against the known TE sequences from Wormbase (WS279.transposons.fa). TEs were only considered to match if the alignment length was bigger than 100. If for a query multiple TEs were matched we used the TE with the highest 'bit score'.

Repeat elements near break points

All *de novo* F30 break points (BNDs) were annotated to their nearest known repeat element in the ce11 genome. The known repeat elements were downloaded from the crhomOut.tar.gz file from https://hgdownload.soe.ucsc.edu/goldenPath/ce11/bigZips/. Only repeats that were within 10bp of the break point were considered.

CeNDR analysis

We downloaded the 20231213_c_elegans_transposon_calls.bed file from the *C. elegans* Natural Diversity Resource (CeNDR) https://caendr.org/data/data-release/c-elegans/latest [103]. This file contains the count of several transposable element classes within 152 isotypes for *C. elegans*. For each isotype, the proportion of each transposable element family was calculate by dividing the number of TEs in each family by the total number of TEs identified in that strain.

Data quantification, handling and statistical analysis

All data are presented as mean ± standard deviation (SD) or indicated in the figures and corresponding figure legends. The number of independent experiments (ℕ), biological replicates (N), and individual organisms (nematodes, n) are specified in the figures and corresponding figure legends. The specific statistical tests applied are detailed in the figure legends, with p-values

bioRxiv preprint doi: https://doi.org/10.1101/2024.12.02.626368; this version posted December 5, 2024. The copyright holder for this preprint (which was not certified by peer review) is the author/funder. All rights reserved. No reuse allowed without permission.

reported directly in the diagrams. Boxplots are shown with the center line depicting the median value, the box limits showing the top and bottom quartiles, and the whiskers showing the 1.5x interquartile range. Linear regression plots are shown with the 95% confidence interval. Data handling, statistical testing, and plotting were conducted using Microsoft Excel 2019, R version 4.3.2, GraphPad Prism 9, and with Seaborn-0.11.0[104] and Matplotlib-3.3.0[105] in Python 3.6.10.

***C. elegans* strains used for this study**

Strain	description	Genotype	origin
N2 Bristol	wild type		CGC
GN112	AFD split caspase ablated - AFD:SCA	*pgIs2 [gcy-8p::TU#813 + gcy-8p::TU#814 + unc-122p::GFP + gcy-8p::mCherry + gcy-8p::GFP + ttx-3p::GFP].*	CGC
BFF96	AFD neuron specific trangenic hitamine gated cloride channel expressing strain	*pgcy-8::HisCl1::SL2::mCherry::rab-3 3'UTR, pgcy-8::GCaMP6::rab-3 3'UTR; rol-6(GOF)*	Rechavi lab
BJS1062	The integrated version of of the BFF96 - AFD:HisCl1	*pgcy-8::HisCl1::SL2::mCherry::rab-3 3'UTR, pgcy-8::GCaMP6::rab-3 3'UTR; rol-6(GOF)*	Generated by us
IK597	AFD triple mutant	*gcy-23(nj37) gcy-8(oy44) gcy-18(nj38) IV.*	CGC

Primers used for this study

Name	Purpose	Sequence 5' - 3'
tbg-1F	RT-qPCR housekeeper gene	CAATGTGCCCATCAATTCGG
tbg-1R	RT-qPCR housekeeper gene	AACAAGAAGCGAGTGACGTC
act-1-F	RT-qPCR housekeeper gene	CCACCATGTACCCAGGAATT
act-1-R	RT-qPCR housekeeper gene	AGAGGGAAGCGAGGATAGAT
eif-3.C-F	RT-qPCR housekeeper gene	ACACTTGACGAGCCCACCGAC
eif-3.C-R	RT-qPCR housekeeper gene	TGCCGCTCGTTCCTTCCTGG
rpl-32 - F	RT-qPCR housekeeper gene	CAAGGTCGTCAAGAAGAAGC
rpl-32 - R	RT-qPCR housekeeper gene	GGCTACACGACGGTATCTGT
Tc1(D) - F	RT-qPCR target gene	ACCAGCACTTCCATGGGCCC
Tc1(D) - R	RT-qPCR target gene	ACGAAGCCACGGCCCACATT
Tc1(E) - F	RT-qPCR target gene	TCGCTTTGAGAATCTCGCCCGG
Tc1(E) - R	RT-qPCR target gene	CGTGGCGGTCCTATGCGGAT
Mirage(D) - F	RT-qPCR target gene	AGCTTCTCCCCAGGCCCTCA

bioRxiv preprint doi: https://doi.org/10.1101/2024.12.02.626368; this version posted December 5, 2024. The copyright holder for this preprint (which was not certified by peer review) is the author/funder. All rights reserved. No reuse allowed without permission.

Mirage(D) - R	RT-qPCR target gene	ATCCGCTTTCCAGGCCACTCC
Mirage(E) - F	RT-qPCR target gene	ACGGGGAAATTCGTTATCCGGTCG
Mirage(E) - R	RT-qPCR target gene	ACAGTTGACTTCGCTCGTCGCA
unc-22B-F1	genotyping *unc-22:Tc1* locus	TTTTGAGACACCCGACGCTT
unc-22B-R1	genotyping *unc-22:Tc1* locus	GTGGTGGTGGCAGGATGATT
unc-22B-F2	genotyping *unc-22:Tc1* locus	CGTGTCACTGGACTTCGTCA
unc-22B-R2	genotyping *unc-22:Tc1* locus	ATGGGCGGTGAGTCCAAAAT
unc-22B-F3	genotyping *unc-22:Tc1* locus	TCACGGAAGGCCACGAATAC
unc-22B-R3	genotyping *unc-22:Tc1* locus	GAAGTCCAGTGACACGAGCA
unc-22B-F4	genotyping *unc-22:Tc1* locus	ACAACATTTTGATTTTCAGTTCCG
unc-22B-R4	genotyping *unc-22:Tc1* locus	TGGAGCAGACGGTCTATCTT
unc-22B-F5	genotyping *unc-22:Tc1* locus	CCATCTGCAATGCGATCTGA
unc-22B-R5	genotyping *unc-22:Tc1* locus	GACACGGAACTGAAAATCAAAATG
unc-22B-F6	genotyping *unc-22:Tc1* locus	ACTTCTTATTTCAGAACCGCCG
unc-22B-R6	genotyping *unc-22:Tc1* locus	TTCCGCATTCTTGCCAGTCT
unc-22B-F7	genotyping *unc-22:Tc1* locus	TACGCCACGTGTAAGACCAC
unc-22B-R7	genotyping *unc-22:Tc1* locus	GGCAACGGGTTCAGGAAACT
gcy-8-F1	genotyping AFD triple mutant	ATGGGTCTTCCCACGAGAAAAC
gcy-8-R1	genotyping AFD triple mutant	GAGAACATTGGATTCACGGACC
gcy-8-F2	genotyping AFD triple mutant	AATCCCAAAGAAGCTGGCCTAC
gcy-8-R2	genotyping AFD triple mutant	GACAGCTAGTACATGGGTGAGC
gcy-18-F1	genotyping AFD triple mutant	ATCGCTACAAACACCGGAAG
gcy-18-R1	genotyping AFD triple mutant	CCGATGAATAAAGCTTCGGA
gcy-18-F2	genotyping AFD triple mutant	TCGAAGAAATCATGCACAGG
gcy-18-R2	genotyping AFD triple mutant	CGTAGGCTGGTAGGAGTTGG
gcy-23-F1	genotyping AFD triple mutant	CGGTTTATGCGGCATTCTAT
gcy-23-R1	genotyping AFD triple mutant	AGACTCCATTCTCGAGGCAA
gcy-23-F2	genotyping AFD triple mutant	AACTGGATTCTGGCCGTCTA
gcy-23-R2	genotyping AFD triple mutant	ATAGGCAATAACGAGGTGCG
mut-16(mg461)F	genotyping AFD triple mutant for *mut-16(mg461)* background	CCCGCCGATACAGAAACTAA
mut-16(mg461)R	genotyping AFD triple mutant for *mut-16(mg461)* background	AATATTCGATCGGCAAGCAG

bioRxiv preprint doi: https://doi.org/10.1101/2024.12.02.626368; this version posted December 5, 2024. The copyright holder for this preprint (which was not certified by peer review) is the author/funder. All rights reserved. No reuse allowed without permission.

Key resources, consumables, instruments used for this study

Reagents:	**Source**	**Identifier**
Nematode growth medium (NGM) agar	[78]	
M9 buffer	[78]	
Trizol® reagent	Invitrogen	15596018
Bromochloropropane (BCP)	Sigma-Aldrich	B9673
SuperScript® III Reverse Transcriptase	Invitrogen	18080085
PowerUp™ SYBR™ Green Master Mix	Thermo Fisher Scientific	A25742
Histamine dihydrochloride	Sigma	H7250-10G
Nicotine	Sigma	N3876
Materials:		
qPCR plates (96 x 0.1 ml plate)	BIOplastics	B60101
200 µl wide-bore pipette tips	Merck	AXYT205WBCRS
1 ml wide-bore pipette tips	Merck	AXYT1005WBCRS
E. coli OP50 strain	CGC	N/A
E. coli NA22 strain	CGC	N/A
QIAGEN Puregene Cell and Tissue Kit	QIAGEN	158388
Qiagen RNeasy Mini Kit®	QIAGEN	175032139
Instruments and Machines:		
Biobeam 8000	Eckert & Ziegler, Gamma Service Medical GmbH	
Centrifuge	Eppendorf	5424 R
Nanodrop spectrophotometer	Thermo Scientific	N/A
CFX Connect real-time PCR detection system	BioRad	#1855201
CFX96 Touch real-time PCR detection system	BioRad	#1854096
Agilent TapeStation System	Agilent	Agilent
Dissecting microscope	Leica	CLS 150X
Axio Imager.M2	Carl Zeiss	N/A
Softwares:		
CFX Manager Software	BioRad	#1845000
Microsoft Excel 2019	Microsoft	
R version 4.3.2		

bioRxiv preprint doi: https://doi.org/10.1101/2024.12.02.626368; this version posted December 5, 2024. The copyright holder for this preprint (which was not certified by peer review) is the author/funder. All rights reserved. No reuse allowed without permission.

GraphPad Prism 9	GraphPad	

Declaration of generative AI and AI-assisted technologies in the writing process.

During the preparation of this work the authors used OpenAI ChatGPT-4o (2023) in order to grammatically proofread the text. After using this tool/service, the authors reviewed and edited the content as needed and take full responsibility for the content of the published article.

Data availability statement

The RNA-seq data are available from the Gene Expression Omnibus (GEO) under the accession number GSE282988.

The proteomics data used in this study have been deposited to the PRIDE database with the accession number PXD056414.

The whole genome sequencing data are available in the BioProject database under the accession number PRJNA1190919.

References

1. Wang, Y., Su, M., Chen, Y., Huang, X., Ruan, L., Lv, Q., and Li, L. (2023). Research progress on the role and mechanism of DNA damage repair in germ cell development. Front Endocrinol (Lausanne) *14*, 1234280. https://doi.org/10.3389/fendo.2023.1234280.

2. Stergiou, L., and Hengartner, M.O. (2004). Death and more: DNA damage response pathways in the nematode C. elegans. Cell Death Differ *11*, 21–28. https://doi.org/10.1038/sj.cdd.4401340.

3. Bujarrabal-Dueso, A., Sendtner, G., Meyer, D.H., Chatzinikolaou, G., Stratigi, K., Garinis, G.A., and Schumacher, B. (2023). The DREAM complex functions as conserved master regulator of somatic DNA-repair capacities. Nat Struct Mol Biol *30*, 475–488. https://doi.org/10.1038/s41594-023-00942-8.

4. Tóth, K.F., Pezic, D., Stuwe, E., and Webster, A. (2016). The piRNA Pathway Guards the Germline Genome Against Transposable Elements. Adv Exp Med Biol *886*, 51–77. https://doi.org/10.1007/978-94-017-7417-8_4.

5. Weng, C., Kosalka, J., Berkyurek, A.C., Stempor, P., Feng, X., Mao, H., Zeng, C., Li, W.-J., Yan, Y.-H., Dong, M.-Q., et al. (2019). The USTC co-opts an ancient machinery to drive piRNA transcription in C. elegans. Genes Dev *33*, 90–102. https://doi.org/10.1101/gad.319293.118.

bioRxiv preprint doi: https://doi.org/10.1101/2024.12.02.626368; this version posted December 5, 2024. The copyright holder for this preprint (which was not certified by peer review) is the author/funder. All rights reserved. No reuse allowed without permission.

6. Weismann, A. (1893). The Germ-plasm: a theory of heredity. Translated by W. Newton Parker and Harriet Rönnfeldt (Scribner) https://doi.org/10.5962/bhl.title.25196.

7. Rechavi, O., and Lev, I. (2017). Principles of Transgenerational Small RNA Inheritance in Caenorhabditis elegans. Current Biology *27*, R720–R730. https://doi.org/10.1016/j.cub.2017.05.043.

8. Ryan, C.P., Brownlie, J.C., and Whyard, S. (2016). Hsp90 and Physiological Stress Are Linked to Autonomous Transposon Mobility and Heritable Genetic Change in Nematodes. Genome Biology and Evolution *8*, 3794–3805. https://doi.org/10.1093/gbe/evw284.

9. Rogers, A.K., and Phillips, C.M. (2020). RNAi pathways repress reprogramming of C. elegans germ cells during heat stress. Nucleic Acids Research *48*, 4256–4273. https://doi.org/10.1093/nar/gkaa174.

10. Kurhanewicz, N.A., Dinwiddie, D., Bush, Z.D., and Libuda, D.E. (2020). Elevated temperatures cause transposon-associated DNA damage in C. elegans spermatocytes. Curr Biol *30*, 5007-5017.e4. https://doi.org/10.1016/j.cub.2020.09.050.

11. Sijen, T., and Plasterk, R.H.A. (2003). Transposon silencing in the Caenorhabditis elegans germ line by natural RNAi. Nature *426*, 310–314. https://doi.org/10.1038/nature02107.

12. Tabara, H., Sarkissian, M., Kelly, W.G., Fleenor, J., Grishok, A., Timmons, L., Fire, A., and Mello, C.C. (1999). The rde-1 Gene, RNA Interference, and Transposon Silencing in C. elegans. Cell *99*, 123–132. https://doi.org/10.1016/S0092-8674(00)81644-X.

13. Ketting, R.F., Fischer, S.E.J., and Plasterk, R.H.A. (1997). Target choice determinants of the Tc1 transposon of Caenorhabditis elegans. Nucleic Acids Research *25*, 4041–4047. https://doi.org/10.1093/nar/25.20.4041.

14. Ketting, R.F., Haverkamp, T.H.A., Luenen, H.G.A.M. van, and Plasterk, R.H.A. (1999). mut-7 of C. elegans, Required for Transposon Silencing and RNA Interference, Is a Homolog of Werner Syndrome Helicase and RNaseD. Cell *99*, 133–141. https://doi.org/10.1016/S0092-8674(00)81645-1.

15. Fischer, S.E.J. (2024). Activity and Silencing of Transposable Elements in C. elegans. DNA *4*, 129–140. https://doi.org/10.3390/dna4020007.

16. Curran, S.P., Wu, X., Riedel, C.G., and Ruvkun, G. (2009). A soma-to-germline transformation in long-lived Caenorhabditis elegans mutants. Nature *459*, 1079–1084. https://doi.org/10.1038/nature08106.

17. Uszkoreit, S., Meyer, D.H., Rechavi, O., and Schumacher, B. (2022). Sensory neurons safeguard from mutational inheritance by controlling the CEP-1/p53-mediated DNA damage response in primordial germ cells. Preprint at bioRxiv, https://doi.org/10.1101/2022.07.19.500657 https://doi.org/10.1101/2022.07.19.500657.

bioRxiv preprint doi: https://doi.org/10.1101/2024.12.02.626368; this version posted December 5, 2024. The copyright holder for this preprint (which was not certified by peer review) is the author/funder. All rights reserved. No reuse allowed without permission.

18. Ermolaeva, M.A., Segref, A., Dakhovnik, A., Ou, H.-L., Schneider, J.I., Utermöhlen, O., Hoppe, T., and Schumacher, B. (2013). DNA damage in germ cells induces an innate immune response that triggers systemic stress resistance. Nature *501*, 416–420. https://doi.org/10.1038/nature12452.

19. Kasper, D.M., Gardner, K.E., and Reinke, V. (2014). Homeland security in the C. elegans germ line: Insights into the biogenesis and function of piRNAs. Epigenetics *9*, 62–74. https://doi.org/10.4161/epi.26647.

20. Bagijn, M.P., Goldstein, L.D., Sapetschnig, A., Weick, E.-M., Bouasker, S., Lehrbach, N.J., Simard, M.J., and Miska, E.A. (2012). Function, Targets, and Evolution of Caenorhabditis elegans piRNAs. Science *337*, 574–578. https://doi.org/10.1126/science.1220952.

21. Lee, H.-C., Gu, W., Shirayama, M., Youngman, E., Conte, D., and Mello, C.C. (2012). *C. elegans* piRNAs Mediate the Genome-wide Surveillance of Germline Transcripts. Cell *150*, 78–87. https://doi.org/10.1016/j.cell.2012.06.016.

22. Das, P.P., Bagijn, M.P., Goldstein, L.D., Woolford, J.R., Lehrbach, N.J., Sapetschnig, A., Buhecha, H.R., Gilchrist, M.J., Howe, K.L., Stark, R., et al. (2008). Piwi and piRNAs Act Upstream of an Endogenous siRNA Pathway to Suppress Tc3 Transposon Mobility in the *Caenorhabditis elegans* Germline. Molecular Cell *31*, 79–90. https://doi.org/10.1016/j.molcel.2008.06.003.

23. Kimura, K.D., Miyawaki, A., Matsumoto, K., and Mori, I. (2004). The *C. elegans* Thermosensory Neuron AFD Responds to Warming. Current Biology *14*, 1291–1295. https://doi.org/10.1016/j.cub.2004.06.060.

24. Clark, D.A., Biron, D., Sengupta, P., and Samuel, A.D.T. (2006). The AFD Sensory Neurons Encode Multiple Functions Underlying Thermotactic Behavior in Caenorhabditis elegans. J. Neurosci. *26*, 7444–7451. https://doi.org/10.1523/JNEUROSCI.1137-06.2006.

25. Goodman, M.B., and Sengupta, P. (2018). The extraordinary AFD thermosensor of C. elegans. Pflugers Arch *470*, 839–849. https://doi.org/10.1007/s00424-017-2089-5.

26. Wang, D., O'Halloran, D., and Goodman, M.B. (2013). GCY-8, PDE-2, and NCS-1 are critical elements of the cGMP-dependent thermotransduction cascade in the AFD neurons responsible for C. elegans thermotaxis. Journal of General Physiology *142*, 437–449. https://doi.org/10.1085/jgp.201310959.

27. Prahlad, V., Cornelius, T., and Morimoto, R.I. (2008). Regulation of the Cellular Heat Shock Response in Caenorhabditis elegans by Thermosensory Neurons. Science *320*, 811–814. https://doi.org/10.1126/science.1156093.

28. Posner, R., Toker, I.A., Antonova, O., Star, E., Anava, S., Azmon, E., Hendricks, M., Bracha, S., Gingold, H., and Rechavi, O. (2019). Neuronal Small RNAs Control Behavior Transgenerationally. Cell *177*, 1814-1826.e15. https://doi.org/10.1016/j.cell.2019.04.029.

bioRxiv preprint doi: https://doi.org/10.1101/2024.12.02.626368; this version posted December 5, 2024. The copyright holder for this preprint (which was not certified by peer review) is the author/funder. All rights reserved. No reuse allowed without permission.

29. Devanapally, S., Ravikumar, S., and Jose, A.M. (2015). Double-stranded RNA made in C. elegans neurons can enter the germline and cause transgenerational gene silencing. Proc Natl Acad Sci U S A *112*, 2133–2138. https://doi.org/10.1073/pnas.1423333112.

30. Wallis, D.C., Nguyen, D.A.H., Uebel, C.J., and Phillips, C.M. (2019). Visualization and Quantification of Transposon Activity in Caenorhabditis elegans RNAi Pathway Mutants. G3 (Bethesda) *9*, 3825–3832. https://doi.org/10.1534/g3.119.400639.

31. Pokala, N., Liu, Q., Gordus, A., and Bargmann, C.I. (2014). Inducible and titratable silencing of Caenorhabditis elegans neurons in vivo with histamine-gated chloride channels. Proceedings of the National Academy of Sciences *111*, 2770–2775. https://doi.org/10.1073/pnas.1400615111.

32. El Mouridi, S., AlHarbi, S., and Frøkjær-Jensen, C. A histamine-gated channel is an efficient negative selection marker for C. elegans transgenesis. MicroPubl Biol *2021*, 10.17912/micropub.biology.000349. https://doi.org/10.17912/micropub.biology.000349.

33. Dishart, J.G., Pender, C.L., Shen, K., Zhang, H., Ly, M., Webb, M.B., and Dillin, A. (2024). Olfaction regulates peripheral mitophagy and mitochondrial function. Science Advances *10*, eadn0014. https://doi.org/10.1126/sciadv.adn0014.

34. Inada, H., Ito, H., Satterlee, J., Sengupta, P., Matsumoto, K., and Mori, I. (2006). Identification of Guanylyl Cyclases That Function in Thermosensory Neurons of Caenorhabditis elegans. Genetics *172*, 2239–2252. https://doi.org/10.1534/genetics.105.050013.

35. Takeishi, A., Yu, Y.V., Hapiak, V.M., Bell, H.W., O'Leary, T., and Sengupta, P. (2016). Receptor-type Guanylyl Cyclases Confer Thermosensory Responses in C. elegans. Neuron *90*, 235–244. https://doi.org/10.1016/j.neuron.2016.03.002.

36. Yu, Y.V., Bell, H.W., Glauser, D., Van Hooser, S.D., Goodman, M.B., and Sengupta, P. (2014). CaMKI-dependent regulation of sensory gene expression mediates experience-dependent plasticity in the operating range of a thermosensory neuron. Neuron *84*, 919–926. https://doi.org/10.1016/j.neuron.2014.10.046.

37. Ippolito, D., Thapliyal, S., and Glauser, D.A. (2021). Ca2+/CaM binding to CaMKI promotes IMA-3 importin binding and nuclear translocation in sensory neurons to control behavioral adaptation. eLife *10*, e71443. https://doi.org/10.7554/eLife.71443.

38. Kobayashi, K., Nakano, S., Amano, M., Tsuboi, D., Nishioka, T., Ikeda, S., Yokoyama, G., Kaibuchi, K., and Mori, I. (2016). Single-Cell Memory Regulates a Neural Circuit for Sensory Behavior. Cell Reports *14*, 11–21. https://doi.org/10.1016/j.celrep.2015.11.064.

39. mut-16(mg461), an RNAi-defective mutation found in the background of several strains (2009). The WBG. http://wbg.wormbook.org/2009/12/01/mut-16mg461-an-rnai-defective-mutation-found-in-the-background-of-several-strains/.

bioRxiv preprint doi: https://doi.org/10.1101/2024.12.02.626368; this version posted December 5, 2024. The copyright holder for this preprint (which was not certified by peer review) is the author/funder. All rights reserved. No reuse allowed without permission.

40. Servello, F.A., Fernandes, R., Eder, M., Harris, N., Martin, O.M., Oswal, N., Lindberg, A., Derosiers, N., Sengupta, P., Stroustrup, N., et al. (2022). Neuronal temperature perception induces specific defenses that enable C. elegans to cope with the enhanced reactivity of hydrogen peroxide at high temperature. eLife *11*, e78941. https://doi.org/10.7554/eLife.78941.

41. Claycomb, J.M., Batista, P.J., Pang, K.M., Gu, W., Vasale, J.J., Wolfswinkel, J.C. van, Chaves, D.A., Shirayama, M., Mitani, S., Ketting, R.F., et al. (2009). The Argonaute CSR-1 and its 22G-RNA co-factors target germline genes and are required for holocentric chromosome segregation. Cell *139*, 123. https://doi.org/10.1016/j.cell.2009.09.014.

42. Seth, M., Shirayama, M., Gu, W., Ishidate, T., Darryl Conte, J., and Mello, C.C. (2013). The C. elegans CSR-1 Argonaute pathway counteracts epigenetic silencing to promote germline gene expression. Developmental cell *27*, 656. https://doi.org/10.1016/j.devcel.2013.11.014.

43. Kirshner, J.A., Picard, C.L., Weiser, N.E., Mehta, N., Feng, S., Murphy, V.N., Vakhnovetsky, A., Alessi, A.F., Xiao, C., Inoki, K., et al. (2024). MORC-1 is a key component of the C. elegans CSR-1 germline gene licensing mechanism. Preprint at bioRxiv, https://doi.org/10.1101/2024.10.02.616347 https://doi.org/10.1101/2024.10.02.616347.

44. Aljohani, M.D., El Mouridi, S., Priyadarshini, M., Vargas-Velazquez, A.M., and Frøkjær-Jensen, C. (2020). Engineering rules that minimize germline silencing of transgenes in simple extrachromosomal arrays in C. elegans. Nat Commun *11*, 6300. https://doi.org/10.1038/s41467-020-19898-0.

45. Padeken, J., Methot, S., Zeller, P., Delaney, C.E., Kalck, V., and Gasser, S.M. (2021). Argonaute NRDE-3 and MBT domain protein LIN-61 redundantly recruit an H3K9me3 HMT to prevent embryonic lethality and transposon expression. Genes Dev. *35*, 82–101. https://doi.org/10.1101/gad.344234.120.

46. Lee, S.-J., and Kenyon, C. (2009). Regulation of the Longevity Response to Temperature by Thermosensory Neurons in Caenorhabditis elegans. Current Biology *19*, 715–722. https://doi.org/10.1016/j.cub.2009.03.041.

47. Tatum, M.C., Ooi, F.K., Chikka, M.R., Chauve, L., Martinez-Velazquez, L.A., Steinbusch, H.W.M., Morimoto, R.I., and Prahlad, V. (2015). Neuronal Serotonin Release Triggers the Heat Shock Response in C. elegans in the Absence of Temperature Increase. Current Biology *25*, 163–174. https://doi.org/10.1016/j.cub.2014.11.040.

48. Chen, Y.-C., Chen, H.-J., Tseng, W.-C., Hsu, J.-M., Huang, T.-T., Chen, C.-H., and Pan, C.-L. (2016). A C. elegans Thermosensory Circuit Regulates Longevity through crh-1/CREB-Dependent flp-6 Neuropeptide Signaling. Developmental Cell *39*, 209–223. https://doi.org/10.1016/j.devcel.2016.08.021.

bioRxiv preprint doi: https://doi.org/10.1101/2024.12.02.626368; this version posted December 5, 2024. The copyright holder for this preprint (which was not certified by peer review) is the author/funder. All rights reserved. No reuse allowed without permission.

49. Soltanmohammadi, N., Wang, S., and Schumacher, B. (2022). Somatic PMK-1/p38 signaling links environmental stress to germ cell apoptosis and heritable euploidy. Nat Commun *13*, 701. https://doi.org/10.1038/s41467-022-28225-8.

50. Akay, A., Di Domenico, T., Suen, K.M., Nabih, A., Parada, G.E., Larance, M., Medhi, R., Berkyurek, A.C., Zhang, X., Wedeles, C.J., et al. (2017). The Helicase Aquarius/EMB-4 Is Required to Overcome Intronic Barriers to Allow Nuclear RNAi Pathways to Heritably Silence Transcription. Dev Cell *42*, 241-255.e6. https://doi.org/10.1016/j.devcel.2017.07.002.

51. Ohta, A., Sato, Y., Isono, K., Kajino, T., Tanaka, K., Taji, T., and Kuhara, A. (2024). The intron binding protein EMB-4 is an opposite regulator of cold and high temperature tolerance in Caenorhabditis elegans. PNAS Nexus *3*, pgae293. https://doi.org/10.1093/pnasnexus/pgae293.

52. Corrêa, R.L., Steiner, F.A., Berezikov, E., and Ketting, R.F. (2010). MicroRNA–Directed siRNA Biogenesis in Caenorhabditis elegans. PLOS Genetics *6*, e1000903. https://doi.org/10.1371/journal.pgen.1000903.

53. Wu, Z., Senchuk, M.M., Dues, D.J., Johnson, B.K., Cooper, J.F., Lew, L., Machiela, E., Schaar, C.E., DeJonge, H., Blackwell, T.K., et al. (2018). Mitochondrial unfolded protein response transcription factor ATFS-1 promotes longevity in a long-lived mitochondrial mutant through activation of stress response pathways. BMC Biology *16*, 147. https://doi.org/10.1186/s12915-018-0615-3.

54. Jiang, H., Guo, R., and Powell-Coffman, J.A. (2001). The Caenorhabditis elegans hif-1 gene encodes a bHLH-PAS protein that is required for adaptation to hypoxia. Proceedings of the National Academy of Sciences of the United States of America *98*, 7916. https://doi.org/10.1073/pnas.141234698.

55. Doering, K.R., Cheng, X., Milburn, L., Ratnappan, R., Ghazi, A., Miller, D.L., and Taubert, S. (2022). Nuclear hormone receptor NHR-49 acts in parallel with HIF-1 to promote hypoxia adaptation in Caenorhabditis elegans. eLife *11*, e67911. https://doi.org/10.7554/eLife.67911.

56. Bai, H., Zou, W., Zhou, W., Zhang, K., and Huang, X. (2021). Deficiency of Innate Immunity against Pseudomonas aeruginosa Enhances Behavioral Avoidance via the HECW-1/NPR-1 Module in Caenorhabditis elegans. Infection and Immunity *89*. https://doi.org/10.1128/iai.00067-21.

57. Edmonds, J.W., McKinney, S.L., Prasain, J.K., and Miller, M.A. (2011). The gap junctional protein INX-14 functions in oocyte precursors to promote C. elegans sperm guidance. Dev Biol *359*, 47–58. https://doi.org/10.1016/j.ydbio.2011.08.014.

bioRxiv preprint doi: https://doi.org/10.1101/2024.12.02.626368; this version posted December 5, 2024. The copyright holder for this preprint (which was not certified by peer review) is the author/funder. All rights reserved. No reuse allowed without permission.

58. Tran, T.D., and Luallen, R.J. (2024). An organismal understanding of *C. elegans* innate immune responses, from pathogen recognition to multigenerational resistance. Seminars in Cell & Developmental Biology *154*, 77–84. https://doi.org/10.1016/j.semcdb.2023.03.005.

59. Singh, V., and Aballay, A. (2012). Endoplasmic reticulum stress pathway required for immune homeostasis is neurally controlled by arrestin-1. J Biol Chem *287*, 33191–33197. https://doi.org/10.1074/jbc.M112.398362.

60. Mertenskötter, A., Keshet, A., Gerke, P., and Paul, R.J. (2013). The p38 MAPK PMK-1 shows heat-induced nuclear translocation, supports chaperone expression, and affects the heat tolerance of *Caenorhabditis elegan*s. Cell Stress and Chaperones *18*, 293–306. https://doi.org/10.1007/s12192-012-0382-y.

61. Alam, T., Maruyama, H., Li, C., Pastuhov, S.I., Nix, P., Bastiani, M., Hisamoto, N., and Matsumoto, K. (2016). Axotomy-induced HIF-serotonin signalling axis promotes axon regeneration in C. elegans. Nat Commun *7*, 10388. https://doi.org/10.1038/ncomms10388.

62. Das, S., Ooi, F.K., Cruz Corchado, J., Fuller, L.C., Weiner, J.A., and Prahlad, V. (2020). Serotonin signaling by maternal neurons upon stress ensures progeny survival. eLife *9*, e55246. https://doi.org/10.7554/eLife.55246.

63. Berendzen, K.M., Durieux, J., Shao, L.-W., Tian, Y., Kim, H., Wolff, S., Liu, Y., and Dillin, A. (2016). Neuroendocrine Coordination of Mitochondrial Stress Signaling and Proteostasis. Cell *166*, 1553-1563.e10. https://doi.org/10.1016/j.cell.2016.08.042.

64. Littlejohn, N.K., Seban, N., Liu, C.-C., and Srinivasan, S. (2020). A feedback loop governs the relationship between lipid metabolism and longevity. eLife *9*, e58815. https://doi.org/10.7554/eLife.58815.

65. Mori, I., Benian, G.M., Moerman, D.G., and Waterston, R.H. (1988). Transposable Element Tc1 of Caenorhabditis elegans Recognizes Specific Target Sequences for Integration. Proceedings of the National Academy of Sciences of the United States of America *85*, 861–864.

66. Benian, G.M., L'Hernault, S.W., and Morris, M.E. (1993). Additional sequence complexity in the muscle gene, unc-22, and its encoded protein, twitchin, of Caenorhabditis elegans. Genetics *134*, 1097–1104. https://doi.org/10.1093/genetics/134.4.1097.

67. Moerman, D.G., Benian, G.M., and Waterston, R.H. (1986). Molecular cloning of the muscle gene unc-22 in Caenorhabditis elegans by Tc1 transposon tagging. Proc Natl Acad Sci U S A *83*, 2579–2583. https://doi.org/10.1073/pnas.83.8.2579.

68. Sang, Y., Gao, B., Diaby, M., Zong, W., Chen, C., Shen, D., Wang, S., Wang, Y., Ivics, Z., and Song, C. (2019). Incomer, a DD36E family of Tc1/mariner transposons newly discovered in animals. Mobile DNA *10*, 45. https://doi.org/10.1186/s13100-019-0188-x.

bioRxiv preprint doi: https://doi.org/10.1101/2024.12.02.626368; this version posted December 5, 2024. The copyright holder for this preprint (which was not certified by peer review) is the author/funder. All rights reserved. No reuse allowed without permission.

69. Dupeyron, M., Baril, T., Bass, C., and Hayward, A. (2020). Phylogenetic analysis of the Tc1/mariner superfamily reveals the unexplored diversity of pogo-like elements. Mobile DNA *11*, 21. https://doi.org/10.1186/s13100-020-00212-0.

70. Plasterk, R.H.A., Izsvák, Z., and Ivics, Z. (1999). Resident aliens: the Tc1/*mariner* superfamily of transposable elements. Trends in Genetics *15*, 326–332. https://doi.org/10.1016/S0168-9525(99)01777-1.

71. Tosi, L.R.O., and Beverley, S.M. (2000). cis and trans factors affecting Mos1 mariner evolution and transposition in vitro, and its potential for functional genomics. Nucleic Acids Res *28*, 784–790.

72. Vos, J.C., De Baere, I., and Plasterk, R.H. (1996). Transposase is the only nematode protein required for in vitro transposition of Tc1. Genes Dev *10*, 755–761. https://doi.org/10.1101/gad.10.6.755.

73. Lampe, D.J., Churchill, M.E., and Robertson, H.M. (1996). A purified mariner transposase is sufficient to mediate transposition in vitro. EMBO J *15*, 5470–5479.

74. Fischer, S.E.J., Wienholds, E., and Plasterk, R.H.A. (2003). Continuous Exchange of Sequence Information Between Dispersed Tc1 Transposons in the Caenorhabditis elegans Genome. Genetics *164*, 127–134. https://doi.org/10.1093/genetics/164.1.127.

75. Pabis, K., Barardo, D., Sirbu, O., Selvarajoo, K., Gruber, J., and Kennedy, B.K. (2023). A concerted increase in readthrough and intron retention drives transposon expression during aging and senescence. Preprint at bioRxiv, https://doi.org/10.1101/2022.12.29.522277 https://doi.org/10.1101/2022.12.29.522277.

76. Galhardo, R.S., Hastings, P.J., and Rosenberg, S.M. (2007). Mutation as a stress response and the regulation of evolvability. Crit Rev Biochem Mol Biol *42*, 399–435. https://doi.org/10.1080/10409230701648502.

77. Foster, P.L. (2007). Stress-induced mutagenesis in bacteria. Crit Rev Biochem Mol Biol *42*, 373–397. https://doi.org/10.1080/10409230701648494.

78. Stiernagle, T. (2006). Maintenance of C. elegans. WormBook. https://doi.org/10.1895/wormbook.1.101.1.

79. Chambers, M.C., Maclean, B., Burke, R., Amodei, D., Ruderman, D.L., Neumann, S., Gatto, L., Fischer, B., Pratt, B., Egertson, J., et al. (2012). A cross-platform toolkit for mass spectrometry and proteomics. Nat Biotechnol *30*, 918–920. https://doi.org/10.1038/nbt.2377.

80. Tyanova, S., Temu, T., Sinitcyn, P., Carlson, A., Hein, M.Y., Geiger, T., Mann, M., and Cox, J. (2016). The Perseus computational platform for comprehensive analysis of (prote)omics data. Nat Methods *13*, 731–740. https://doi.org/10.1038/nmeth.3901.

bioRxiv preprint doi: https://doi.org/10.1101/2024.12.02.626368; this version posted December 5, 2024. The copyright holder for this preprint (which was not certified by peer review) is the author/funder. All rights reserved. No reuse allowed without permission.

81. Chen, S., Zhou, Y., Chen, Y., and Gu, J. (2018). fastp: an ultra-fast all-in-one FASTQ preprocessor. Bioinformatics *34*, i884–i890. https://doi.org/10.1093/bioinformatics/bty560.

82. Patro, R., Duggal, G., Love, M.I., Irizarry, R.A., and Kingsford, C. (2017). Salmon provides fast and bias-aware quantification of transcript expression. Nat Methods *14*, 417–419. https://doi.org/10.1038/nmeth.4197.

83. Davis, P., Zarowiecki, M., Arnaboldi, V., Becerra, A., Cain, S., Chan, J., Chen, W.J., Cho, J., da Veiga Beltrame, E., Diamantakis, S., et al. (2022). WormBase in 2022-data, processes, and tools for analyzing Caenorhabditis elegans. Genetics *220*, iyac003. https://doi.org/10.1093/genetics/iyac003.

84. Soneson, C., Love, M.I., and Robinson, M.D. (2015). Differential analyses for RNA-seq: transcript-level estimates improve gene-level inferences. F1000Res *4*, 1521. https://doi.org/10.12688/f1000research.7563.2.

85. Robinson, M.D., McCarthy, D.J., and Smyth, G.K. (2010). edgeR: a Bioconductor package for differential expression analysis of digital gene expression data. Bioinformatics *26*, 139–140. https://doi.org/10.1093/bioinformatics/btp616.

86. Szklarczyk, D., Kirsch, R., Koutrouli, M., Nastou, K., Mehryary, F., Hachilif, R., Gable, A.L., Fang, T., Doncheva, N.T., Pyysalo, S., et al. (2023). The STRING database in 2023: protein-protein association networks and functional enrichment analyses for any sequenced genome of interest. Nucleic Acids Res *51*, D638–D646. https://doi.org/10.1093/nar/gkac1000.

87. Zou, Z., Ohta, T., and Oki, S. (2024). ChIP-Atlas 3.0: a data-mining suite to explore chromosome architecture together with large-scale regulome data. Nucleic Acids Research *52*, W45–W53. https://doi.org/10.1093/nar/gkae358.

88. Yang, W., Dierking, K., and Schulenburg, H. (2016). WormExp: a web-based application for a Caenorhabditis elegans-specific gene expression enrichment analysis. Bioinformatics *32*, 943–945. https://doi.org/10.1093/bioinformatics/btv667.

89. Korotkevich, G., Sukhov, V., Budin, N., Shpak, B., Artyomov, M.N., and Sergushichev, A. (2021). Fast gene set enrichment analysis. Preprint at bioRxiv, https://doi.org/10.1101/060012 https://doi.org/10.1101/060012.

90. Rauluseviciute, I., Riudavets-Puig, R., Blanc-Mathieu, R., Castro-Mondragon, J.A., Ferenc, K., Kumar, V., Lemma, R.B., Lucas, J., Chèneby, J., Baranasic, D., et al. (2024). JASPAR 2024: 20th anniversary of the open-access database of transcription factor binding profiles. Nucleic Acids Research *52*, D174–D182. https://doi.org/10.1093/nar/gkad1059.

91. Heinz, S., Benner, C., Spann, N., Bertolino, E., Lin, Y.C., Laslo, P., Cheng, J.X., Murre, C., Singh, H., and Glass, C.K. (2010). Simple combinations of lineage-determining transcription factors

bioRxiv preprint doi: https://doi.org/10.1101/2024.12.02.626368; this version posted December 5, 2024. The copyright holder for this preprint (which was not certified by peer review) is the author/funder. All rights reserved. No reuse allowed without permission.

prime cis-regulatory elements required for macrophage and B cell identities. Molecular cell *38*, 576. https://doi.org/10.1016/j.molcel.2010.05.004.

92. Zhang, X., Wang, Y., Cai, Z., Wan, Z., Aihemaiti, Y., and Tu, H. (2023). A gonadal gap junction INX-14/Notch GLP-1 signaling axis suppresses gut defense through an intestinal lysosome pathway. Front Immunol *14*, 1249436. https://doi.org/10.3389/fimmu.2023.1249436.

93. Tyc, K.M., Nabih, A., Wu, M.Z., Wedeles, C.J., Sobotka, J.A., and Claycomb, J.M. (2017). The Conserved Intron Binding Protein EMB-4 Plays Differential Roles in Germline Small RNA Pathways of C. elegans. Dev Cell *42*, 256-270.e6. https://doi.org/10.1016/j.devcel.2017.07.003.

94. Lachmann, A., Torre, D., Keenan, A.B., Jagodnik, K.M., Lee, H.J., Wang, L., Silverstein, M.C., and Ma'ayan, A. (2018). Massive mining of publicly available RNA-seq data from human and mouse. Nat Commun *9*, 1366. https://doi.org/10.1038/s41467-018-03751-6.

95. Feng, D., Qu, L., and Powell-Coffman, J.A. (2024). Whole genome profiling of short-term hypoxia induced genes and identification of HIF-1 binding sites provide insights into HIF-1 function in Caenorhabditis elegans. PLoS One *19*, e0295094. https://doi.org/10.1371/journal.pone.0295094.

96. Bond, M.R., Ghosh, S.K., Wang, P., and Hanover, J.A. (2014). Conserved nutrient sensor O-GlcNAc transferase is integral to C. elegans pathogen-specific immunity. PLoS One *9*, e113231. https://doi.org/10.1371/journal.pone.0113231.

97. Clough, E., Barrett, T., Wilhite, S.E., Ledoux, P., Evangelista, C., Kim, I.F., Tomashevsky, M., Marshall, K.A., Phillippy, K.H., Sherman, P.M., et al. (2024). NCBI GEO: archive for gene expression and epigenomics data sets: 23-year update. Nucleic Acids Research *52*, D138–D144. https://doi.org/10.1093/nar/gkad965.

98. Sellegounder, D., Liu, Y., Wibisono, P., Chen, C.-H., Leap, D., and Sun, J. (2019). Neuronal GPCR NPR-8 regulates C. elegans defense against pathogen infection. Sci Adv *5*, eaaw4717. https://doi.org/10.1126/sciadv.aaw4717.

99. Kovács, D., Biró, J.B., Ahmed, S., Kovács, M., Sigmond, T., Hotzi, B., Varga, M., Vincze, V.V., Mohammad, U., Vellai, T., et al. (2024). Age-dependent heat shock hormesis to HSF-1 deficiency suggests a compensatory mechanism mediated by the unfolded protein response and innate immunity in young Caenorhabditis elegans. Aging Cell *23*, e14246. https://doi.org/10.1111/acel.14246.

100. Gu, Z., Gu, L., Eils, R., Schlesner, M., and Brors, B. (2014). circlize implements and enhances circular visualization in R. Bioinformatics *30*, 2811–2812. https://doi.org/10.1093/bioinformatics/btu393.

101. Cingolani, P., Platts, A., Wang, L.L., Coon, M., Nguyen, T., Wang, L., Land, S.J., Lu, X., and Ruden, D.M. (2012). A program for annotating and predicting the effects of single

bioRxiv preprint doi: https://doi.org/10.1101/2024.12.02.626368; this version posted December 5, 2024. The copyright holder for this preprint (which was not certified by peer review) is the author/funder. All rights reserved. No reuse allowed without permission.

nucleotide polymorphisms, SnpEff: SNPs in the genome of Drosophila melanogaster strain w1118; iso-2; iso-3. Fly (Austin) *6*, 80–92. https://doi.org/10.4161/fly.19695.

102. Camacho, C., Coulouris, G., Avagyan, V., Ma, N., Papadopoulos, J., Bealer, K., and Madden, T.L. (2009). BLAST+: architecture and applications. BMC Bioinformatics *10*, 421. https://doi.org/10.1186/1471-2105-10-421.

103. Crombie, T.A., McKeown, R., Moya, N.D., Evans, K.S., Widmayer, S.J., LaGrassa, V., Roman, N., Tursunova, O., Zhang, G., Gibson, S.B., et al. (2024). CaeNDR, the Caenorhabditis Natural Diversity Resource. Nucleic Acids Research *52*, D850–D858. https://doi.org/10.1093/nar/gkad887.

104. Waskom, M.L. (2021). seaborn: statistical data visualization. Journal of Open Source Software *6*, 3021. https://doi.org/10.21105/joss.03021.

105. Hunter, J.D. (2007). Matplotlib: A 2D Graphics Environment. Computing in Science & Engineering *9*, 90–95. https://doi.org/10.1109/MCSE.2007.55.

Figure legends

Figure 1. AFD dysfunction triggers transposon expression

RT-qPCR was performed to quantify the differential expression of transposase mRNA in various AFD neuron-depleted *C. elegans* strains. The experiment was repeated three times, each time with independently set up three independent cohorts consisting of 3000 nematodes. All biological replicate was measured in technical triplicates. Each data point represents the mean of a biological replicate, with data from these nine independent populations combined ($\mathbb{N}=3$, $N=9$).

Target transposases, were measured with: Tc1 (B) for Tc1 transposase, and Mirage1 (B) for Mirage transposase. The Mirage1 (B) target was measure in two independent experiments, resulting in a total of six biological replicates.

Relative quantities were calculated using the $2^{\Delta Ct}$ method and normalized using a normal factor derived from the relative quantities of the housekeeping genes tbg-1, act-1, eif-3.C, and rpl-32. This provided the normalized fold change (FC) values for the target transposases.

Statistical significance was determined using an unpaired t-test with Welch's correction, following normality assessment with the Shapiro-Wilk test. The p-values for the comparisons are indicated on the figure, along with the percentage change where relevant.

bioRxiv preprint doi: https://doi.org/10.1101/2024.12.02.626368; this version posted December 5, 2024. The copyright holder for this preprint (which was not certified by peer review) is the author/funder. All rights reserved. No reuse allowed without permission.

A) Differential expression of transposase mRNAs in AFD split caspase-depleted strain (AFD:SCA) and wild type in comparison.
B) Differential expression of transposase mRNAs in AFD histamine-gated chloride channel strain (AFD:HisCl1) compared to the wild type control. Populations were cultured on standard NGM and NGM supplemented with 1 mM histamine.
C) Model of the thermosensory response pathway in the AFD neuron, adapted from [36].
D) Differential expression of transposase mRNAs in AFD triple mutant strain compared to the wild type control, cultured under normal experimental temperatures and heat-stress conditions.
E) The barplot shows the mean logFC of all transposable elements in WS291 in the respective pairwise comparisons. The error bar indicates the 95% confidence interval.

Figure 2. Transcriptome and Proteome analysis reveal desilencing mechanisms triggers in AFD triple mutants.

Each strain and condition comprise five biological replicates, with independent nematode populations consisting of 3000 individuals (N=5).

A) Two examples for additively changing genes upon heat stress (HS) in the wild type and the AFD triple mutant. The y-axis depicts the log normalized expression values. The boxplots show the quartiles of the datasets as boxes, the 1.5x interquartile range as the whiskers, and samples outside of this range as diamonds.
B) Enriched pathways from an enrichment analysis with STRING[86] for the additively downregulated genes, i.e. genes that are significantly downregulated in the AFD triple mutant, and upon HS irrespective of the strain. The x-axis shows the -log10 of the enrichment false discovery rate. For the full list see (**Supplementary Table 1**).
C) Genes that are significantly regulated in the AFD triple mutant RNA-seq and proteomics are significantly positively correlated (Pearson correlation=0.9). The x-axis shows the logFC of the RNA-seq, the y-axis the logFC of the proteomics dataset.
D) Overview of genes involved in the regulation of sRNAs. The color code shows the logFC of the comparison AFD triple mutant vs. WT in the RNA-seq data (left boxes), or proteomics (right boxes). *<0.05, **<0.01, ***<0.001, ns>=0.05, n.d.: not detected.

bioRxiv preprint doi: https://doi.org/10.1101/2024.12.02.626368; this version posted December 5, 2024. The copyright holder for this preprint (which was not certified by peer review) is the author/funder. All rights reserved. No reuse allowed without permission.

E) The significantly upregulated genes in the comparison AFD triple mutant vs. WT are enriched in heterochromatin modification peaks in public datasets. ChIP-Atlas[87] was used for the enrichment analysis (see methods for details) and all over-enriched histone modifications are plotted. The y-axis shows the fold change enrichment. Every dot is one publicly available sample. The boxplots show the quartiles of the datasets as boxes, the 1.5x interquartile range as the whiskers.

Figure 3. Transcriptome analysis identifies AFD-germline pathway regulating TE expression.

A) Heatmap of logFC of the respective pairwise RNA-seq comparisons for genes known to be affected by the AFD neuron. The color code shows the logFC of the respective comparisons. *<0.05, **<0.01, ***<0.001, ns>=0.05

B) Neuropeptides are significantly upregulated in the AFD triple mutant compared to WT worms. The x-axis shows the logFC, the y-axis the -log10 false discovery rate. Red dots display significantly upregulated genes, blue dots significantly downregulated genes, and grey dots genes with an FDR >0.05.

C) Comparison of publicly available differentially expressed gene sets with differentially expressed genes in the AFD triple mutant. WormExp[88] was used to calculate the overlap of publicly available data with the significantly upregulated (red), respective downregulated (blue), genes in the AFD triple mutant. Five selected public datasets are shown, for the whole list see (**Supplementary Table 2**). The x-axis shows the overlap, i.e. the observed number of genes divided by the expected number of genes. *<0.05, **<0.01, ***<0.001

D) Genes regulated in the constitutive active *atfs-1 (et15)* mutant are similarly regulated in the AFD triple mutant. The correlation plot in Figure 3C is colored depending on whether the genes is significantly upregulated in the *atfs-1(et15)* mutant (red), significantly downregulated (blue), or not significantly changed (grey).

E) The top 10 hits of a transcription factor motif enrichment analysis for the AFD triple mutant vs WT comparison (see method for details). The x-axis shows the -log10 of the multiple test adjusted p-value. The searched motif is depicted on the right side of each row.

F) The results of gene set enrichment analyses for the sRNA regulation related genes from Figure 2D in public datasets. Each bar depicts the normalized enrichment score of the sRNA

bioRxiv preprint doi: https://doi.org/10.1101/2024.12.02.626368; this version posted December 5, 2024. The copyright holder for this preprint (which was not certified by peer review) is the author/funder. All rights reserved. No reuse allowed without permission.

regulation related gene set in the specified dataset. A negative value indicates that the gene set is enriched in the downregulated genes. *<0.05, **<0.01, ***<0.001, ns>=0.05

Figure 4. Phenotypic and genetic analysis shows *de novo* Tc1 insertion mutagenesis.

A) Schematic representation of the experimental design and workflow for the twitching screen, including a description of the genetic background contributing to the observed twitching phenotype.

B) Results of four independent experiments (N=4) assessing the penetrance of the twitching phenotype in populations N2 wild-type and AFD triple mutant strains, derived from a single non-twitching mother. Data presented include population size (n), penetrance (expressed as ratio), and the number of nematodes displaying the twitching phenotype (n). The statistical comparison between the two strains was performed using the Mann-Whitney test, the p-value is indicated in the figure.

C) Analysis of the inheritance pattern of the twitching phenotype in the F1 progeny from five individual worms (line A-E), isolated from the third and fourth independent experiments using the AFD triple mutant background. Penetrance of the twitching phenotype was assessed in these progenies. The F1 population size (n), penetrance (%) nematodes displaying the twitching phenotype (n) represented on the figure.

D) Single-worm genotyping PCR analysis of the D-line isolate mother after the completion of egg-laying, as described in panel C. Seven primer pairs were used to genotype the *unc-22* genomic locus (38,311 bp). The figure shows the results for the first and second primer pairs, including wild-type control and AFD triple mutant D-line, with two technical replicates of the PCR. The primer set 2 revealed an insertion with expected wild-type product size of 3047 bp and a Tc1 transposon insertion size of 1032 bp.

E) Schematic reconstruction of the *unc-22* genomic locus based on sequencing results. The annotation includes the *unc-22* gene (blue), Tc1 insertion (orange), and Tc1 flanking regions (dark blue lines), with a scale bar (bp) starting from the *unc-22* start codon.

Figure 5. AFD neurons control inheritable TE insertion accumulation.

A) Experimental design of the mutation accumulation experiment

bioRxiv preprint doi: https://doi.org/10.1101/2024.12.02.626368; this version posted December 5, 2024. The copyright holder for this preprint (which was not certified by peer review) is the author/funder. All rights reserved. No reuse allowed without permission.

B) Circos plots showing *de novo* translocation events in the 5 independent F30 lines for WT (top row) and the AFD triple mutant (bottom row). Each line within the circles shows a translocation event that was not existent in the respective P0 sample.

C) Quantification of heterozygous *de novo* structural variants (SV) in the WT F30 samples (blue), and the AFD triple mutant (orange). The y-axis shows the count of each SV type in the respective samples. Each dot is an independent repeat.

D) Quantification of repeat element classes nearby (<10bp) the translocation break points.

E) Quantification of homozygous *de novo* structural variants (SV) in the WT F30 samples (blue), and the AFD triple mutant (orange). The y-axis shows the count of each SV type in the respective samples. Each dot is an independent repeat.

F) Quantification of transposable element classes in the homozygous inserted sequences.

Figure 6. Model of the AFD neuron mediated transposon activation in the germ line based on our results.

Supplementary Figure Legends

Supplementary Figure 1.

A) RT-qPCR primer binding sites for transposase mRNA measurements. Two independent primer pairs targeting the same transposase consensus sequence in their respective TE families were used. A For the Tc1 transposase, the green primer pair Tc1(A) and the blue primer pair Tc1(B) were used. For the Mirage transposase, the yellow primer pair Mirage(A) and the red primer pair Mirage(B) were employed.

RT-qPCR was performed to quantify the differential expression of transposase mRNA in various AFD neuron-depleted *C. elegans* strains. The experiment was repeated three times, each time with independently set up three independent cohorts consisting of 3000 nematodes. All biological replicate was measured in technical triplicates. Each data point represents the mean of a biological replicate, with data from these nine independent populations combined (ℕ=3, N=9). Target transposases, were measured with: Tc1(A) for Tc1 transposase, and Mirage1(A) for Mirage transposase. Relative quantities were calculated using the 2ΔCt method and normalized using a normal factor derived from the relative quantities of the housekeeping genes *tbg-1*, *act-1*, *eif-3.C*, and *rpl-32*. This provided the normalized fold change (FC) values for the target transposases.

bioRxiv preprint doi: https://doi.org/10.1101/2024.12.02.626368; this version posted December 5, 2024. The copyright holder for this preprint (which was not certified by peer review) is the author/funder. All rights reserved. No reuse allowed without permission.

Statistical significance was determined using an unpaired t-test with Welch's correction, following normality assessment with the Shapiro-Wilk test. The p-values for the comparisons are indicated on the figure, along with the percentage change where relevant.

B) Differential expression of transposase mRNAs in AFD split caspase-depleted strain (AFD:SCA) and wild type in comparison.

C) Differential expression of transposase mRNAs in AFD histamine-gated chloride channel strain (AFD:HisCl1) and wild type in comparison. Populations were cultured on standard NGM and NGM supplemented with 1 mM histamine.

D) Differential expression of transposase mRNAs in AFD triple mutant strain compared to the wild type control, cultured under normal experimental temperatures and heat-stress conditions.

Supplementary Figure 2.

Genotyping of individual worms using single-worm PCR for the AFD triple mutant in the *mut-16(mg461*) background, compared to a wild-type control. PCR was performed on three randomly selected nematodes (N=3) from their respective population. The expected PCR product size for the wild-type allele is 824 bp, while the expected product size for the *mut-16(mg461)* allele is 373 bp.

Supplementary Figure 3.

A) Overview of gene set enrichment analyses (GSEA) for transposable elements in the annotated pairwise RNA-seq comparisons. The y-axis shows the normalized enrichment score of a GSEA. A positive value indicates the enrichment of transposable element genes in the upregulated genes of the respective pairwise comparison. The underlying results are shown in Supplementary Figure 3B-G *<0.05, **<0.01, ***<0.001, ns>=0.05.

B) GSEA of the transposable element genes in the WT heat stress vs. control RNA-seq comparison. The y-axis shows the enrichment score. The x-axis the gene rank, with the highest expressed gene being rank 0. TE genes are shown as lines on the bottom. The red dashed lines show the peaks of the running sum of the enrichment score (green line).

C) The same as B) but for the comparison AFD triple mutant vs WT.

D) The same as B) but for the comparison AFD triple mutant heat stress vs AFD triple mutant control.

bioRxiv preprint doi: https://doi.org/10.1101/2024.12.02.626368; this version posted December 5, 2024. The copyright holder for this preprint (which was not certified by peer review) is the author/funder. All rights reserved. No reuse allowed without permission.

E) The same as B) but for the comparison AFD triple mutant heat stress vs WT heat stress.

F) The same as B) but for the comparison AFD:SCA vs WT

G) The same as B) but for the comparison AFD:HisCl1 histamine vs WT control.

H) Heatmap of the average logFC of the transposable element classes of the respective RNA-seq comparisons. The color code shows the average logFC.

I) Heatmap of the normalized enrichment score of the transposable element classes with at least 5 genes. The color code shows the normalized enrichment score calculated via a GSEA. The hierarchical clustering of the columns was done with a correlation metric and the Ward method.

Supplementary Figure 4

A) The distribution of genes significantly downregulated (blue) or upregulated (red) in the constitutive active *crh-1(tz2)* mutant in the differentially expressed genes in the comparison AFD triple mutant vs. WT. The x-axis shows the logFC of the AFD triple mutant. The density plots show the distribution of the genes that are significantly upregulated (red), respective downregulated (blue), in the *crh-1(tz2)* dataset.

B) The same as A) but for the *pmk-1(km25)* dataset.

C) The same as A) but for the *emb-4(hc60)* dataset.

D) The same as A) but for the *miR-243(n4759)* dataset.

E) The same as A) but for the *atfs-1(et15)* dataset.

Supplementary Figure 5

Heatmap of the public datasets shown in Figure 3F. All genes from the sRNA regulation pathway (Figure 2D) and genes known to be affected by the AFD neuron (Figure 3A) are shown. The color code shows the logFC. The hierarchical clustering was done with a correlation metric and the Ward method.

Supplementary Figure 6

Single GSEA plots of the sRNA regulation related genes for Figure 3F.

bioRxiv preprint doi: https://doi.org/10.1101/2024.12.02.626368; this version posted December 5, 2024. The copyright holder for this preprint (which was not certified by peer review) is the author/funder. All rights reserved. No reuse allowed without permission.

A) AFD triple mutant vs. WT RNA-seq comparison. The y-axis shows the enrichment score. The x-axis the gene rank, with the highest expressed gene being rank 0. sRNA regulation related genes are shown as lines on the bottom. The red dashed lines show the peaks of the running sum of the enrichment score (green line).
B) The same as A) but for the public dataset *lin-13(n770)* vs WT.
C) The same as A) but for the public dataset *flp-6(ok3056)* vs WT.
D) The same as A) but for the public dataset *inx-14* RNAi vs Control.
E) The same as A) but for the public dataset *emb-4(hc60)* vs WT.
F) The same as A) but for the public dataset *atfs-1(et15)* vs WT.
G) The same as A) but for the public dataset Pseudomonas aeruginosa (PA14) vs Control.
H) The same as A) but for the public dataset Hypoxia vs Control.
I) The same as A) but for the public dataset *pmk-1(km25)* vs WT.
J) The same as A) but for the public dataset *hsf-1(sy441)* vs WT.

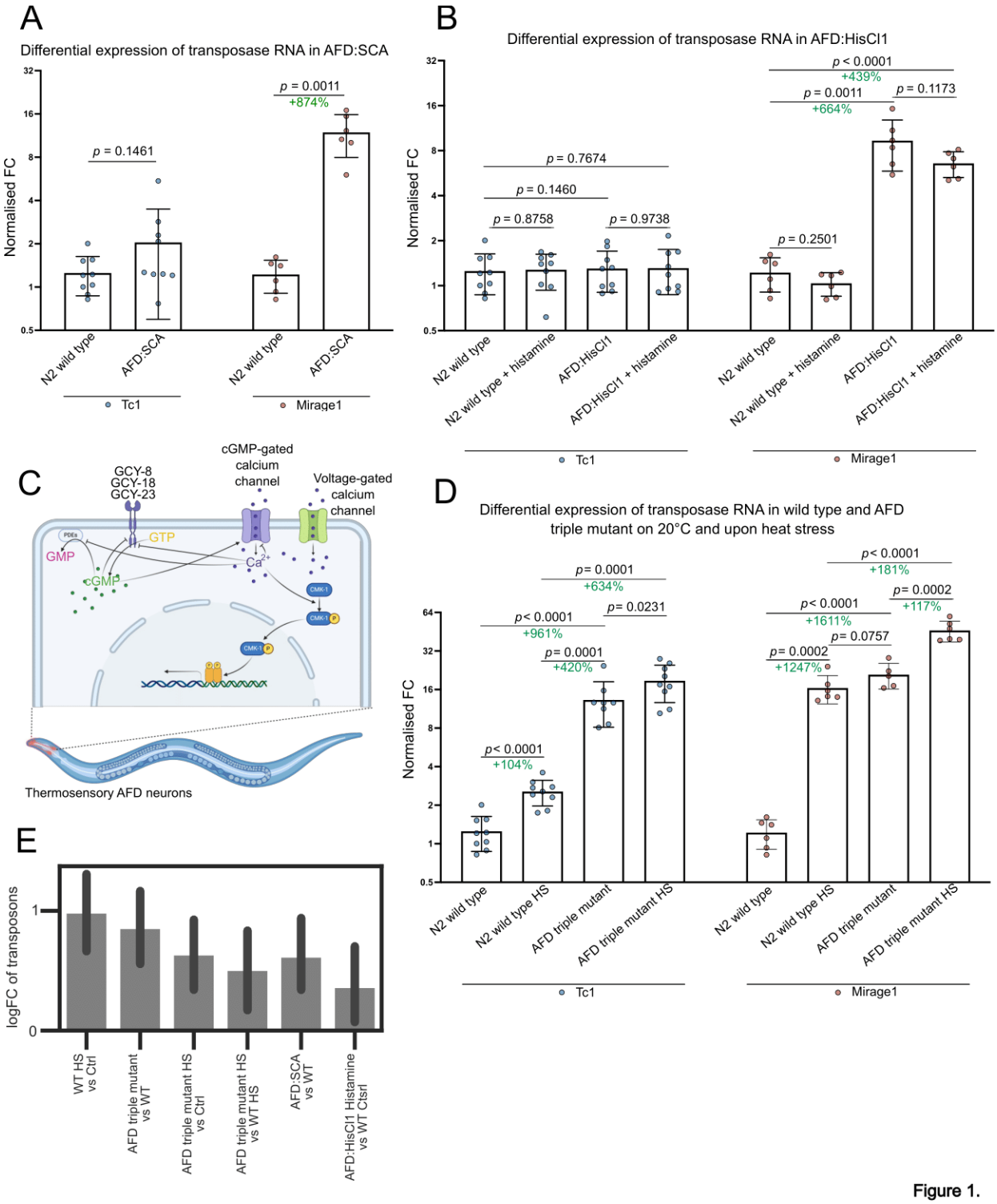
A
Differential expression of transposase RNA in AFD:SCA
Normalised FC
p = 0.1461
p = 0.0011
+874%
N2 wild type
AFD:SCA
N2 wild type
AFD:SCA
Tc1
Mirage1
B
Differential expression of transposase RNA in AFD:HisCl1
p < 0.0001
+439%
p = 0.0011
+664%
p = 0.1173
p = 0.7674
p = 0.1460
p = 0.8758
p = 0.9738
p = 0.2501
N2 wild type
N2 wild type + histamine
AFD:HisCl1
AFD:HisCl1 + histamine
N2 wild type
N2 wild type + histamine
AFD:HisCl1
AFD:HisCl1 + histamine
Tc1
Mirage1
C
GCY-8
GCY-18
GCY-23
cGMP-gated calcium channel
Voltage-gated calcium channel
GTP
GMP
cGMP
Ca2+
CMK-1
Thermosensory AFD neurons
D
Differential expression of transposase RNA in wild type and AFD triple mutant on 20°C and upon heat stress
Normalised FC
p< 0.0001
+104%
p= 0.0001
+634%
p< 0.0001
+961%
p= 0.0231
p= 0.0001
+420%
p< 0.0001
+181%
p< 0.0001
+1611%
p= 0.0002
+117%
p= 0.0002
+1247%
p= 0.0757
N2 wild type
N2 wild type HS
AFD triple mutant
AFD triple mutant HS
N2 wild type
N2 wild type HS
AFD triple mutant
AFD triple mutant HS
Tc1
Mirage1
E
logFC of transposons
WT HS vs Ctrl
AFD triple mutant vs WT
AFD triple mutant HS vs Ctrl
AFD triple mutant HS vs WT HS
AFD:SCA vs WT
AFD:HisCl1 Histamine vs WT Ctsrl

Figure 1.

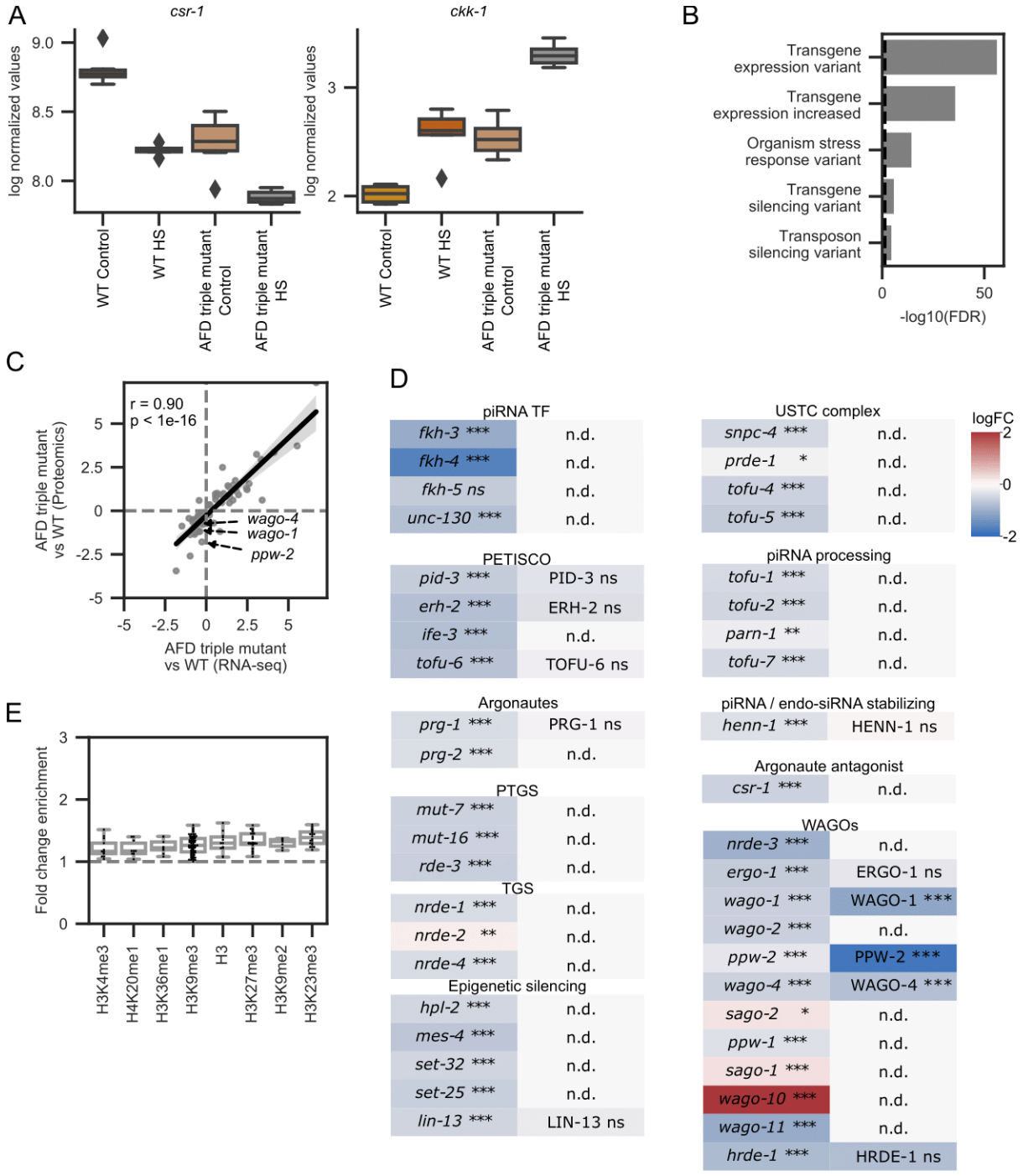
A
csr-1
ckk-1
log normalized values
WT Control
WT HS
AFD triple mutant Control
AFD triple mutant HS
B
Transgene expression variant
Transgene expression increased
Organism stress response variant
Transgene silencing variant
Transposon silencing variant
-log10(FDR)
C
r = 0.90
p < 1e-16
AFD triple mutant vs WT (Proteomics)
AFD triple mutant vs WT (RNA-seq)
wago-4
wago-1
ppw-2
D
logFC
piRNA TF
fkh-3 *** n.d.
fkh-4 *** n.d.
fkh-5 ns n.d.
unc-130 *** n.d.
PETISCO
pid-3 *** PID-3 ns
erh-2 *** ERH-2 ns
ife-3 *** n.d.
tofu-6 *** TOFU-6 ns
Argonautes
prg-1 *** PRG-1 ns
prg-2 *** n.d.
PTGS
mut-7 *** n.d.
mut-16 *** n.d.
rde-3 *** n.d.
TGS
nrde-1 *** n.d.
nrde-2 ** n.d.
nrde-4 *** n.d.
Epigenetic silencing
hpl-2 *** n.d.
mes-4 *** n.d.
set-32 *** n.d.
set-25 *** n.d.
lin-13 *** LIN-13 ns
USTC complex
snpc-4 *** n.d.
prde-1 * n.d.
tofu-4 *** n.d.
tofu-5 *** n.d.
piRNA processing
tofu-1 *** n.d.
tofu-2 *** n.d.
parn-1 ** n.d.
tofu-7 *** n.d.
piRNA / endo-siRNA stabilizing
henn-1 *** HENN-1 ns
Argonaute antagonist
csr-1 *** n.d.
WAGOs
nrde-3 *** n.d.
ergo-1 *** ERGO-1 ns
wago-1 *** WAGO-1 ***
wago-2 *** n.d.
ppw-2 *** PPW-2 ***
wago-4 *** WAGO-4 ***
sago-2 * n.d.
ppw-1 *** n.d.
sago-1 *** n.d.
wago-10 *** n.d.
wago-11 *** n.d.
hrde-1 *** HRDE-1 ns
E
Fold change enrichment
H3K4me3
H4K20me1
H3K36me1
H3K9me3
H3
H3K27me3
H3K9me2
H3K23me3

Figure 2.

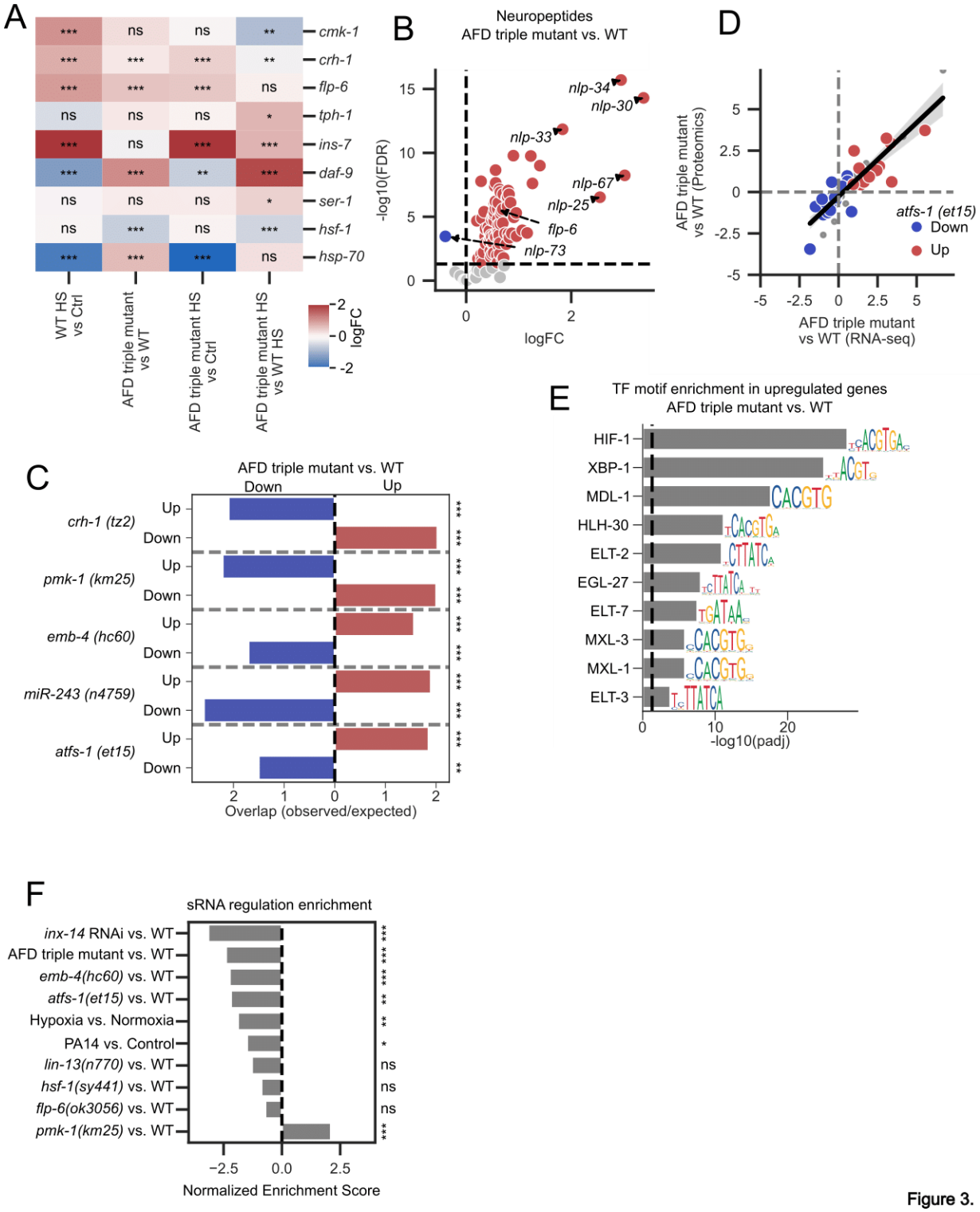
A
cmk-1
crh-1
flp-6
tph-1
ins-7
daf-9
ser-1
hsf-1
hsp-70
WT HS vs Ctrl
AFD triple mutant vs WT
AFD triple mutant HS vs Ctrl
AFD triple mutant HS vs WT HS
logFC
B
Neuropeptides
AFD triple mutant vs. WT
-log10(FDR)
logFC
nlp-34
nlp-30
nlp-33
nlp-67
nlp-25
flp-6
nlp-73
C
AFD triple mutant vs. WT
Down
Up
crh-1 (tz2)
pmk-1 (km25)
emb-4 (hc60)
miR-243 (n4759)
atfs-1 (et15)
Overlap (observed/expected)
D
AFD triple mutant vs WT (Proteomics)
AFD triple mutant vs WT (RNA-seq)
atfs-1 (et15)
Down
Up
E
TF motif enrichment in upregulated genes
AFD triple mutant vs. WT
HIF-1
XBP-1
MDL-1
HLH-30
ELT-2
EGL-27
ELT-7
MXL-3
MXL-1
ELT-3
-log10(padj)
F
sRNA regulation enrichment
inx-14 RNAi vs. WT
AFD triple mutant vs. WT
emb-4(hc60) vs. WT
atfs-1(et15) vs. WT
Hypoxia vs. Normoxia
PA14 vs. Control
lin-13(n770) vs. WT
hsf-1(sy441) vs. WT
flp-6(ok3056) vs. WT
pmk-1(km25) vs. WT
Normalized Enrichment Score

Figure 3.

A

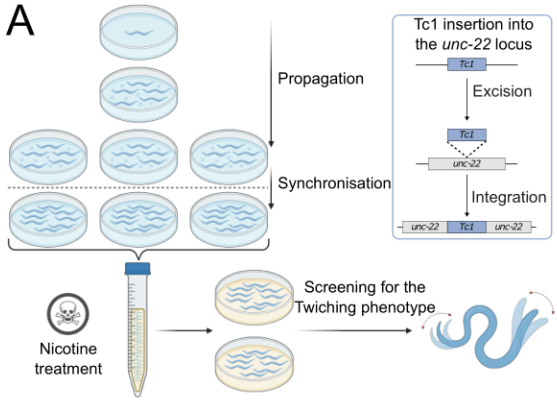

B

Strain	Indpendent experiment	Population size (n)	Penetrance	Nematodes with twiching phemotype (n)	
N2 Wild type	1st	83100	0	Non were found	
	2nd	161600	0	Non were found	
	3rd	309120	0	Non were found	
	4th	379200	0	Non were found	
AFD triple mutant	1st	185310	2.16E-05	4	p =0.0286
	2nd	442880	2.48E-5	11	
	3rd	262650	1.14E-05	3	
	4th	546500	5.49E-06	3	

C

Isolated nematode	Population size (n)	Penetrance (%)	Nematodes with twiching phenotype (n)
A	43	100	43
B	44	100	44
C	50	100	50
D	16	100	16
E	37	100	37

D

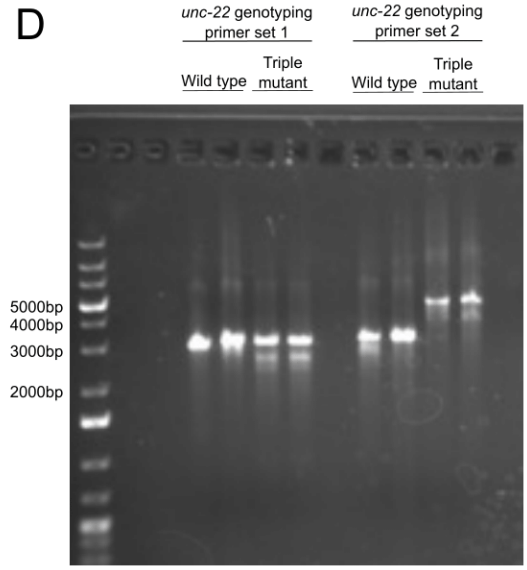

E

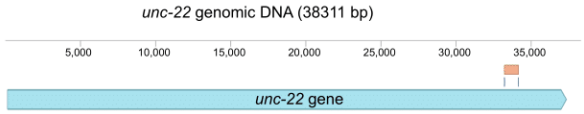

Figure 4.

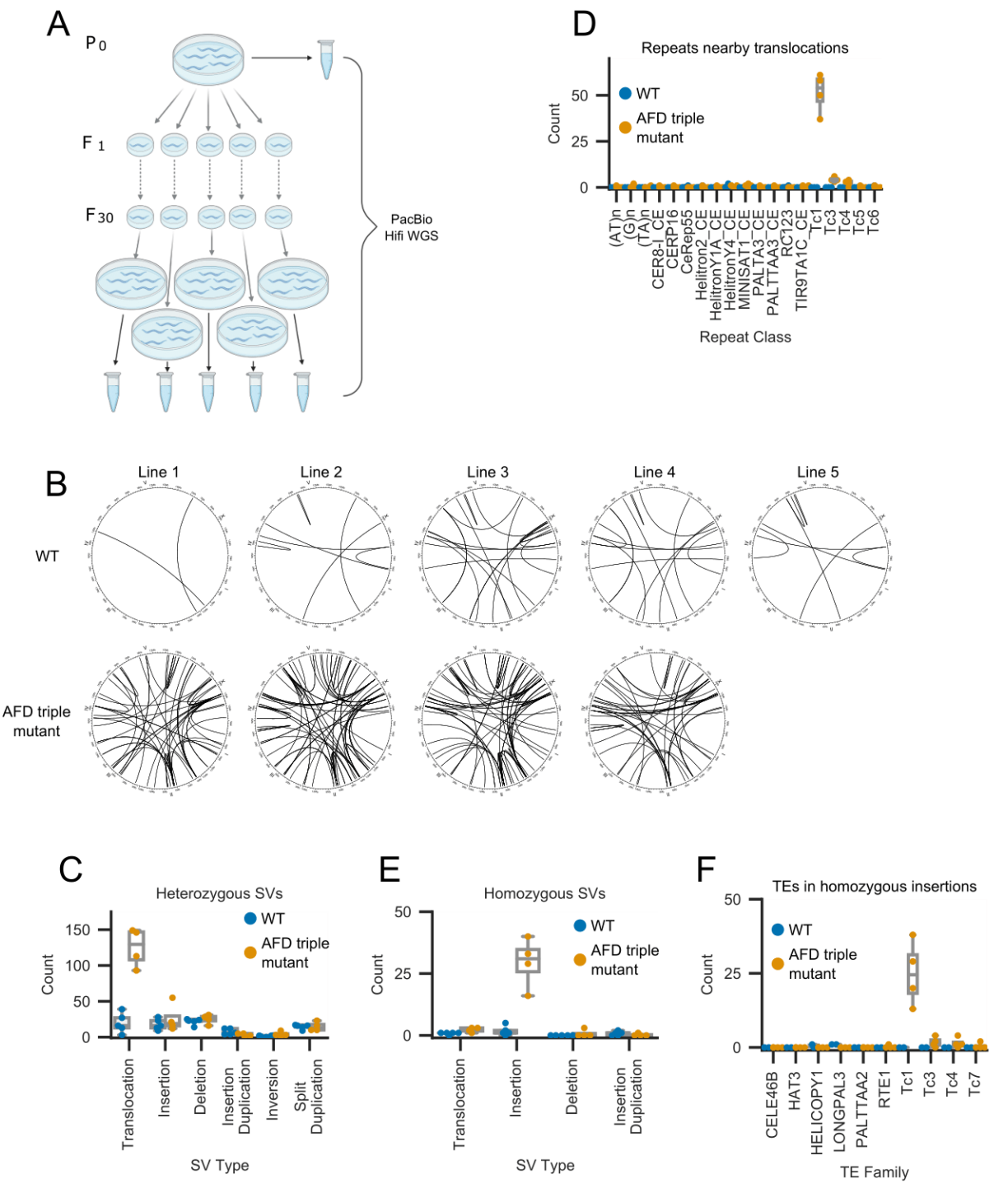
A
P 0
F 1
F 30
PacBio
Hifi WGS
D
Repeats nearby translocations
WT
AFD triple
mutant
Count
50
25
0
(AT)n
(G)n
(TA)n
CER8-I_CE
CERP16
CeRep55
Helitron2_CE
HelitronY1A_CE
HelitronY4_CE
MINISAT1_CE
PALTA3_CE
PALTTAA3_CE
RC123
TIR9TA1C_CE
Tc1
Tc3
Tc4
Tc5
Tc6
Repeat Class
B
Line 1
Line 2
Line 3
Line 4
Line 5
WT
AFD triple
mutant
C
Heterozygous SVs
WT
AFD triple
mutant
Count
150
100
50
0
Translocation
Insertion
Deletion
Insertion
Duplication
Inversion
Split
Duplication
SV Type
E
Homozygous SVs
WT
AFD triple
mutant
Count
50
25
0
Translocation
Insertion
Deletion
Insertion
Duplication
SV Type
F
TEs in homozygous insertions
WT
AFD triple
mutant
Count
50
25
0
CELE46B
HAT3
HELICOPY1
LONGPAL3
PALTTAA2
RTE1
Tc1
Tc3
Tc4
Tc7
TE Family

Figure 5.

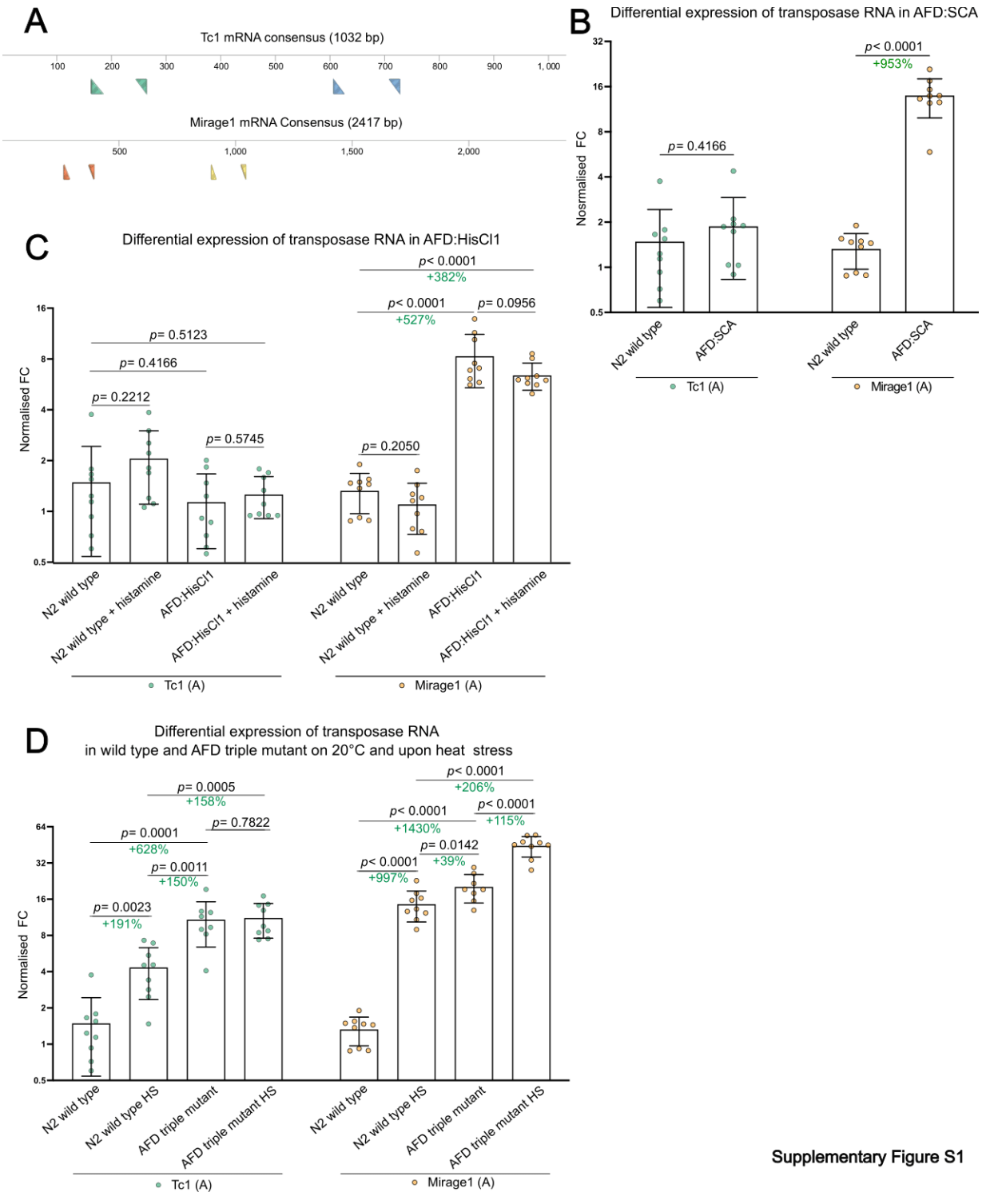

Supplementary Figure S1

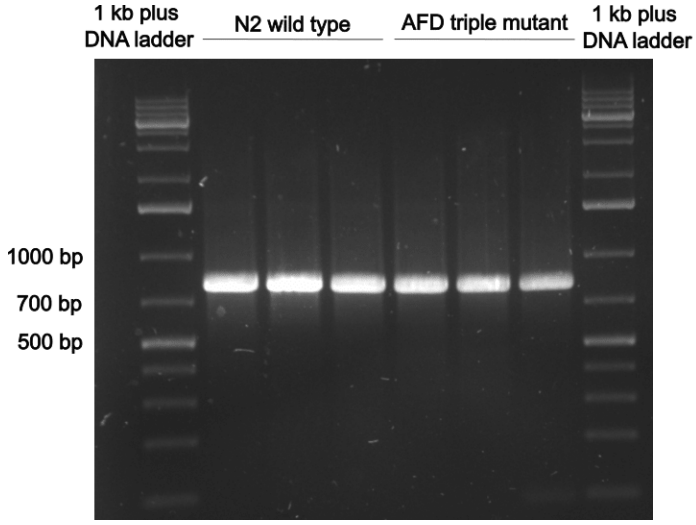

Supplementary Figure S2

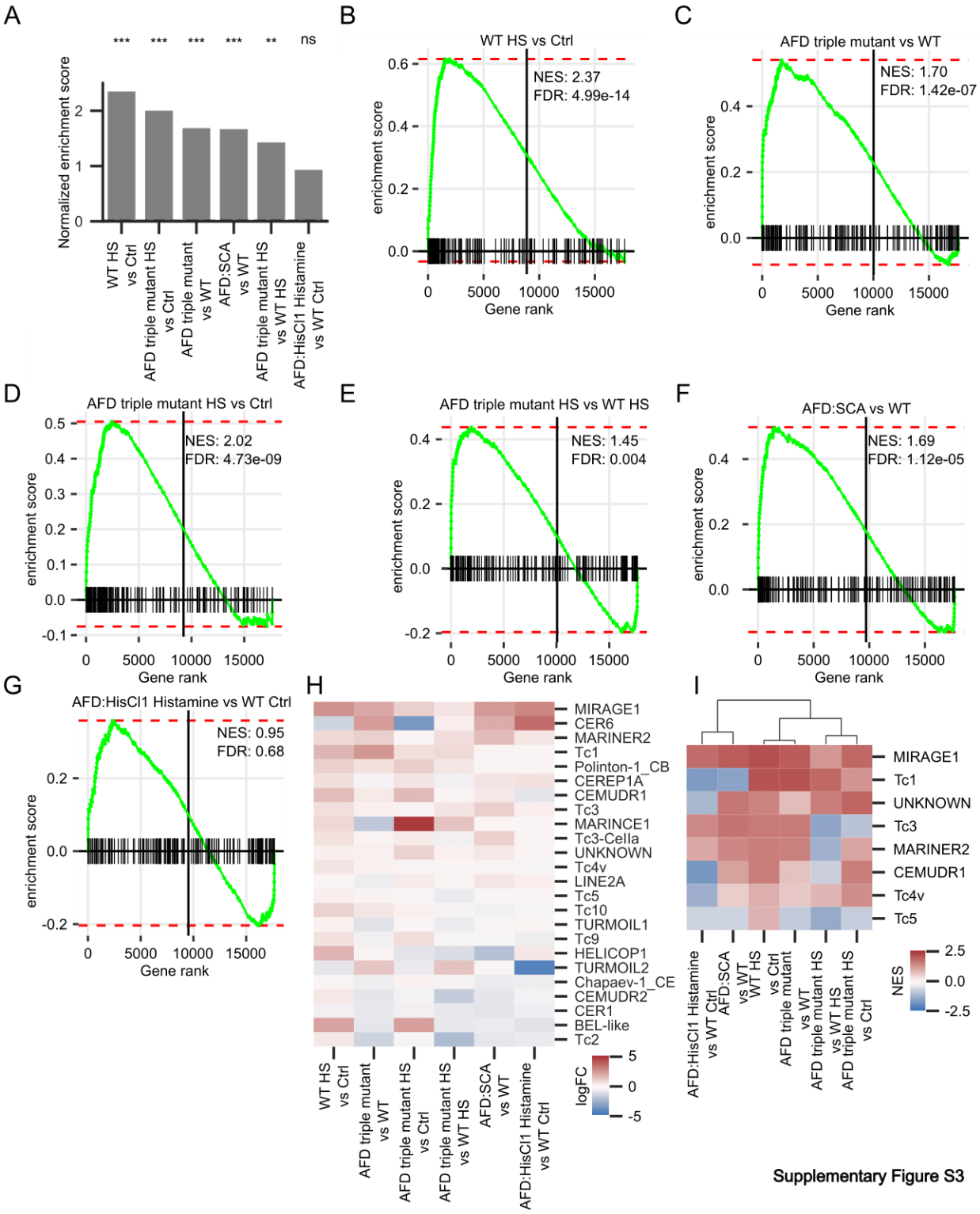

Supplementary Figure S3

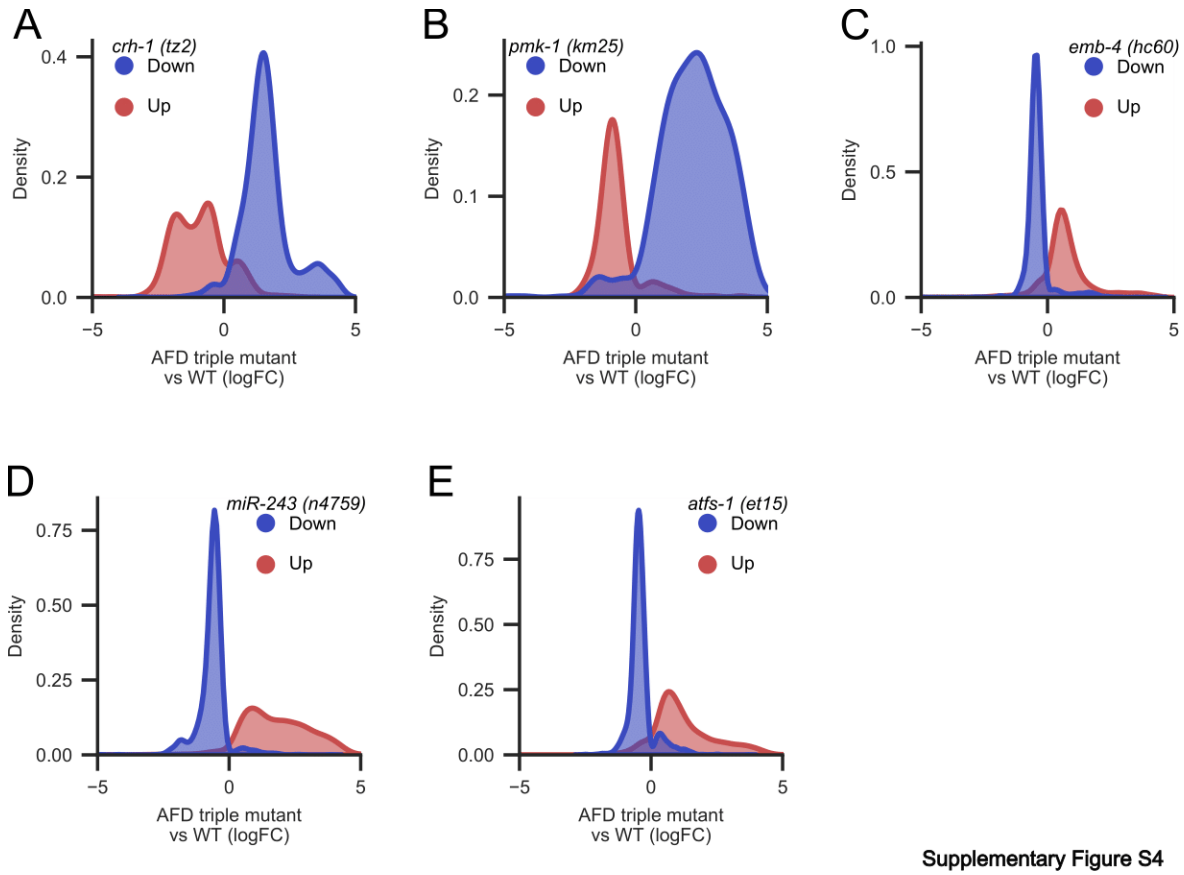

Supplementary Figure S4

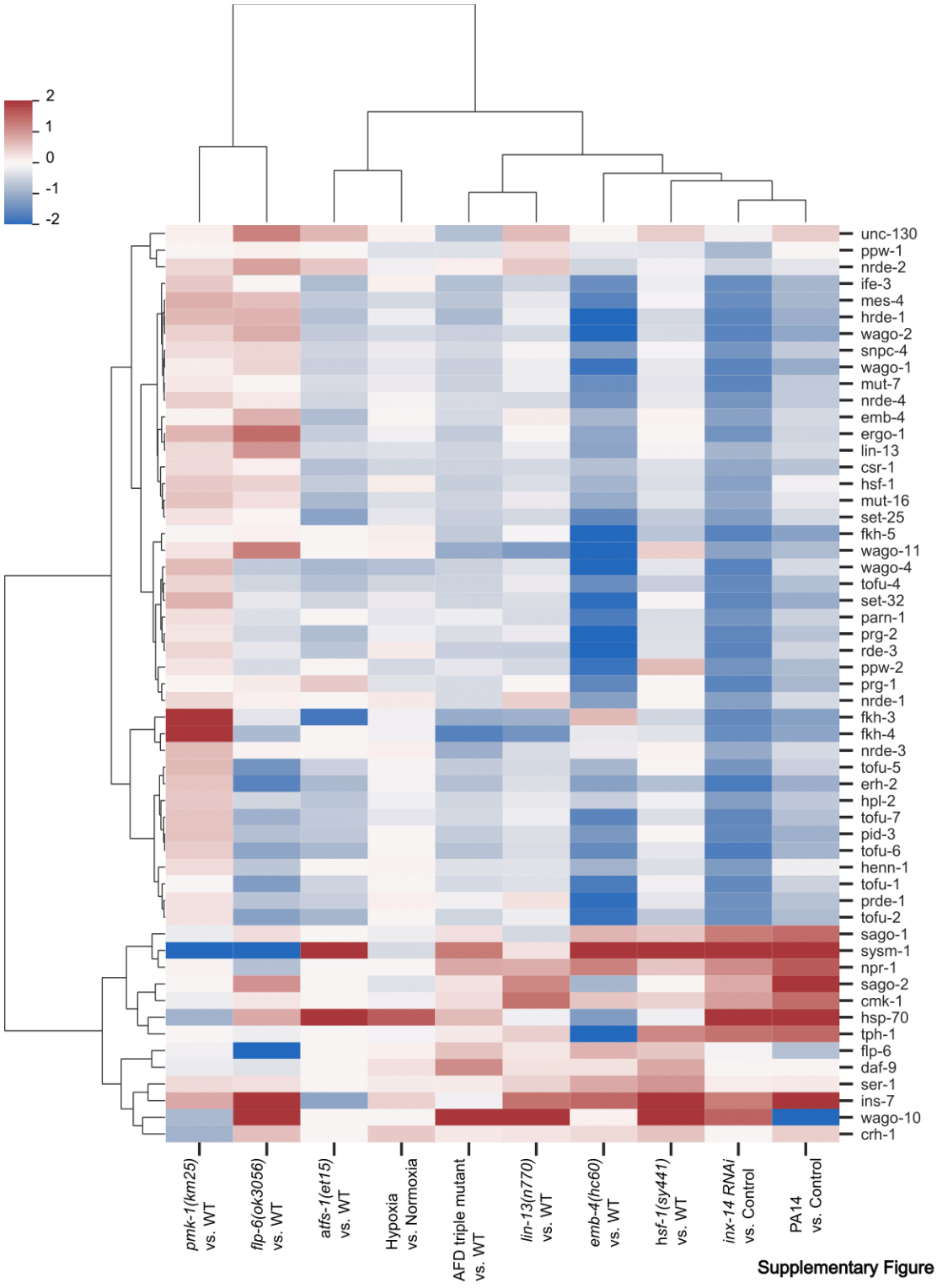

Supplementary Figure S5

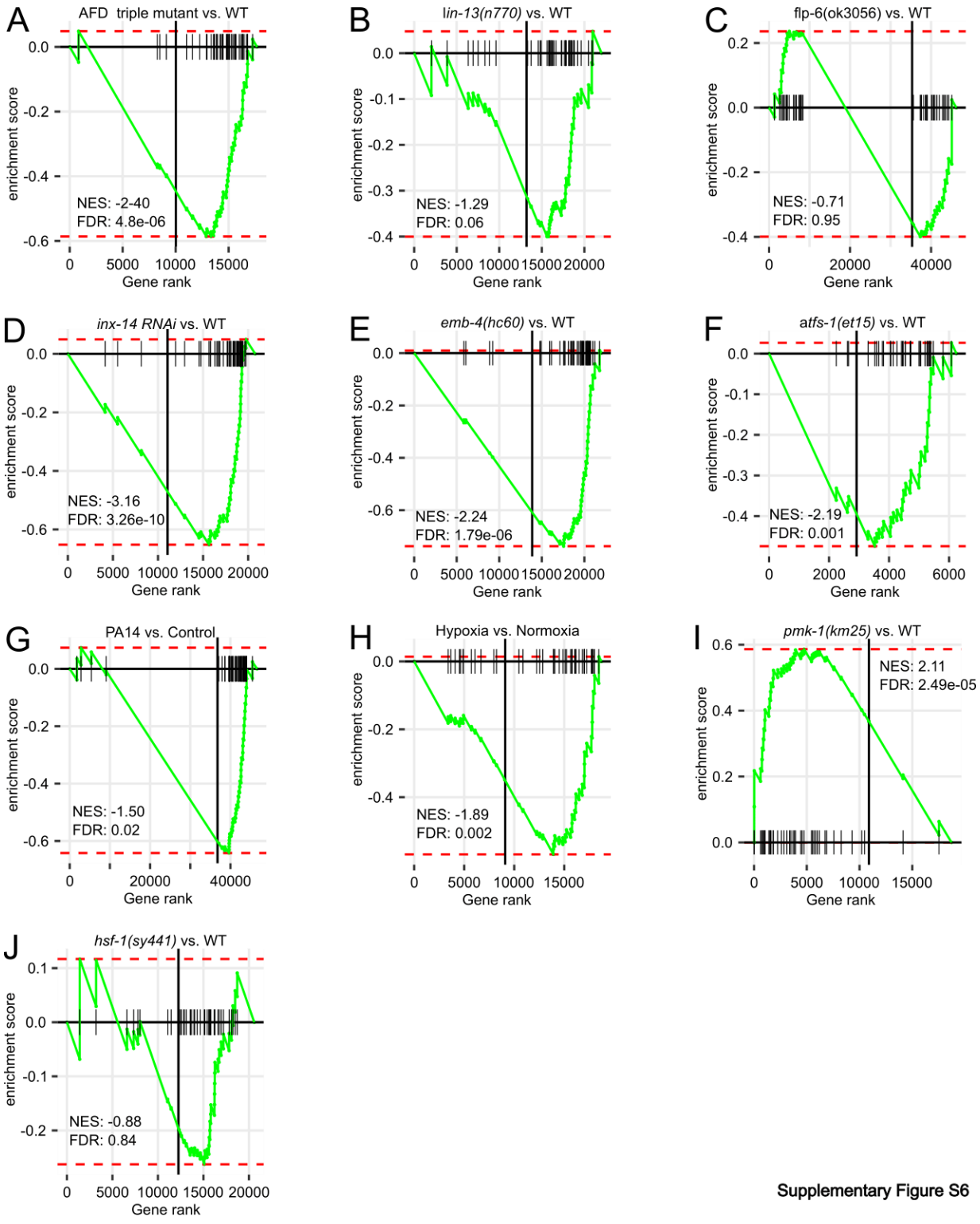

Supplementary Figure S6

3.2 Effect of candidate mediator genes that link AFD neuron signaling to germline transposable element activity

To further investigate the pathway connecting the AFD neuron to the germline, I followed up on our omics-based predictions by employing mutant strains for candidate mediator genes. To evaluate their involvement more effectively, I designed an experimental approach to assess the potential transgenerational persistence of TE expression change, and to determine whether this regulation is mirrored or counteracted by the candidate genes. In this setup, nematode cultures were first synchronized by bleaching to generate a P0 population, which was cultured at 20 °C. Expression levels of the Tc1 and Mirage TE families were measured **(Figure 3.6 A)**. A portion of this P0 population was then bleach-synchronized again to produce the F1 generation, which was cultured under mild heat stress at 26 °C, and TE expression was measured again **(Figure 3.6 B)**. Finally, a subset of the F1 population was bleach-synchronized to produce the F2 generation, which was cultured at 20 °C, and TE expression was measured once more **(Figure 3.6 C)**. Additionally, I compared the fold change in TE induction upon heat stress across the different mutant strains **(Figure 3.6 D)**. The results show that as before the AFD triple mutant reliably shows elevated expression of Tc1 and Mirage already at 20 °C in the P0 generation, with even stronger expression under heat stress. Interestingly, while WT animals also show significant TE induction under heat stress, normalization of each strain to its own untreated control reveals that the AFD triple mutant exhibits a slightly lower fold induction of Tc1 (not statistically significant), and a significantly lower induction of Mirage, 92% lower compared to wild type **(Figure 3.6 D)**. This suggests that heat stress–dependent TE activation may reach a saturation point, and that the AFD neuron is indeed a component of this regulatory cascade. In the absence of functional AFD signaling, the mutant may already exhibit a maximally activated state for certain TEs, limiting further induction by heat stress. While the possibility of AFD-independent, cell-autonomous regulation of TEs cannot be ruled out, it is notable that the AFD triple mutant is unable to mount the same fold of TE induction in response to heat stress as wild type. The involvement of *cmk-1* (calcium/calmodulin-dependent protein kinase) remains ambiguous. At 20 °C, both Tc1 and Mirage expression levels are slightly, but not significantly, elevated compared to wild type **(Figure 3.6 A)**. Under heat stress, Tc1 shows a non-significant reduction in induction relative to wild type, while Mirage displays a non-significant increase **(Figure 3.6 B)**. When comparing the heat-stressed condition to the non-heat-stressed baseline within the *cmk-1* mutant, both TEs show reduced induction, with Tc1 showing a non-significant decrease and Mirage exhibiting a significant 48% reduction **(Figure 3.6 C)**. As *cmk-1* most probably is dispensable for basal TE repression but required for the full heat-induced activation of Mirage, pointing to a modulatory rather than essential role in AFD-mediated TE regulation. The *flp-6* is a neuropeptide reportedly secreted by AFD neurons[293]. At 20 °C, *flp-6* mutants show no change in Tc1 expression and a non-significant 139% increase in Mirage expression compared to wild type **(Figure 3.6 A)**. Under heat stress, Tc1 expression is significantly more induced than in wild type, while Mirage expression remains comparable **(Figure 3.6 B)**. When normalized to the mutant's own untreated control, Tc1 shows a fold change similar to that of wild type under heat stress, but Mirage displays a

significantly lower fold change **(Figure 3.6 C)**. However, this should be interpreted in the context of its already elevated basal expression at 20 °C. These data suggest that while *flp-6* is not an exclusive regulator, it may play a limited role in heat stress induced TE activation. The *tph-1* shows a non-significant increase in Tc1 expression and a significant 286% induction of Mirage at 20 °C **(Figure 3.6A)**. This pattern is mirrored under heat stress: compared to heat-stressed wild type, *tph-1* exhibits an additional non-significant increase in Tc1 and a significant 70% further increase in Mirage expression **(Figure 3.6B)**. When comparing heat-stressed *tph-1* to its 20 °C-cultivated counterpart, the fold induction of Tc1 is similar to that observed in wild type, while Mirage shows a significantly lower fold change relative to heat-stressed wild type. This reflects a pattern similar to that of the AFD triple mutant, suggesting that the elevated basal expression of Mirage at 20 °C in *tph-1* may limit further induction under heat stress **(Figure 3.6D)**. This pattern suggests that *tph-1* may act as a positive regulator in AFD neuron–dependent, heat stress–induced germline transposable element regulation. Lastly, *pmk-1* at 20 °C shows no change in Tc1 expression and a non-significant reduction in Mirage expression **(Figure 3.6A)**. Under heat stress, compared to heat-stressed wild type, *pmk-1* exhibits a non-significant reduction in Tc1 induction and a strongly significant 83% decrease in Mirage expression **(Figure 3.6B)**. When comparing heat-stressed *pmk-1* to its 20 °C counterpart, the fold induction of both TE families is lower than in wild type, with Mirage showing a significantly reduced fold change **(Figure 3.6D)**. These results suggest that *pmk-1* functions as a negative regulator of AFD neuron–dependent, heat stress–induced germline transposable element regulation. Differential expression of transposase mRNAs in the F1 generation under mild heat stress. FC values were normalized to the respective 20 °C grown counterpart strain. In the F2 generation, following return to 20 °C after the heat-stressed state of F1, no significant deviations were observed relative to the P0 20 °C condition. This indicates that TE expression levels largely return to their original state, with some variation that does not reach statistical significance.

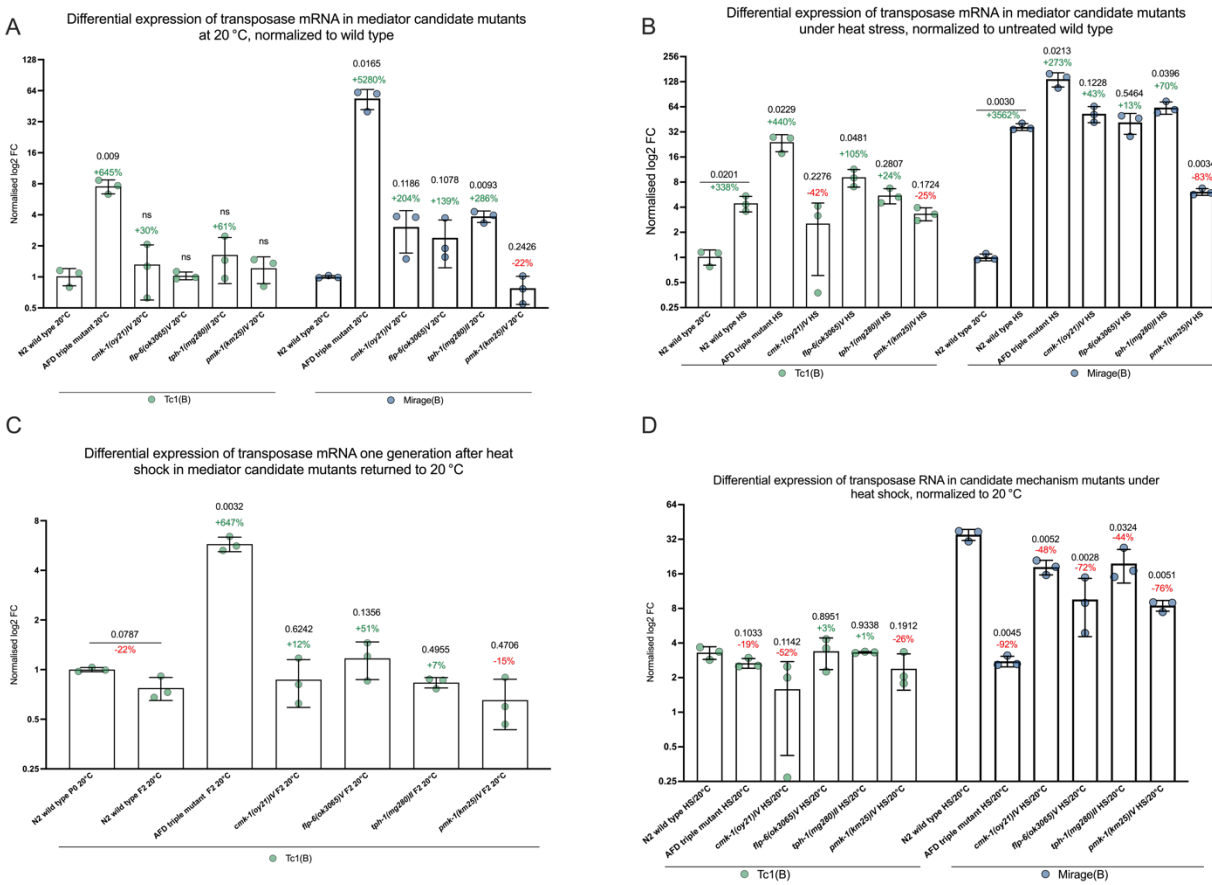

Figure 3.6 RT-qPCR measurement of differential expression of transposase mRNA in the AFD neuron-germ line signaling mediator candidate *C. elegans* strains. The experiment was performed in three independent cohorts consisting of 3000 nematodes as three biological replicates. All biological replicate was measured in technical triplicates. Each data point represents the mean of a biological replicate (N=3). Target transposases, were measured with: Tc1 (B) primers for Tc1 transposase, and Mirage1 (B) primers for Mirage transposase. Relative quantities were calculated using the 2ΔCt method and normalized using a normal factor derived from the relative quantities of the housekeeping genes *tbg-1, act-1, eif-3.C*, and *rpl-32*. This provided the normalized fold change (FC) values for the target transposases. Statistical significance was determined using an unpaired t-test with Welch's correction, following normality assessment with the Shapiro-Wilk test. The p-values for the comparisons are indicated on the figure, along with the percentage change. **A)** Differential expression of transposase mRNAs in the P0 generation of the experimental setup at 20 °C. FC was normalized to the WT control. Statistical comparisons display p-values and percentage changes, with each strain compared to the WT. **B)** Differential expression of transposase mRNAs in the F1 generation under mild HS. FC values were normalized to the WT control grown at 20 °C. Statistical comparisons display p-values and percentage changes, with each strain compared to the HS WT, the HS WT to the 20°C grown WT. **C)** Differential expression of transposase mRNAs in the F2 generation, following the return of progeny to 20 °C from HS F1. FC values were normalized to the P0 WT control grown at 20 °C. Statistical comparisons display

p-values and percentage changes, with each strain compared to the F2 WT at 20°C, and the F2 WT at 20°C to the P0 WT at 20°C **D)** Comparison of F1 HS strains normalized to their 20 °C-grown P0 counterparts. Statistical comparisons display p-values and percentage changes, with each strain compared to the heat-stressed wild type.

3.3 The effect of AFD neuron impairment on fertility and germ cell apoptosis

I conducted an experiment to assess the effect of various methods of AFD neuron depletion (AFD triple mutant, AFD:SCA, and AFD:HisCl1) on *C. elegans* fertility.

The AFD triple mutant did not show any statistically significant changes in viable progeny or total egg-laying capacity, although a non-significant decreasing trend was observed. Notably, the number of unhatched eggs was significantly higher, which may indicate that increased TE activity compromises embryonic viability. The AFD:SCA strain exhibited a strong and statistically significant fertility impairment. Brood size was reduced to less than half that of the wild type, with a pronounced decrease in viable progeny. Although the number of unhatched eggs was also higher, this difference did not reach statistical significance **(Figure 3.7 A)**.

The AFD:HisCl1 strain, when cultivated on standard NGM without histamine, did not differ significantly from the wild type, though a downward trend was observed in both egg-laying capacity and viable progeny count. However, the number of unhatched eggs was significantly higher than in the wild-type control. Histamine treatment alone had no significant effect on the fertility of wild-type animals. In contrast, when histamine was supplemented in the AFD:HisCl1 strain, a marked reduction in both egg-laying capacity and viable progeny count was observed. These reductions were statistically significant when compared to both untreated wild-type and histamine-treated wild-type controls. The number of unhatched eggs in the histamine-treated AFD:HisCl1 group did not show a significant change **(Figure 3.7 B)**

It is important to note that this experiment was conducted with five animals per condition and in a single replicate; therefore, the statistical power is limited. Nonetheless, the observed trends provide valuable preliminary insight.

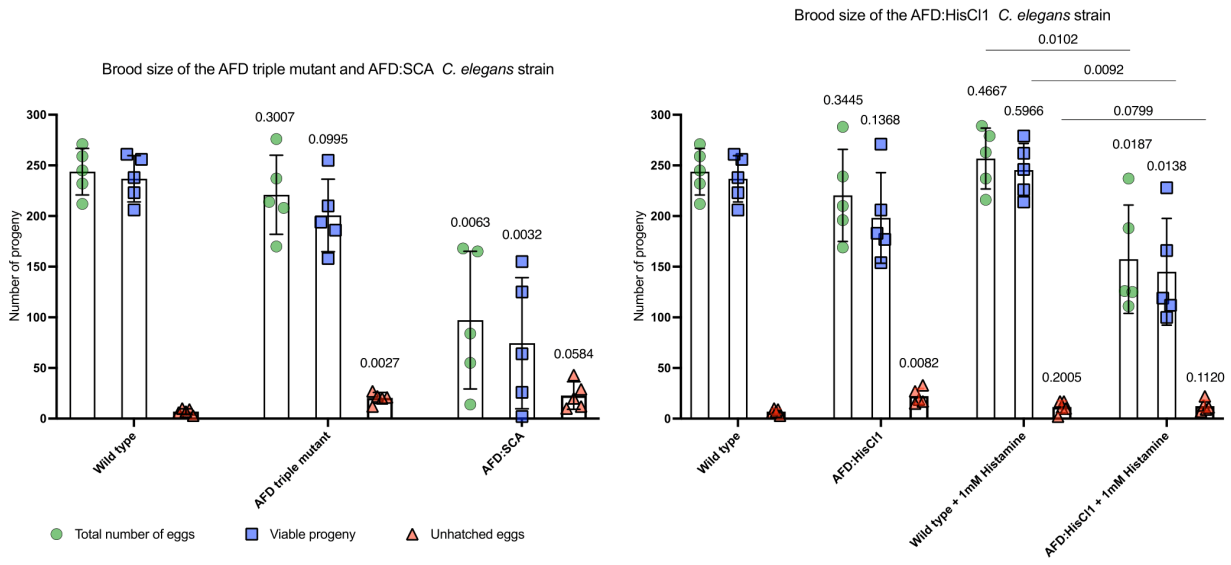

Figure 3.7 Brood size of AFD neuron-depleted strains: AFD triple mutant, AFD:SCA **A)**, and AFD:HisCl1 with and without 1 mM histamine treatment **B)**, compared to their corresponding wild-type controls. Each data point represents the total progeny of a single nematode throughout its reproductive lifespan. All recordings were performed simultaneously and are shown in separate panels (**A** and **B**) for clarity; note that the non-treated wild-type values are shared across both panels. Statistical significance was calculated using a two-tailed unpaired t-test with Welch's correction. P-values for comparisons against the non-treated wild type are indicated above each dataset, while p-values for the comparison between histamine-treated wild type and AFD:HisCl1 are shown above the connecting lines.

To further assess how the AFD neuron influences germline maintenance, I performed an apoptosis assay to examine germ cell apoptosis in the AFD triple mutant. In this experimental setup, YA worms were subjected to ionizing radiation (30 Gy or 90 Gy), heat shock (34 °C for 2 hours), or a combination of both, with radiation applied immediately after the heat shock when both treatments were used. Apoptotic corpses in the gonad were quantified 6 hours after treatment. To evaluate the impact on fertility, individual worms were then singled out, and allowed to lay eggs for 24h, then their progeny were assessed the following two days.

When comparing germline apoptosis between the AFD triple mutant and the wild type, a mild increasing trend was observed across all the conditions; however, it did not reach statistical significance **(Figure 3.8 A)**. These trends were also reflected in the fertility of the worms following treatment. The total egg-laying capacity of the AFD triple mutant showed a non-significant decrease **(Figure 3.8 B)**, and a similar trend was observed in the number of viable progeny **(Figure 3.8 C)**. This was further reflected in the egg survival rate, where a smaller proportion of eggs hatched in the AFD triple mutant compared to wild type across all conditions, though again, the differences were not statistically significant **(Figure 3.8 D)**. Although not statistically confirmed, the consistent trends of elevated apoptosis, reduced fertility, and lower egg viability suggest that

AFD triple mutant impair germ cell maintenance and embryo viability. The increase in genomic instability may contribute to both germline apoptosis and the transmission of sublethal damage affecting embryonic survival. However, due to the limited statistical power of this single replicate, additional experimental repetitions are required to validate these observations.

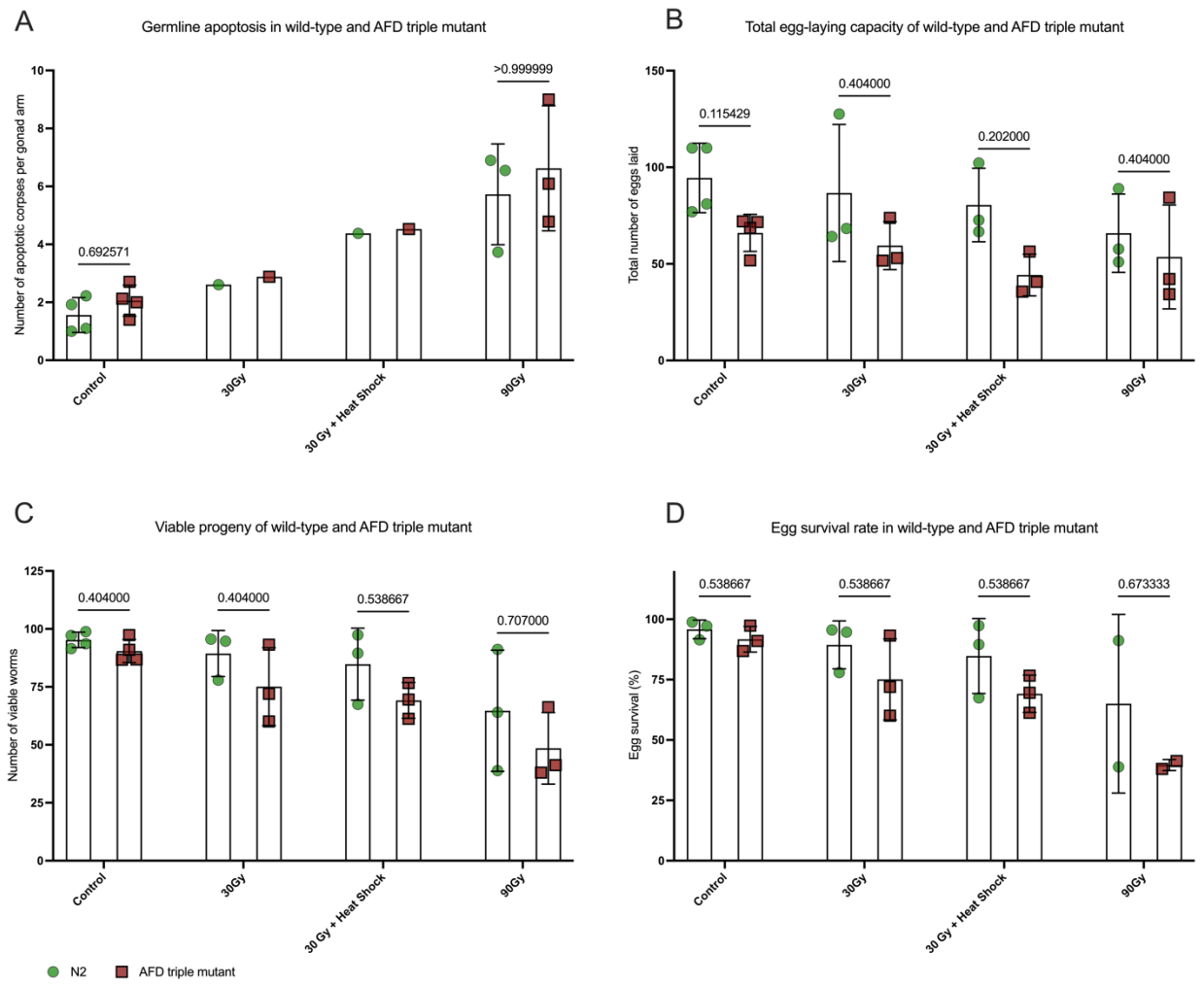

Figure 3.8 Germ cell apoptosis and fertility of the AFD triple mutant. **A)** Germ cell apoptosis assay. Each data point represents the average of an independent experiment, in which the number of apoptotic corpses per gonad arm was quantified in 15–20 worms. **B)** Total egg-laying capacity. Each data point represents the average of an independent experiment, where five individual nematodes were plated after treatment, and the total number of eggs laid was quantified the following day after removal of the adults. **C)** Viable progeny count. The number of viable progeny was quantified over the two days following egg laying. **D)** Egg survival (hatching ratio) was calculated by dividing the number of viable progeny (**C**) by the total number of eggs laid (**B**). In each case statistical analysis was performed using the Mann–Whitney test, a non-parametric, rank-based method for assessing differences between groups.

4 Results II: The impact of transposable element activity on aging and fertility in *C. elegans*

TE activation has been implicated in aging, neurodegeneration, and inflammation. Most relevant to this work, TE activity also impacts reproductive aging and oocyte quality, as demonstrated by Wasserzug-Pash et al[155]. In this chapter, I investigate whether pharmacological inhibition of transposases can modulate reproductive and somatic aging phenotypes in *C. elegans*, based on the hypothesis that TE suppression may promote improved healthspan and lifespan. Specifically, I present findings from experiments using a transposase inhibitor, including its application in a transposon-silencing-deficient mutant with severely impaired fertility, to evaluate potential phenotypic rescue. I also examine the effects of the inhibitor on fertility in wild-type animals and the feminized *fog-2* mutant, which serves as a model for studying oocyte aging and reproductive lifespan. Finally, I assess the impact of the inhibitor on overall lifespan in both wild-type and AFD triple mutant *C. elegans*.

4.1 Transposase inhibitor: Raltegravir

The drug Isentress® INN-Raltegravir was originally developed as an antiretroviral treatment for HIV, acting by binding to the catalytic domain of HIV integrase. Notably, HIV integrase shares structural similarities with the Mos1 transposase, which has prompted interest in raltegravir as a potential inhibitor of transposase activity in vivo. A key study by Wolkowicz et al. (2014) demonstrated that raltegravir binds and inhibits Mos1 transposase in the presence of Mg^{2+} or Mn^{2+}, without requiring transposon DNA. This inhibition is specific to raltegravir, and the study revealed that the drug adopts a compact and unique binding conformation, providing a structural basis for the development of targeted transposase inhibitors.

Raltegravir's specificity and unique mechanism make it a promising candidate for in vivo transposase inhibition. By selectively blocking transposase function, it becomes possible to assess the phenotypic effects of transposon activity, particularly in relation to lifespan and healthspan. In *Drosophila*, a study where mobilization of the mariner TE family in the *white* gene causes mosaic red eye spots, showed the strongest suppression phenotype when raltegravir was added to the medium at 210 µM. The observed inhibition of the Drosophila mariner family is particularly relevant, since, as discussed in Results Chapter I, the Tc1/mariner family is the most abundant and active transposon family in *C. elegans*, contributing significantly to transposon-induced genomic instability. Based on these findings, I chose to supplement *C. elegans* NGM with 200 µM raltegravir for experimentation, dissolving the drug in Dimethylsulfoxid (DMSO) and supplying administering it into NGM plates in 0.1 V/V% final concentration.

4.2 Establishing Raltegravir treatment and conducting a brood size assay.

As pilot experimentation to initially assess the effect of raltegravir, I employed the TE-silencing-deficient *C. elegans* strain *mut-16(pk710)I*, it is a key Argonaute-associated gene expressed in the

germline and is involved in several aspects of germline maintenance, including the repression of transposable elements through sRNA pathway.
To verify the literature-based expectation of increased TE expression in the *mut-16(pk710)I* strain, I performed RT-qPCR to assess the expression levels of the Tc1 and Mirage transposon families. As expected, both TE families showed a significant upregulation in expression. (**Figure 4.1)**.

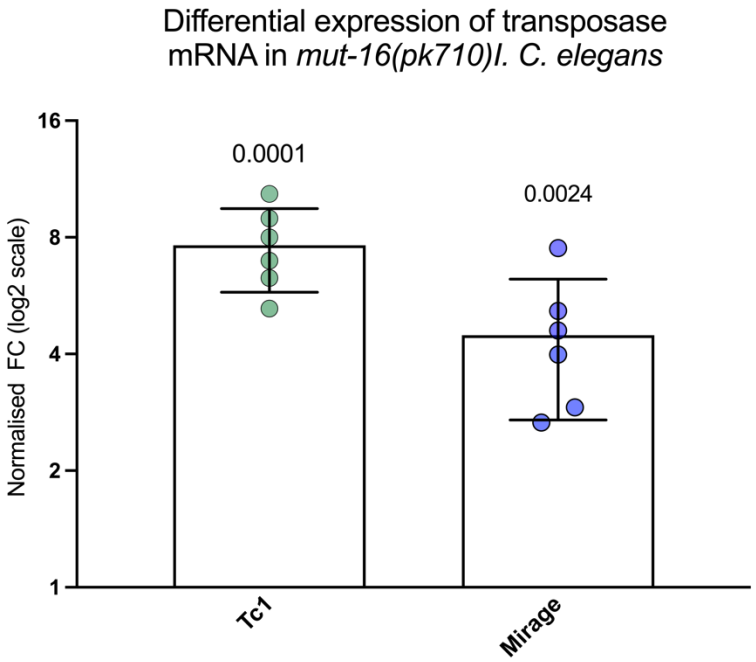

Figure 4.1 Differential expression of transposase mRNA level of the Tc1 and Mirage transposon families in the *mut-16(pk710)I. C. elegans*. Every data point represents the average value of one biological replicate (N=6) normalized to the wild type level (baseline). Statistical significance was determined using an unpaired t-test with Welch's correction, following normality assessment with the Shapiro-Wilk test. The p-values for the comparisons are indicated on the figure.

Based on these findings, I conducted a fertility assay using *mut-16(pk710)I* to evaluate the expected impairment in fertility, as previously reported. In addition, I aimed to assess whether treatment with the transposase inhibitor raltegravir could rescue this defect. The brood size assay revealed a pronounced fertility impairment in *mut-16(pk710)I.* Under DMSO control conditions, animals laid an average of only 5–15 eggs, with fewer than 5 viable progeny, compared to the 250–300 viable progeny typically observed in wild-type animals, which also exhibit near-complete hatching rates. Raltegravir treatment led to a significant, though partial, rescue of the phenotype. Treated animals laid significantly more eggs; however, this increase was largely due to a higher number of unhatched, non-viable eggs. While the number of viable progeny was slightly higher than in the control group, the increase did not reach statistical significance (**Figure 4.2**).

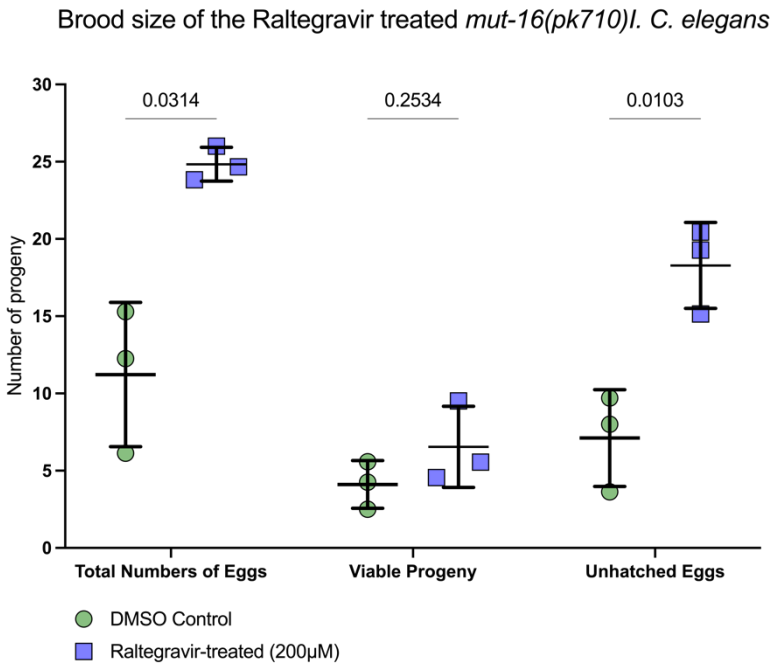

Figure 4.2 Brood size of *mut-16(pk710)I C. elegans*, treated with DMSO (control) or raltegravir (200 µM). Each data point represents the average value from an independent biological replicate. Total egg count, viable progeny, and unhatched eggs were quantified. Statistical significance was determined using an unpaired t-test with Welch's correction.

As three independent repetitions of the assay consistently showed that raltegravir treatment can partially rescue the impaired fertility of the TE-silencing-deficient *mut-16(pk710)I* strain, but did not improve progeny viability and instead led to an increase in non-viable eggs (**Figure 4.2**), the next step was to assess whether the treatment affects germ cell apoptosis in the *mut-16(pk710)I* background. Since *mut-16(pk710)I* affects more than just TE regulation, other mechanisms may contribute synergistically to the observed fertility impairment. It is also possible that TE activity alone could trigger apoptosis of damaged germ cells, particularly if chromatin maintenance is compromised due to downstream disruption of RNAi-mediated epigenetic silencing pathways in the absence of functional MUT-16. The results show that *mut-16(pk710)I* animals treated with DMSO exhibit an increased number of apoptotic corpses compared to untreated wild-type animals. However, this comparison is limited by the absence of a parallel wild-type control group, as the wild-type data were obtained from a previous experiment and are included only to illustrate the expected basal level of apoptosis, typically only a few apoptotic corpses per gonad arm. Notably, when comparing *mut-16(pk710)I* animals treated with DMSO to the ones treated with raltegravir, a significant reduction in apoptotic corpses was observed in the raltegravir-treated group (**Figure 4.3**).

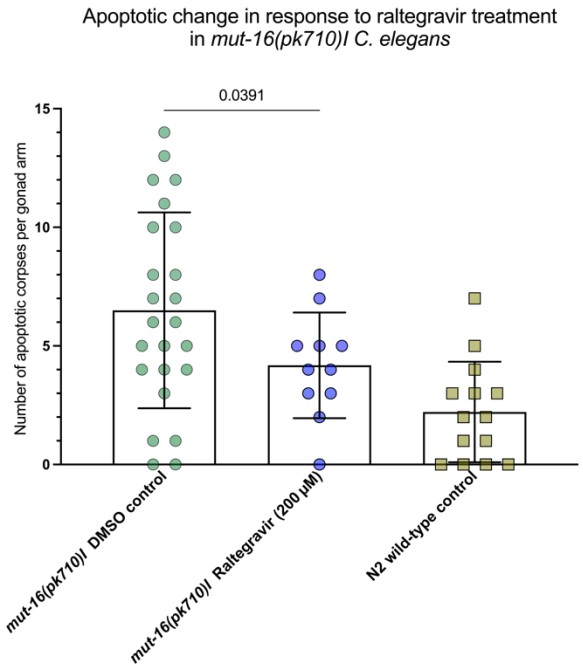

Figure 4.3 Number of apoptotic corpses per gonad arm. Each data point represents the count from a single animal. Statistical comparison was performed using a two-tailed unpaired t-test with Welch's correction. Bar charts represent the mean ± standard deviation (SD).

An interesting observation made during this experiment was that raltegravir-treated animals appeared to retain more intact gonad morphology (**Figure 4.4**); however, no quantification was performed, hence conclusions cannot be stated.

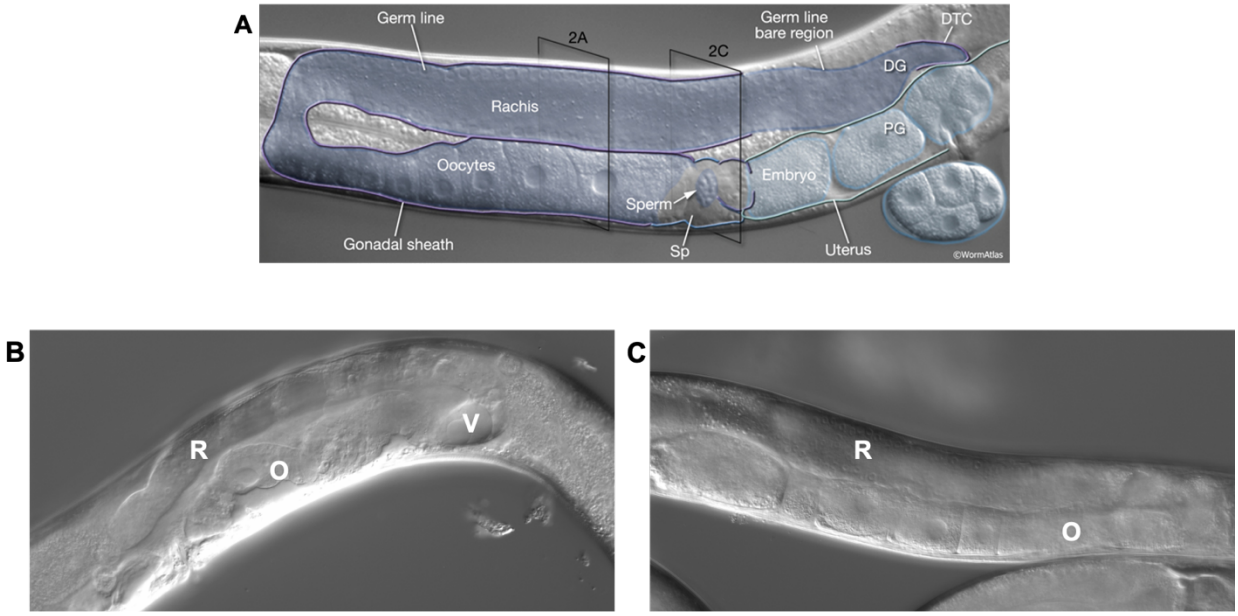

Figure 4.4 Morphological changes in the gonad of day 3 adult *mut-16(pk710)I* worms under DMSO control and raltegravir (200 µM) treatment. A) Healthy anatomically annotated gonad

(adapted from WormAtlas[272]). B) DMSO control. C) Raltegravir-treated worm. Legend: R – rachis; O – oocytes; V – vacuole.

4.3 The effect of transposon inhibitor treatment on fertility in wild type under normal and mild heat stress conditions.

Since raltegravir treatment showed promising results in partially rescuing fertility impairment in a known TE silencing deficient mutant, including improvements in brood size and reductions in germline apoptosis, the next step was to test its effect in wild-type *C. elegans* under standard cultivation at 20 °C and under elevated temperature conditions at 25 °C, where increased TE activity is expected.

Compared to the DMSO control, raltegravir treatment showed no significant changes in any aspect of brood size at 20 °C. However, at 25 °C, raltegravir treatment resulted in a significant increase in the total number of eggs laid and in the number of viable progeny. A slight but statistically significant increase in the number of unhatched eggs was also observed. These findings suggest that fertility impairment caused by cultivation at 25 °C, a temperature considered to be at the lower limit of mild heat stress, can be partially alleviated by treatment with the raltegravir (**Figure 4.4)**.

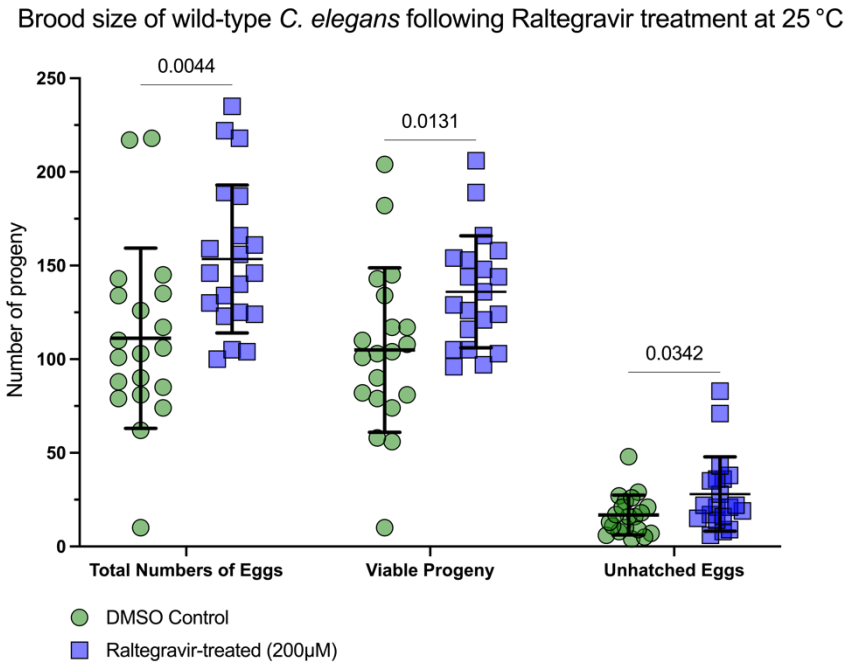

Figure 4.4 Raltegravir treatment and DMSO control in wild-type *C. elegans* at 25 °C. Each data point represents the brood of a single worm, including the total number of eggs laid, viable progeny, and unhatched eggs. Statistical comparisons were performed using an unpaired t-test with Welch's correction. [1] (Adapted from Lahav, n.d. [302])

[1] The experiments were carried out by my mentee, Bachelor's student Gali Lahav, as part of her lab internship and were published in her thesis titled The Effectiveness of a Transposon Inhibitor on the Aging of *C. elegans*,

4.4 The effect of transposon inhibitor treatment on fertility and reproductive aging in *fog-2* feminized *C. elegans*.

To assess the effect of the raltegravir on reproductive aging, *fog-2(q71)V* feminized worms were used. This mutant strain has impaired sperm production, resulting in animals that possess only female gametes. Since the oocytes remain intact, this strain is referred to as a feminized mutant. This allows for the separation of oocyte- and sperm-specific effects, making it possible to study reproductive aging in the different gametes. In this experimental setup, a pool of developmentally synchronized worms, obtained by timed egg-laying, were individually isolated, and their progeny were assessed throughout their reproductive lifespan. To exclude any confounding effects from sperm aging, a fresh pool of young males was provided daily for mating.

Raltegravir treatment resulted in a statistically significant increase in total brood size, with a higher number of viable offspring without a change in the number of unhatched eggs. Analysis of daily progeny distribution revealed no extension of the reproductive lifespan, as all worms ceased egg-laying by day seven of adulthood. Thus, the increase in progeny was confined to the normal fertile window. Pairwise comparisons of daily progeny counts showed no significant differences, with the increase reaching statistical significance only in the cumulative brood size across the full reproductive period (**Figure 4.5)**.

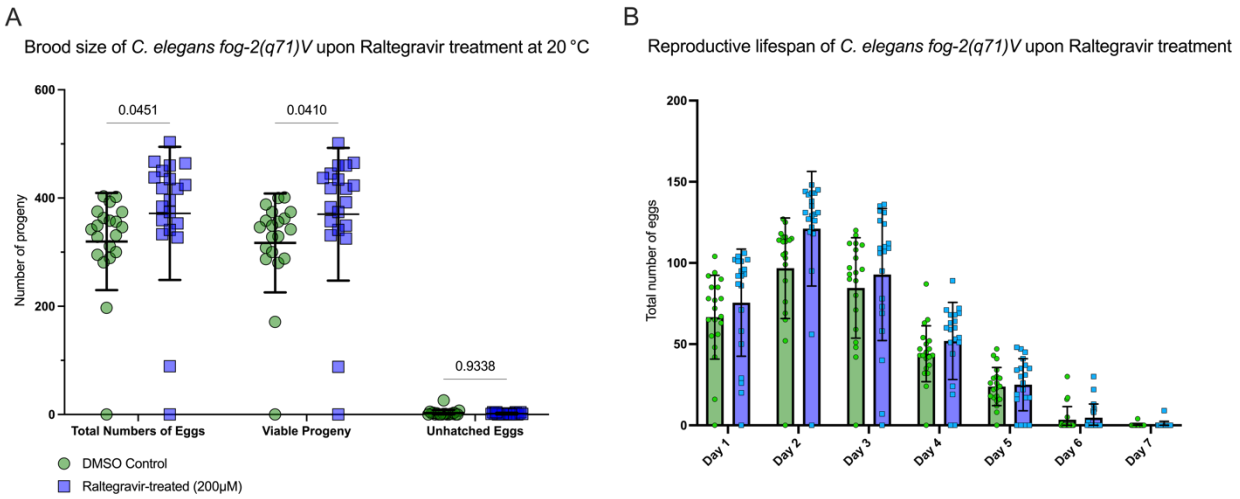

Figure 4.5 The effect of raltegravir treatment on brood size and reproductive lifespan in *fog-2(q71)V* animals under DMSO control and raltegravir treatment (200 µM). Each data point represents the progeny count of a single animal. **A)** Brood size, showing total number of eggs laid, viable progeny, and unhatched eggs. **B)** Reproductive lifespan, represented by the daily

submitted to the University of Applied Sciences Bonn-Rhein-Sieg, Department of Natural Sciences. It is included here as a citation to present the complete experimental workflow.

distribution of total eggs laid. Statistical significance was evaluated using the Wilcoxon matched-pairs signed-rank test.[2]

4.5 The effect of transposon inhibitor treatment on the lifespan of *C. elegans*

Previous studies have implicated age-dependent TE activation as a contributor to aging, primarily through increased genomic instability and processes such as inflammaging, as discussed in Introduction Chapter 1.6. Based on this, I tested whether pharmacological TE inhibition could impact aging in *C. elegans*. Lifespan assays were performed in wild-type animals treated with raltegravir to evaluate its potential effect on longevity.

Initially, the effect of raltegravir treatment was assessed in wild type *C. elegans* at 20 °C, using a DMSO supplemented control. To test for potential germline-dependent effects, 5'-fluorodeoxyuridine (FUdR) was added to the NGM at a final concentration of 50 µM in an additional condition. Both DMSO control and raltegravir treatment conditions were applied with and without the presence of FUdR. The experiment was conducted using a blinded approach to minimize bias (**Figure 4.6**).

[2] The experimentation was carried out by my mentee Mater´s student Titash Chandra Sarker as part of a laboratory practical rotation module.

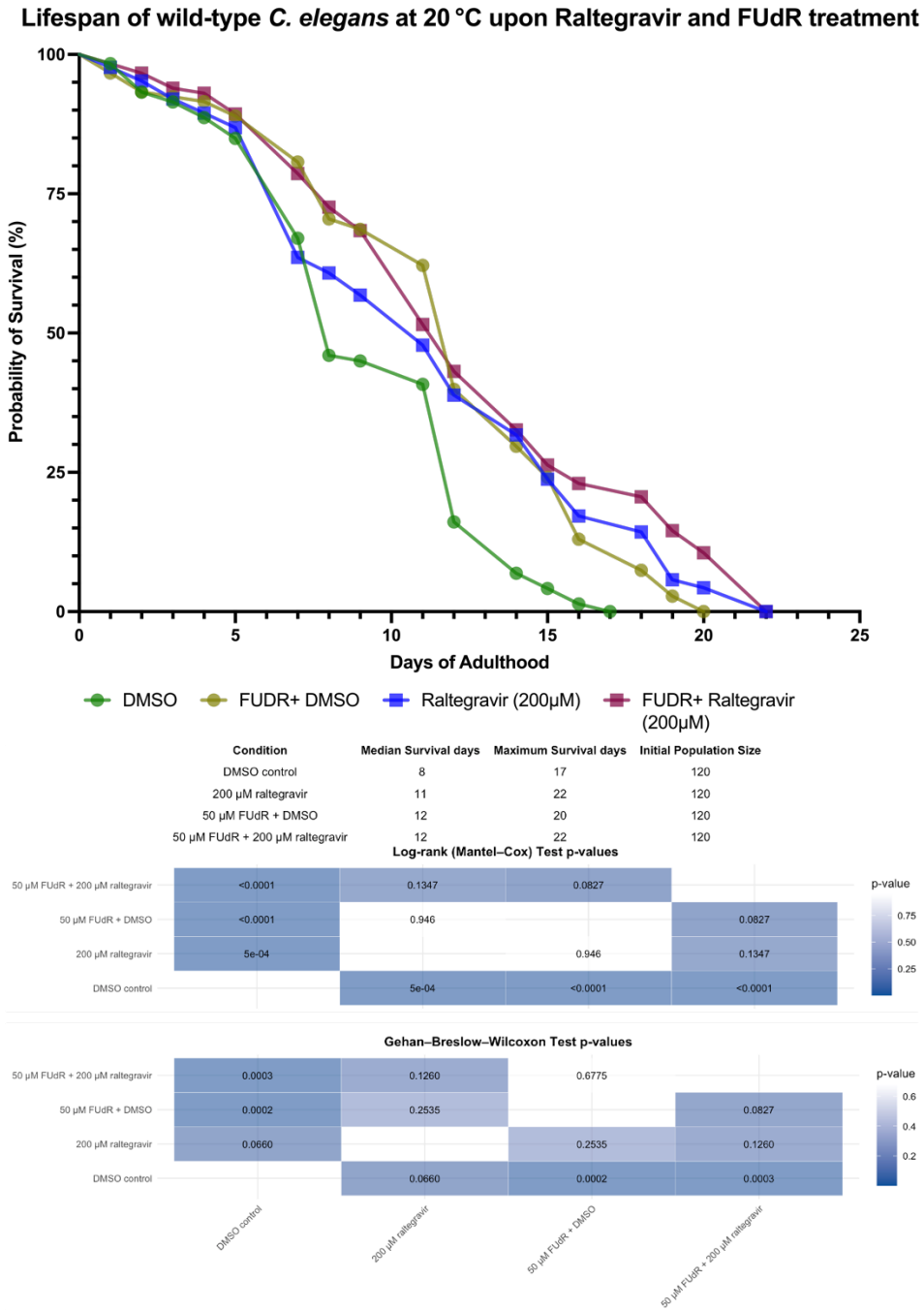

Figure 4.6 Lifespan of wild-type N2 *C. elegans* at 20 °C treated with DMSO (control), 50 µM FUdR, 200 µM raltegravir, and a combination of 50 µM FUdR + 200 µM raltegravir. Statistical evaluation was performed using the Log-rank (Mantel–Cox) test and the Gehan–Breslow–Wilcoxon test.[3] (Adapted from Lahav, n.d. [302])

[3] The experiments were carried out by my mentee, Bachelor's student Gali Lahav, as part of her lab internship and were published in her thesis titled The Effectiveness of a Transposon Inhibitor on the Aging of C. elegans, submitted to the University of Applied Sciences Bonn-Rhein-Sieg, Department of Natural Sciences. It is included here as a citation to present the complete experimental workflow.

Raltegravir treatment extended the lifespan of *C. elegans* compared to the DMSO control, with an increase of 3 days in median lifespan and 5 days in maximum lifespan. This effect was observed in the absence of FUdR. The extension was statistically significant in the later stages of life, as indicated by the log-rank (Mantel-Cox) test, while early-life survival curves showed no significant difference, as confirmed by the Gehan-Breslow-Wilcoxon test.

As expected, FUdR treatment alone also extended lifespan relative to the DMSO-only control, with a median increase of 4 days and a 3 day increase in maximum lifespan. Finally, the combination of FUdR and raltegravir did not significantly differ from raltegravir alone; however, the combination showed the most pronounced effect overall. Notably, while FUdR alone extended both median and maximum lifespan during late-age survival, raltegravir alone produced a stronger effect on maximum lifespan. The maximum lifespan remained the same between the raltegravir and raltegravir combined with FUdR conditions (**Figure 4.6**).

To verify the effect of raltegravir on lifespan extension, the experiment with wild-type animals was repeated at 20 °C without FUdR supplementation. The experiment was again conducted using a blinded setup to minimize bias (**Figure 4.7**).

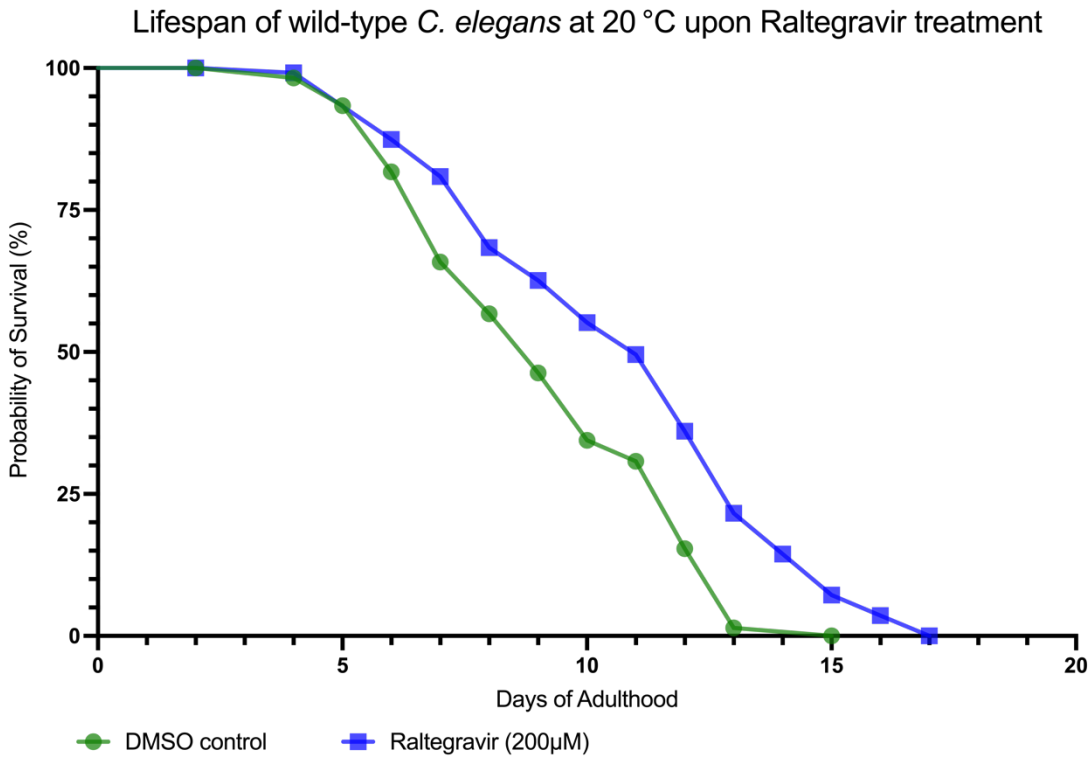

Figure 4.7 Lifespan of wild-type *C. elegans* at 20°C with treated raltegravir (200 µM) at 20 °C. Median survival was 9 days in the DMSO control group and 11 days in the raltegravir-treated group. Statistical evaluation showed a highly significant difference by Log-rank (Mantel–Cox) test

($p < 0.0001$) and a significant difference by Gehan–Breslow–Wilcoxon test ($p = 0.0016$). n=120 worms per condition. [4]

In this second repetition, raltegravir treatment significantly increased the lifespan of *C. elegans* at 20 °C compared to the DMSO control, with an increase of 2 days in median survival. While the effect was not dramatic, it demonstrates that the pharmacological TE inhibitor is capable of extending lifespan. Overall, the data confirm that raltegravir treatment produces a mild but statistically significant extension of lifespan, with median lifespan increased by 3 days (approximately 30–35%) and maximum lifespan extended by 2 to 5 days (up to 30%).

To further investigate the interaction between mild heat stress and transposon inhibition, I conducted a lifespan assay in wild-type *C. elegans* at 25 °C. The experimental conditions included DMSO control and raltegravir treatment, consistent with previous assays performed at 20 °C. The experiment was performed in 2 repetitions(**Figure 4.8**).

The effect of raltegravir treatment at 25 °C appears modest. In the first trial, it had no impact on median survival but resulted in a statistically significant one-day increase in maximum lifespan. In the second repetition, raltegravir significantly affected both early and late survival, increasing median lifespan by one day and maximum lifespan by two days (**Figure 4.8)**.

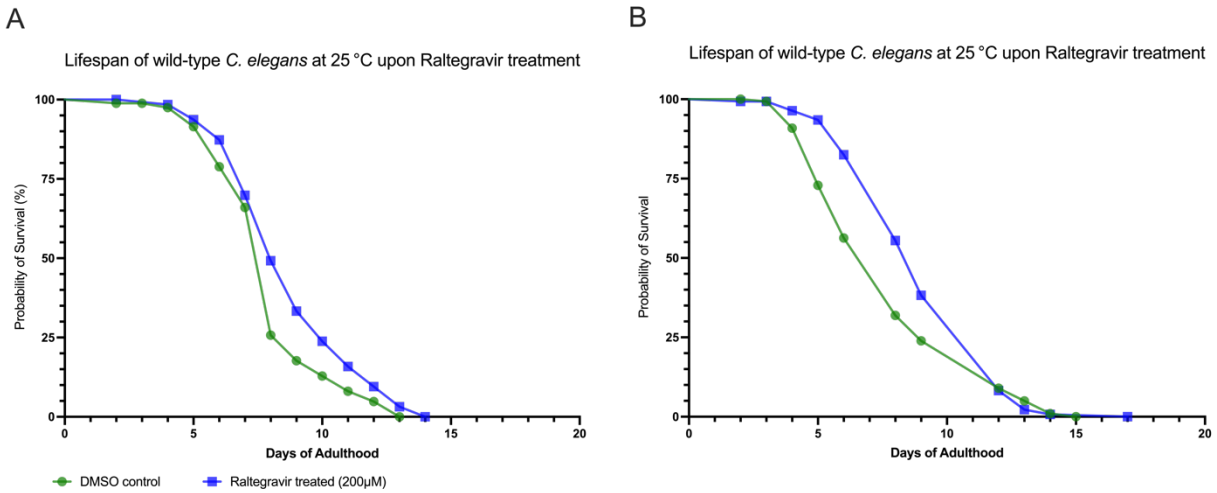

Figure 4.8 Lifespan of wild-type *C. elegans* at 25 °C treated with raltegravir (200 µM) **A)** In the first independent experiment, both the DMSO control (n=90) and raltegravir-treated(n=70) groups showed a median survival of 8 days. Statistical comparison indicated a modest but significant difference using the Log-rank (Mantel–Cox) test ($p = 0.042$) and the Gehan–Breslow–Wilcoxon test ($p = 0.0442$). **B)** In the second independent experiment, raltegravir-treated (n=150) animals had a median survival of 9 days compared to 8 days in the DMSO control (n=150). The difference was statistically significant by both the Log-rank (Mantel–Cox) test ($p = 0.0022$) and the Gehan–Breslow–Wilcoxon test ($p < 0.0001$).

[4] The experimentation was carried out by my mentee Mater´s student Titash Chandra Sarker as part of a laboratory practical rotation module.

Taken together, these findings indicate that the antiretroviral drug raltegravir is capable of producing a moderate but statistically significant extension of lifespan in *C. elegans*.
During my experiments with raltegravir treatment at 25 °C in wild-type *C. elegans*, I observed a higher incidence of internal hatching (bagging) in the DMSO control condition compared to the raltegravir-treated group. This observation prompted a follow-up quantification (**Figure 4.9)**.

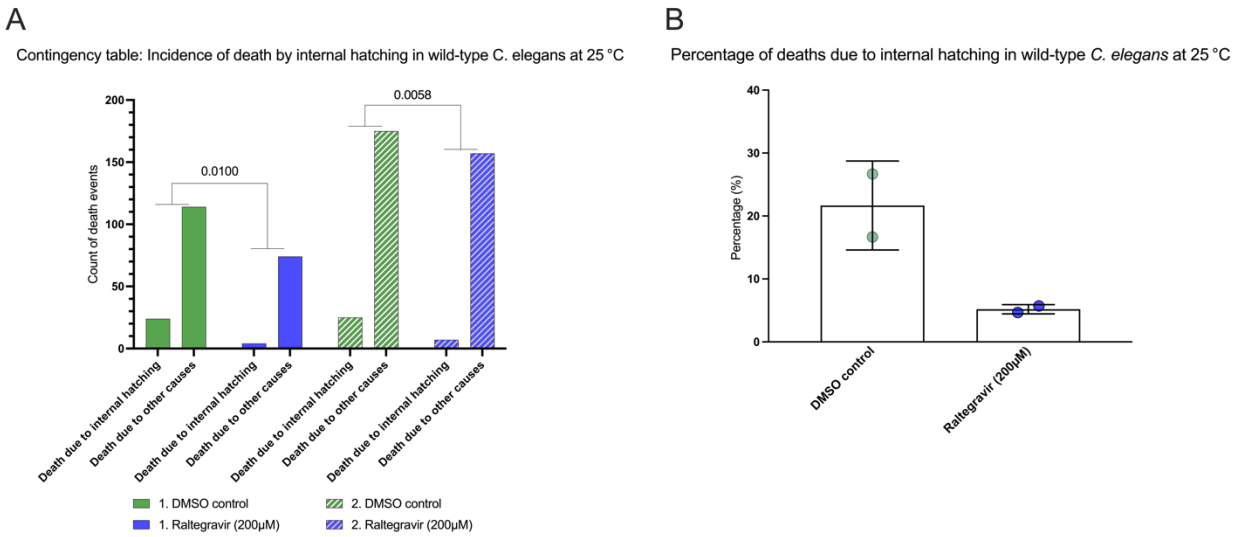

Figure 4.9 A) Contingency analysis of the internal hatching phenotype observed during the first and second lifespan experiments, showing the number of deaths caused by internal hatching compared to all other causes of death. **B)** Percentage representation of deaths attributed to internal hatching. Statistical evaluation was performed using a Chi-square test, p-values represented on the figure.

Raltegravir treatment significantly reduced the incidence of internal hatching in both independent experiments. This finding suggests that heat-induced transposable element activation may contribute to the increased incidence of internal hatching, and that raltegravir treatment can alleviate this phenotype.
It has been reported that the AFD triple mutant strain IK597 exhibits a shortened lifespan at 20 °C compared to wild type[293]. Given that my previous results showed increased TE activity, an intriguing question emerged: could raltegravir treatment extend the lifespan of the AFD triple mutant? To address this, the same experimental conditions were applied as in previous assays, using the AFD triple mutant at 20 °C with DMSO control and raltegravir treatment.
Raltegravir treatment did not affect the lifespan of the AFD triple mutant compared to the DMSO control (**Figure 4.10)**. This outcome is consistent with previous reports suggesting that the reduced lifespan in this mutant is primarily due to effects on *daf-9* and *ins-7* signaling[293], likely independent of TE activity. Therefore, raltegravir is unlikely to rescue this phenotype. However, an interesting observation was made regarding a higher incidence of internal hatching in the AFD mutant. To

explore this further, I quantified and compared the incidence of internal hatching in wild-type animals treated with raltegravir at 20 °C and in the AFD triple mutant under the same treatment conditions. The results show that raltegravir treatment had minimal effect on internal hatching in wild type animals at 20 °C. In contrast, the AFD triple mutant exhibited a high incidence of internal hatching, with 68% of animals dying from this phenotype. Remarkably, raltegravir treatment reduced this incidence to 25%. However, as the experiment was conducted with only one replicate, the findings cannot be statistically validated. Nonetheless, the observation suggests a potential link between TE activity and internal hatching, supported by the statistically significant reduction observed in wild type animals under 25 °C conditions and the similar trend seen in the AFD triple mutant at 20 °C (**Figure 4.11)**.

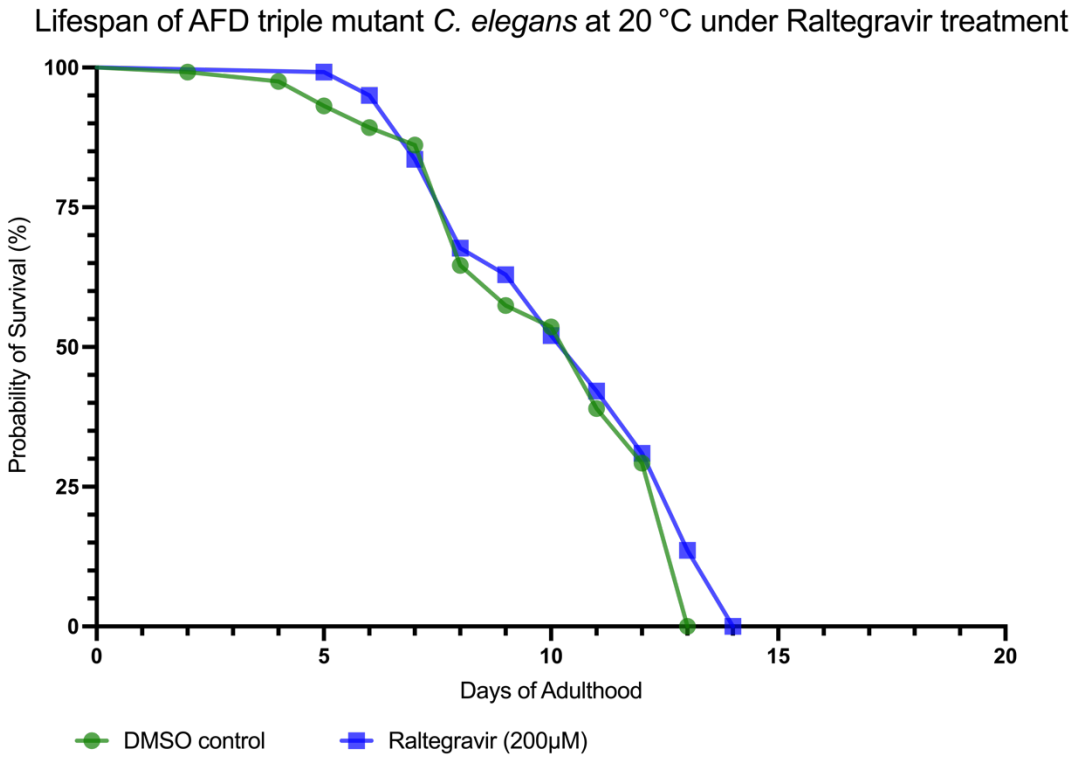

Figure 4.10 Lifespan of the Raltegravir-treated AFD triple mutant at 20 °C. Both the DMSO control and Raltegravir-treated groups showed a median survival of 11 days. Statistical comparisons indicated no significant difference between the groups, as assessed by the Log-rank (Mantel–Cox) test ($p = 0.3354$) and the Gehan–Breslow–Wilcoxon test ($p = 0.3274$). n=120 worms per condition.[5]

[5] The experimentation was carried out by my mentee Mater´s student Titash Chandra Sarker as part of a laboratory practical rotation module.

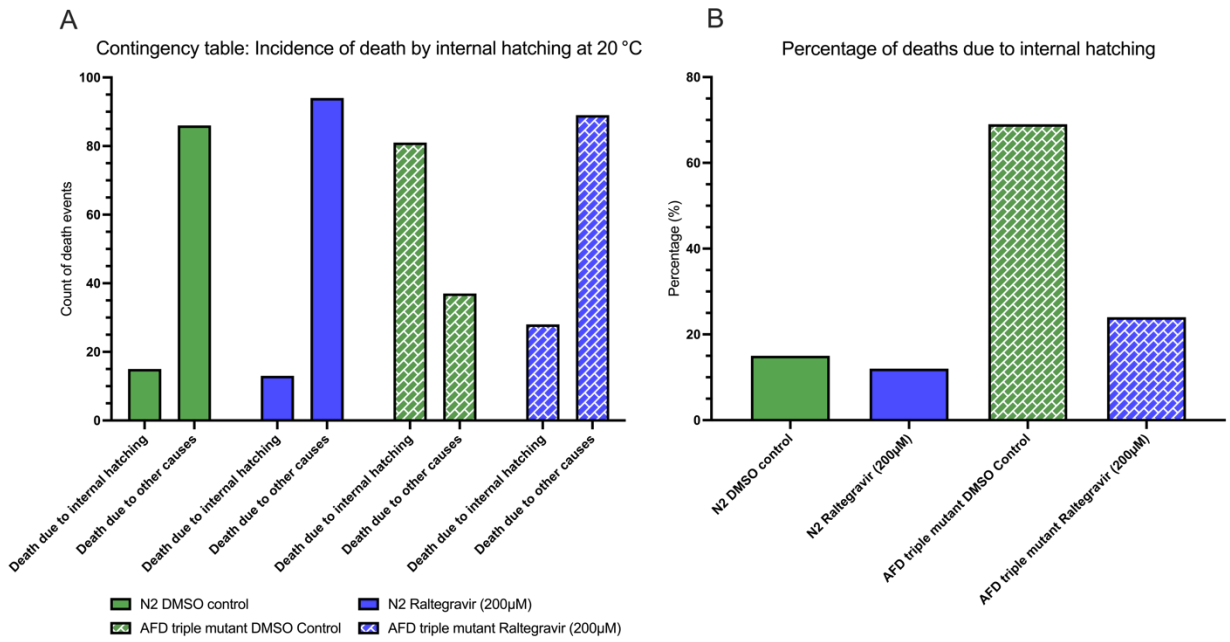

Figure 4.11 The effect of Raltegravir treatment on internal hatching was assessed based on lifespan assay recordings, using data from wild-type animals (**Figure 4.7**) and the AFD triple mutant (**Figure 4.9**). **A**) Contingency analysis of internal hatching-related deaths, based on total number of occurrences. **B**) Percentage of internal hatching events relative to total deaths.

5 Discussion

My investigation revealed that the AFD thermosensory neuron non-cell-autonomously regulates TE activity in the germline, effectively breaching the long-held Weismann barrier. These findings demonstrate that somatic neuronal regulation can directly influence germline genome maintenance, subsequently altering the frequency of heritable mutations **(Figure 5.1)**. As detailed in the attached paper and discussed in Chapter Results I, dysfunction of the AFD neuron significantly impacts TE expression **(Figure 3.1** and **Supplementary Figure S3 H, I)**. This alteration increases the frequency of mutation inheritance across generations **(Figure 3.4)**, ultimately leading to a progressive accumulation of *de novo* Tc1 insertions over generations **(Figure 3.5)**. The neuronal control of germline mutation rates may have far-reaching implications for evolutionary biology. Since TEs are known to facilitate genetic diversity, and according to the "epi-transposon hypothesis" and the "TE-thrust hypothesis," they may act as evolutionary accelerators, especially during population bottlenecks or habitat shifts[97]. Under prolonged environmental stress, neuronal sensing of stress signals can trigger TE mobilization in germ cells, leading to an increased mutation rate and the generation of novel genetic variation. This is particularly significant because TEs often harbor regulatory elements, such as enhancers and transcription factor binding sites. Thus, stress-induced TE bursts can drive large-scale regulatory innovation. In addition, TE-mediated duplications and genomic rearrangements can give rise to new gene copies that are free from the constraints of the original gene's function, allowing them to diverge and potentially acquire adaptive roles. Together, these mechanisms may help populations cope with environmental challenges and bottleneck events by accelerating evolutionary responses. The observations from my study raise intriguing questions about how neuronal regulation of germ cell TE activity could open new avenues for investigating mechanisms of adaptive evolution in animals.

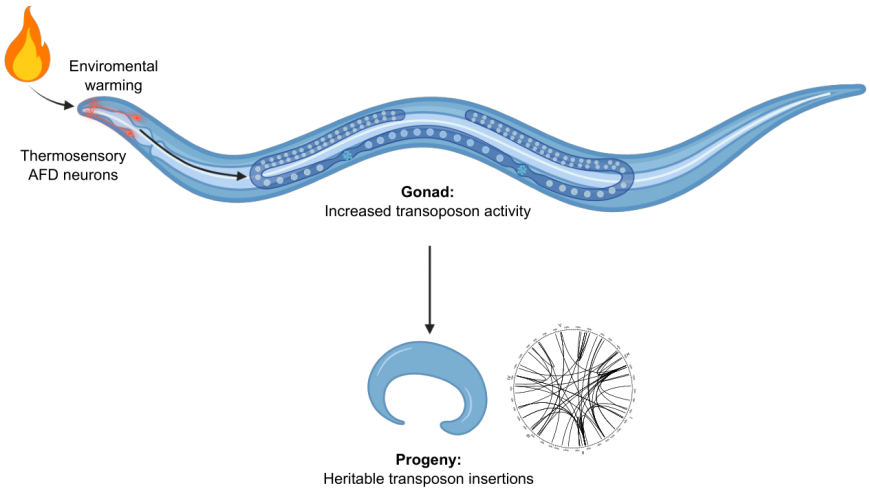

Figure 5.1 Working model: Heat stress sensed by the AFD neuron induces TE expression and mobilization in the germline, leading to heritable mutations through de novo insertions and the accumulation of mutations across generations[3].

An important question to address regarding observation from the transcriptomic analysis is the broad dysregulation of multiple TE families. However, notably, only the Tc1 family significantly contributes to *de novo* insertions. As highlighted in Results I, despite elevated RNA expression across several TE families, including Mirage, *de novo* insertions were exclusively attributed to the Tc1 family. While it remains intriguing to question what differentiates these families in their insertion-inducing behavior, the most probable explanation resides in their distinct molecular transposition machinery rather than selective signaling or regulatory mechanisms targeting individual families. This specificity likely reflects evolutionary adaptations shaping the molecular mechanisms underpinning transposition efficiency[303–306]. Prior studies emphasize the relatively recent origin and ongoing activity of the Tc1 family and the closely related Mariner family, both belonging to the Tc1/Mariner superfamily[307]. Unlike evolutionarily older TE families that predominantly generate nonfunctional transcripts or depend heavily on multiple cofactors, often encoded by separate elements, the Tc1 family encodes its own fully functional proteins essential for mobilization[303–306]. Remarkably, even though only a small fraction of Tc1 transcripts are correctly processed, this limited pool is sufficient to yield functional transposase proteins capable of robust transposition[303–306]. Importantly, the Tc1 element possesses a single open reading frame encoding a highly efficient transposase enzyme, known for its aggressive catalytic activity[304,305]. This transposase has been shown to independently facilitate Tc1 mobilization both in vitro and heterologously as a transgene in other organisms, a rare and defining trait among TEs[303–306]. Consistent with this interpretation, investigation of wild isotypes of *C. elegans* confirms that the

Tc1/Mariner superfamily remains the most actively mobilized group in the recent evolutionary past, as reported in **Supplementary Table 5** of the attached paper. Thus, while numerous TE-related transcripts become upregulated following AFD neuron dysfunction, the predominant genetic alterations originate specifically from the Tc1 elements, underscoring their unique capacity to drive inheritable genetic diversity across successive generations.

It is important to note the difference between the three AFD neuron depletion strains, as discussed in the attached paper in the Results I chapter, these differences limited experimentation with the AFD:SCA, and AFD:HisCl1 strains. The three strains, AFD triple mutant, AFD:SCA, and AFD:HisCl1, exhibit varying degrees of TE activation. Notably, Tc1 family activation is exclusive to the AFD triple mutant, while Mirage1 is expressed across all three. At the transcriptome level, an interesting pattern emerges **(Supplementary Figure S3 H–I)**: the clustering of TE expression profiles shows that AFD:SCA and AFD:HisCl1 group together, while the AFD triple mutant clusters with both the wild type under heat stress and the AFD triple mutant under normal conditions. This suggests that the triple *gcy* gene mutations in the AFD triple mutant may induce a persistent heat stress–like sensing state, in which the neuron remains structurally intact and functional but behaves as though under heat stress, at least in terms of the germline TE regulation phenotype. In contrast, the other two strains represent pathological inactivation of the AFD neurons. In AFD:SCA, the neurons are ablated via apoptosis, while in AFD:HisCl1, permanent hyperpolarization is induced by a transgenic chloride channel, rendering the neurons inactive. This discrepancy is further supported by brood size assessments. The AFD triple mutant shows the least fertility impairment, while AFD:SCA displays severe fertility defects and a heavy reproductive burden. Although not quantitatively measured during my experiments, AFD:SCA animals also exhibited developmental delay, further complicating experimentation. Interestingly, AFD:HisCl1 shows TE induction even without histamine treatment, and in this state, fertility is not severely impaired. However, upon histamine treatment, fertility is strongly compromised, a phenotype not observed in wild type controls under the same conditions, this is suggestive of a TE independent impact on fertility in response to AFD neuron impairment. Taken together, these observations led to the choice of the AFD triple mutant as the primary model to study the role of AFD neurons in germline TE regulation.

As presented and discussed in Chapter Results I, my investigation focused on elucidating the genetic consequences of TE mobilization resulting from dysfunctions in AFD neuron activity. TE silencing in germline cells is predominantly mediated by sRNAs, described as "the guardians of the genome"[308,309]. Complementing this study, the accompanying paper by Teichman et al.[310] reports significant epigenetic effects arising from AFD neuron impairments, specifically highlighting disrupted transgenerational sRNA inheritance, consequently causing germline desilencing of transgenic elements. Multiple lines of evidence support the notion that transgene silencing and TE silencing in the *C. elegans* germline share overlapping molecular machineries[2,311–313]. Nevertheless, the exact molecular signaling pathways connecting AFD neuron activity to germline TE regulation remain incompletely characterized. This study provides valuable insights, proposing that the consistent effects of AFD neuron dysfunction on

transgenerational sRNA inheritance and TE activation likely originate from a common molecular mechanism, plausibly triggered by chronic heat stress responses specifically within AFD neurons. Mechanistically, our integrated transcriptomic and proteomic analyses implicate well-characterized mediators of AFD signaling. In particular, HIF-1 mediated serotonin signaling appears to modulate the transcription factor ATFS-1 and its downstream effector EMB-4, potentially operating in parallel with PMK-1-dependent activation of SYSM-1 and repression of HSF-1. Collectively, these pathways converge to suppress sRNA biogenesis and functionality, resulting in TE derepression and subsequent *de novo* Tc1-driven germline mutagenesis. These proposed molecular mechanisms strongly align with genetic evidence presented in the accompanying Teichman et al.[310] paper.

To further explore this connection, I analyzed TE expression levels in these relevant mutant backgrounds under standard conditions at 20°C and during heat stress (**Figure 3.6)**. The results indicated that serotonin signaling via TPH-1 functions as a negative regulator of heat-induced TE activation. This is demonstrated by the enhanced induction of TE expression in *tph-1* mutants compared to wild-type under heat stress conditions. Conversely, PMK-1 signaling appears to act as a positive regulator in this context, as *pmk-1* mutation resulted in reduced TE induction relative to wild-type. Additionally, it is noteworthy that the triple AFD mutant showed a lower fold-induction of TE expression in response to heat stress compared to wild-type animals, suggesting partial occlusion of heat-induced TE activation, potentially indicating that TE activation approaches a plateau level. Nonetheless, the potential contribution of parallel cell-autonomous mechanisms cannot be entirely excluded based on these results.

Furthermore, interpreting **Figure 3.6** in combination with **Figure 3.3F** and **Supplementary Figure S5** provides additional insights. Comparative analysis of the publicly available RNA-seq datasets, as shown in **Figure 3.3F** and **Supplementary Figure S5**, revealed significant enrichment of genes (sRNA pathway components) within the *pmk-1* mutant, which are downregulated in our AFD triple mutant transcriptome analysis **Figure 3.2D**. This suggests that PMK-1 normally represses genes involved in the sRNA pathways, which itself inhibits TE expression. Consequently, in *pmk-1* mutants, the repression of sRNA-related factors is lifted, allowing the reactivation of TEs. These observations are consistent with the reduced heat-induced TE expression observed in the *pmk-1* mutant background relative to wild-type upon **Figure 3.6**.

These observations further imply that heat-induced TE activity depends on AFD neuron function, and importantly, the effects seen in the mutant candidates support a model of cell-nonautonomous regulation, as these mediators are not expressed in the germline. This experimentation and the extended comparative analysis suggest that heat stress sensed by the AFD neuron influences germline TE activity through two potentially parallel signaling pathways. The first pathway involves HIF-1-mediated serotonin signaling that activates ATFS-1, subsequently restricting EMB-4, a factor essential for germline piRNA and sRNA-mediated TE regulation. In parallel, the second pathway operates through PMK-1 signaling, which presumably represses the germline-expressed transcription factor HSF-1, a known regulator of several piRNA and sRNA factors involved in controlling TE expression **Figure 5.2**. It is important to note the key limitation, the

proposed pathway remains hypothetical, inferred from the exploratory data analysis and the effects of the aforementioned individual gene mutations under heat stress condition. To validate this model, it is essential to establish epistatic relationships. Specifically, it must be determined whether the aforementioned mutations in the AFD triple mutant background replicates the same effects on TE expression as observed under heat stress conditions in **Figure 3.6**. Further investigation should explore the combined impact of these pathways. If the two proposed signaling routes indeed regulate germline TE expression in parallel, then combining the *pmk-1* knockout and/or RNAi knockdown with serotonin supplementation should produce a significant rescue of the TE expression induction phenotype seen in the AFD triple mutant. As a next step, testing this epistatic interaction hypothesis is necessary to confirm the mechanistic framework suggested by these findings.

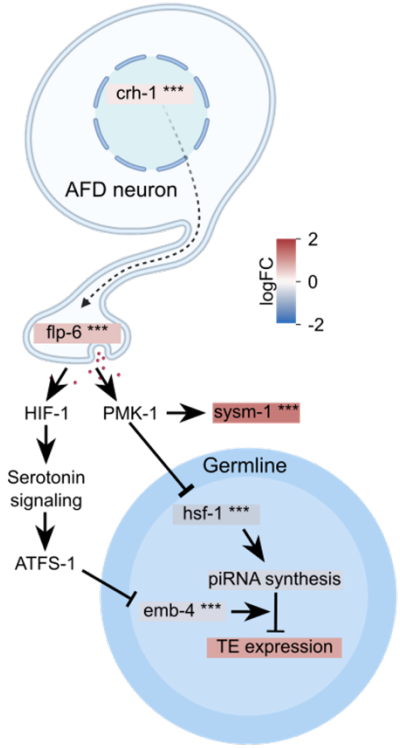

Figure 5.2 Proposed signaling pathway mechanism linking the AFD neuron to the germline.

To further characterize the effect of the AFD neuron on germ cells, I aimed to assess the fertility in the AFD neuron-depleted strains, which revealed that dysfunction of the AFD neuron affects worm fertility to varying degrees. The AFD triple mutant exhibits a slight, non-significant reduction in egg-laying capacity and progeny viability; however, it shows a significant increase in the number of unhatched eggs, suggesting elevated embryonic lethality. In contrast, the AFD:HisCl1 strain without histamine treatment does not display significant changes in brood size or progeny viability. Interestingly, in this condition, TE expression is already significantly upregulated. When histamine is added, there is no further significant increase in TE expression,

but a severe reduction in brood size is observed. This differs from the AFD:SCA strain, which shows both dramatic brood size reduction and reduced progeny viability. These results suggest that the AFD neuron influences fertility and progeny viability. However, given the small sample size and some inconsistencies between TE expression and reproductive outcomes, a definitive causal link between AFD neuron-induced TE activity and impaired fertility is indicated but cannot yet be conclusively established. While a TE-independent effect on germ cell maintenance and, consequently, fertility is plausible.

As the second aim of my work, I aimed to establish a pharmacological method to inhibit TE activity in vivo in worms and assess its effect on brood size, reproductive lifespan, oocyte aging, and overall lifespan.

Based on previous reports, I selected the antiretroviral HIV integrase inhibitor drug Isentress® INN: Raltegravir, which has been shown to effectively bind to Mos1 transposase and also inhibit Mariner transposon activity in *Drosophila* somatic tissues[314,315]. Therefore, it presents a promising candidate for testing in *C. elegans* to assess whether it can extend reproductive lifespan and overall lifespan. I aimed to evaluate the drug's efficacy in a well-characterized TE-silencing mutant, *mut-16(pk710)I*, in which transposable element expression and mobilization are significantly elevated, accompanied by reduced fertility. Treatment with raltegravir resulted in a significant but partial rescue of the impaired fertility phenotype. Furthermore, although not yet replicated, initial observations suggest a rescue of the increased germline apoptosis phenotype, and based on non-quantified assessments, the gonadal morphology appeared more preserved. While these latter findings require further validation, the observed improvement in brood size supports the suitability of raltegravir for additional experiments aimed at assessing its potential impact on reproductive aging and lifespan.

As a next step, I aimed to test the effect of raltegravir in wild-type worms. At 20°C, treatment did not result in a significant change in brood size. However, since heat stress is known to induce transposable element activity, as previously reported and supported by my findings in the Results I chapter, we extended the analysis to 25°C. Under these mild heat stress conditions, raltegravir treatment led to a significant increase in both brood size and the number of viable progeny. Interestingly, there was also an increase in the number of unhatched eggs. This observation suggests that while the drug improves overall fertility, certain aspects of embryonic development remain impaired. This finding is particularly intriguing in light of the hypothesis that transposable elements may act as physiological mediators of inflammation. As discussed in Introduction chapter 1.6, transposable elements can trigger inflammatory responses when genome stability is compromised. For example, chromatin dysregulation can lead to the activation of transposable elements, which not only further destabilizes the genome but also results in the accumulation of cytoplasmic double-stranded DNA. This, in turn, can trigger innate immune responses. In this context, transposable elements may act as internal biomarkers of disrupted genome maintenance. Therefore, it is plausible to hypothesize that in our study, chromatin instability activates transposable elements as part of an apoptotic or stress signaling cascade. Inhibiting these elements

with raltegravir may suppress both their mutagenic and pro-inflammatory effects, thereby allowing certain compromised embryos to proceed through development by bypassing cellular damage checkpoints. Because these initial experiments were conducted in wild-type hermaphrodites, which are self-fertilizing and produce sperm only during development, they could not differentiate between sperm- and oocyte-specific effects. To address this and focus specifically on oocyte aging, I employed the *fog-2(q71)V* mutant strain, which produces functional oocytes but lacks sperm, allowing controlled mating and the exclusion of sperm aging as a confounding factor. We conducted a reproductive aging experiment using this strain. Raltegravir treatment significantly increased brood size and viable progeny counts; however, it did not extend the reproductive window, as all worms ceased egg-laying by day 7. This result could indicate that raltegravir's inhibition of transposable element activity is only partial and that further improvements in dosage or the use of more potent inhibitors may be necessary. It is also possible that mechanisms independent of TE activity contribute to reproductive aging and the cessation of fertility.
These fertility experiments demonstrate that transposable element inhibition, in principle, and raltegravir, as a candidate drug, hold potential for enhancing brood size and improving early reproductive output. However, limitations in experimental replication and the need for dosage optimization highlight important directions for future research to assess the viability of TE inhibition as a strategy for improving reproductive health and lifespan. It is also essential to consider the potential risks associated with transposable elements having dedicated physiological roles, such as acting as immune mediators. If this turns out to be the case, rather than aiming for complete suppression, a more cautious and selective repression strategy may be necessary to maintain the appropriate balance between TE repression and expression.

Previous studies have reported that transposable element activity increases with age and may contribute to age-related pathologies, as discussed in Introduction chapter 1.6. Moreover, RNAi-based repression of transposable element activity has been shown to influence lifespan[316]. This suggests that pharmacological inhibition of transposable elements could offer a promising strategy for extending both lifespan and healthspan. Our experiments demonstrated a modest but significant and reproducible extension of lifespan at both 20°C and 25°C in wild-type *C. elegans* treated with raltegravir. Additional experiments involving co-treatment with FUdR provided further insight. raltegravir did not lead to additional lifespan extension when administered alongside FUdR, whereas FUdR alone was sufficient to extend lifespan. This result suggests that the beneficial effect of raltegravir on lifespan may depend on germ line-specific activity. However, the possibility that FUdR also inhibits TE activity cannot be excluded. As a future direction, genetic ablation of the germline could help clarify this question. During the lifespan experiments, I observed a notably lower incidence of internal hatching in worms treated with raltegravir compared to wild type. This effect was consistently reproducible at 25°C but not observed at 20°C, suggesting a temperature-dependent phenotype. A dramatic increase in internal hatching was also seen in the AFD triple mutant, which was almost completely reduced to wild-type levels at 20°C following raltegravir treatment. Although the connection remains unclear, this is an intriguing

observation. Internal hatching typically occurs when worms fail to lay eggs and embryos hatch within the body cavity. It raises the question of how raltegravir, and more broadly how TE activity, might influence such a severe phenotype, potentially through effects on reproductive or neuromuscular pathways involved in egg-laying. Exploring this connection could be a valuable direction for future research. Taken together these results lay the preliminary groundwork for further exploring the lifespan-extending effects of pharmacological transposable element inhibition. As a future direction, additional dose optimization and experimental replication will be necessary for validation, then expanding into the mechanistic framework of the observed phenotypes.

6 Conclusion

To conclude, during my work, I investigated the effects of various models to deplete the AFD neuron. This investigation led to the discovery that AFD neuron depletion results in increased transposon expression. This effect is particularly pronounced in the AFD triple mutant, where the Tc1 transposable element family not only shows elevated expression but also mobilization in germ cells, leading to de novo insertions that are heritable across generations. Our findings further demonstrate that these TE-induced insertions accumulate over successive generations. Taken together, these results reveal that the AFD thermosensory neuron regulates transposable element activity in germ cells and can influence the germline mutation rate. This challenges the final postulate of the Weismann barrier by showing that somatic neuronal activity can indeed affect the germline genome, with potential evolutionary consequences.
Furthermore, during this study established the use of raltegravir to study TE inhibition in *C. elegans* in the context of aging and reproductive aging. With further validation and replication, these findings could support a potential new application and repurposing of the drug.

References

1. Han, M., Perkins, M.H., Novaes, L.S., Xu, T., and Chang, H. (2023). Advances in transposable elements: from mechanisms to applications in mammalian genomics. Front Genet *14*, 1290146. https://doi.org/10.3389/fgene.2023.1290146.

2. Fischer, S.E.J. (2024). Activity and Silencing of Transposable Elements in C. elegans. DNA *4*, 129–140. https://doi.org/10.3390/dna4020007.

3. Szántó, P.R., Meyer, D.H., Teichman, G., Pérez-Llanos, F.J., Rickert, D., Köhrer, K.-E., Rechavi, O., and Schumacher, B. (2024). Thermosensory neurons control genetic inheritance through regulation of germline transposons. Preprint, https://doi.org/10.1101/2024.12.02.626368 https://doi.org/10.1101/2024.12.02.626368.

4. On the origin of species by means of natural selection, or the preservation of favoured races in the struggle for life(first edition) (1859).

5. Stenseth, N.Chr., Andersson, L., and Hoekstra, H.E. (2022). Gregor Johann Mendel and the development of modern evolutionary biology. Proceedings of the National Academy of Sciences *119*, e2201327119. https://doi.org/10.1073/pnas.2201327119.

6. Weismann, A. (1893). The Germ-plasm: a theory of heredity. Translated by W. Newton Parker and Harriet Rönnfeldt (Scribner) https://doi.org/10.5962/bhl.title.25196.

7. Cooper, G.M. (2000). Heredity, Genes, and DNA. In The Cell: A Molecular Approach. 2nd edition (Sinauer Associates).

8. Wang, Y., Su, M., Chen, Y., Huang, X., Ruan, L., Lv, Q., and Li, L. (2023). Research progress on the role and mechanism of DNA damage repair in germ cell development. Front Endocrinol (Lausanne) *14*, 1234280. https://doi.org/10.3389/fendo.2023.1234280.

9. Stergiou, L., and Hengartner, M.O. (2004). Death and more: DNA damage response pathways in the nematode C. elegans. Cell Death Differ *11*, 21–28. https://doi.org/10.1038/sj.cdd.4401340.

10. Bujarrabal-Dueso, A., Sendtner, G., Meyer, D.H., Chatzinikolaou, G., Stratigi, K., Garinis, G.A., and Schumacher, B. (2023). The DREAM complex functions as conserved master regulator of somatic DNA-repair capacities. Nat Struct Mol Biol *30*, 475–488. https://doi.org/10.1038/s41594-023-00942-8.

11. Ayarpadikannan, S., and Kim, H.-S. (2014). The Impact of Transposable Elements in Genome Evolution and Genetic Instability and Their Implications in Various Diseases. Genomics Inform *12*, 98–104. https://doi.org/10.5808/GI.2014.12.3.98.

12. Liao, X., Zhu, W., Zhou, J., Li, H., Xu, X., Zhang, B., and Gao, X. (2023). Repetitive DNA sequence detection and its role in the human genome. Commun Biol *6*, 954. https://doi.org/10.1038/s42003-023-05322-y.

13. Brown, T.A. (2002). Mutation, Repair and Recombination. In Genomes. 2nd edition (Wiley-Liss).

14. Chatterjee, N., and Walker, G.C. (2017). Mechanisms of DNA damage, repair and mutagenesis. Environ Mol Mutagen *58*, 235–263. https://doi.org/10.1002/em.22087.

15. Zamudio, N., and Bourc'his, D. (2010). Transposable elements in the mammalian germline: a comfortable niche or a deadly trap? Heredity *105*, 92–104. https://doi.org/10.1038/hdy.2010.53.

16. Ewe, C.K., and Rechavi, O. (2023). The third barrier to transgenerational inheritance in animals: somatic epigenetic resetting. EMBO Rep *24*, e56615. https://doi.org/10.15252/embr.202256615.

17. Nilsson, E.E., Maamar, M.B., and Skinner, M.K. (2020). Environmentally Induced Epigenetic Transgenerational Inheritance and the Weismann Barrier: The Dawn of Neo-Lamarckian Theory. J Dev Biol *8*, 28. https://doi.org/10.3390/jdb8040028.

18. Rieger, I., Weintraub, G., Lev, I., Goldstein, K., Bar-Zvi, D., Anava, S., Gingold, H., Shaham, S., and Rechavi, O. Nucleus-independent transgenerational small RNA inheritance in Caenorhabditis elegans. Sci Adv *9*, eadj8618. https://doi.org/10.1126/sciadv.adj8618.

19. Barucci, G., Cornes, E., Singh, M., Li, B., Ugolini, M., Samolygo, A., Didier, C., Dingli, F., Loew, D., Quarato, P., et al. (2020). Small RNA-mediated transgenerational silencing of histone genes impairs fertility in piRNA mutants. Nat Cell Biol *22*, 235–245. https://doi.org/10.1038/s41556-020-0462-7.

20. McClintock, B. (1950). The origin and behavior of mutable loci in maize. Proceedings of the National Academy of Sciences *36*, 344–355. https://doi.org/10.1073/pnas.36.6.344.

21. Feschotte, C., and Pritham, E.J. (2007). DNA Transposons and the Evolution of Eukaryotic Genomes. Annual Review of Genetics *41*, 331–368. https://doi.org/10.1146/annurev.genet.40.110405.090448.

22. The C. elegans Sequencing Consortium (1998). Genome Sequence of the Nematode C. elegans: A Platform for Investigating Biology. Science *282*, 2012–2018. https://doi.org/10.1126/science.282.5396.2012.

23. Schnable, P.S., Ware, D., Fulton, R.S., Stein, J.C., Wei, F., Pasternak, S., Liang, C., Zhang, J., Fulton, L., Graves, T.A., et al. (2009). The B73 Maize Genome: Complexity, Diversity, and Dynamics. Science *326*, 1112–1115. https://doi.org/10.1126/science.1178534.

24. Chuong, E.B., Elde, N.C., and Feschotte, C. (2017). Regulatory activities of transposable elements: from conflicts to benefits. Nat Rev Genet *18*, 71–86. https://doi.org/10.1038/nrg.2016.139.

25. International Human Genome Sequencing Consortium, Whitehead Institute for Biomedical Research, Center for Genome Research:, Lander, E.S., Linton, L.M., Birren, B., Nusbaum, C., Zody, M.C., Baldwin, J., Devon, K., Dewar, K., et al. (2001). Initial sequencing and analysis of the human genome. Nature *409*, 860–921. https://doi.org/10.1038/35057062.

26. Feschotte, C. (2008). Transposable elements and the evolution of regulatory networks. Nat Rev Genet *9*, 397–405. https://doi.org/10.1038/nrg2337.

27. Mobile Elements: Drivers of Genome Evolution | Science https://www.science.org/doi/10.1126/science.1089670.

28. Slotkin, R.K., and Martienssen, R. (2007). Transposable elements and the epigenetic regulation of the genome. Nat Rev Genet *8*, 272–285. https://doi.org/10.1038/nrg2072.

29. Goodier, J.L. (2016). Restricting retrotransposons: a review. Mobile DNA *7*, 16. https://doi.org/10.1186/s13100-016-0070-z.

30. Levin, H.L., and Moran, J.V. (2011). Dynamic interactions between transposable elements and their hosts. Nat Rev Genet *12*, 615–627. https://doi.org/10.1038/nrg3030.

31. Rebollo, R., Romanish, M.T., and Mager, D.L. (2012). Transposable Elements: An Abundant and Natural Source of Regulatory Sequences for Host Genes. Annu. Rev. Genet. *46*, 21–42. https://doi.org/10.1146/annurev-genet-110711-155621.

32. Chuong, E.B., Elde, N.C., and Feschotte, C. (2016). Regulatory evolution of innate immunity through co-option of endogenous retroviruses. Science *351*, 1083–1087. https://doi.org/10.1126/science.aad5497.

33. Pearson, E.R. (2018). Pharmacogenetics and target identification in diabetes. Current Opinion in Genetics & Development *50*, 68–73. https://doi.org/10.1016/j.gde.2018.02.005.

34. Logsdon, G.A., Vollger, M.R., and Eichler, E.E. (2020). Long-read human genome sequencing and its applications. Nat Rev Genet *21*, 597–614. https://doi.org/10.1038/s41576-020-0236-x.

35. Anzalone, A.V., Randolph, P.B., Davis, J.R., Sousa, A.A., Koblan, L.W., Levy, J.M., Chen, P.J., Wilson, C., Newby, G.A., Raguram, A., et al. (2019). Search-and-replace genome editing without double-strand breaks or donor DNA. Nature *576*, 149–157. https://doi.org/10.1038/s41586-019-1711-4.

36. Shmakov, S., Smargon, A., Scott, D., Cox, D., Pyzocha, N., Yan, W., Abudayyeh, O.O., Gootenberg, J.S., Makarova, K.S., Wolf, Y.I., et al. (2017). Diversity and evolution of class 2 CRISPR–Cas systems. Nat Rev Microbiol *15*, 169–182. https://doi.org/10.1038/nrmicro.2016.184.

37. Bourque, G., Burns, K.H., Gehring, M., Gorbunova, V., Seluanov, A., Hammell, M., Imbeault, M., Izsvák, Z., Levin, H.L., Macfarlan, T.S., et al. (2018). Ten things you should know about transposable elements. Genome Biology *19*, 199. https://doi.org/10.1186/s13059-018-1577-z.

38. Finnegan, D.J. (1989). Eukaryotic transposable elements and genome evolution. Trends Genet *5*, 103–107. https://doi.org/10.1016/0168-9525(89)90039-5.

39. Wells, J.N., and Feschotte, C. (2020). A Field Guide to Eukaryotic Transposable Elements. Annu. Rev. Genet. *54*, 539–561. https://doi.org/10.1146/annurev-genet-040620-022145.

40. Wicker, T., Sabot, F., Hua-Van, A., Bennetzen, J.L., Capy, P., Chalhoub, B., Flavell, A., Leroy, P., Morgante, M., Panaud, O., et al. (2007). A unified classification system for eukaryotic transposable elements. Nat Rev Genet *8*, 973–982. https://doi.org/10.1038/nrg2165.

41. Johnson, W.E. (2019). Origins and evolutionary consequences of ancient endogenous retroviruses. Nat Rev Microbiol *17*, 355–370. https://doi.org/10.1038/s41579-019-0189-2.

42. Marín, I., and Lloréns, C. (2000). Ty3/Gypsy Retrotransposons: Description of New Arabidopsis thaliana Elements and Evolutionary Perspectives Derived from Comparative Genomic Data. Molecular Biology and Evolution *17*, 1040–1049. https://doi.org/10.1093/oxfordjournals.molbev.a026385.

43. Dodonova, S.O., Prinz, S., Bilanchone, V., Sandmeyer, S., and Briggs, J.A.G. (2019). Structure of the Ty3/Gypsy retrotransposon capsid and the evolution of retroviruses. Proceedings of the National Academy of Sciences *116*, 10048–10057. https://doi.org/10.1073/pnas.1900931116.

44. Kapitonov, V.V., Tempel, S., and Jurka, J. (2009). Simple and fast classification of non-LTR retrotransposons based on phylogeny of their RT domain protein sequences. Gene *448*, 207–213. https://doi.org/10.1016/j.gene.2009.07.019.

45. Ghanim, G.E., Hu, H., Boulanger, J., and Nguyen, T.H.D. (2025). Structural mechanism of LINE-1 target-primed reverse transcription. Science *388*, eads8412. https://doi.org/10.1126/science.ads8412.

46. Zingler, N., Willhoeft, U., Brose, H.-P., Schoder, V., Jahns, T., Hanschmann, K.-M.O., Morrish, T.A., Löwer, J., and Schumann, G.G. (2005). Analysis of 5′ junctions of human LINE-1 and Alu retrotransposons suggests an alternative model for 5′-end attachment requiring microhomology-mediated end-joining. Genome Res *15*, 780–789. https://doi.org/10.1101/gr.3421505.

47. Kramerov, D.A., and Vassetzky, N.S. (2011). Origin and evolution of SINEs in eukaryotic genomes. Heredity (Edinb) *107*, 487–495. https://doi.org/10.1038/hdy.2011.43.

48. Lu, C., Chen, J., Zhang, Y., Hu, Q., Su, W., and Kuang, H. (2012). Miniature Inverted–Repeat Transposable Elements (MITEs) Have Been Accumulated through Amplification Bursts and Play Important Roles in Gene Expression and Species Diversity in Oryza sativa. Mol Biol Evol *29*, 1005–1017. https://doi.org/10.1093/molbev/msr282.

49. Poulter, R.T.M., and Butler, M.I. (2015). Tyrosine Recombinase Retrotransposons and Transposons. Microbiology Spectrum *3*, 10.1128/microbiolspec.mdna3-0036–2014. https://doi.org/10.1128/microbiolspec.mdna3-0036-2014.

50. Poulter, R.T.M., and Goodwin, T.J.D. (2005). DIRS-1 and the other tyrosine recombinase retrotransposons. Cytogenet Genome Res *110*, 575–588. https://doi.org/10.1159/000084991.

51. Evgen'ev, M.B., and Arkhipova, I.R. (2005). Penelope-like elements--a new class of retroelements: distribution, function and possible evolutionary significance. Cytogenet Genome Res *110*, 510–521. https://doi.org/10.1159/000084984.

52. Siguier, P., Gourbeyre, E., Varani, A., Ton-Hoang, B., and Chandler, M. (2015). Everyman's Guide to Bacterial Insertion Sequences. Microbiology Spectrum *3*, 10.1128/microbiolspec.mdna3-0030–2014. https://doi.org/10.1128/microbiolspec.mdna3-0030-2014.

53. Wilson, M.H., Coates, C.J., and George, A.L. (2007). PiggyBac Transposon-mediated Gene Transfer in Human Cells. Molecular Therapy *15*, 139–145. https://doi.org/10.1038/sj.mt.6300028.

54. Tellier, M., Bouuaert, C.C., and Chalmers, R. (2015). Mariner and the ITm Superfamily of Transposons. Microbiology Spectrum *3*, 10.1128/microbiolspec.mdna3-0033–2014. https://doi.org/10.1128/microbiolspec.mdna3-0033-2014.

55. Phylogenetic Relationships and Ancient Incomplete Lineage Sorting Among Cichlid Fishes in Lake Tanganyika as Revealed by Analysis of the Insertion of Retroposons | Molecular Biology and Evolution | Oxford Academic https://academic.oup.com/mbe/article/18/11/2057/1063082.

56. Kapitonov, V.V., and Jurka, J. (2001). Rolling-circle transposons in eukaryotes. Proceedings of the National Academy of Sciences *98*, 8714–8719. https://doi.org/10.1073/pnas.151269298.

57. Garrigues, J.M., Tsu, B.V., Daugherty, M.D., and Pasquinelli, A.E. (2019). Diversification of the Caenorhabditis heat shock response by Helitron transposable elements. eLife *8*, e51139. https://doi.org/10.7554/eLife.51139.

58. Krupovic, M., Makarova, K.S., Forterre, P., Prangishvili, D., and Koonin, E.V. (2014). Casposons: a new superfamily of self-synthesizing DNA transposons at the origin of prokaryotic CRISPR-Cas immunity. BMC Biology *12*, 36. https://doi.org/10.1186/1741-7007-12-36.

59. Kramerov, D.A., and Vassetzky, N.S. (2005). Short Retroposons in Eukaryotic Genomes. In International Review of Cytology A Survey of Cell Biology. (Academic Press), pp. 165–221. https://doi.org/10.1016/S0074-7696(05)47004-7.

60. Raskina, O., Barber, J.C., Nevo, E., and Belyayev, A. (2008). Repetitive DNA and chromosomal rearrangements: speciation-related events in plant genomes. Cytogenetic and Genome Research *120*, 351–357. https://doi.org/10.1159/000121084.

61. Hickman, A.B., and Dyda, F. (2015). Mechanisms of DNA Transposition. Microbiology Spectrum *3*, 10.1128/microbiolspec.mdna3-0034–2014. https://doi.org/10.1128/microbiolspec.mdna3-0034-2014.

62. Szafran, M.J., Jakimowicz, D., and Elliot, M.A. (2020). Compaction and control—the role of chromosome-organizing proteins in Streptomyces. FEMS Microbiology Reviews *44*, 725–739. https://doi.org/10.1093/femsre/fuaa028.

63. Malik, H.S., and Eickbush, T.H. (1999). Modular Evolution of the Integrase Domain in the Ty3/Gypsy Class of LTR Retrotransposons. Journal of Virology *73*, 5186–5190. https://doi.org/10.1128/jvi.73.6.5186-5190.1999.

64. Wessler, S.R. (2006). Transposable elements and the evolution of eukaryotic genomes. Proceedings of the National Academy of Sciences *103*, 17600–17601. https://doi.org/10.1073/pnas.0607612103.

65. Schaack, S., Gilbert, C., and Feschotte, C. (2010). Promiscuous DNA: horizontal transfer of transposable elements and why it matters for eukaryotic evolution. Trends Ecol Evol *25*, 537–546. https://doi.org/10.1016/j.tree.2010.06.001.

66. Palazzo, A., Caizzi, R., Viggiano, L., and Marsano, R.M. (2017). Does the Promoter Constitute a Barrier in the Horizontal Transposon Transfer Process? Insight from Bari Transposons. Genome Biol Evol *9*, 1637–1645. https://doi.org/10.1093/gbe/evx122.

67. Loreto, E.L.S., Carareto, C.M.A., and Capy, P. (2008). Revisiting horizontal transfer of transposable elements in Drosophila. Heredity *100*, 545–554. https://doi.org/10.1038/sj.hdy.6801094.

68. Walsh, A.M., Kortschak, R.D., Gardner, M.G., Bertozzi, T., and Adelson, D.L. (2013). Widespread horizontal transfer of retrotransposons. Proc Natl Acad Sci U S A *110*, 1012–1016. https://doi.org/10.1073/pnas.1205856110.

69. Malik, H.S., and Eickbush, T.H. (2001). Phylogenetic analysis of ribonuclease H domains suggests a late, chimeric origin of LTR retrotransposable elements and retroviruses. Genome Res *11*, 1187–1197. https://doi.org/10.1101/gr.185101.

70. Dewannieux, M., Esnault, C., and Heidmann, T. (2003). LINE-mediated retrotransposition of marked Alu sequences. Nat Genet *35*, 41–48. https://doi.org/10.1038/ng1223.

71. Ullu, E., and Tschudi, C. (1984). Alu sequences are processed 7SL RNA genes. Nature *312*, 171–172. https://doi.org/10.1038/312171a0.

72. Thomas, J., Phillips, C.D., Baker, R.J., and Pritham, E.J. (2014). Rolling-Circle Transposons Catalyze Genomic Innovation in a Mammalian Lineage. Genome Biology and Evolution *6*, 2595–2610. https://doi.org/10.1093/gbe/evu204.

73. Sundaram, V., and Wang, T. (2018). Transposable element mediated innovation in gene regulatory landscapes of cells: Re-visiting the ‘gene-battery’ model. Bioessays *40*, 10.1002/bies.201700155. https://doi.org/10.1002/bies.201700155.

74. Garrigues, J.M., and Pasquinelli, A.E. (2022). Caenorhabditis elegans transposable elements harbor diverse transcription factor DNA-binding sites. G3 (Bethesda) *12*, jkac009. https://doi.org/10.1093/g3journal/jkac009.

75. Tollis, M., and Boissinot, S. (2012). The evolutionary dynamics of transposable elements in eukaryote genomes. Genome Dyn *7*, 68–91. https://doi.org/10.1159/000337126.

76. Laricchia, K.M., Zdraljevic, S., Cook, D.E., and Andersen, E.C. (2017). Natural Variation in the Distribution and Abundance of Transposable Elements Across the Caenorhabditis elegans Species. Mol Biol Evol *34*, 2187–2202. https://doi.org/10.1093/molbev/msx155.

77. Pardue, M.-L., and DeBaryshe, P.G. (2011). Retrotransposons that maintain chromosome ends. Proceedings of the National Academy of Sciences *108*, 20317–20324. https://doi.org/10.1073/pnas.1100278108.

78. Pardue, M.L., and DeBaryshe, P.G. (1999). Telomeres and telomerase: more than the end of the line. Chromosoma *108*, 73–82. https://doi.org/10.1007/s004120050354.

79. Huang, S., Tao, X., Yuan, S., Zhang, Y., Li, P., Beilinson, H.A., Zhang, Y., Yu, W., Pontarotti, P., Escriva, H., et al. (2016). Discovery of an Active RAG Transposon Illuminates the Origins of V(D)J Recombination. Cell *166*, 102–114. https://doi.org/10.1016/j.cell.2016.05.032.

80. Dupressoir, A., Marceau, G., Vernochet, C., Bénit, L., Kanellopoulos, C., Sapin, V., and Heidmann, T. (2005). Syncytin-A and syncytin-B, two fusogenic placenta-specific murine envelope genes of retroviral origin conserved in Muridae. Proceedings of the National Academy of Sciences *102*, 725–730. https://doi.org/10.1073/pnas.0406509102.

81. Kapitonov, V.V., and Jurka, J. (2005). RAG1 Core and V(D)J Recombination Signal Sequences Were Derived from Transib Transposons. PLOS Biology *3*, e181. https://doi.org/10.1371/journal.pbio.0030181.

82. Lavialle, C., Cornelis, G., Dupressoir, A., Esnault, C., Heidmann, O., Vernochet, C., and Heidmann, T. (2013). Paleovirology of 'syncytins', retroviral env genes exapted for a role in placentation. Philosophical Transactions of the Royal Society B: Biological Sciences *368*, 20120507. https://doi.org/10.1098/rstb.2012.0507.

83. Van't Hof, A.E., Campagne, P., Rigden, D.J., Yung, C.J., Lingley, J., Quail, M.A., Hall, N., Darby, A.C., and Saccheri, I.J. (2016). The industrial melanism mutation in British peppered moths is a transposable element. Nature *534*, 102–105. https://doi.org/10.1038/nature17951.

84. de Souza, F.S.J., Franchini, L.F., and Rubinstein, M. (2013). Exaptation of Transposable Elements into Novel Cis-Regulatory Elements: Is the Evidence Always Strong? Molecular Biology and Evolution *30*, 1239–1251. https://doi.org/10.1093/molbev/mst045.

85. Castanera, R., Morales-Diaz, N., Gupta, S., Purugganan, M., and Casacuberta, J.M. (2023). Transposons are important contributors to gene expression variability under selection in rice populations. eLife *12*. https://doi.org/10.7554/eLife.86324.2.

86. Kaessmann, H., Vinckenbosch, N., and Long, M. (2009). RNA-based gene duplication: mechanistic and evolutionary insights. Nat Rev Genet *10*, 19–31. https://doi.org/10.1038/nrg2487.

87. Brosius, J. (1991). Retroposons—Seeds of Evolution. Science *251*, 753–753. https://doi.org/10.1126/science.1990437.

88. The life history of retrocopies illuminates the evolution of new mammalian genes https://genome.cshlp.org/content/26/3/301.

89. Parker, H.G., VonHoldt, B.M., Quignon, P., Margulies, E.H., Shao, S., Mosher, D.S., Spady, T.C., Elkahloun, A., Cargill, M., Jones, P.G., et al. (2009). An Expressed Fgf4 Retrogene Is Associated with Breed-Defining Chondrodysplasia in Domestic Dogs. Science *325*, 995–998. https://doi.org/10.1126/science.1173275.

90. Gray, Y.H.M. (2000). It takes two transposons to tango:transposable-element-mediated chromosomal rearrangements. Trends in Genetics *16*, 461–468. https://doi.org/10.1016/S0168-9525(00)02104-1.

91. Bailey, J.A., and Eichler, E.E. (2006). Primate segmental duplications: crucibles of evolution, diversity and disease. Nat Rev Genet *7*, 552–564. https://doi.org/10.1038/nrg1895.

92. Cáceres, M., Ranz, J.M., Barbadilla, A., Long, M., and Ruiz, A. (1999). Generation of a Widespread Drosophila Inversion by a Transposable Element. Science *285*, 415–418. https://doi.org/10.1126/science.285.5426.415.

93. Gu, W., Zhang, F., and Lupski, J.R. (2008). Mechanisms for human genomic rearrangements. PathoGenetics *1*, 4. https://doi.org/10.1186/1755-8417-1-4.

94. Hastings, P.J., Lupski, J.R., Rosenberg, S.M., and Ira, G. (2009). Mechanisms of change in gene copy number. Nat Rev Genet *10*, 551–564. https://doi.org/10.1038/nrg2593.

95. Ichiyanagi, T., Ichiyanagi, K., Ogawa, A., Kuramochi-Miyagawa, S., Nakano, T., Chuma, S., Sasaki, H., and Udono, H. (2014). HSP90α plays an important role in piRNA biogenesis and retrotransposon repression in mouse. Nucleic Acids Res *42*, 11903–11911. https://doi.org/10.1093/nar/gku881.

96. Errbii, M., Keilwagen, J., Hoff, K.J., Steffen, R., Altmüller, J., Oettler, J., and Schrader, L. (2021). Transposable elements and introgression introduce genetic variation in the invasive ant Cardiocondyla obscurior. Mol Ecol *30*, 6211–6228. https://doi.org/10.1111/mec.16099.

97. Oliver, K.R., and Greene, W.K. (2011). Mobile DNA and the TE-Thrust hypothesis: supporting evidence from the primates. Mob DNA *2*, 8. https://doi.org/10.1186/1759-8753-2-8.

98. Kurhanewicz, N.A., Dinwiddie, D., Bush, Z.D., and Libuda, D.E. (2020). Elevated temperatures cause transposon-associated DNA damage in C. elegans spermatocytes. Curr Biol *30*, 5007-5017.e4. https://doi.org/10.1016/j.cub.2020.09.050.

99. Cryderman, D.E., Tang, H., Bell, C., Gilmour, D.S., and Wallrath, L.L. (1999). Heterochromatic silencing of Drosophila heat shock genes acts at the level of promoter potentiation. Nucleic Acids Res *27*, 3364–3370. https://doi.org/10.1093/nar/27.16.3364.

100. Kim, A.I., and Belyaeva, E.S. (1991). Transposition of mobile elements gypsy (mdg4) and hobo in germ-line and somatic cells of a genetically unstable mutator strain of Drosophila melanogaster. Molec. Gen. Genet. *229*, 437–444. https://doi.org/10.1007/BF00267467.

101. Characterization of a heat-activated retrotransposon in natural accessions of *Arabidopsis thaliana* https://www.jstage.jst.go.jp/article/ggs/91/6/91_16-00045/_article/-char/ja/.

102. Ryan, C.P., Brownlie, J.C., and Whyard, S. (2016). Hsp90 and Physiological Stress Are Linked to Autonomous Transposon Mobility and Heritable Genetic Change in Nematodes. Genome Biology and Evolution *8*, 3794–3805. https://doi.org/10.1093/gbe/evw284.

103. Della Valle, F., Reddy, P., Aguirre Vazquez, A., and Izpisua Belmonte, J.C. (2025). Reactivation of retrotransposable elements is associated with environmental stress and ageing. Nat Rev Genet, 1–12. https://doi.org/10.1038/s41576-025-00829-y.

104. Figueiredo, J.C., Grau, M.V., Wallace, K., Levine, A.J., Shen, L., Hamdan, R., Chen, X., Bresalier, R.S., McKeown-Eyssen, G., Haile, R.W., et al. (2009). Global DNA Hypomethylation (LINE-1) in the Normal Colon and Lifestyle Characteristics, Dietary and Genetic Factors. Cancer Epidemiol Biomarkers Prev *18*, 1041–1049. https://doi.org/10.1158/1055-9965.EPI-08-0926.

105. JCI Insight - SARS-CoV-2 infection mediates differential expression of human endogenous retroviruses and long interspersed nuclear elements https://insight.jci.org/articles/view/147170.

106. Srinivasachar Badarinarayan, S., Shcherbakova, I., Langer, S., Koepke, L., Preising, A., Hotter, D., Kirchhoff, F., Sparrer, K.M.J., Schotta, G., and Sauter, D. (2020). HIV-1 infection activates endogenous retroviral promoters regulating antiviral gene expression. Nucleic Acids Res *48*, 10890–10908. https://doi.org/10.1093/nar/gkaa832.

107. Spike, C.A., Huelgas-Morales, G., Tsukamoto, T., and Greenstein, D. (2018). Multiple Mechanisms Inactivate the LIN-41 RNA-Binding Protein To Ensure a Robust Oocyte-to-Embryo Transition in Caenorhabditis elegans. Genetics *210*, 1011–1037. https://doi.org/10.1534/genetics.118.301421.

108. Seroussi, U., Li, C., Sundby, A.E., Lee, T.L., Claycomb, J.M., and Saltzman, A.L. (2022). Mechanisms of epigenetic regulation by *C. elegans* nuclear RNA interference pathways. Seminars in Cell & Developmental Biology *127*, 142–154. https://doi.org/10.1016/j.semcdb.2021.11.018.

109. Matzke, M.A., and Mosher, R.A. (2014). RNA-directed DNA methylation: an epigenetic pathway of increasing complexity. Nat Rev Genet *15*, 394–408. https://doi.org/10.1038/nrg3683.

110. Brennecke, J., Aravin, A.A., Stark, A., Dus, M., Kellis, M., Sachidanandam, R., and Hannon, G.J. (2007). Discrete Small RNA-Generating Loci as Master Regulators of Transposon Activity in Drosophila. Cell *128*, 1089–1103. https://doi.org/10.1016/j.cell.2007.01.043.

111. Ghildiyal, M., and Zamore, P.D. (2009). Small silencing RNAs: an expanding universe. Nat Rev Genet *10*, 94–108. https://doi.org/10.1038/nrg2504.

112. Ozata, D.M., Gainetdinov, I., Zoch, A., O'Carroll, D., and Zamore, P.D. (2019). PIWI-interacting RNAs: small RNAs with big functions. Nat Rev Genet *20*, 89–108. https://doi.org/10.1038/s41576-018-0073-3.

113. Siomi, M.C., Sato, K., Pezic, D., and Aravin, A.A. (2011). PIWI-interacting small RNAs: the vanguard of genome defence. Nat Rev Mol Cell Biol *12*, 246–258. https://doi.org/10.1038/nrm3089.

114. Koonin, E.V. (2017). Evolution of RNA- and DNA-guided antivirus defense systems in prokaryotes and eukaryotes: common ancestry vs convergence. Biology Direct *12*, 5. https://doi.org/10.1186/s13062-017-0177-2.

115. Ipsaro, J.J., Haase, A.D., Knott, S.R., Joshua-Tor, L., and Hannon, G.J. (2012). The structural biochemistry of Zucchini implicates it as a nuclease in piRNA biogenesis. Nature *491*, 279–283. https://doi.org/10.1038/nature11502.

116. Zheng, K., Xiol, J., Reuter, M., Eckardt, S., Leu, N.A., McLaughlin, K.J., Stark, A., Sachidanandam, R., Pillai, R.S., and Wang, P.J. (2010). Mouse MOV10L1 associates with Piwi proteins and is an essential component of the Piwi-interacting RNA (piRNA) pathway. Proceedings of the National Academy of Sciences *107*, 11841–11846. https://doi.org/10.1073/pnas.1003953107.

117. Sampathi, S., Acharya, P., Zhao, Y., Wang, J., Stengel, K.R., Liu, Q., Savona, M.R., and Hiebert, S.W. (2019). The CDK7 inhibitor THZ1 alters RNA polymerase dynamics at the 5′ and 3′ ends of genes. Nucleic Acids Research *47*, 3921–3936. https://doi.org/10.1093/nar/gkz127.

118. Han, B.W., Wang, W., Li, C., Weng, Z., and Zamore, P.D. (2015). piRNA-guided transposon cleavage initiates Zucchini-dependent, phased piRNA production. Science *348*, 817–821. https://doi.org/10.1126/science.aaa1264.

119. Stein, C.B., Genzor, P., Mitra, S., Elchert, A.R., Ipsaro, J.J., Benner, L., Sobti, S., Su, Y., Hammell, M., Joshua-Tor, L., et al. (2019). Decoding the 5′ nucleotide bias of PIWI-interacting RNAs. Nat Commun *10*, 828. https://doi.org/10.1038/s41467-019-08803-z.

120. Horwich, M.D., Li, C., Matranga, C., Vagin, V., Farley, G., Wang, P., and Zamore, P.D. (2007). The Drosophila RNA methyltransferase, DmHen1, modifies germline piRNAs and single-stranded siRNAs in RISC. Curr Biol *17*, 1265–1272. https://doi.org/10.1016/j.cub.2007.06.030.

121. Sato, K., Iwasaki, Y.W., Shibuya, A., Carninci, P., Tsuchizawa, Y., Ishizu, H., Siomi, M.C., and Siomi, H. (2015). Krimper Enforces an Antisense Bias on piRNA Pools by Binding AGO3 in the Drosophila Germline. Mol Cell *59*, 553–563. https://doi.org/10.1016/j.molcel.2015.06.024.

122. Dodson, A.E., and Kennedy, S. (2020). Phase Separation in Germ Cells and Development. Dev Cell *55*, 4–17. https://doi.org/10.1016/j.devcel.2020.09.004.

123. Sankaranarayanan, M., and Weil, T.T. (2020). Granule regulation by phase separation during Drosophila oogenesis. Emerg Top Life Sci *4*, 355–364. https://doi.org/10.1042/ETLS20190155.

124. Suyama, R., and Kai, T. piRNA processing within non-membrane structures is governed by constituent proteins and their functional motifs. The FEBS Journal *n/a*. https://doi.org/10.1111/febs.17360.

125. Lim, L.-X., Isshiki, W., Iki, T., Kawaguchi, S., and Kai, T. (2022). The Tudor Domain-Containing Protein, Kotsubu (CG9925), Localizes to the Nuage and Functions in piRNA Biogenesis in D. melanogaster. Front. Mol. Biosci. *9*. https://doi.org/10.3389/fmolb.2022.818302.

126. Aravin, A.A., Heijden, G.W. van der, Castañeda, J., Vagin, V.V., Hannon, G.J., and Bortvin, A. (2009). Cytoplasmic Compartmentalization of the Fetal piRNA Pathway in Mice. PLOS Genetics *5*, e1000764. https://doi.org/10.1371/journal.pgen.1000764.

127. Manakov, S.A., Pezic, D., Marinov, G.K., Pastor, W.A., Sachidanandam, R., and Aravin, A.A. (2015). MIWI2 and MILI Have Differential Effects on piRNA Biogenesis and DNA Methylation. Cell Rep *12*, 1234–1243. https://doi.org/10.1016/j.celrep.2015.07.036.

128. Du, L., Chen, W., Zhang, D., Cui, Y., and He, Z. (2024). The functions and mechanisms of piRNAs in mediating mammalian spermatogenesis and their applications in reproductive medicine. Cell Mol Life Sci *81*, 379. https://doi.org/10.1007/s00018-024-05399-6.

129. Cecere, G., Zheng, G.X.Y., Mansisidor, A.R., Klymko, K.E., and Grishok, A. (2012). Promoters recognized by forkhead proteins exist for individual 21U-RNAs. Mol Cell *47*, 734–745. https://doi.org/10.1016/j.molcel.2012.06.021.

130. Svendsen, J.M., Reed, K.J., Vijayasarathy, T., Montgomery, B.E., Tucci, R.M., Brown, K.C., Marks, T.N., Nguyen, D.A.H., Phillips, C.M., and Montgomery, T.A. (2019). henn-1/HEN1 Promotes Germline Immortality in Caenorhabditis elegans. Cell Rep *29*, 3187-3199.e4. https://doi.org/10.1016/j.celrep.2019.10.114.

131. Rogers, A.K., and Phillips, C.M. (2020). A Small-RNA-Mediated Feedback Loop Maintains Proper Levels of 22G-RNAs in *C. elegans*. Cell Reports *33*, 108279. https://doi.org/10.1016/j.celrep.2020.108279.

132. Cordeiro Rodrigues, R.J., de Jesus Domingues, A.M., Hellmann, S., Dietz, S., de Albuquerque, B.F.M., Renz, C., Ulrich, H.D., Sarkies, P., Butter, F., and Ketting, R.F. (2019). PETISCO is a novel protein complex required for 21U RNA biogenesis and embryonic viability. Genes Dev *33*, 857–870. https://doi.org/10.1101/gad.322446.118.

133. Buckley, B.A., Burkhart, K.B., Gu, S.G., Spracklin, G., Kershner, A., Fritz, H., Kimble, J., Fire, A., and Kennedy, S. (2012). A nuclear Argonaute promotes multigenerational epigenetic inheritance and germline immortality. Nature *489*, 447–451. https://doi.org/10.1038/nature11352.

134. Guang, S., Bochner, A.F., Burkhart, K.B., Burton, N., Pavelec, D.M., and Kennedy, S. (2010). Small regulatory RNAs inhibit RNA polymerase II during the elongation phase of transcription. Nature *465*, 1097–1101. https://doi.org/10.1038/nature09095.

135. Ashe, A., Sapetschnig, A., Weick, E.-M., Mitchell, J., Bagijn, M.P., Cording, A.C., Doebley, A.-L., Goldstein, L.D., Lehrbach, N.J., Le Pen, J., et al. (2012). piRNAs can trigger a multigenerational epigenetic memory in the germline of C. elegans. Cell *150*, 88–99. https://doi.org/10.1016/j.cell.2012.06.018.

136. Claycomb, J.M., Batista, P.J., Pang, K.M., Gu, W., Vasale, J.J., van Wolfswinkel, J.C., Chaves, D.A., Shirayama, M., Mitani, S., Ketting, R.F., et al. (2009). The Argonaute CSR-1 and its 22G-RNA cofactors are required for holocentric chromosome segregation. Cell *139*, 123–134. https://doi.org/10.1016/j.cell.2009.09.014.

137. Simon, M., Sarkies, P., Ikegami, K., Doebley, A.-L., Goldstein, L.D., Mitchell, J., Sakaguchi, A., Miska, E.A., and Ahmed, S. (2014). Reduced insulin/IGF-1 signaling restores germ cell immortality to Caenorhabditis elegans Piwi mutants. Cell Rep *7*, 762–773. https://doi.org/10.1016/j.celrep.2014.03.056.

138. Shi, J., Zhou, T., and Chen, Q. (2022). Exploring the expanding universe of small RNAs. Nat Cell Biol *24*, 415–423. https://doi.org/10.1038/s41556-022-00880-5.

139. Lewis, S.H., Quarles, K.A., Yang, Y., Tanguy, M., Frézal, L., Smith, S.A., Sharma, P.P., Cordaux, R., Gilbert, C., Giraud, I., et al. (2018). Pan-arthropod analysis reveals somatic piRNAs as an ancestral defence against transposable elements. Nat Ecol Evol *2*, 174–181. https://doi.org/10.1038/s41559-017-0403-4.

140. Patel, M.Z., Jiang, Y., and Kakumani, P.K. (2024). Somatic piRNA and PIWI-mediated post-transcriptional gene regulation in stem cells and disease. Front Cell Dev Biol *12*, 1495035. https://doi.org/10.3389/fcell.2024.1495035.

141. Palakodeti, D., Smielewska, M., Lu, Y.-C., Yeo, G.W., and Graveley, B.R. (2008). The PIWI proteins SMEDWI-2 and SMEDWI-3 are required for stem cell function and piRNA expression in planarians. RNA *14*, 1174–1186. https://doi.org/10.1261/rna.1085008.

142. Juliano, C.E., Reich, A., Liu, N., Götzfried, J., Zhong, M., Uman, S., Reenan, R.A., Wessel, G.M., Steele, R.E., and Lin, H. (2014). PIWI proteins and PIWI-interacting RNAs function in Hydra somatic stem cells. Proc Natl Acad Sci U S A *111*, 337–342. https://doi.org/10.1073/pnas.1320965111.

143. Nandi, S., Chandramohan, D., Fioriti, L., Melnick, A.M., Hébert, J.M., Mason, C.E., Rajasethupathy, P., and Kandel, E.R. (2016). Roles for small noncoding RNAs in silencing of retrotransposons in the mammalian brain. Proceedings of the National Academy of Sciences *113*, 12697–12702. https://doi.org/10.1073/pnas.1609287113.

144. Chen, X., Xie, W., Zhang, M., Shi, Y., Xu, S., Cheng, H., Wu, L., Pathak, J.L., and Zheng, Z. (2022). The Emerging Role of Non-Coding RNAs in Osteogenic Differentiation of

Human Bone Marrow Mesenchymal Stem Cells. Front Cell Dev Biol *10*, 903278. https://doi.org/10.3389/fcell.2022.903278.

145. Saxe, J.P., Chen, M., Zhao, H., and Lin, H. (2013). Tdrkh is essential for spermatogenesis and participates in primary piRNA biogenesis in the germline. EMBO J *32*, 1869–1885. https://doi.org/10.1038/emboj.2013.121.

146. Yu, B., Ikhlas, S., Ruan, C., Zhong, X., and Cai, D. (2020). Innate and Adaptive Immunity of Murine Neural Stem Cell-Derived piRNA Exosomes/Microvesicles against Pseudotyped SARS-CoV-2 and HIV-Based Lentivirus. iScience *23*. https://doi.org/10.1016/j.isci.2020.101806.

147. Padeken, J., Zeller, P., Towbin, B., Katic, I., Kalck, V., Methot, S.P., and Gasser, S.M. (2019). Synergistic lethality between BRCA1 and H3K9me2 loss reflects satellite derepression. Genes Dev. *33*, 436–451. https://doi.org/10.1101/gad.322495.118.

148. Chang, C., Pagano, D.J., Lowe, D.D., and Kennedy, S. (2022). DNA Repair Strategy Sets Transposon Mobilization Rates in Caenorhabditis elegans. Preprint at bioRxiv, https://doi.org/10.1101/2022.08.01.502254 https://doi.org/10.1101/2022.08.01.502254.

149. Luo, S., Zhang, H., Duan, Y., Yao, X., Clark, A.G., and Lu, J. (2020). The evolutionary arms race between transposable elements and piRNAs in Drosophila melanogaster. BMC Evolutionary Biology *20*, 14. https://doi.org/10.1186/s12862-020-1580-3.

150. Pastore, B., Hertz, H.L., and Tang, W. Comparative analysis of piRNA sequences, targets and functions in nematodes. RNA Biol *19*, 1276–1292. https://doi.org/10.1080/15476286.2022.2149170.

151. Hoogstrate, S.W., Volkers, R.J., Sterken, M.G., Kammenga, J.E., and Snoek, L.B. (2014). Nematode endogenous small RNA pathways. Worm *3*, e28234. https://doi.org/10.4161/worm.28234.

152. Parhad, S.S., and Theurkauf, W.E. (2019). Rapid evolution and conserved function of the piRNA pathway. Open Biol *9*, 180181. https://doi.org/10.1098/rsob.180181.

153. Reilly, M.T., Faulkner, G.J., Dubnau, J., Ponomarev, I., and Gage, F.H. (2013). The Role of Transposable Elements in Health and Diseases of the Central Nervous System. J Neurosci *33*, 17577–17586. https://doi.org/10.1523/JNEUROSCI.3369-13.2013.

154. Merenciano, M., Larue, A., Garambois, C., Nunes, W.V.B., and Vieira, C. (2025). Exploring the relationship of transposable elements and ageing: causes and consequences. Genome Biol Evol, evaf088. https://doi.org/10.1093/gbe/evaf088.

155. Wasserzug-Pash, P., Rothman, R., Reich, E., Zecharyahu, L., Schonberger, O., Weiss, Y., Srebnik, N., Cohen-Hadad, Y., Weintraub, A., Ben-Ami, I., et al. (2022). Loss of heterochromatin and retrotransposon silencing as determinants in oocyte aging. Aging Cell *21*, e13568. https://doi.org/10.1111/acel.13568.

156. Peaston, A.E., Evsikov, A.V., Graber, J.H., Vries, W.N. de, Holbrook, A.E., Solter, D., and Knowles, B.B. (2004). Retrotransposons Regulate Host Genes in Mouse Oocytes and Preimplantation Embryos. Developmental Cell *7*, 597–606. https://doi.org/10.1016/j.devcel.2004.09.004.

157. Hajkova, P., Ancelin, K., Waldmann, T., Lacoste, N., Lange, U.C., Cesari, F., Lee, C., Almouzni, G., Schneider, R., and Surani, M.A. (2008). Chromatin dynamics during epigenetic reprogramming in the mouse germ line. Nature *452*, 877–881. https://doi.org/10.1038/nature06714.

158. Jachowicz, J.W., Bing, X., Pontabry, J., Bošković, A., Rando, O.J., and Torres-Padilla, M.-E. (2017). LINE-1 activation after fertilization regulates global chromatin accessibility in the early mouse embryo. Nat Genet *49*, 1502–1510. https://doi.org/10.1038/ng.3945.

159. Sakashita, A., Kitano, T., Ishizu, H., Guo, Y., Masuda, H., Ariura, M., Murano, K., and Siomi, H. (2023). Transcription of MERVL retrotransposons is required for preimplantation embryo development. Nat Genet *55*, 484–495. https://doi.org/10.1038/s41588-023-01324-y.

160. Vaquero, A., Scher, M., Erdjument-Bromage, H., Tempst, P., Serrano, L., and Reinberg, D. (2007). SIRT1 regulates the histone methyl-transferase SUV39H1 during heterochromatin formation. Nature *450*, 440–444. https://doi.org/10.1038/nature06268.

161. Malki, S., van der Heijden, G.W., O'Donnell, K.A., Martin, S.L., and Bortvin, A. (2014). A Role for Retrotransposon LINE-1 in Fetal Oocyte Attrition in Mice. Dev Cell *29*, 521–533. https://doi.org/10.1016/j.devcel.2014.04.027.

162. Zhao, Y., Simon, M., Seluanov, A., and Gorbunova, V. (2023). DNA damage and repair in age-related inflammation. Nat Rev Immunol *23*, 75–89. https://doi.org/10.1038/s41577-022-00751-y.

163. Franke, V., Ganesh, S., Karlic, R., Malik, R., Pasulka, J., Horvat, F., Kuzman, M., Fulka, H., Cernohorska, M., Urbanova, J., et al. (2017). Long terminal repeats power evolution of genes and gene expression programs in mammalian oocytes and zygotes. Genome Res *27*, 1384–1394. https://doi.org/10.1101/gr.216150.116.

164. De Cecco, M., Criscione, S.W., Peterson, A.L., Neretti, N., Sedivy, J.M., and Kreiling, J.A. (2013). Transposable elements become active and mobile in the genomes of aging mammalian somatic tissues. Aging (Albany NY) *5*, 867–883. https://doi.org/10.18632/aging.100621.

165. Djeghloul, D., Kuranda, K., Kuzniak, I., Barbieri, D., Naguibneva, I., Choisy, C., Bories, J.-C., Dosquet, C., Pla, M., Vanneaux, V., et al. (2016). Age-Associated Decrease of the Histone Methyltransferase SUV39H1 in HSC Perturbs Heterochromatin and B Lymphoid Differentiation. Stem Cell Reports *6*, 970–984. https://doi.org/10.1016/j.stemcr.2016.05.007.

166. Chamani, I.J., and Keefe, D.L. (2019). Epigenetics and Female Reproductive Aging. Front. Endocrinol. *10*. https://doi.org/10.3389/fendo.2019.00473.

167. Ge, Z.-J., Schatten, H., Zhang, C.-L., and Sun, Q.-Y. (2015). Oocyte ageing and epigenetics. Reproduction *149*, R103–R114. https://doi.org/10.1530/REP-14-0242.

168. Tsutsumi, M., Fujiwara, R., Nishizawa, H., Ito, M., Kogo, H., Inagaki, H., Ohye, T., Kato, T., Fujii, T., and Kurahashi, H. (2014). Age-Related Decrease of Meiotic Cohesins in Human Oocytes. PLOS ONE *9*, e96710. https://doi.org/10.1371/journal.pone.0096710.

169. Lister, L.M., Kouznetsova, A., Hyslop, L.A., Kalleas, D., Pace, S.L., Barel, J.C., Nathan, A., Floros, V., Adelfalk, C., Watanabe, Y., et al. (2010). Age-Related Meiotic Segregation Errors in Mammalian Oocytes Are Preceded by Depletion of Cohesin and Sgo2. Current Biology *20*, 1511–1521. https://doi.org/10.1016/j.cub.2010.08.023.

170. Mihalas, B.P., Pieper, G.H., Aboelenain, M., Munro, L., Srsen, V., Currie, C.E., Kelly, D.A., Hartshorne, G.M., Telfer, E.E., McAinsh, A.D., et al. (2024). Age-dependent loss of cohesion protection in human oocytes. Current Biology *34*, 117-131.e5. https://doi.org/10.1016/j.cub.2023.11.061.

171. Félix, M.-A., Ashe, A., Piffaretti, J., Wu, G., Nuez, I., Bélicard, T., Jiang, Y., Zhao, G., Franz, C.J., Goldstein, L.D., et al. (2011). Natural and Experimental Infection of Caenorhabditis Nematodes by Novel Viruses Related to Nodaviruses. PLOS Biology *9*, e1000586. https://doi.org/10.1371/journal.pbio.1000586.

172. Rechavi, O., Houri-Ze'evi, L., Anava, S., Sho Goh, W.S., Kerk, S.Y., Hannon, G.J., and Hobert, O. (2014). Starvation-Induced Transgenerational Inheritance of Small RNAs in C. elegans. Cell *158*, 277–287. https://doi.org/10.1016/j.cell.2014.06.020.

173. Dennis, S., Sheth, U., Feldman, J.L., English, K.A., and Priess, J.R. (2012). C. elegans Germ Cells Show Temperature and Age-Dependent Expression of Cer1, a Gypsy/Ty3-Related Retrotransposon. PLoS Pathog *8*, e1002591. https://doi.org/10.1371/journal.ppat.1002591.

174. Jones, B.C., Wood, J.G., Chang, C., Tam, A.D., Franklin, M.J., Siegel, E.R., and Helfand, S.L. (2016). A somatic piRNA pathway in the Drosophila fat body ensures metabolic homeostasis and normal lifespan. Nat Commun *7*, 13856. https://doi.org/10.1038/ncomms13856.

175. Roy, M., Viginier, B., Saint-Michel, É., Arnaud, F., Ratinier, M., and Fablet, M. (2020). Viral infection impacts transposable element transcript amounts in Drosophila. Proceedings of the National Academy of Sciences *117*, 12249–12257. https://doi.org/10.1073/pnas.2006106117.

176. Wang, L., Tracy, L., Su, W., Yang, F., Feng, Y., Silverman, N., and Zhang, Z.Z. (2022). Retrotransposon activation during Drosophila metamorphosis conditions adult antiviral responses. Nat Genet *54*, 1933–1945. https://doi.org/10.1038/s41588-022-01214-9.

177. Garschall, K., and Flatt, T. (2018). The interplay between immunity and aging in Drosophila. F1000Res *7*, 160. https://doi.org/10.12688/f1000research.13117.1.

178. Gorbunova, V., Seluanov, A., Mita, P., McKerrow, W., Fenyö, D., Boeke, J.D., Linker, S.B., Gage, F.H., Kreiling, J.A., Petrashen, A.P., et al. (2021). The role of retrotransposable elements in aging and age-associated diseases. Nature *596*, 43–53. https://doi.org/10.1038/s41586-021-03542-y.

179. Blumenstiel, J.P., Erwin, A.A., and Hemmer, L.W. (2016). What Drives Positive Selection in the Drosophila piRNA Machinery? The Genomic Autoimmunity Hypothesis. Yale J Biol Med *89*, 499–512.

180. Voichek, M., Bernhard, A., Novatchkova, M., Handler, D., Möseneder, P., Rafanel, B., Duchek, P., Senti, K.-A., and Brennecke, J. (2025). Direct cell-to-cell transmission of retrotransposons. Preprint at bioRxiv, https://doi.org/10.1101/2025.03.14.642691 https://doi.org/10.1101/2025.03.14.642691.

181. Cecco, M.D., Ito, T., Petrashen, A.P., Elias, A.E., Skvir, N.J., Criscione, S.W., Caligiana, A., Brocculi, G., Adney, E.M., Boeke, J.D., et al. (2019). LINE-1 derepression in senescent cells triggers interferon and inflammaging. Nature *566*, 73. https://doi.org/10.1038/s41586-018-0784-9.

182. Sundaram, V., Cheng, Y., Ma, Z., Li, D., Xing, X., Edge, P., Snyder, M.P., and Wang, T. (2014). Widespread contribution of transposable elements to the innovation of gene regulatory networks. Genome Res *24*, 1963–1976. https://doi.org/10.1101/gr.168872.113.

183. Kassiotis, G., and Stoye, J.P. (2016). Immune responses to endogenous retroelements: taking the bad with the good. Nat Rev Immunol *16*, 207–219. https://doi.org/10.1038/nri.2016.27.

184. Larouche, J.-D., Laumont, C.M., Trofimov, A., Vincent, K., Hesnard, L., Brochu, S., Côté, C., Humeau, J., Bonneil, É., Lanoix, J., et al. (2024). Transposable elements regulate thymus development and function. eLife *12*. https://doi.org/10.7554/eLife.91037.2.

185. Zhao, K., Du, J., Peng, Y., Li, P., Wang, S., Wang, Y., Hou, J., Kang, J., Zheng, W., Hua, S., et al. (2018). LINE1 contributes to autoimmunity through both RIG-I- and MDA5-mediated RNA sensing pathways. J Autoimmun *90*, 105–115. https://doi.org/10.1016/j.jaut.2018.02.007.

186. Volkman, H.E., and Stetson, D.B. (2014). The enemy within: endogenous retroelements and autoimmune disease. Nat Immunol *15*, 415–422. https://doi.org/10.1038/ni.2872.

187. Censi, S.T., Mariani-Costantini, R., Granzotto, A., Tomassini, V., and Sensi, S.L. (2024). Endogenous retroviruses in multiple sclerosis: A network-based etiopathogenic model. Ageing Research Reviews *99*, 102392. https://doi.org/10.1016/j.arr.2024.102392.

188. DNA hypomethylation leads to cGAS-induced autoinflammation in the epidermis | The EMBO Journal https://www.embopress.org/doi/full/10.15252/embj.2021108234.

189. Harding, S.M., Benci, J.L., Irianto, J., Discher, D.E., Minn, A.J., and Greenberg, R.A. (2017). Mitotic progression following DNA damage enables pattern recognition within micronuclei. Nature *548*, 466–470. https://doi.org/10.1038/nature23470.

190. Zhao, Y., Oreskovic, E., Zhang, Q., Lu, Q., Gilman, A., Lin, Y.S., He, J., Zheng, Z., Lu, J.Y., Lee, J., et al. (2021). Transposon-triggered innate immune response confers cancer resistance to the blind mole rat. Nat Immunol *22*, 1219–1230. https://doi.org/10.1038/s41590-021-01027-8.

191. Roers, A., Hiller, B., and Hornung, V. (2016). Recognition of Endogenous Nucleic Acids by the Innate Immune System. Immunity *44*, 739–754. https://doi.org/10.1016/j.immuni.2016.04.002.

192. Smith, C.C., Beckermann, K.E., Bortone, D.S., Cubas, A.A.D., Bixby, L.M., Lee, S.J., Panda, A., Ganesan, S., Bhanot, G., Wallen, E.M., et al. (2019). Endogenous retroviral signatures predict immunotherapy response in clear cell renal cell carcinoma. J Clin Invest *128*, 4804–4820. https://doi.org/10.1172/JCI121476.

193. Chiappinelli, K.B., Strissel, P.L., Desrichard, A., Li, H., Henke, C., Akman, B., Hein, A., Rote, N.S., Cope, L.M., Snyder, A., et al. (2015). Inhibiting DNA Methylation Causes an Interferon Response in Cancer via dsRNA Including Endogenous Retroviruses. Cell *162*, 974–986. https://doi.org/10.1016/j.cell.2015.07.011.

194. Bhat, A., Ghatage, T., Bhan, S., Lahane, G.P., Dhar, A., Kumar, R., Pandita, R.K., Bhat, K.M., Ramos, K.S., and Pandita, T.K. (2022). Role of Transposable Elements in Genome Stability: Implications for Health and Disease. International Journal of Molecular Sciences *23*, 7802. https://doi.org/10.3390/ijms23147802.

195. Muotri, A.R., Chu, V.T., Marchetto, M.C.N., Deng, W., Moran, J.V., and Gage, F.H. (2005). Somatic mosaicism in neuronal precursor cells mediated by L1 retrotransposition. Nature *435*, 903–910. https://doi.org/10.1038/nature03663.

196. Erwin, J.A., Marchetto, M.C., and Gage, F.H. (2014). Mobile DNA elements in the generation of diversity and complexity in the brain. Nat Rev Neurosci *15*, 497–506. https://doi.org/10.1038/nrn3730.

197. Singer, T., McConnell, M.J., Marchetto, M.C.N., Coufal, N.G., and Gage, F.H. (2010). LINE-1 retrotransposons: mediators of somatic variation in neuronal genomes? Trends in Neurosciences *33*, 345–354. https://doi.org/10.1016/j.tins.2010.04.001.

198. Erwin, J.A., Paquola, A.C.M., Singer, T., Gallina, I., Novotny, M., Quayle, C., Bedrosian, T.A., Alves, F.I.A., Butcher, C.R., Herdy, J.R., et al. (2016). L1-associated genomic regions are deleted in somatic cells of the healthy human brain. Nat Neurosci *19*, 1583–1591. https://doi.org/10.1038/nn.4388.

199. Baillie, J.K., Barnett, M.W., Upton, K.R., Gerhardt, D.J., Richmond, T.A., De Sapio, F., Brennan, P.M., Rizzu, P., Smith, S., Fell, M., et al. (2011). Somatic retrotransposition alters

the genetic landscape of the human brain. Nature *479*, 534–537. https://doi.org/10.1038/nature10531.

200. Sundaram, V., and Wysocka, J. (2020). Transposable elements as a potent source of diverse cis-regulatory sequences in mammalian genomes. Philosophical Transactions of the Royal Society B: Biological Sciences *375*, 20190347. https://doi.org/10.1098/rstb.2019.0347.

201. Notwell, J.H., Chung, T., Heavner, W., and Bejerano, G. (2015). A family of transposable elements co-opted into developmental enhancers in the mouse neocortex. Nat Commun *6*, 6644. https://doi.org/10.1038/ncomms7644.

202. Kapusta, A., Kronenberg, Z., Lynch, V.J., Zhuo, X., Ramsay, L., Bourque, G., Yandell, M., and Feschotte, C. (2013). Transposable Elements Are Major Contributors to the Origin, Diversification, and Regulation of Vertebrate Long Noncoding RNAs. PLOS Genetics *9*, e1003470. https://doi.org/10.1371/journal.pgen.1003470.

203. Padeken, J., Methot, S.P., and Gasser, S.M. (2022). Establishment of H3K9-methylated heterochromatin and its functions in tissue differentiation and maintenance. Nat Rev Mol Cell Biol *23*, 623–640. https://doi.org/10.1038/s41580-022-00483-w.

204. Ecco, G., Cassano, M., Kauzlaric, A., Duc, J., Coluccio, A., Offner, S., Imbeault, M., Rowe, H.M., Turelli, P., and Trono, D. (2016). Transposable elements and their KRAB-ZFP controllers regulate gene expression in adult tissues. Dev Cell *36*, 611–623. https://doi.org/10.1016/j.devcel.2016.02.024.

205. Van Meter, M., Kashyap, M., Rezazadeh, S., Geneva, A.J., Morello, T.D., Seluanov, A., and Gorbunova, V. (2014). SIRT6 represses LINE1 retrotransposons by ribosylating KAP1 but this repression fails with stress and age. Nat Commun *5*, 5011. https://doi.org/10.1038/ncomms6011.

206. Patoori, S., Barnada, S.M., Large, C., Murray, J.I., and Trizzino, M. (2022). Young transposable elements rewired gene regulatory networks in human and chimpanzee hippocampal intermediate progenitors. Development *149*, dev200413. https://doi.org/10.1242/dev.200413.

207. Thomas, E.O., Zuniga, G., Sun, W., and Frost, B. (2020). Awakening the dark side: Retrotransposon activation in neurodegenerative disorders. Curr Opin Neurobiol *61*, 65–72. https://doi.org/10.1016/j.conb.2020.01.012.

208. Zierhut, C., and Funabiki, H. (2020). Regulation and Consequences of cGAS Activation by Self-DNA. Trends Cell Biol *30*, 594–605. https://doi.org/10.1016/j.tcb.2020.05.006.

209. Gázquez-Gutiérrez, A., Witteveldt, J., Heras, S.R., and Macias, S. (2021). Sensing of transposable elements by the antiviral innate immune system. RNA *27*, 735–752. https://doi.org/10.1261/rna.078721.121.

210. Takahashi, T., Stoiljkovic, M., Song, E., Gao, X.-B., Yasumoto, Y., Kudo, E., Carvalho, F., Kong, Y., Park, A., Shanabrough, M., et al. (2022). LINE-1 activation in the cerebellum drives ataxia. Neuron *110*, 3278-3287.e8. https://doi.org/10.1016/j.neuron.2022.08.011.

211. Terry, D.M., and Devine, S.E. (2020). Aberrantly High Levels of Somatic LINE-1 Expression and Retrotransposition in Human Neurological Disorders. Front Genet *10*, 1244. https://doi.org/10.3389/fgene.2019.01244.

212. Römer, C. (2021). Viruses and Endogenous Retroviruses as Roots for Neuroinflammation and Neurodegenerative Diseases. Front Neurosci *15*, 648629. https://doi.org/10.3389/fnins.2021.648629.

213. Ramirez, P., Zuniga, G., Sun, W., Beckmann, A., Ochoa, E., DeVos, S.L., Hyman, B., Chiu, G., Roy, E.R., Cao, W., et al. (2022). Pathogenic tau accelerates aging-associated activation of transposable elements in the mouse central nervous system. Prog Neurobiol *208*, 102181. https://doi.org/10.1016/j.pneurobio.2021.102181.

214. Wahl, D., Smith, M.E., McEntee, C.M., Cavalier, A.N., Osburn, S.C., Burke, S.D., Grant, R.A., Nerguizian, D., Lark, D.S., Link, C.D., et al. (2023). The reverse transcriptase inhibitor 3TC protects against age-related cognitive dysfunction. Aging Cell *22*, e13798. https://doi.org/10.1111/acel.13798.

215. Grow, E.J., Flynn, R.A., Chavez, S.L., Bayless, N.L., Wossidlo, M., Wesche, D.J., Martin, L., Ware, C.B., Blish, C.A., Chang, H.Y., et al. (2015). Intrinsic retroviral reactivation in human preimplantation embryos and pluripotent cells. Nature *522*, 221–225. https://doi.org/10.1038/nature14308.

216. Pontis, J., Planet, E., Offner, S., Turelli, P., Duc, J., Coudray, A., Theunissen, T.W., Jaenisch, R., and Trono, D. (2019). Hominoid-Specific Transposable Elements and KZFPs Facilitate Human Embryonic Genome Activation and Control Transcription in Naive Human ESCs. Cell Stem Cell *24*, 724-735.e5. https://doi.org/10.1016/j.stem.2019.03.012.

217. Jang, H.S., Shah, N.M., Du, A.Y., Dailey, Z.Z., Pehrsson, E.C., Godoy, P.M., Zhang, D., Li, D., Xing, X., Kim, S., et al. (2019). Transposable elements drive widespread expression of oncogenes in human cancers. Nat Genet *51*, 611–617. https://doi.org/10.1038/s41588-019-0373-3.

218. Babaian, A., and Mager, D.L. (2016). Endogenous retroviral promoter exaptation in human cancer. Mobile DNA *7*, 24. https://doi.org/10.1186/s13100-016-0080-x.

219. Roulois, D., Loo Yau, H., Singhania, R., Wang, Y., Danesh, A., Shen, S.Y., Han, H., Liang, G., Jones, P.A., Pugh, T.J., et al. (2015). DNA-Demethylating Agents Target Colorectal Cancer Cells by Inducing Viral Mimicry by Endogenous Transcripts. Cell *162*, 961–973. https://doi.org/10.1016/j.cell.2015.07.056.

220. Treangen, T.J., and Salzberg, S.L. (2011). Repetitive DNA and next-generation sequencing: computational challenges and solutions. Nat Rev Genet *13*, 36–46. https://doi.org/10.1038/nrg3117.

221. Moerman, D.G., Benian, G.M., Barstead, R.J., Schriefer, L.A., and Waterston, R.H. (1988). Identification and intracellular localization of the unc-22 gene product of Caenorhabditis elegans. Genes Dev. *2*, 93–105. https://doi.org/10.1101/gad.2.1.93.

222. Moerman, D.G., Benian, G.M., and Waterston, R.H. (1986). Molecular cloning of the muscle gene unc-22 in Caenorhabditis elegans by Tc1 transposon tagging. Proceedings of the National Academy of Sciences *83*, 2579–2583. https://doi.org/10.1073/pnas.83.8.2579.

223. Rubin, G.M., and Spradling, A.C. (1982). Genetic Transformation of *Drosophila* with Transposable Element Vectors. Science *218*, 348–353. https://doi.org/10.1126/science.6289436.

224. Geyer, P.K., Green, M.M., and Corces, V.G. (1988). Reversion of a gypsy-induced mutation at the yellow (y) locus of Drosophila melanogaster is associated with the insertion of a newly defined transposable element. Proceedings of the National Academy of Sciences *85*, 3938–3942. https://doi.org/10.1073/pnas.85.11.3938.

225. Metzker, M.L. (2010). Sequencing technologies — the next generation. Nat Rev Genet *11*, 31–46. https://doi.org/10.1038/nrg2626.

226. Eid, J., Fehr, A., Gray, J., Luong, K., Lyle, J., Otto, G., Peluso, P., Rank, D., Baybayan, P., Bettman, B., et al. (2009). Real-Time DNA Sequencing from Single Polymerase Molecules. Science *323*, 133–138. https://doi.org/10.1126/science.1162986.

227. Jain, M., Koren, S., Miga, K.H., Quick, J., Rand, A.C., Sasani, T.A., Tyson, J.R., Beggs, A.D., Dilthey, A.T., Fiddes, I.T., et al. (2018). Nanopore sequencing and assembly of a human genome with ultra-long reads. Nat Biotechnol *36*, 338–345. https://doi.org/10.1038/nbt.4060.

228. Nurk, S., Koren, S., Rhie, A., Rautiainen, M., Bzikadze, A.V., Mikheenko, A., Vollger, M.R., Altemose, N., Uralsky, L., Gershman, A., et al. (2022). The complete sequence of a human genome. Science *376*, 44–53. https://doi.org/10.1126/science.abj6987.

229. Bao, W., Kojima, K.K., and Kohany, O. (2015). Repbase Update, a database of repetitive elements in eukaryotic genomes. Mobile DNA *6*, 11. https://doi.org/10.1186/s13100-015-0041-9.

230. Quesneville, H., Bergman, C.M., Andrieu, O., Autard, D., Nouaud, D., Ashburner, M., and Anxolabehere, D. (2005). Combined Evidence Annotation of Transposable Elements in Genome Sequences. PLOS Computational Biology *1*, e22. https://doi.org/10.1371/journal.pcbi.0010022.

231. Jain, M., Olsen, H.E., Paten, B., and Akeson, M. (2016). The Oxford Nanopore MinION: delivery of nanopore sequencing to the genomics community. Genome Biology *17*, 239. https://doi.org/10.1186/s13059-016-1103-0.

232. Rang, F.J., Kloosterman, W.P., and de Ridder, J. (2018). From squiggle to basepair: computational approaches for improving nanopore sequencing read accuracy. Genome Biology *19*, 90. https://doi.org/10.1186/s13059-018-1462-9.

233. Wick, R.R., Judd, L.M., Gorrie, C.L., and Holt, K.E. (2017). Unicycler: Resolving bacterial genome assemblies from short and long sequencing reads. PLOS Computational Biology *13*, e1005595. https://doi.org/10.1371/journal.pcbi.1005595.

234. RNA and cDNA sequencing for isoform-level transcriptomics Oxford Nanopore Technologies. https://nanoporetech.com/applications/techniques/rna-and-cdna-sequencing.

235. Smits, N., and Faulkner, G.J. (2023). Nanopore Sequencing to Identify Transposable Element Insertions and Their Epigenetic Modifications. In Transposable Elements: Methods and Protocols, M. R. Branco and A. de Mendoza Soler, eds. (Springer US), pp. 151–171. https://doi.org/10.1007/978-1-0716-2883-6_9.

236. Wenger, A.M., Peluso, P., Rowell, W.J., Chang, P.-C., Hall, R.J., Concepcion, G.T., Ebler, J., Fungtammasan, A., Kolesnikov, A., Olson, N.D., et al. (2019). Accurate circular consensus long-read sequencing improves variant detection and assembly of a human genome. Nat Biotechnol *37*, 1155–1162. https://doi.org/10.1038/s41587-019-0217-9.

237. Sharon, D., Tilgner, H., Grubert, F., and Snyder, M. (2013). A single-molecule long-read survey of the human transcriptome. Nat Biotechnol *31*, 1009–1014. https://doi.org/10.1038/nbt.2705.

238. Rhoads, A., and Au, K.F. (2015). PacBio Sequencing and Its Applications. Genomics, Proteomics & Bioinformatics *13*, 278–289. https://doi.org/10.1016/j.gpb.2015.08.002.

239. LoRTE: Detecting transposon-induced genomic variants using low coverage PacBio long read sequences. - PacBio https://www.pacb.com/publications/lorte-detecting-transposon-induced-genomic-variants-using-low-coverage-pacbio-long-read-sequences/.

240. Yasir, M., Turner, A.K., Lott, M., Rudder, S., Baker, D., Bastkowski, S., Page, A.J., Webber, M.A., and Charles, I.G. (2022). Long-read sequencing for identification of insertion sites in large transposon mutant libraries. Sci Rep *12*, 3546. https://doi.org/10.1038/s41598-022-07557-x.

241. Kahles, A., Behr, J., and Rätsch, G. (2016). MMR: a tool for read multi-mapper resolution. Bioinformatics *32*, 770–772. https://doi.org/10.1093/bioinformatics/btv624.

242. Bendall, M.L., Mulder, M. de, Iñiguez, L.P., Lecanda-Sánchez, A., Pérez-Losada, M., Ostrowski, M.A., Jones, R.B., Mulder, L.C.F., Reyes-Terán, G., Crandall, K.A., et al. (2019). Telescope: Characterization of the retrotranscriptome by accurate estimation of transposable element expression. PLOS Computational Biology *15*, e1006453. https://doi.org/10.1371/journal.pcbi.1006453.

243. Handzlik, J.E., Tastsoglou, S., Vlachos, I.S., and Hatzigeorgiou, A.G. (2020). Manatee: detection and quantification of small non-coding RNAs from next-generation sequencing data. Sci Rep *10*, 705. https://doi.org/10.1038/s41598-020-57495-9.

244. Axtell, M.J. (2013). ShortStack: Comprehensive annotation and quantification of small RNA genes. RNA *19*, 740–751. https://doi.org/10.1261/rna.035279.112.

245. O'Neill, K., Brocks, D., and Hammell, M.G. (2020). Mobile genomics: tools and techniques for tackling transposons. Philos Trans R Soc Lond B Biol Sci *375*, 20190345. https://doi.org/10.1098/rstb.2019.0345.

246. Wang, K., Hoeksema, J., and Liang, C. (2018). piRNN: deep learning algorithm for piRNA prediction. PeerJ *6*, e5429. https://doi.org/10.7717/peerj.5429.

247. Wang, K., Liang, C., Liu, J., Xiao, H., Huang, S., Xu, J., and Li, F. (2014). Prediction of piRNAs using transposon interaction and a support vector machine. BMC Bioinformatics *15*, 419. https://doi.org/10.1186/s12859-014-0419-6.

248. Sović, I., Šikić, M., Wilm, A., Fenlon, S.N., Chen, S., and Nagarajan, N. (2016). Fast and sensitive mapping of nanopore sequencing reads with GraphMap. Nat Commun *7*, 11307. https://doi.org/10.1038/ncomms11307.

249. Bustin, S.A., Benes, V., Garson, J.A., Hellemans, J., Huggett, J., Kubista, M., Mueller, R., Nolan, T., Pfaffl, M.W., Shipley, G.L., et al. (2009). The MIQE guidelines: minimum information for publication of quantitative real-time PCR experiments. Clin Chem *55*, 611–622. https://doi.org/10.1373/clinchem.2008.112797.

250. Wallis, D.C., Nguyen, D.A.H., Uebel, C.J., and Phillips, C.M. (2019). Visualization and Quantification of Transposon Activity in Caenorhabditis elegans RNAi Pathway Mutants. G3 (Bethesda) *9*, 3825–3832. https://doi.org/10.1534/g3.119.400639.

251. Hindson, B.J., Ness, K.D., Masquelier, D.A., Belgrader, P., Heredia, N.J., Makarewicz, A.J., Bright, I.J., Lucero, M.Y., Hiddessen, A.L., Legler, T.C., et al. (2011). High-Throughput Droplet Digital PCR System for Absolute Quantitation of DNA Copy Number. Anal. Chem. *83*, 8604–8610. https://doi.org/10.1021/ac202028g.

252. TEtools facilitates big data expression analysis of transposable elements and reveals an antagonism between their activity and that of piRNA genes | Nucleic Acids Research | Oxford Academic https://academic.oup.com/nar/article/45/4/e17/2290912.

253. Jin, Y., Tam, O.H., Paniagua, E., and Hammell, M. (2015). TEtranscripts: a package for including transposable elements in differential expression analysis of RNA-seq datasets. Bioinformatics *31*, 3593–3599. https://doi.org/10.1093/bioinformatics/btv422.

254. Yang, W.R., Ardeljan, D., Pacyna, C.N., Payer, L.M., and Burns, K.H. (2019). SQuIRE reveals locus-specific regulation of interspersed repeat expression. Nucleic Acids Research *47*, e27. https://doi.org/10.1093/nar/gky1301.

255. Navarro, F.C., Hoops, J., Bellfy, L., Cerveira, E., Zhu, Q., Zhang, C., Lee, C., and Gerstein, M.B. (2019). TeXP: Deconvolving the effects of pervasive and autonomous transcription of transposable elements. PLOS Computational Biology *15*, e1007293. https://doi.org/10.1371/journal.pcbi.1007293.

256. LIONS: analysis suite for detecting and quantifying transposable element initiated transcription from RNA-seq | Bioinformatics | Oxford Academic https://academic.oup.com/bioinformatics/article/35/19/3839/5355055?login=false.

257. Zhang, Z., and Xing, Y. (2017). CLIP-seq analysis of multi-mapped reads discovers novel functional RNA regulatory sites in the human transcriptome. Nucleic Acids Res *45*, 9260–9271. https://doi.org/10.1093/nar/gkx646.

258. Feng, X., Hao, X., Shi, R., Xia, Z., Huang, L., Yu, Q., and Zhou, F. (2020). Detection and Comparative Analysis of Methylomic Biomarkers of Rheumatoid Arthritis. Front Genet *11*, 238. https://doi.org/10.3389/fgene.2020.00238.

259. Sun, D., Xi, Y., Rodriguez, B., Park, H.J., Tong, P., Meong, M., Goodell, M.A., and Li, W. (2014). MOABS: model based analysis of bisulfite sequencing data. Genome Biology *15*, R38. https://doi.org/10.1186/gb-2014-15-2-r38.

260. Stuart, T., Eichten, S.R., Cahn, J., Karpievitch, Y.V., Borevitz, J.O., and Lister, R. (2016). Population scale mapping of transposable element diversity reveals links to gene regulation and epigenomic variation. eLife *5*, e20777. https://doi.org/10.7554/eLife.20777.

261. Daron, J., and Slotkin, R.K. (2017). EpiTEome: Simultaneous detection of transposable element insertion sites and their DNA methylation levels. Genome Biology *18*, 91. https://doi.org/10.1186/s13059-017-1232-0.

262. Garza, R., Sharma, Y., Atacho, D.A.M., Thiruvalluvan, A., Abu Hamdeh, S., Jönsson, M.E., Horvath, V., Adami, A., Ingelsson, M., Jern, P., et al. (2023). Single-cell transcriptomics of human traumatic brain injury reveals activation of endogenous retroviruses in oligodendroglia. Cell Reports *42*, 113395. https://doi.org/10.1016/j.celrep.2023.113395.

263. Groza, C., Chen, X., Wheeler, T.J., Bourque, G., and Goubert, C. (2024). A unified framework to analyze transposable element insertion polymorphisms using graph genomes. Nat Commun *15*, 8915. https://doi.org/10.1038/s41467-024-53294-2.

264. THE GENETICS OF CAENORHABDITIS ELEGANS | Genetics | Oxford Academic https://academic.oup.com/genetics/article-abstract/77/1/71/5991065?redirectedFrom=fulltext.

265. Byerly, L., Cassada, R.C., and Russell, R.L. (1976). The life cycle of the nematode *Caenorhabditis elegans*. Developmental Biology *51*, 23–33. https://doi.org/10.1016/0012-1606(76)90119-6.

266. Sulston, J.E., Schierenberg, E., White, J.G., and Thomson, J.N. (1983). The embryonic cell lineage of the nematode Caenorhabditis elegans. Dev Biol *100*, 64–119. https://doi.org/10.1016/0012-1606(83)90201-4.

267. Hodgkin, J., Horvitz, H.R., and Brenner, S. (1979). Nondisjunction Mutants of the Nematode CAENORHABDITIS ELEGANS. Genetics *91*, 67–94. https://doi.org/10.1093/genetics/91.1.67.

268. Ellis, H.M., and Horvitz, H.R. (1986). Genetic control of programmed cell death in the nematode C. elegans. Cell *44*, 817–829. https://doi.org/10.1016/0092-8674(86)90004-8.

269. Dickinson, D.J., Ward, J.D., Reiner, D.J., and Goldstein, B. (2013). Engineering the Caenorhabditis elegans genome using Cas9-triggered homologous recombination. Nat Methods *10*, 1028–1034. https://doi.org/10.1038/nmeth.2641.

270. Top community curators Google Docs. https://docs.google.com/spreadsheets/d/1u2EuEEeeo5pa7hLZ_mw08qhS1yJQKyRZxCNTYm90ULQ/pubhtml?gid=873251968&single=true&widget=true&headers=false&usp=embed_facebook.

271. WormBook http://www.wormbook.org/.

272. Meneely, P.M., Dahlberg, C.L., and Rose, J.K. (2019). Working with Worms: *Caenorhabditis elegans* as a Model Organism. CP Essential Lab Tech *19*, e35. https://doi.org/10.1002/cpet.35.

273. Evolution of the Caenorhabditis elegans Genome | Molecular Biology and Evolution | Oxford Academic https://academic.oup.com/mbe/article/26/6/1199/1040527.

274. Corsi, A.K., Wightman, B., and Chalfie, M. (2018). A Transparent window into biology: A primer on Caenorhabditis elegans. In WormBook: The Online Review of C. elegans Biology [Internet] (WormBook).

275. Cook, D.E., Zdraljevic, S., Roberts, J.P., and Andersen, E.C. (2017). CeNDR, the Caenorhabditis elegans natural diversity resource. Nucleic Acids Res *45*, D650–D657. https://doi.org/10.1093/nar/gkw893.

276. Braendle, C., and Paaby, A. (2024). Life history in Caenorhabditis elegans: from molecular genetics to evolutionary ecology. Genetics *228*, iyae151. https://doi.org/10.1093/genetics/iyae151.

277. Kenyon, C.J. (2010). The genetics of ageing. Nature *464*, 504–512. https://doi.org/10.1038/nature08980.

278. Noble, L.M., Chelo, I., Guzella, T., Afonso, B., Riccardi, D.D., Ammerman, P., Dayarian, A., Carvalho, S., Crist, A., Pino-Querido, A., et al. (2017). Polygenicity and Epistasis Underlie Fitness-Proximal Traits in the Caenorhabditis elegans Multiparental Experimental

Evolution (CeMEE) Panel. Genetics *207*, 1663–1685. https://doi.org/10.1534/genetics.117.300406.

279. Bessereau, J.-L. (2006). Transposons in C. elegans. WormBook. https://doi.org/10.1895/wormbook.1.70.1.

280. Sarkies, P., and Miska, E.A. (2014). Small RNAs break out: the molecular cell biology of mobile small RNAs. Nat Rev Mol Cell Biol *15*, 525–535. https://doi.org/10.1038/nrm3840.

281. Vastenhouw, N.L., Fischer, S.E.J., Robert, V.J.P., Thijssen, K.L., Fraser, A.G., Kamath, R.S., Ahringer, J., and Plasterk, R.H.A. (2003). A Genome-Wide Screen Identifies 27 Genes Involved in Transposon Silencing in C. elegans. Current Biology *13*, 1311–1316. https://doi.org/10.1016/S0960-9822(03)00539-6.

282. Cecere, G. (2021). Small RNAs in epigenetic inheritance: from mechanisms to trait transmission. FEBS Lett *595*, 2953–2977. https://doi.org/10.1002/1873-3468.14210.

283. Barucci, G., Cornes, E., Singh, M., Li, B., Ugolini, M., Samolygo, A., Didier, C., Dingli, F., Loew, D., Quarato, P., et al. (2020). Small-RNA-mediated transgenerational silencing of histone genes impairs fertility in piRNA mutants. Nat Cell Biol *22*, 235–245. https://doi.org/10.1038/s41556-020-0462-7.

284. Winston, W.M., Molodowitch, C., and Hunter, C.P. (2002). Systemic RNAi in C. elegans requires the putative transmembrane protein SID-1. Science *295*, 2456–2459. https://doi.org/10.1126/science.1068836.

285. Maniar, J.M., and Fire, A.Z. (2011). EGO-1, a C. elegans RdRP, Modulates Gene Expression via Production of mRNA-Templated Short Antisense RNAs. Curr Biol *21*, 449–459. https://doi.org/10.1016/j.cub.2011.02.019.

286. Towbin, B.D., González-Aguilera, C., Sack, R., Gaidatzis, D., Kalck, V., Meister, P., Askjaer, P., and Gasser, S.M. (2012). Step-wise methylation of histone H3K9 positions heterochromatin at the nuclear periphery. Cell *150*, 934–947. https://doi.org/10.1016/j.cell.2012.06.051.

287. Price, I.F., Wagner, J.A., Pastore, B., Hertz, H.L., and Tang, W. (2023). C. elegans germ granules sculpt both germline and somatic RNAome. Nat Commun *14*, 5965. https://doi.org/10.1038/s41467-023-41556-4.

288. Mori, I., and Ohshima, Y. (1995). Neural regulation of thermotaxis in Caenorhabditis elegans. Nature *376*, 344–348. https://doi.org/10.1038/376344a0.

289. Matsuyama, H.J., and Mori, I. (2020). Neural Coding of Thermal Preferences in the Nematode Caenorhabditis elegans. eNeuro *7*, ENEURO.0414-19.2020. https://doi.org/10.1523/ENEURO.0414-19.2020.

290. Servello, F.A., Fernandes, R., Eder, M., Harris, N., Martin, O.M., Oswal, N., Lindberg, A., Derosiers, N., Sengupta, P., Stroustrup, N., et al. (2022). Neuronal temperature perception

induces specific defenses that enable C. elegans to cope with the enhanced reactivity of hydrogen peroxide at high temperature. eLife *11*, e78941. https://doi.org/10.7554/eLife.78941.

291. Lee, S.-J., and Kenyon, C. (2009). Regulation of the Longevity Response to Temperature by Thermosensory Neurons in Caenorhabditis elegans. Curr Biol *19*, 715–722. https://doi.org/10.1016/j.cub.2009.03.041.

292. Lin, C.-T., He, C.-W., Huang, T.-T., and Pan, C.-L. (2017). Longevity control by the nervous system: Sensory perception, stress response and beyond. Translational Medicine of Aging *1*, 41–51. https://doi.org/10.1016/j.tma.2017.07.001.

293. Chen, Y.-C., Chen, H.-J., Tseng, W.-C., Hsu, J.-M., Huang, T.-T., Chen, C.-H., and Pan, C.-L. (2016). A *C. elegans* Thermosensory Circuit Regulates Longevity through *crh-1*/CREB-Dependent *flp-6* Neuropeptide Signaling. Developmental Cell *39*, 209–223. https://doi.org/10.1016/j.devcel.2016.08.021.

294. Luo, S., and Murphy, C.T. (2011). Caenorhabditis elegans reproductive aging: Regulation and underlying mechanisms. Genesis *49*, 53–65. https://doi.org/10.1002/dvg.20694.

295. Tatum, M.C., Ooi, F.K., Chikka, M.R., Chauve, L., Martinez-Velazquez, L.A., Steinbusch, H.W.M., Morimoto, R.I., and Prahlad, V. (2015). Neuronal Serotonin Release Triggers the Heat Shock Response in C. elegans in the Absence of Temperature Increase. Curr Biol *25*, 163–174. https://doi.org/10.1016/j.cub.2014.11.040.

296. Friday, A.J., Henderson, M.A., Morrison, J.K., Hoffman, J.L., and Keiper, B.D. (2015). Spatial and temporal translational control of germ cell mRNAs mediated by the eIF4E isoform IFE-1. Journal of Cell Science *128*, 4487–4498. https://doi.org/10.1242/jcs.172684.

297. Kato, M., and Slack, F.J. (2013). Ageing and the small, non-coding RNA world. Ageing Research Reviews *12*, 429–435. https://doi.org/10.1016/j.arr.2012.03.012.

298. Gebel, J., Tuppi, M., Sänger, N., Schumacher, B., and Dötsch, V. (2020). DNA Damaged Induced Cell Death in Oocytes. Molecules *25*, 5714. https://doi.org/10.3390/molecules25235714.

299. Waskom, M.L. (2021). seaborn: statistical data visualization. Journal of Open Source Software *6*, 3021. https://doi.org/10.21105/joss.03021.

300. Hunter, J.D. (2007). Matplotlib: A 2D Graphics Environment. Computing in Science & Engineering *9*, 90–95. https://doi.org/10.1109/MCSE.2007.55.

301. Stiernagle, T. (2006). Maintenance of C. elegans. WormBook. https://doi.org/10.1895/wormbook.1.101.1.

302. Lahav, G. The Effectiveness of a Transposon Inhibitor on the Aging of C. elegans.

303. Tosi, L.R.O., and Beverley, S.M. (2000). cis and trans factors affecting Mos1 mariner evolution and transposition in vitro, and its potential for functional genomics. Nucleic Acids Res *28*, 784–790.

304. Vos, J.C., De Baere, I., and Plasterk, R.H. (1996). Transposase is the only nematode protein required for in vitro transposition of Tc1. Genes Dev *10*, 755–761. https://doi.org/10.1101/gad.10.6.755.

305. Lampe, D.J., Churchill, M.E., and Robertson, H.M. (1996). A purified mariner transposase is sufficient to mediate transposition in vitro. EMBO J *15*, 5470–5479.

306. Fischer, S.E.J., Wienholds, E., and Plasterk, R.H.A. (2003). Continuous Exchange of Sequence Information Between Dispersed Tc1 Transposons in the Caenorhabditis elegans Genome. Genetics *164*, 127–134. https://doi.org/10.1093/genetics/164.1.127.

307. Dupeyron, M., Baril, T., Bass, C., and Hayward, A. (2020). Phylogenetic analysis of the Tc1/mariner superfamily reveals the unexplored diversity of pogo-like elements. Mobile DNA *11*, 21. https://doi.org/10.1186/s13100-020-00212-0.

308. Kasper, D.M., Gardner, K.E., and Reinke, V. (2014). Homeland security in the C. elegans germ line: Insights into the biogenesis and function of piRNAs. Epigenetics *9*, 62–74. https://doi.org/10.4161/epi.26647.

309. Bagijn, M.P., Goldstein, L.D., Sapetschnig, A., Weick, E.-M., Bouasker, S., Lehrbach, N.J., Simard, M.J., and Miska, E.A. (2012). Function, Targets, and Evolution of Caenorhabditis elegans piRNAs. Science *337*, 574–578. https://doi.org/10.1126/science.1220952.

310. Teichman, G., Sela, M., Ewe, C.K., Rieger, I., Anava, S., Mor, Y., Szántó, P., Meyer, D.H., Doron, H., Shachar, O., et al. (2024). Perception of Temperature Even in the Absence of Actual Change is Sufficient to Drive Transgenerational Epigenetic Inheritance. Preprint at bioRxiv, https://doi.org/10.1101/2024.12.02.626416 https://doi.org/10.1101/2024.12.02.626416.

311. Sijen, T., and Plasterk, R.H.A. (2003). Transposon silencing in the Caenorhabditis elegans germ line by natural RNAi. Nature *426*, 310–314. https://doi.org/10.1038/nature02107.

312. Tabara, H., Sarkissian, M., Kelly, W.G., Fleenor, J., Grishok, A., Timmons, L., Fire, A., and Mello, C.C. (1999). The rde-1 Gene, RNA Interference, and Transposon Silencing in C. elegans. Cell *99*, 123–132. https://doi.org/10.1016/S0092-8674(00)81644-X.

313. Aljohani, M.D., El Mouridi, S., Priyadarshini, M., Vargas-Velazquez, A.M., and Frøkjær-Jensen, C. (2020). Engineering rules that minimize germline silencing of transgenes in simple extrachromosomal arrays in C. elegans. Nat Commun *11*, 6300. https://doi.org/10.1038/s41467-020-19898-0.

314. Wolkowicz, U.M., Morris, E.R., Robson, M., Trubitsyna, M., and Richardson, J.M. (2014). Structural Basis of Mos1 Transposase Inhibition by the Anti-retroviral Drug Raltegravir. ACS Chem Biol *9*, 743–751. https://doi.org/10.1021/cb400791u.

315. Cancian, M., and Loreto, E.L.S. (2018). A Mos1 transposase in vivo assay to screen new HIV-1 integrase inhibitors. Genetica *146*, 243–247. https://doi.org/10.1007/s10709-018-0007-1.

316. Sturm, Á., Saskői, É., Hotzi, B., Tarnóci, A., Barna, J., Bodnár, F., Sharma, H., Kovács, T., Ari, E., Weinhardt, N., et al. (2023). Downregulation of transposable elements extends lifespan in Caenorhabditis elegans. Nat Commun *14*, 5278. https://doi.org/10.1038/s41467-023-40957-9.